PFC/RR-89-3 DOE/ID-01570-4

THE CHEMICAL KINETICS OF THE REACTIONS OF LITHIUM WITH STEAM-AIR MIXTURES

D.S. Barnett and M.S. Kazimi

April 1989

Plasma Fusion Center
and the
Department of Nuclear Engineering
Massachusetts Institute of Technology
Cambridge, MA 02139 U.S.A.

*This work was supported by EG&G Idaho, Inc. and the U.S. Department of Energy, Idaho Operations Office under DOE Contract No. DE-AC07-761ID01570

THE CHEMICAL KINETICS OF THE REACTIONS OF LITHIUM WITH STEAM–AIR MIXTURES

by
D.S. Barnett and M.S. Kazimi

ABSTRACT

This work involved the experimental and analytical determination of the consequences of lithium fires in the presence of steam. Experiments were performed to characterize the chemical reactions of lithium with steam–nitrogen and steam–air mixtures. Models were introduced in the LITFIRE code to describe lithium fires in the presence of steam inside the containment building and plasma chamber of a hypothetical fusion reactor. The code was also equipped with the capability to determine the effects of decay heat and lithium fires on the temperature response of the reactor first wall in the event of a coolant disturbance.

Forty–two kinetics experiments were performed in which a stream of steam–nitrogen or steam–air was passed over and reacted with approximately three grams of lithium heated to a predetermined temperature. The lithium reaction rates with the constituent gases were measured and characterized for a wide range of lithium temperatures and gas compositions. Experiments were performed with steam molar concentrations of 5, 15 and 30% and lithium temperatures ranging from 400 to 1100° C, inclusive.

The results of the kinetics experiments showed that the steam served to catalyze the lithium–nitrogen reaction at temperatures under 700° C. The catalytic effect was observed to decrease exponentially as a function of the lithium temperature until it vanished above 700° C. The catalytic effect was greater in the steam–air experiments than in the steam–nitrogen experiments. The lithium–steam reaction rates were observed to be independent of the lithium temperature but they were reduced by the presence of oxygen in air. If nitrogen was used as a reactor cover gas it would have to be kept dry, as a lithium–nitrogen fire in the presence of steam could burn more fiercely than was previously thought.

The LITFIRE code was modified to enable it to model the interactions of lithium with steam–air atmospheres. The results of the reaction kinetics experiments were used in the reaction model, and the heat transfer model was expanded to allow it to handle condensible atmospheres. Three groups of accidents were investigated: a spill on the containment building floor, a spill inside the reactor plasma chamber, and a spill inside the plasma chamber with steam injection to the containment building simulating a steam line break. The results were compared to dry air cases under the same conditions. The results of all three groups showed that the most important effect of the presence of water vapor was the increased heat transfer to the cell gases, primarily due to the higher gas thermal emissivity. In the containment building fire, where the lithium pool was relatively insulated, the measured emissivity served to increase the gas temperature and pressure with little effect on the pool or combustion zone. The maximum predicted pool and combustion zone temperatures were 1000° C and 1250° C, respectively. In the plasma chamber fires, the lithium pool was cooled indirectly by the containment building atmosphere and the maximum pool and combustion zone temperatures were found to be 650 and 850° C. The gas temperature and pressure were changed only slightly while the structural temperatures were reduced below those of the dry air cases. Significant concentrations of hydrogen were also predicted to occur in the plasma chamber.

Models of the heat transfer pathways and decay heat generation in the blanket and shield structures of a tokamak were added to LITFIRE. Calculations for a typical reactor indicated that the simultaneous occurrence of a lithium fire and a loss of flow accident would raise the maximum temperature of the first wall from 650°C due to decay heat alone to 875°C. The addition of a fire to a loss of coolant accident would raise the maximum first wall temperature from 1000 to 1100°C.

ACKNOWLEDGMENT

This report is based on the thesis submitted by the first author in partial fulfillment of the requirements for a Ph.D. in Nuclear Engineering at MIT. The authors would like to thank Ernesto Cabello for his assistance with the lithium–steam kinetics experiments.

Contents

List of Figures

List of Tables

Chapter 1

Introduction

1.1 Motivation

Nuclear fusion has the potential to be a safe, limitless source of energy, fulfilling much of the world's energy need in the future. With plentiful inexpensive fuel supplies, even first generation reactors employing deuterium and tritium as fuel could make a considerable contribution to solving the energy problem without the negative environmental impact associated with fossil fuels and the safety concerns over nuclear fission. In order to realize its potential, however, fusion must learn from and avoid the mistakes of the past.

The experience of the nuclear industry can serve as a lesson for fusion. In the early days of nuclear power, it was described as being perfectly clean, absolutely safe and "too cheap to meter". In the thirty years since the first commercial nuclear power plant came on line, it has been seen that while nuclear power has certainly been cleaner than fossil fuel power—it doesn't spew carbon dioxide or noxious gases into the atmosphere—the nuclear waste issue has emerged as a difficult political, if not technical, problem in this country. The safety of nuclear power both with regard to the public and the financial well-being of the utility has come into question with the accidents at Three Mile Island and Chernobyl resulting in the total loss of the

reactors in both cases and fatalities among personnel responding to the emergency at Chernobyl. The cost of electricity from fission has increased over the years as more reactor safety systems have been required (with some having been added after the plants were built) and the time and cost of plant construction have gone up. This is not to say that nuclear fission should not be utilized as a significant source of energy, but rather that fusion should strive to avoid the pitfalls that have beset the nuclear industry.

One of the central aspects in which fusion can profit from past fission experience is the aspect of safety—safety of the public, safety of the environment and safety of the investment. The safety of fusion reactors will be crucial to their gaining and maintaining public and investor confidence. Since fusion will be a new technology, both the public and the investor will be wary of embracing it as the solution to the energy problem unless they perceive the risk from using it to be low. By emphasizing safety from the beginning risk can be minimized. Potential accidents can be anticipated and prevented or mitigated. Necessary safety features can be incorporated into plant designs before they are built, resulting in considerable savings in cost. The reduction of both risk and cost makes it quite beneficial to consider safety early on in the development of fusion energy.

As stated earlier, the first generation of fusion reactors would most likely use deuterium and tritium as fuel due to their higher reactivity. Other fusion fuel cycles such as catalyzed deuterium or deuterium-helium-3 are more difficult to operate although they may be used farther in the future. Since tritium occurs naturally only in trace amounts, it must be bred in order to fuel the reactors. The easiest way to breed tritium is to bombard lithium with neutrons from the fusion reaction:

$$^{6}_{3}\mathrm{Li} + \mathrm{n} \longrightarrow ^{4}_{2}\mathrm{He} + ^{3}_{1}\mathrm{T} + 4.78\ \mathrm{MeV} \tag{1.1}$$

$$^{7}_{3}\mathrm{Li} + \mathrm{n} \longrightarrow ^{4}_{2}\mathrm{He} + ^{3}_{1}\mathrm{T} + \mathrm{n} - 2.47\ \mathrm{MeV} \tag{1.2}$$

the neutron capture reactions will result in the production of tritium and, with

lithium-7, a neutron. The tritium must then be extracted from the lithium in the blanket around the plasma chamber for use as fuel in the reactor.

The lithium may exist within the reactor blanket in a variety of forms: pure liquid lithium, liquid lithium-lead eutectic, or solid compounds of lithium such as Li_2O or $LiAlO_2$. Liquid lithium is advantageous to use in that it can also serve as the coolant of the reactor, simplifying blanket design and allowing the reactor to take advantage of lithium's superior coolant and tritium breeding properties. Other forms of breeder do not have such options available to them. One of the significant drawbacks to using liquid lithium, in addition to the MHD pressure drop associated with pumping a liquid metal across a magnetic field, is its property of reacting easily and exothermically with oxygen, nitrogen, water vapor and carbon dioxide in the atmosphere and various compounds in concrete. The reactions of interest and the energy released by them are shown in Table 1.1 below:[1]

In the event of a large lithium spill the lithium would catch fire and burn until it or the atmospheric gas supply was totally consumed. Such a fire could cause considerable damage to the reactor and the containment building through both the direct heat of the fire and containment overpressurization. The total amount of potential chemical energy contained in the lithium present in a commercial sized reactor using lithium as a coolant would be on the order of 10^9 kJ[2].

1.2 Previous Work

Because of the potential for a severe accident to result from the employment of liquid lithium as a breeder/coolant, much work has been done to characterize the lithium reactions experimentally and to use computer modeling to predict the consequences of large lithium fires. Beginning in 1978 tests were performed at Hanford Engineering Development Laboratory (HEDL) to characterize lithium reactions with dry and moist air, nitrogen, carbon dioxide, steam and concrete. These tests involved

Table 1.1: Reactions of lithium with various materials in the containment atmosphere and concrete

Reactions of Lithium with Constituents in the Atmosphere and in Concrete			
Reaction			Energy (ΔH_{298} kJ/mol Li)
Atmosphere:			
$4Li + O_2$	$\longrightarrow$	$2Li_2O$	-298
$2Li + O_2$	$\longrightarrow$	Li_2O_2	-318
$6Li + N_2$	$\longrightarrow$	$2Li_3N$	-67
$2Li + 2H_2O$	$\longrightarrow$	$2LiOH + H_2$	-244
$2Li + H_2O$	$\longrightarrow$	$Li_2O + H_2$	-177
$2Li + 2LiOH$	$\longrightarrow$	$2Li_2O + H_2$	-111
$2Li + H_2$	$\longrightarrow$	$2LiH$	-10.8
$4Li + 3CO_2$	$\longrightarrow$	$2Li_2CO_3 + C$	-313
$2Li + 2C$	$\longrightarrow$	Li_2C_2	-7.1
Concrete:			
$8Li + Fe_3O_4$	$\longrightarrow$	$4Li_2O + 3Fe$	-158
$4Li + SiO_2$	$\longrightarrow$	$2Li_2O + Si$	-83

the burning of 10–100 kg of lithium in a small sealed test vessel. The quantities measured during the experiments included cell temperatures, gas pressures, overall reaction rates and reaction product distributions[3]. These tests will be reviewed in greater detail in Chapter 2.

About the same time the LITFIRE (LIThium FIRE) code was developed at MIT for the purpose of predicting the temperature and pressure response of the reactor containment to a large lithium spill and fire[2]. The code has the ability to model different spill and containment geometries, with various containment structural materials and atmospheric gases; it has been augmented over the years with the capabilities to model lithium-lead fires, a two-room reactor containment, a concrete-walled containment building, lithium-concrete reactions and an insulated pan holding the lithium or lithium-lead. Since it is not practical to burn very large amounts of lithium to test the accuracy of the code, the results of the HEDL experiments have been used to do so in the past.

Beginning in 1984 small lithium pool reaction kinetics experiments were begun at MIT to determine the maximum reaction rates of lithium with nitrogen and oxygen as functions of lithium temperature and gas composition[4,1]. These experiments involved the burning of about three grams of lithium in a reaction chamber with the reactant gases supplied by forced convection. The data from these experiments was then used to improve the accuracy of LITFIRE.

In addition to the MIT kinetics experiments, lithium and lithium lead kinetics experiments have been performed at the Joint Research Center (JRC) at Ispra, Italy to characterize lithium and lithium-lead interactions with pure steam[5]. These experiments involved the burning of 0.68 to 100 g of lithium and lithium-lead at temperatures from 350°C to 800°C in the presence of a surplus of steam. Lithium-steam reaction rates were calculated from measurements of the hydrogen generation rates. A review of the lithium fire experiments will be given in Chapter 2 and a detailed description of the structure and capabilities of LITFIRE will be given in Chapter 5.

1.3 This Work

The purpose of this work is to increase knowledge of the consequences of accidental lithium spills and fires associated with conceptual fusion reactors. The investigative effort has been two-pronged: first, the lithium fire modeling capabilities of the LITFIRE code have been enhanced by the addition of the ability to simulate a condensible steam containment atmosphere and the ability to simulate radioactive decay heat produced in the reactor blanket and shield structures; second, chemical kinetics tests have been performed to characterize the reaction rates of lithium with steam-nitrogen and steam-air mixtures over a number of different steam concentrations and over a wide range of lithium temperatures.

The LITFIRE code has been modified by the addition of the ability to model condensible steam atmospheres. The modification involved the addition of pools of condensed water on the floor of each cell with heat and mass transfer to and from the pools, the modification of heat transfer to and from containment structures to account for condensation and the modification of the emissivity of the cell gas to account for the presence of water vapor. The code was also modified to model a lithium spill and fire inside the plasma chamber. This involved the addition of models for the blanket and shield structures (with their thermal resistances and heat capacities) and the radioactive decay heat produced by them during an accident. The new code was then used to predict the consequences of various accidents in order to gain some insight into their mitigation.

The lithium kinetics experiments involved the design and construction of a new apparatus to handle lithium-steam reactions, the testing of the apparatus and approximately 40 individual runs. The experiments were performed with steam-nitrogen, steam-air (20% oxygen) and steam-nitrogen-oxygen (10% oxygen) mixtures with steam contents of five, 15 and 30 percent. Lithium reaction rates with each of the gases were measured for each gas composition at lithium temperatures of 400–900 °C. at 100 °C. intervals. The results of the experiments were quantified in terms of

the lithium reaction rates and the effect of the presence of steam on the reaction rate of lithium and nitrogen. The results of the experiments were then utilized to further increase the accuracy of the LITFIRE code.

This work will be detailed in the chapters that follow. Chapter 2 will review the lithium fire experiments conducted at HEDL, JRC Ispra and MIT. An overview of the tests and a characterization and summary of the results will be given.

A description of the experimental apparatus and procedures used to conduct the lithium-steam-air kinetics tests will be given in Chapter 3. Each portion of the apparatus and every phase of the procedures will be covered in detail.

The results of the experiments and the analysis of the data will be shown in Chapter 4. The results will be expressed in terms of the lithium reaction rates with the various gas constituents and the observations made during the course of the experiments. Experimental difficulties and sources of error will also be covered. The data analysis will be presented to characterize the kinetics of the lithium reactions and illustrate the effect of the presence of steam.

Chapter 5 will present a complete description of the workings and capabilities of the LITFIRE code, emphasizing the modeling of large lithium fires and the options available to simulate various accident scenarios. This chapter will cover all work done on LITFIRE prior to the present effort.

Chapter 6 will present a description of the modeling of lithium-steam-air interactions and the associated development of LITFIRE. It will also include the results of calculations made with LITFIRE to predict the consequences of lithium fires in the presence of steam and a characterization of the effects of the presence of steam in general.

Chapter 7 will cover the determination of the effects of a simultaneous loss of coolant or loss of flow accident and lithium fire. Specifically, the LITFIRE code was enhanced to enable it to model a lithium fire inside the plasma chamber and the decay heat generated in the reactor blanket and shield structures. Both the modeling and

the results of the calculations will be detailed.

Finally, the conclusions drawn from the results of this work, and recommendations for further work will be presented in Chapter 8.

Chapter 2

Review of Previous Lithium Fire Experiments

Since liquid lithium was being considered for use as a breeder and coolant in fusion reactors, and it was recognized that this posed an accident threat based on the chemical reactivity of lithium, it was necessary to determine more precisely the magnitude of the consequences of large lithium fires. These experiments consisted of lithium pool fires, conducted at HEDL by D.W. Jeppson, lithium reaction kinetics studies, conducted at MIT by W.J. Ijams and T.K. Gil and kinetics studies conducted at JRC-Ispra by H. Kottowski[3,4,1,5]. By better determining the consequences of lithium fires, the experiments aided in the reactor design process and, as an additional benefit, provided experience in handling liquid lithium.

2.1 HEDL Pool Fire Experiments

The first lithium pool fire experiments were begun in 1978 at HEDL to characterize lithium pool interactions with air, nitrogen, carbon dioxide and steam and lithium-lead pool interactions with air[3,6]. The interactions with nitrogen and carbon dioxide were of interest as, in light of the high reactivity of lithium with air, it was suggested

to use nitrogen or carbon dioxide as a cover gas in the reactor containment building. If the nitrogen or carbon dioxide did not react violently with the lithium, the chemical hazard, one of the greatest drawbacks to using lithium, would be greatly reduced. Steam reactions were of interest as it is possible that steam could be present in the containment atmosphere as a result of humidity in the air or as a result of a steam line break.

To perform each test, the desired containment atmosphere was created in the test cell, a 14.3 m^3 cylinder 2.13 m in diameter and 3.7 m high, containing a reaction pan 50 cm long x 40 cm wide x 25 cm deep. One larger scale experiment (LA-3) was performed in a room with a volume of 340 m^3 and two other larger scale air experiments (LA-4 and LA-5) were performed in a larger vessel 7.6 m in diameter and 20.4 m high. Ten kilograms of lithium were loaded into a portable lithium transfer vessel (PLTV) in which the lithium was melted and transferred into the reaction chamber via stainless steel tubing. Larger scale tests (LA-3,-4 and -5) employed 45, 26.7 and 100 kg of lithium while the lithium-lead tests (LPA-1–LPA-3) employed 200 kg of 17Li83Pb (a volume equivalent to that of the 10 kg lithium tests). Once the lithium transfer was started it began to react with the cell atmosphere. Additional gas was added to the cell during the test to maintain cell pressure. Aerosol and gas samples were taken during the test. After the completion of the test reaction product samples were taken from the reaction pan to determine their chemical compositions.[3]

Schematics of the test cell and the reaction pan are shown in Figures 2-1 and 2-2. The reaction pan was heated and insulated to establish the desired lithium temperature at the beginning of the test. Thermocouples were attached to the pan to monitor the temperatures of the pan and the lithium during the test. Thermocouples were also attached to the test cell wall to monitor its temperature and to measure the cell gas temperature. The cell gas composition, humidity and pressure were monitored continuously throughout the test[3].

The lithium pool fire test conditions and results are summarized in Table 2.1[6];

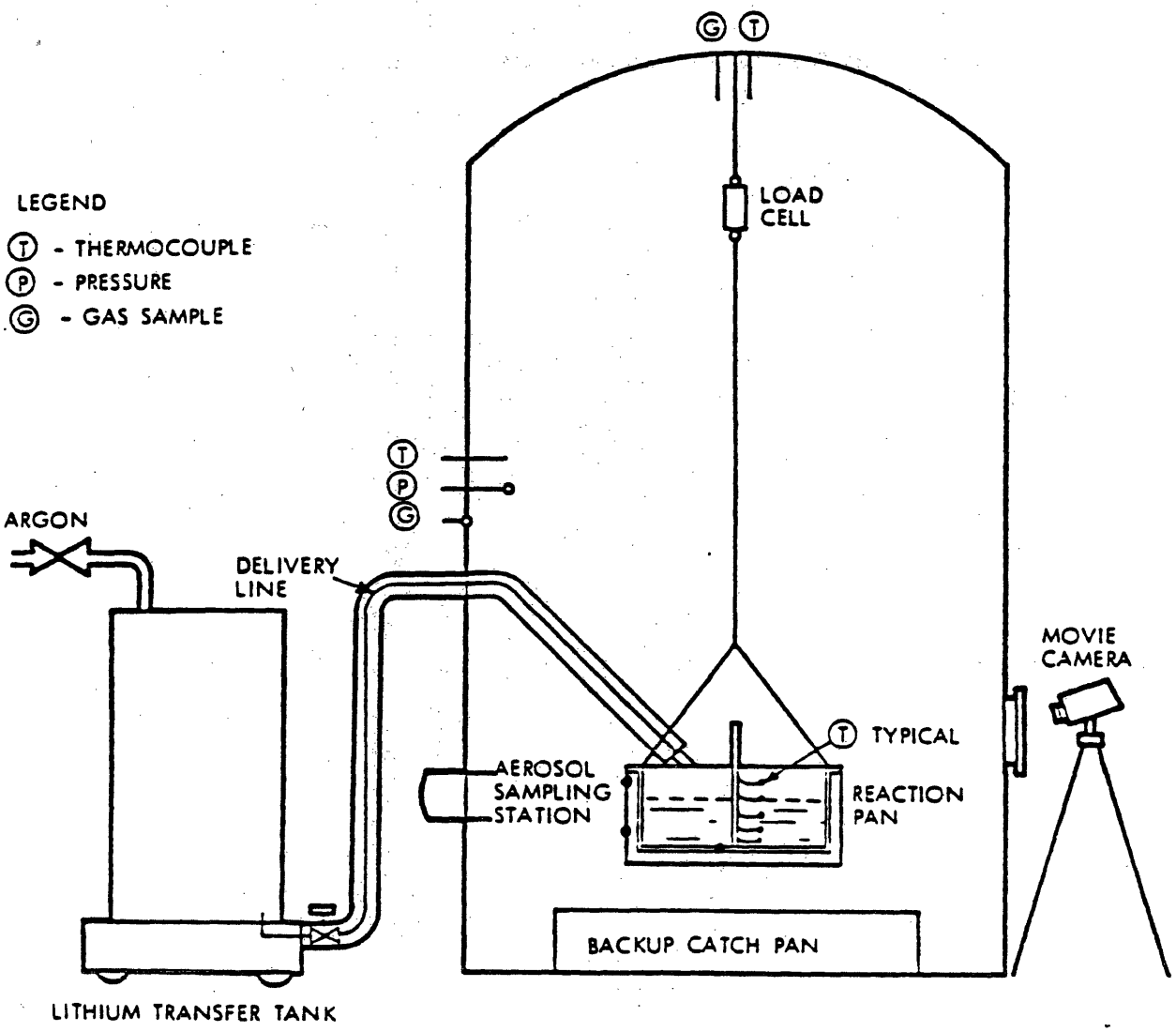

Figure 2-1: HEDL lithium fire test cell

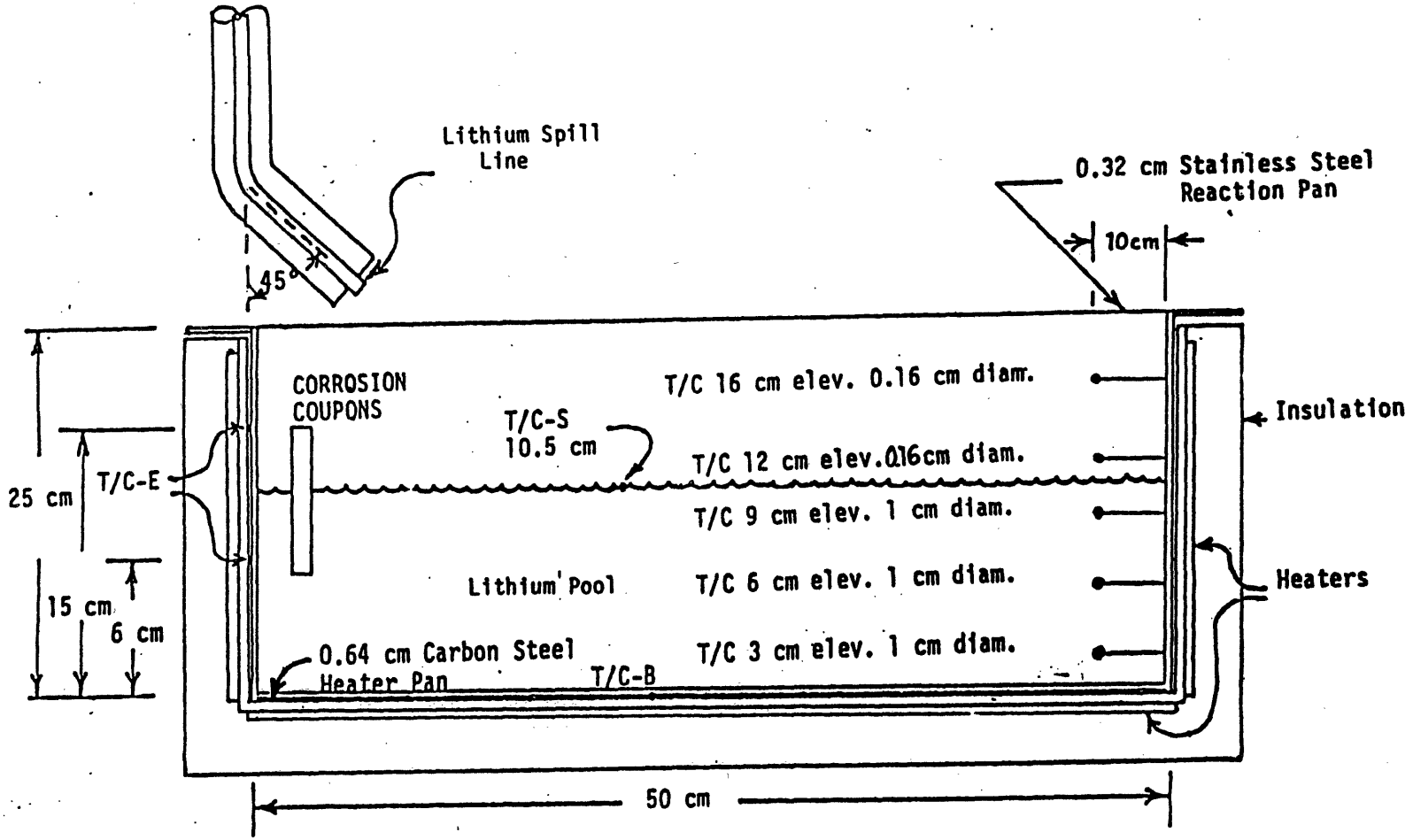

FIGURE 2.2 SCHEMATIC OF LITHIUM POOL-STEAM (LPS-1) REACTION AND HEATER PANS

lithium-lead test results are summarized in Table 2.2[6]. The lithium-dry air experiments (LA-1–LA-5) showed similar results regarding maximum lithium pool and flame temperatures, indicating that they were independent of the initial lithium temperature. Reaction rates were also similar in that the pool temperature reached 1000°C at roughly the same rate, considering the different initial temperatures. The chief differences between the tests involved the generation of combustion products and are shown in Table 2.3[3,7,8,1]. Test LA-3 was performed with an unlimited supply of air and generated a different distribution of reaction products from tests LA-1 and LA-2. A much higher proportion of the reaction product consisted of lithium oxide in the unlimited air test, and much more of the aerosol consisted of lithium carbonate. This may have been due to the fact that lithium reacts more vigorously with oxygen than nitrogen, and in an unlimited air atmosphere, the oxygen supply was also unlimited. The higher fraction of lithium carbonate in the aerosol may have been caused by the higher stability of lithium carbonate relative to lithium oxide and again the presence of unlimited carbon dioxide with the unlimited air atmosphere.[3,7] Test LA-5 showed similar results in that the cell volume was much larger than in tests LA-1 and LA-2, so the supply of oxygen was larger relative to the amount that reacted with the lithium. This would enable the oxygen to compete with the nitrogen for the supply of lithium more readily, thus generating more lithium oxide.

The lithium-nitrogen test results (LN-1–LN-3) indicated that the initial lithium temperature had a strong effect on the extent of the reaction, contrary to the results of the lithium-air tests. In test LN-1 (224°C) about 10% of the lithium reacted; in test LN-2 (532°C) about 15% of the lithium reacted; and in test LN-3 (843°C) all of the lithium reacted. In fact, in test LN-1 no increase in the lithium pool temperature was observed, indicating that the cooling rate was greater than the rate of energy release from the reaction. In test LN-2 the pool temperature rose for about five minutes and then declined, while in test LN-3 the pool temperature increased about 140°C in 6 minutes, levelled off for about 8 minutes, then declined[3]. This indicates that

Table 2.1: HEDL lithium pool fire test summary (temp. in °C)

Gas	Test	Initial lithium temp.	Maximum pool temp.	Maximum combustion zone temp.	% Li aerosol-ized	Comments
N_2	LN-1	222	222	N/A	0	No ignition, 10% Li reacted
	LN-2	532	542	N/A	-	No ignition, 15% Li reacted, peak aerosol 0.07 g-Li/m^3
	LN-3	843	960	N/A	-	Ignited, reaction products to 980°C, 100% Li reacted peak aerosol 0.65 g-Li/m^3
Air	LA-1	243	1038	1260	-	Reaction heated pool to 538°C after 12 min., then rapid rise to 1038°C; peak aerosol 5.2 g-Li/m^3
	LA-2	510	1000	1100	5.5	Temp. excursion sooner; peak aerosol 6.5 g-Li/m^3
	LA-3	232	1040	N/A	7.8	45 kg Li with 0.55 m^2 area, unlimited air supply
	LA-4	600	1070	N/A	10.3	26.7 kg Li, 0.124 m^2 area, lithium leaked into shallow pool with 16.3 kg Li remaining, 2.0 m^2 area
	LA-5	500	1070	N/A	5.9	100 kg Li, 2.0 m^2 area
	LAM-1	248	1060	1150	6.1	Humid, decreased from 43% to 1.5% relative humidity during test, had to be ignited by water droplets, peak aerosol 7 g-Li/m^3
	LAM-2	539	1100	890	7.3	Humid, 14% relative humidity, self-ignited
CO_2	LC-1	238	238	238		Did not ignite
	LC-2	540	>1400	>1400	3	Ignited
H_2O	LPS-1	700	1020	1200	6	75% steam, 25% argon test

Table 2.2: HEDL $Li_{17}Pb_{83}$-air pool fire test summary

Test	Initial $Li_{17}Pb_{83}$ temp. (°C)	Comments
LPA-1	450	No temperature increase, thin oxide coating formed on surface, no detectable aerosol
LPA-2	700	No temperature increase, thin oxide coating formed on surface, maximum aerosol concentration 0.39 mg-Li/m^3 and 0.27 mg-Pb/m^3
LPA-3	714	No temperature increase, thin oxide coating formed on surface, even with pool surface agitation, maximum aerosol concentration 0.05 mg-Li/m^3 and 1.0 mg-Pb/m^3

Table 2.3: HEDL test reaction product summary (% of total Li, not wt.% of reaction products

Test	Li-Air				Li-Moist Air		$Li-CO_2$	Li-Steam
Test Number	LA-1	LA-2	LA-3	LA-5	LAM-1	LAM-2	LC-2	LPS-1
Solid Products:								
Li_3N	44	47	6	25	41	2.7	0	-
Li_2O	45	49	93	75	56	82	92	89
LiOH	9	0.2	<1	-	2	13	0	6
LiH	-	-	-	-	-	-	-	5
Li_2CO_3	<1	0.3	0	-	0	2.4	5	-
Li_2C_2	0	0	0	0	0	0	3	-
Metallic Li	-	-	0	-	0	0	<1	0
Aerosol Products:								
Li_2O	-	76	68	-	8	<1	2.6	0
Li_2CO_3	-	2	12	-	7	<1	97	-
LiOH	-	1	15	-	40	98	0	100
$LiOH \cdot H_2O$	-	-	0	-	40	0	0	0
Li_2C_2	-	-	0	-	0	0	<1	-

depending on the initial temperature of the lithium spill (or the operating temperature of the reactor blanket), a nitrogen cover gas could be an effective means of mitigating the consequences of a lithium fire.

Two lithium-carbon dioxide tests were conducted at HEDL. The first (LC-1) had an initial lithium pool temperature of 238°C. No reaction between the lithium and the carbon dioxide was observed during the test. The pool merely cooled off after the lithium was added to the pan[3]. The second test (LC-2) had an initial pool temperature of 540°C. After the lithium was added the heat of reaction drove the lithium to its boiling point (1347°C) in 2.3 minutes. Thermocouples indicated flame temperatures over 1400°C. After three to three and a half minutes the lithium corroded through the pan and fell into the catch well below. The test cell was flooded with argon and the test was terminated[7]. Thus carbon dioxide was shown to be totally unsuitable for use as a reactor cover gas or as a fire extinguisher. In fact reactor fire extinguishing systems would have to be designed with the extreme reactivity of lithium and carbon dioxide in mind, possibly leading to the choice of an alternative method of fire suppression.

Three tests were performed with steam, two with moist air (LAM-1 and LAM-2) and one with a steam-argon mixture (LPS-1). The first moist air test was conducted in air with 43% humidity and had an initial pool temperature of 248°C. When the test started the lithium did not ignite but slowly reacted with the water vapor in the air. The pool was then ignited by the sprinkling of a few drops of water onto the surface. The test then proceeded in a manner similar to the dry air tests, with a maximum pool temperature of 1060°C and a maximum flame temperature of 1150°C The second test was conducted in air with 14% humidity and had an initial pool temperature of 539°C. It ignited immediately and again showed results similar to the dry air tests and LAM-1, although the flame temperature was measured to be only about 850°C, 1.5 cm above the surface of the pool. That was considerably lower than the flame temperatures measured in the other tests[7].

The reaction products from both LAM-1 and LAM-2 differed from the dry air tests in that a significant amount of lithium hydroxide was present in both LAM-1 and LAM-2. This was caused by the reaction of steam with lithium oxide (formed by the reaction of lithium with oxygen and steam) to form lithium hydroxide. Approximately 7.3% of the lithium was released as an aerosol in LAM-2[7].

The lithium-steam test LPS-1 was conducted in an atmosphere of 75% steam and 25% argon and had an initial lithium temperature of 700°C. During the test the pool temperature rose quickly to just over 1000°C, where it remained until the test was terminated at 12,240 seconds by cell venting and argon flooding. Maximum flame temperatures were found to be as high as 1200°C although they tended to fluctuate around 1100°C for most of the duration of the test. Those results were similar to the results of the dry and moist air tests (LA-1–LA-5 and LAM-1 and LAM-2). However, the cell gas temperature reached a maximum of 270°C, which was considerably higher than that seen in the other tests (approximately 165°C in LAM-2). This was due to the increase in radiative heat transfer from the pool and flames to the gas caused by the presence of steam. The reaction products generated consisted of 87% lithium monoxide, 9% lithium hydroxide and 3% lithium hydride by weight. Six percent of the reacted lithium was released as an aerosol, all as lithium hydroxide[8]. These results indicate that a lithium fire in a steam atmosphere poses just as much threat as one in an air atmosphere and maybe more in that an increase in the containment gas temperature would cause an increase in containment gas pressure, which could threaten containment integrity.

2.2 MIT Kinetics Experiments

In addition to the large lithium fire experiments performed at HEDL, the computer code LITFIRE has been developed at MIT to predict the time dependent temperature and pressure profiles in a fusion reactor containment building during a large lithium

fire[2]. Early on in the development of the code it was used to simulate the HEDL experiments and some difficulty was encountered as it predicted the temperature and pressure profiles of the test cell fairly well, but overpredicted both the oxygen and nitrogen reaction rates[9].

One of the most significant unknowns was the reaction rate of lithium with nitrogen as a function of lithium temperature. It was known previously that the reaction rate was a function of lithium temperature and oxygen concentration but it had not been quantified experimentally[2]. Various "guestimated" curves, shown in Figure 2-3, were used in attempts to capture the effect, but the uncertainty was still a source of error[9].

2.2.1 Lithium-Nitrogen Tests

The lack of information on the lithium-nitrogen reaction rate provided the motivation for the initiation of small scale lithium reaction kinetics experiments. The first series of experiments was conducted by Ijams and involved the measurement of the lithium-nitrogen reaction rate as a function of temperature. In those experiments nitrogen was forced over a small pool of lithium ($\sim$ three grams) fast enough that the reaction rate was influenced only by the diffusion of lithium to the surface of the pool and not by the nitrogen flow rate. This also enabled the effect of the lithium nitride buildup on the pool surface to be characterized[4].

Ijams' apparatus is shown in Figure 2-4. To prepare each experiment, Tank 1 was pressurized with nitrogen (to approximately 450 kPa (65 psig)) which had been passed through a molecular sieve to remove any water from the gas. Tank 2 was filled with argon at atmospheric pressure. The lithium was loaded into the combustion chamber and the combustion chamber was then placed into the furnace. The lithium was kept under argon to prevent contamination and the chamber was heated to the desired temperature. The temperatures of the experiments ranged from 300°C to 1100°C[4].

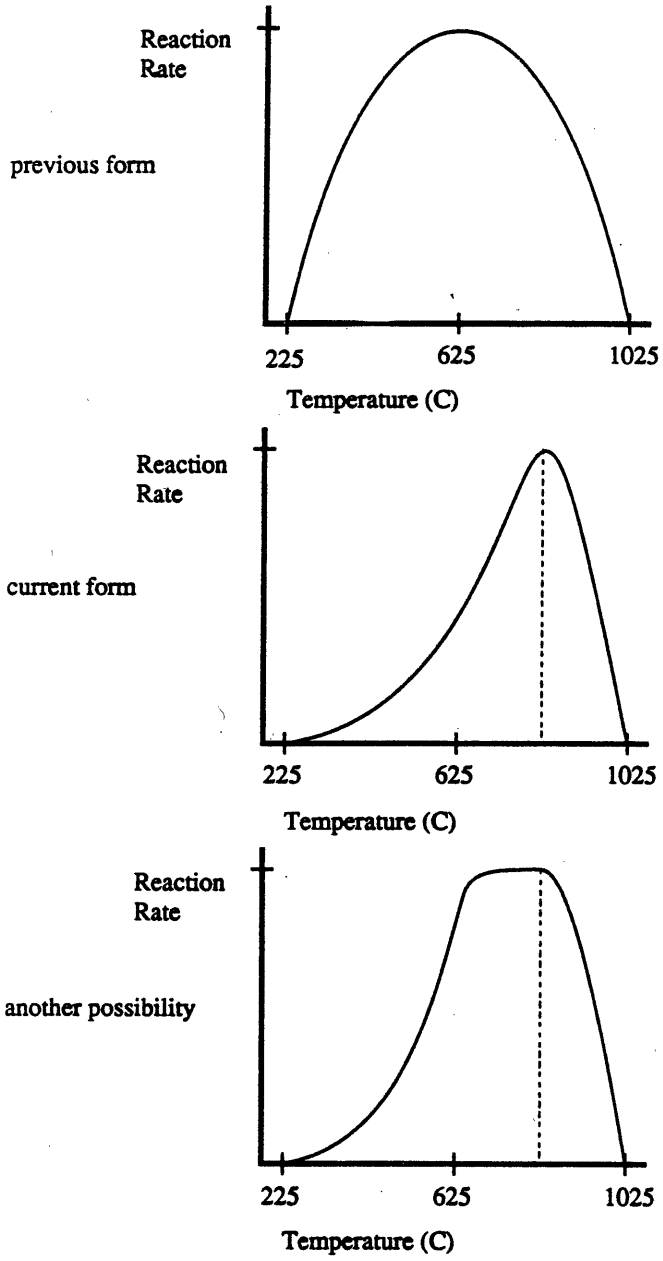

Figure 2-3: Tillack's estimated lithium-nitrogen reaction rate curves

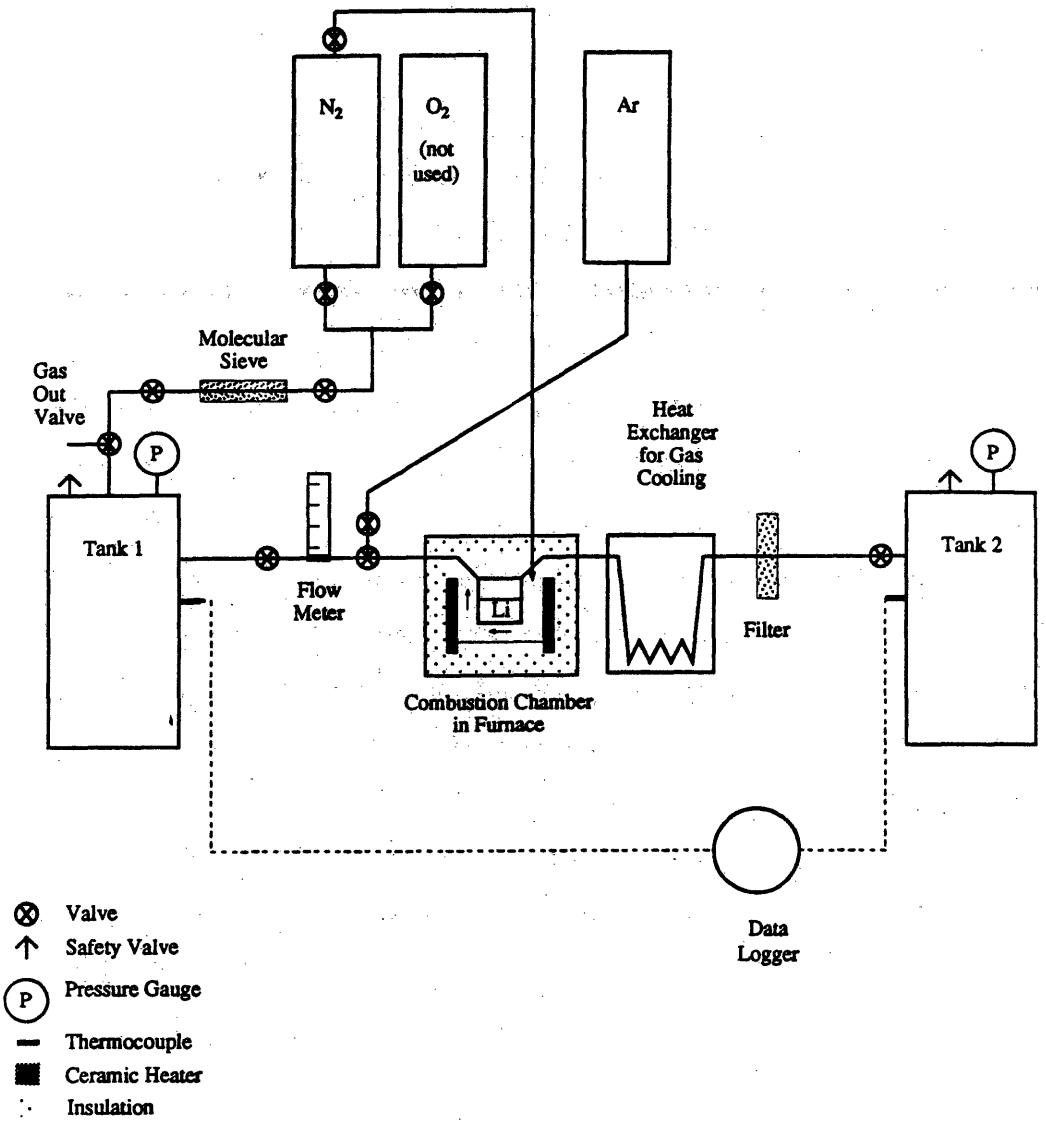

Figure 2-4: Ijams' experimental apparatus

An experiment was begun when the gas from Tank 1 was allowed to flow through the flow meter, into the combustion chamber where it reacted with the lithium. Flow rates of 1.5 to 3.5 liters/min were used, depending on the temperature of the lithium. Higher temperature runs required a higher gas flow rate to ensure that the reaction rate was not gas flow rate dependent. Nevertheless, some of the high temperature runs (over 750°C) did indicate a gas flow rate dependence. The unreacted gas then flowed out of the combustion chamber, through the filter and into Tank 2. After a few seconds into the experiment, pressure readings were taken periodically from which the gas flow rates into and out of the combustion chamber were calculated. The difference between the flow rates gave the nitrogen consumption rate[4].

The results of the experiments, expressed as the lithium-nitrogen reaction rate as a function of lithium temperature, are shown in Figure 2-5[4]. It can be seen that the reaction rate was very low at low temperatures and then increased quickly at about 650°. C. In fact more than one run was performed at the higher temperatures in an attempt to eliminate the flow rate dependence. The curve shows that the reaction kinetics limit is most limiting at low temperatures and could make nitrogen attractive as a reactor cover gas. However, if the lithium ever reached temperatures of 650°C or higher the reaction rate would probably be limited only by the gas flow and therefore a large fire could burn out of control, causing severe damage to the reactor. Figure 2-5 shows the maximum reaction rate measured during the HEDL LN-3 test, conducted at 843°C. It can be seen that the reaction rate measured during the forced convection kinetics experiment was considerably higher.

2.2.2 Lithium-Nitrogen-Oxygen Tests

Since the lithium-nitrogen reaction rate in air was known to be not only a function of the lithium temperature, but also a function of the oxygen content of the atmosphere[2], the next set of kinetics experiments were performed by Gil to determine that dependence. His experiments were similar to those of Ijams, but employed

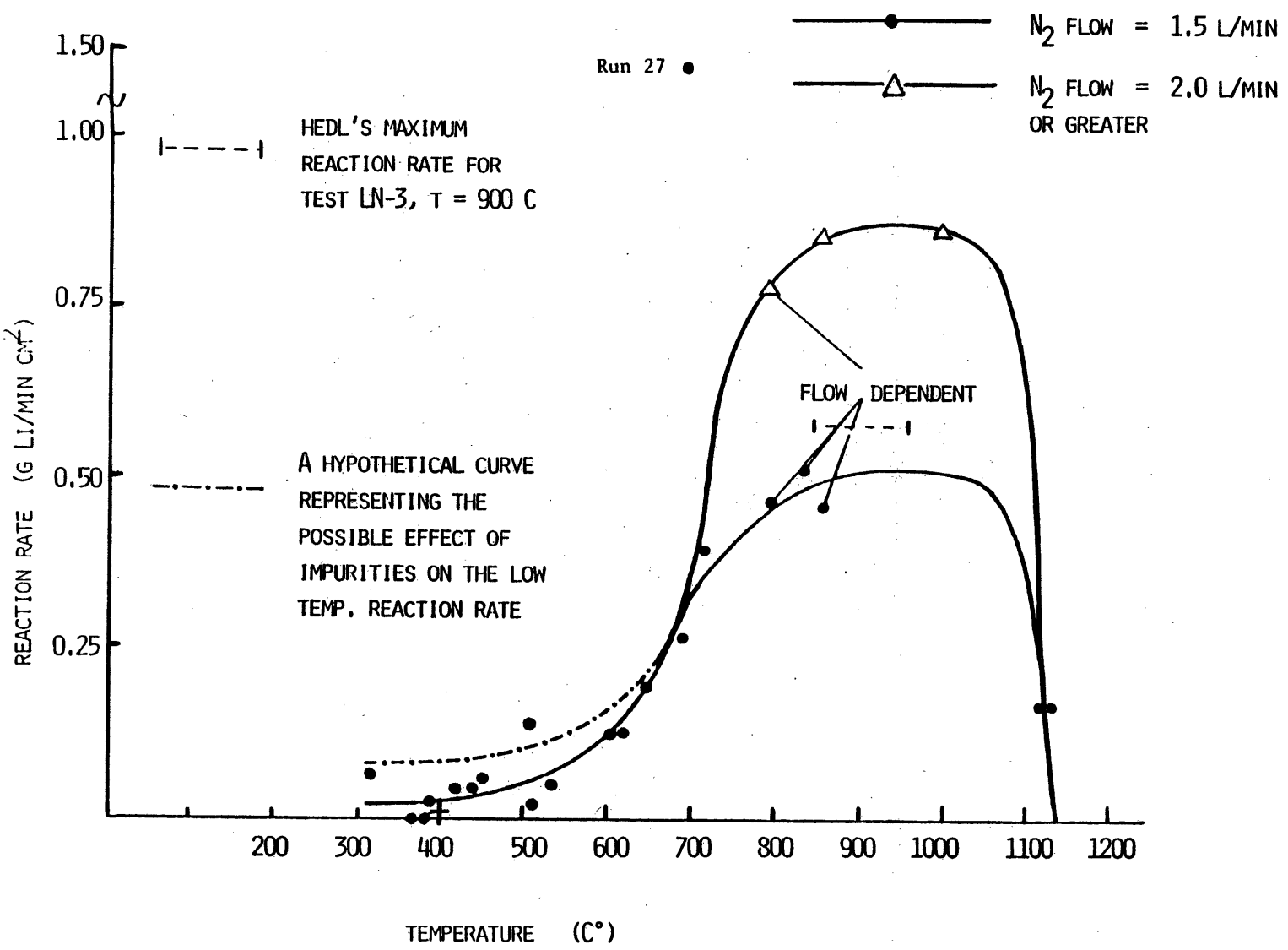

Figure The lithium - nitrogen reaction rate as a function of temperature

gas mixtures of 80% nitrogen and 20% oxygen, 90% nitrogen and 10% oxygen, 95% nitrogen and 5% oxygen, and pure oxygen to quantify the inhibiting effect of the presence of oxygen on the lithium-nitrogen reaction rate and also to measure the lithium-oxygen reaction rate. Approximately forty experiments were conducted in the series[1].

A schematic diagram of the experimental apparatus is shown in Figure 2-6. The basic apparatus was the same as the one used by Ijams, but a number of changes were made to improve experimental accuracy. A new data acquisition system was installed that could track the tank pressures as well as the tank temperatures. It was connected to an IBM-PC which stored the data from each experiment in a separate file[1]. Combined with the replacement of the analog pressure gauges with digital pressure transducers this eliminated the need to monitor the tank pressures manually, a significant source of error according to Ijams[4]. The mounting of the thermocouple housing was moved from the top of the combustion chamber to the bottom to ensure that it was always covered by the lithium pool and not exposed to the lithium flame. Before this modification the housing had been melted during a pure oxygen test, as the flame temperature exceeded 1500°C. The new chamber configuration is shown in Figure 2-7. The gas flow meter was also replaced as it was expected that the mixed gas reaction rates would be higher than the nitrogen reaction rates. The old meter had a maximum capacity of 3.5 liters/min; the new one had a maximum capacity of 14 liters/min[1].

In addition to the improvements made to the system, a means of determining the composition of the gas in Tank 2 was necessary to determine the reaction rates of the lithium with the oxygen and nitrogen. A residual gas analyzer (RGA) was acquired for this purpose. The RGA was connected to Tank 2 by a capillary line and required the gas to be pumped from the tank to the analyzer head at a very low pressure ($< 10^{-3}$ torr). Therefore it was also necessary to acquire a vacuum pumping system. After experiencing some difficulty with a diffusion pump due to oil backstreaming, a

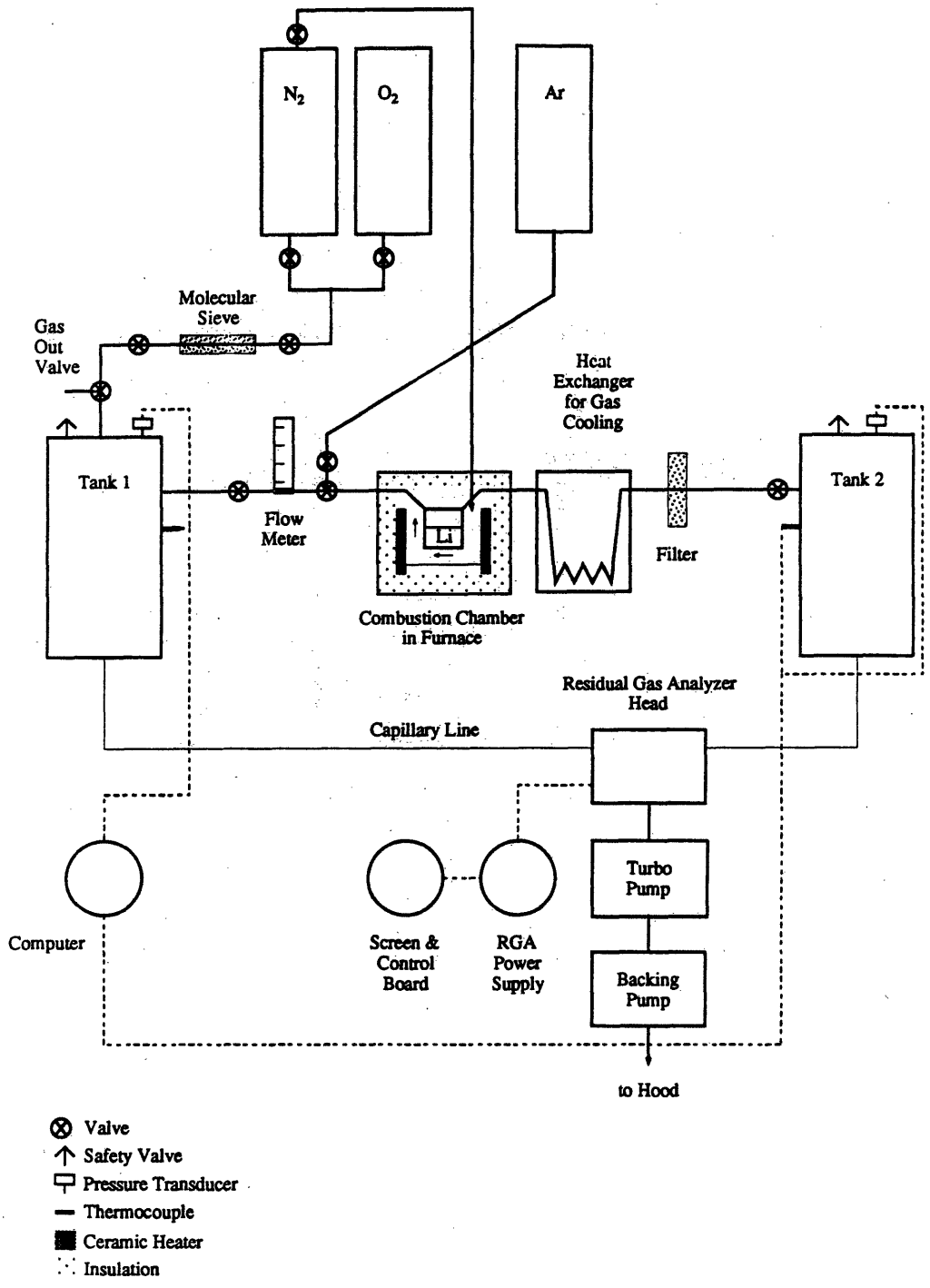

Figure 2-6: Gil's experimental apparatus

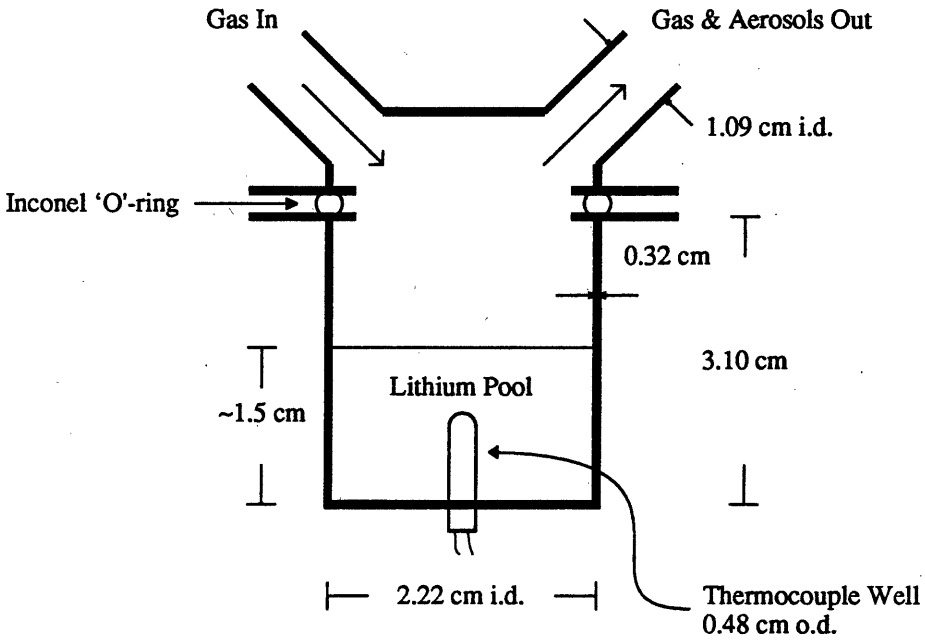

Figure 2-7: Gil's combustion chamber

turbomolecular pump backed by a mechanical roughing pump was selected and used satisfactorily[1].

The procedure used to conduct the experiments was similar to the one used by Ijams. Some changes were necessary due to the addition of the new equipment and some were made to reduce the number of experimental runs discarded[1]. The procedure used by Gil was also similar to the one used to conduct the experiments reported in this work (described in detail in Chapter 3) so only the changes from Ijams' procedure will be described here.

The most important difference between the two procedures involved the analysis of the gas composition in Tank 2. Because it was necessary to determine the lithium reaction rates with each of the various gas constituents, it was necessary to ensure that Tank 2 was filled with pure argon gas before the run. In the preparation stage of each experiment the vacuum system for the RGA was first pumped down for approximately half an hour. Tank 2 was filled with argon gas to about 70 kPa (10 psig) and then the gas was allowed to bleed out of the tank slowly. This was repeated until the gas in Tank 2 was at least 99.9% pure. The RGA was also used to confirm the gas composition in Tank 1[1].

Another potential source of error mentioned by Ijams was the impurity of the lithium pellets[4]. For that reason it was decided to use lithium ribbon of a higher purity. The lithium was handled in an argon filled bag and spots of contamination were cut off before it was loaded into the combustion chamber. In addition, for the lower temperature runs, the lithium was heated up to 600°C and then allowed to cool to the temperature desired[1].

The reaction rates measured by Gil are shown in Figures 2-8 to 2-10[1]. These plots include both the oxygen and nitrogen reaction rates and the sum of the two. Figure 2-11 compares the nitrogen reaction rates to those measured by Ijams, and Figure 2-12 compares the oxygen reaction rates to each other[1]. The plot of the pure nitrogen reaction rates was derived from a curve fit of Ijams' data. It can

be seen from the figures that the nitrogen reaction rate exhibited the same general temperature dependence as it did in the absence of oxygen. The oxygen reaction rate also appeared to be slightly temperature dependent, although since higher gas flow rates were used for the experiments conducted at higher temperatures it may have been gas flow dependent. This is also supported by the appearance of the oxygen reaction rate curves which tended to level off at high temperatures suggesting that the reaction rates were limited by the oxygen supply.

Figure 2-11 shows that the real effect of the oxygen was to inhibit the nitrogen reaction at all temperatures. The lithium-nitrogen reaction rate inhibition factor, defined as the ratio of the lithium-nitrogen reaction rate in the presence of oxygen to the lithium-nitrogen reaction rate in the absence of oxygen, is shown in Figure 2-13 for the gas compositions used in the experiments[1]. It can be seen that the inhibition increased with the fraction of oxygen. The inhibition factor was also a function of the lithium temperature. It was most pronounced around 700°C and then lessened at higher temperatures as the nitrogen reaction rate increased. Thus as the nitrogen reaction became more vigorous at higher temperatures it could actually compete with the oxygen for the available lithium.

The second major phenomenon observed by Gil was the effect of the reaction products on the gas reaction rates. An example of this is shown in Figure 2-14 in which the square of the mass of the lithium consumed is plotted versus time[1]. From the figure it can be seen that the rate seemed to exhibit a linear law, followed by a logarithmic law, finally followed by a parabolic law over most of the duration of the run. From observing similar plots of other runs it was inferred that the the effect was due to the thickening of the lithium nitride layer on top of the pool. The effect was most pronounced at high temperatures as more lithium nitride was produced. It was also observed that cracks in the nitride layer seemed to form momentarily and allow the lithium to react more quickly. These cracks were seen to be more prevalent at higher oxygen concentrations and higher pool temperatures, suggesting that they

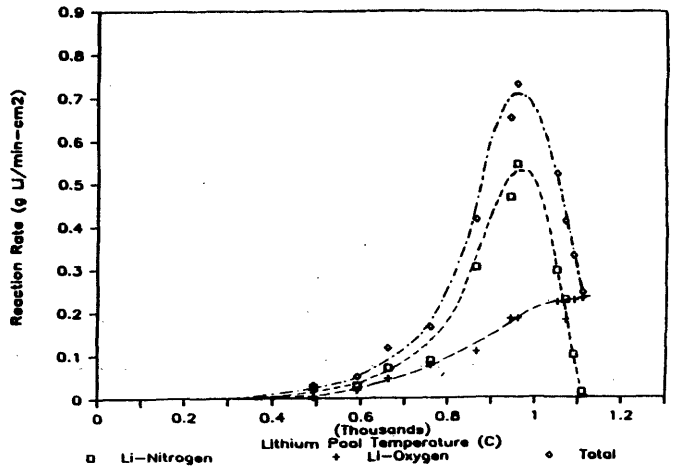

Figure 2-8: Li reaction rates from 80% N_2-20% O_2 experiments

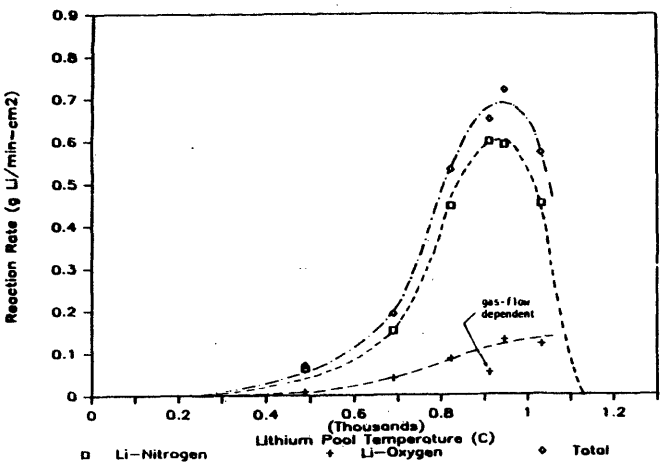

Figure 2-9: Li reaction rates from 90% N_2-10% O_2 experiments

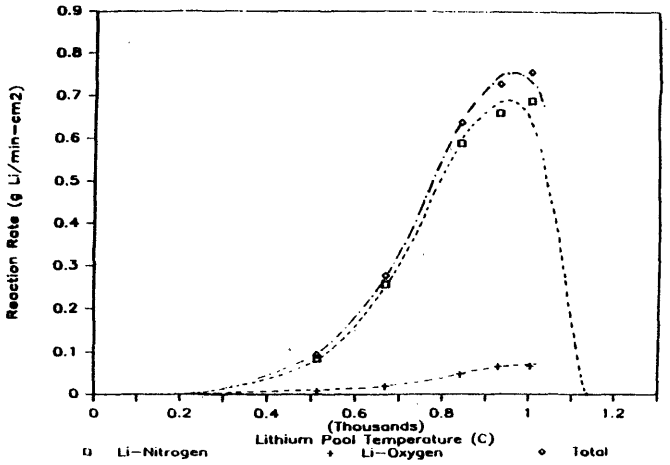

Figure 2-10: Li reaction rates from 95% N_2-5% O_2 experiments

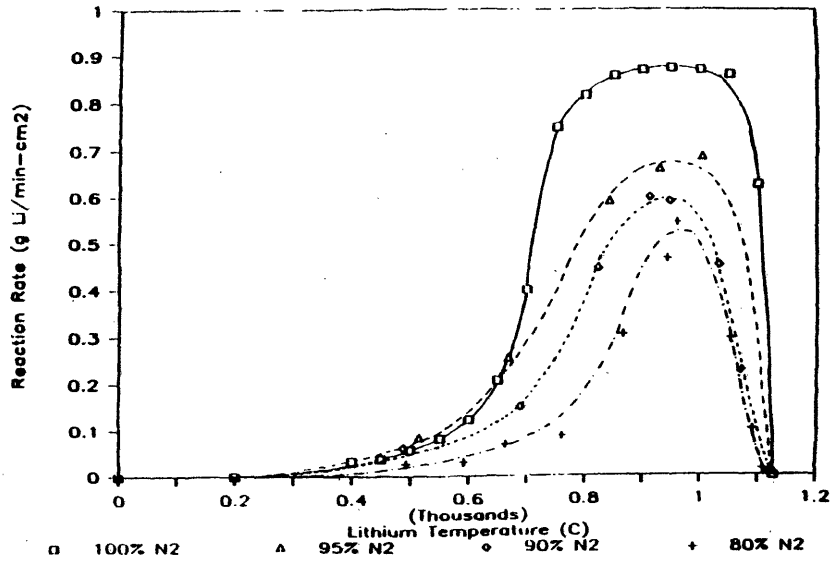

Figure 2-11: Li-N reaction rates from pure and mixed gas (O_2) experiments

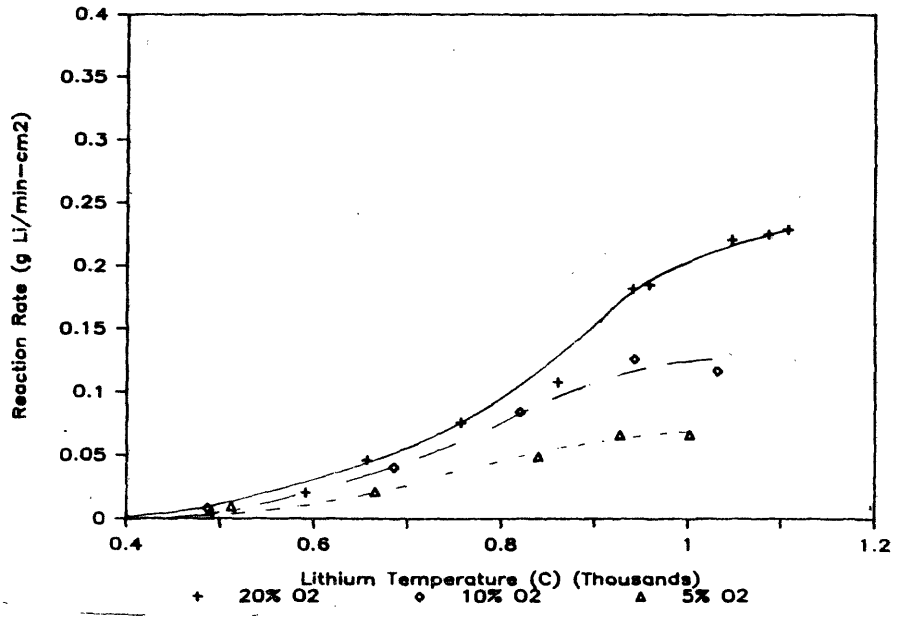

Figure 2-12: Li-O reaction rates from mixed gas (N_2) experiments

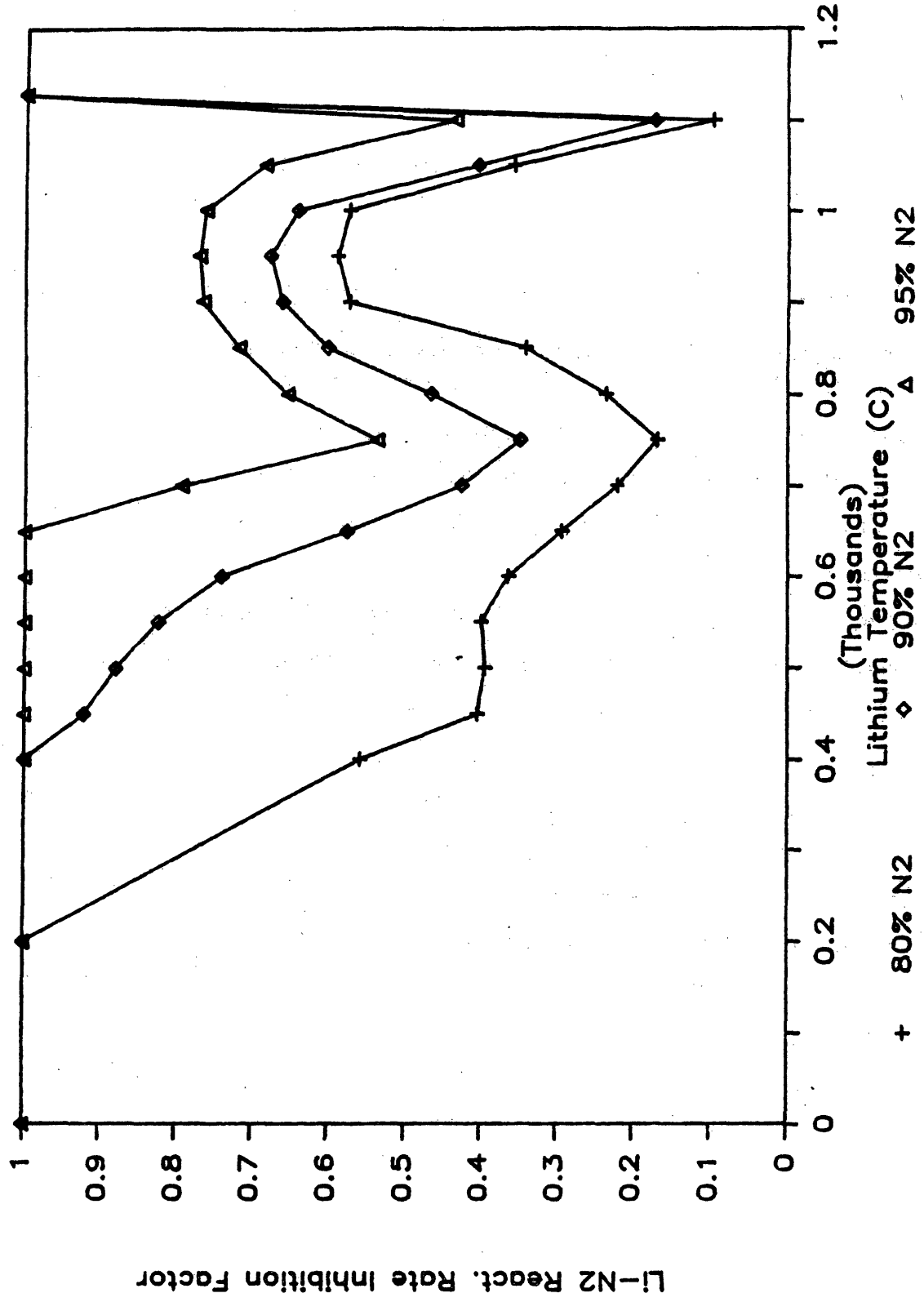

Figure 2-13: Lithium-nitrogen reaction rate inhibition factor in terms of lithium temperature and the fraction oxygen.

were caused by the heat of reaction. For an unknown reason the oxygen reaction rates did not seem to exhibit this phenomenon[1].

2.3 JRC-Ispra Kinetics Experiments

In addition to the kinetics experiments performed at MIT with nitrogen and oxygen-nitrogen mixtures, kinetics experiments have been performed with pure steam at JRC-Ispra. The JRC experiments used $Li_{17}Pb_{83}$, $Li_{50}Pb_{50}$, and Li_7Pb_2 lithium-lead as well as pure lithium as test samples. The tests were conducted in the presence of an excess of steam at 1.0 ± 0.2 bars pressure and the lithium-steam reaction rates were calculated from measurements of the hydrogen generation rates[5].

A matrix of the conditions present for each test is shown in Table 2.4 below. The apparatus used to conduct the experiments is shown in Figure 2-15[5].

To perform an experiment, water was boiled in the steam generator and the steam created passed through a heater to heat it to the desired temperature. The steam then flowed through the test chamber where it reacted with the lithium, producing hydrogen. The hydrogen and the unreacted steam then flowed together through a condenser and into the hydrogen-water separator. The steam was separated from the hydrogen by condensation into the tank of water and the hydrogen was collected in the hydrogen collector. The hydrogen collection rate and the metal pool temperature were monitored throughout the experiment so that the lithium reaction rate could be determined as a function of the pool temperature[5]. A typical experiment ran for about three minutes and the pool temperature increased to as high as 1000°C, so the reaction rates could be measured over a wide range of pool temperatures during a single test.

The hydrogen generation rates measured are plotted versus the metal pool temperature in Figure 2-16[5]. It can be seen from the figure that the lithium reaction rate was about four times higher than the Li_7Pb_2 or $Li_{50}Pb_{50}$ reaction rate, and was

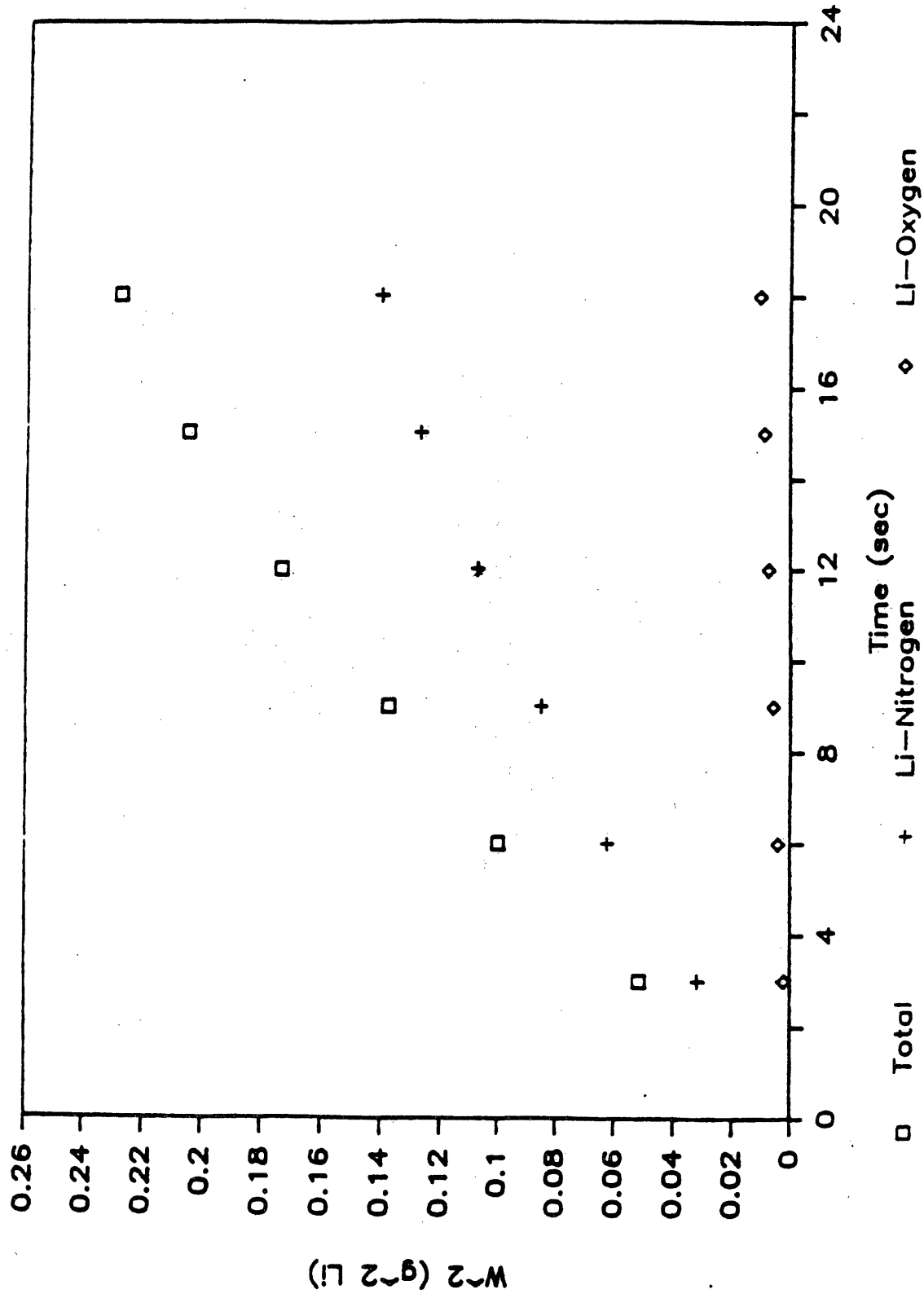

Figure 2-14: Effects of Li_3N layer on reaction rates

Table 2.4: JRC-Ispra test matrix

Metals	Melt Temp. (°C.)	Melt Quantity (g)	Li Inventory (g)	Steam Temp. (°C.)
$Li_{17}Pb_{83}$	350	100	0.68	350
	450	100	0.68	450
	550	100	0.68	550
$Li_{50}Pb_{50}$	450	21.0	0.68	450
	550	21.0	0.68	550
Li_7Pb_2	550	6.48	0.68	550
	~800	6.48	0.68	350
Li	350	0.68	0.68	350
	450	0.68	0.68	450
	550	0.68	0.68	550

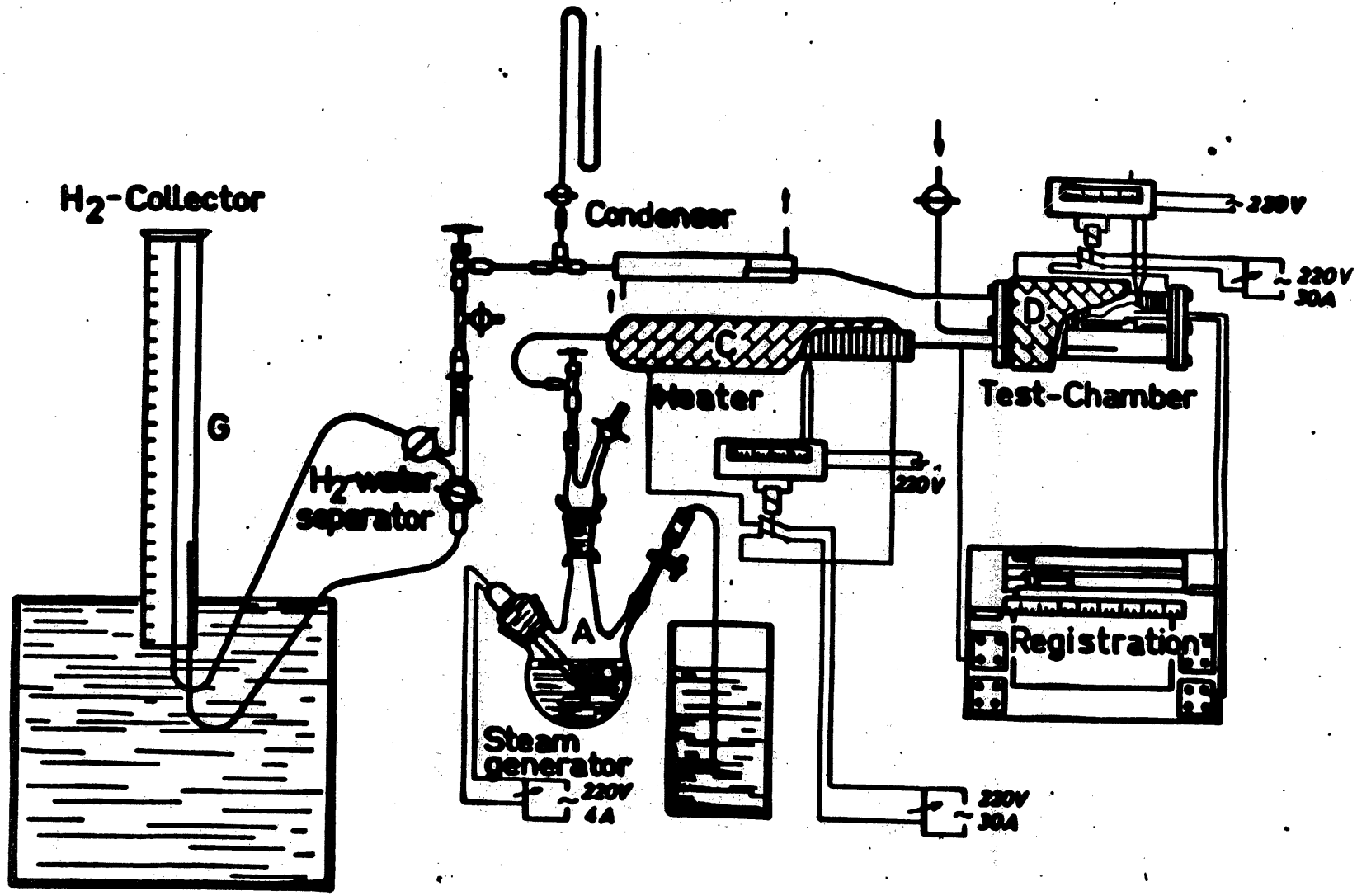

Figure 2-15: JRC-Ispra experimental apparatus

about one hundred times higher than the $Li_{17}Pb_{83}$ reaction rate. Only the $Li_{17}Pb_{83}$ reaction rate seemed to be temperature dependent, increasing by about a factor of three between 300 and 400°C. The others seemed to be fairly constant over the full range of temperatures tested.

Observations after the tests indicated that a solid "porous" crust of reaction products was formed on top of the pools for melt temperatures of less than 450°C. No coherent crust was observed at temperatures over 450°C. It was also suggested that the $Li_{17}Pb_{83}$ reaction was diffusion dominated[5].

2.4 Summary and Comparison

Lithium and lithium-lead fires pose threats of varying degrees to the safety of fusion reactors, depending on the alloy and the containment atmosphere. The relative magnitude of the threats can be summarized and compared to each other by examining the maximum lithium reaction rates and the energy liberation rates per unit area observed for each combination. While it is somewhat misleading to compare kinetics tests, with their surplus gas supply, to pool fire tests, whose gas supply was limited by natural convection, the reaction rates from the kinetics tests can serve to indicate the maximum potential threat posed by a given alloy-gas combination. Table 2.5 summarizes the results of the lithium fire experiments described in this chapter. Only tests for which reaction rate data are available are shown.

It can be seen readily from the table that the lithium-carbon dioxide pool fire had the highest energy release rate by far, so it would be necessary to keep carbon dioxide out of the reactor containment building. The lithium-carbon dioxide fire also had the highest pool temperature.

The next most threatening combination was lithium and air, as the second highest energy release rate was obtained from the lithium-air kinetics test and except for the high temperature nitrogen pool fire, the lithium-air pool fires exhibited the next high-

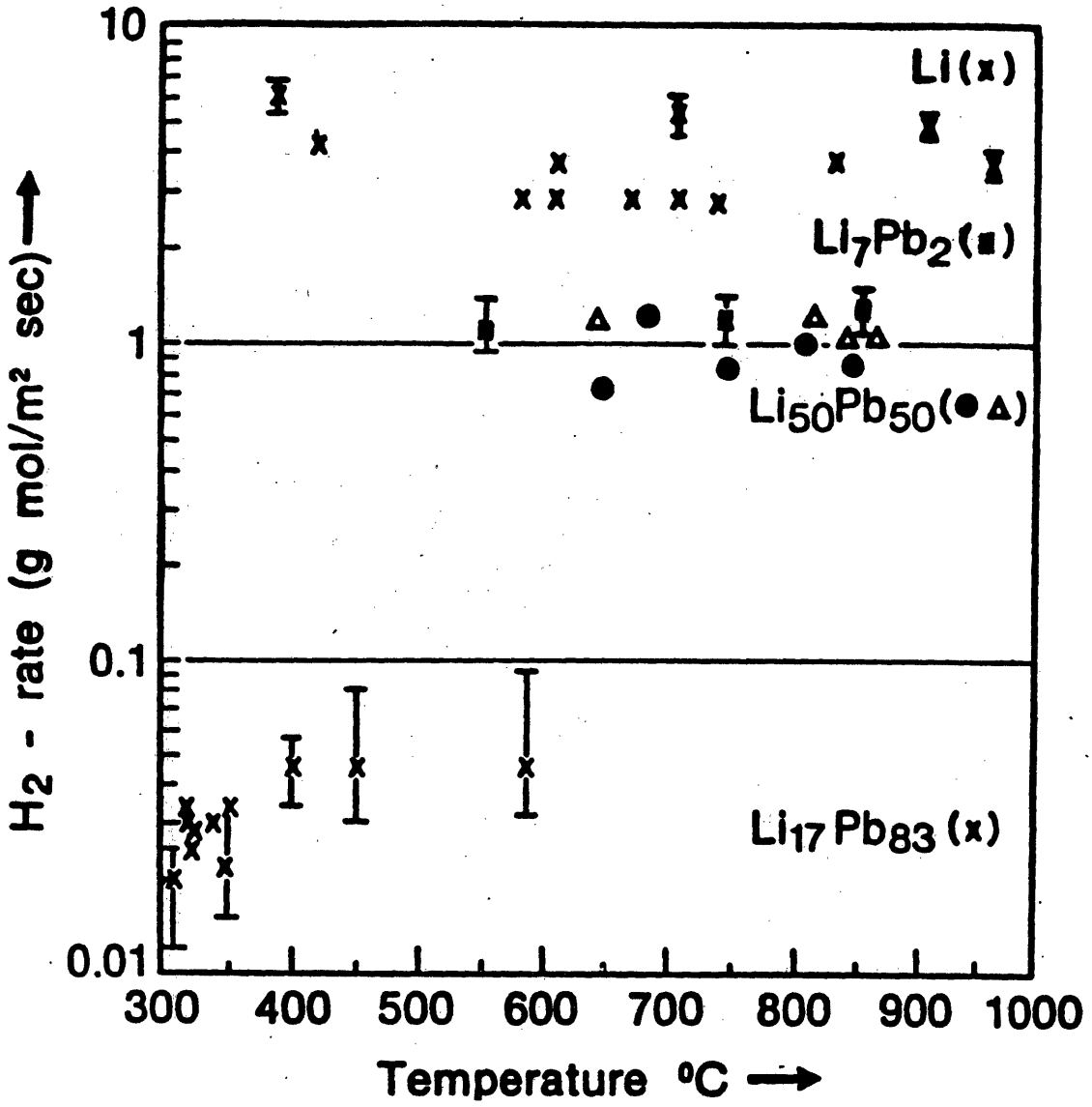

Figure 2-16: JRC-Ispra Li-steam reaction rates

Table 2.5: Lithium fire test summary and comparison

Alloy	Gas	Test name and type	Peak alloy temp. (°C)	Peak reaction rate (g Li/min cm^2)	Peak energy liberation rate (W/cm^2)
Li	N_2	LN-1 pool	224	0	0
		LN-2 pool	542	0.044	7.1
		LN-3 pool	960	0.567	91.2
		MIT kin.	1000	0.854	137.3
	Air	LA-2 pool	1000	0.129	37.7
		LA-3 pool	1040	0.07	50.3
		LA-5 pool	1070	0.0755	46.22
		LAM-1 pool	1060	0.045	18.2
		LAM-2 pool	1100	0.021	8.3
		MIT kin.	960	0.731	230.2
	CO_2	LC-2 pool	>1400	0.69	518.3
	H_2O	LPS-1 pool	1020	0.0172	7.3
		JRC kin.	900	0.4	169.9
Li_7Pb_2	H_2O	JRC kin.	850	0.108	45.9
$Li_{50}Pb_{50}$	H_2O	JRC kin.	870	0.085	36.1
$Li_{17}Pb_{83}$	H_2O	JRC kin.	600	0.0042	1.8

est energy release rates. That would be expected in light of the high heat of reaction for lithium and oxygen (see Table 1.1). The energy release rates and the maximum pool temperatures indicate that a lithium-air fire would also be quite threatening to the safety of the reactor, and that it would be necessary to eliminate contact between spilled lithium and air inside the containment to ensure reactor safety.

The third highest energy release rate overall, and the second highest of the kinetics tests was produced by the lithium-steam reaction. The energy release rate was roughly 73 percent of that of the air kinetics test. However, the energy release rate of the lithium-steam pool fire was about 15 percent of that of the lithium-air pool fires. That indicates that while a lithium-steam fire has the potential to be almost as threatening as a lithium-air fire, something in the pool tests caused the lithium reaction rate to be much lower for the steam fire. That could have been the higher gas temperature, as the natural convection of gas to the reaction site is driven by the temperature difference between the bulk gas and the gas near the pool surface. With a higher bulk gas temperature (caused by enhanced radiative heat transfer from the burning pool to the steam in the gas), the natural convection rate, and thus the lithium reaction rate would be reduced. This is further borne out by the observation that the lithium reaction rates in the humid air pool fires were about half those of the dry air pool fires. For design considerations, however, lithium-steam fires should be considered to be almost as dangerous as lithium-air fires, as, if forced gas flow rate to the reaction site was possible (e.g. through openings or holes in the containment building), the energy release rates could be comparable. Therefore it is also necessary to ensure that a large amount of steam could not be released into the contaiment building during an accident.

The threat posed by a lithium-nitrogen fire seems to be strongly dependent on the initial temperature of the spilled lithium, as the energy release rates seen in the pool fires ranged from near zero, at 224°C, to about one-sixth that of the air fires, at 542°C, to approximately twice that of the air fires, at 960°C. That would seem to

suggest that nitrogen could serve as an effective cover gas for the reactor as long as the lithium spill temperature was not too high. Limiting the nitrogen temperature might be difficult, however, in the event of a loss of coolant or loss of flow accident.

The relatively very high reaction rate and energy release rate of the high temperature nitrogen pool fire (LN-3) was somewhat surprising as the lithium was reacting roughly 65 percent as fast as in the nitrogen kinetics test, while in the air pool fires the lithium was reacting roughly only 10–20 percent as fast in the air kinetics test. During the 542°C nitrogen test (LN-2) the lithium reacted only about five percent as fast as in the nitrogen kinetics test. That serves as an example of how, even under somewhat similar conditions, the gas flow rate to the reaction site in one case could be faster or slower than that in another. Therfore, given the relatively small amount of data available, one should be conservative when estimating potential risk, considering both the observed severity (pool fire tests) and the potential severity (kinetics tests) of a fire. At high temperatures the energy release rate in the nitrogen kinetics test was about half of that in the air kinetics tests and about 80 percent of that in the steam kinetics tests, so the potential risk from a lithium-nitrogen fire is less than that from a lithium-air or lithium-steam fire, but it may or may not be low enough to use nitrogen as a cover gas and consider the reactor to be safe from a chemical reaction point of view.

The energy release rates of the lithium-lead-steam kinetics tests were all considerably lower than that of the lithium-nitrogen kinetics test. Li_7Pb_2 and $Li_{50}Pb_{50}$ were similar, at about 30 percent of the energy release rate of the nitrogen kinetics test, while $Li_{17}Pb_{83}$ was much lower, still, at about one percent. That would indicate that the threat from a lithium-lead-steam interaction would not be nearly as great as that from a lithium-nitrogen fire, and that the

threat from a $Li_{17}Pb_{83}$-steam interaction would be very small. Thus the use of lithium-lead would greatly limit the chemical reaction threat to reactor safety, and, in that regard, lithium-lead would be a superior material to use as a reactor coolant

or breeder. Of course chemical reaction safety is not the only criterion by which a potential coolant or breeder material is judged, and lithium is superior to lithium-lead in other important areas (e.g. radiological safety).

Chapter 3

Apparatus and Procedures for the Steam Experiments

A series of experiments has been conducted to characterize the kinetics of lithium reactions with mixtures of oxygen, nitrogen and steam. Lithium reaction rates with nitrogen-steam and nitrogen-oxygen-steam mixtures were determined as functions of the lithium temperature and the gas composition. Inhibition or catalytic factors were determined where oxygen or steam hindered or boosted the lithium-nitrogen reaction rate.

These experiments were performed as part of a continuing effort to characterize lithium reactions with gases likely to be encountered inside the containment building of a fusion reactor in the event of a lithium spill. In a fusion reactor steam could be present as humidity in the air or as a result of a steam line break during an accident. Since previous experiments had measured lithium reaction rates with nitrogen, nitrogen-oxygen mixtures and carbon dioxide (see Chapter 2), it was desired to determine the effect of the presence of steam on the other gas reactions. It was known that the presence of steam served to catalyze lithium reactions with nitrogen[2], but the effect had never been quantified.

The goal of the experiments was to determine the maximum lithium reaction rates

as limited by the reaction kinetics. In the case of a large fire the reaction rate would probably be limited by the gas flow (due to natural convection) to the reaction site. It was desired to determine whether there existed another, fundamental limit to the lithium reaction rates. Previous experiments had shown that indeed such a limit existed for the lithium-nitrogen reaction, and that the limit was also affected by the presence of oxygen[4,1]. The present experiments were designed to measure the effect of the presence of steam.

The basic approach to the measurements is the passage of gas of a known composition at a monitored flow rate over a small pool of liquid lithium with a fixed surface area. A portion of the gas reacts with the lithium; the unreacted gas is then collected at a measured rate and its composition determined. The total lithium reaction rate can be calculated from the difference between the gas flow rates into and out of the reaction site and the surface area of the lithium pool. The knowledge of the initial and final gas compositions allows the individual gas flow rates to and from the reaction site to be determined. From that the reaction rates of the individual gases can be calculated. In order to properly measure the kinetics, and not gas flow, limit on the reaction rates, care must be taken that no more than half of the incoming gas reacts with the lithium.

In order to obtain the most useful characterization of the reaction kinetics, the experiments were to be performed over a range of temperature from the lowest expected temperature of a lithium spill to the maximum temperature expected during a large fire.

The experiments were designed to follow the previous experiments of Ijams and Gil[4,1]. As such, the apparatus and procedures used to conduct them were similar, although a number of changes were made to account for the presence of steam and to facilitate performance. The apparatus will be described in detail later in this chapter. Forty-two experiments were performed in all, 22 with nitrogen-steam mixtures and 20 with nitrogen-oxygen-steam mixtures. In each experiment, gas of a desired com-

position was passed over lithium preheated to a specific temperature (between 400 and 1100°C). The gas was forced over the lithium fast enough to observe the reaction kinetics. That was taken to mean, as in the previous experiments, that less than half of the gas that flowed into the combustion chamber reacted with the lithium. The lithium reaction rate with each of the gases was measured and any inhibition or catalysis of the reactions due to the presence of steam was observed and quantified.

3.1 Apparatus

The apparatus used to conduct the experiments is shown in Figure 3-1. During an experiment the gas mixture created in Tank 1 was allowed to flow over the lithium that had been preheated to a desired temperature in the combustion chamber. The reaction products and the unreacted gas then passed through the filter (where solid aerosol reaction products were deposited) and into Tank 2. Throughout the experiment the pressures in both Tanks 1 and 2 were monitored and recorded. The pressure histories of both were used to determine the flow rates into and out of the combustion chamber; the difference determined the total reaction rate. A residual gas analyzer (RGA) was used to measure the final composition in the mixed gas tests. From that information the lithium reaction rates with each of the individual gases were determined.

Figure 3-1 identifies the major components of the apparatus. The apparatus is similar to that used in previous experiments but modifications were made to accommodate steam, to ease the performing of the experiments and to increase experimental accuracy. The figure shows the latest configuration.

3.1.1 Gas Preparation and Collection Systems

Tanks 1 and 2 were the same ones used by Ijams and Gil. They were of welded aluminum construction with volumes of 4.16 liters and 14.02 liters, respectively. For

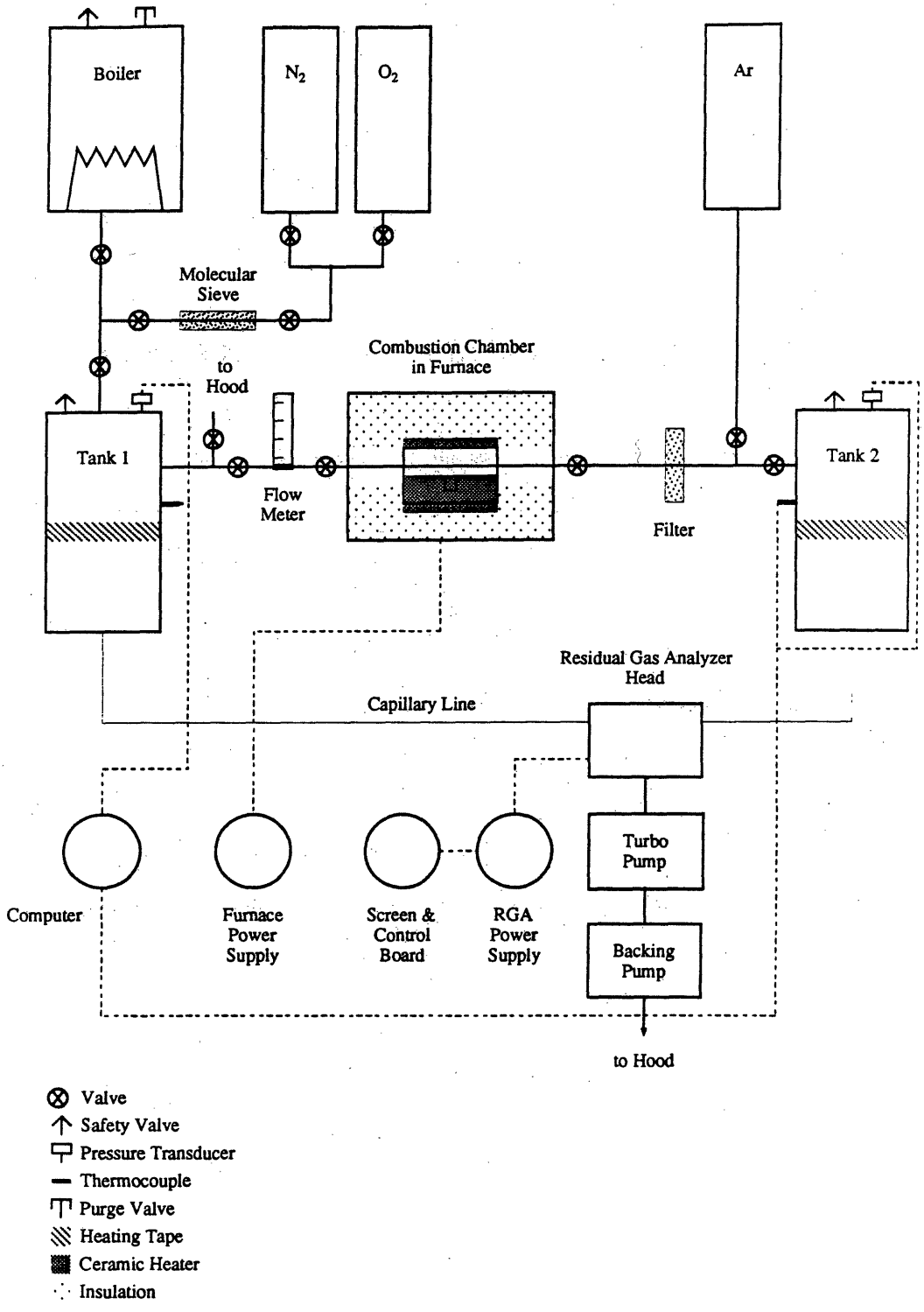

Figure 3-1: Experimental apparatus

the steam tests it was necessary to prevent steam condensation inside the tanks. Therefore they were covered with fiberglass insulation, and they were heated with 100 and 200 W electrical heating tapes. The heating tapes were connected to thermostats for temperature control and a temperature was selected for each tank prior to each experiment. The thermostats were usually set at 130°C., but because the pressure transducer on Tank 2 overheated a number of times, the Tank 2 thermostat was set at 100°C. for the later experiments.

The tanks were connected to the rest of the system with 0.635 cm ($\frac{1}{4}$ in.) copper tubing. The tubing was connected to the gas supply tanks, boiler and combustion chamber by 0.635 cm brass compression fittings and sealed with silicone rubber. Since the tubing was repeatedly connected to and disconnected from the combustion chamber it was not possible to use the permanent silicone sealant. Instead, a silver goop high temperature (815°C) temporary sealant was applied to the combustion chamber fittings before each run.

During an experiment, data were recorded every 1 or 2 seconds. The tank sizes were such that the incremental pressure changes were relatively small but clearly measurable between each reading. The tank pressures were measured with pressure transducers employing capacitance gauges. Their response time to pressure changes was very small (10 milliseconds) and their output was connected directly to the data acquisition system; thus they eliminated the need for manual reading, a source of error in the earlier experiments[4].

The boiler shown in Figure 3-1 was used in the steam experiments and was of welded aluminum construction (30.48 cm (12 in.) dia. and 60.96 cm (24 in.) long), employing a 3000 W immersion heater. The boiler was provided with a safety valve and a purge valve to remove gas impurities, and it was connected to Tank 1 with copper tubing.

A molecular sieve was used between the gas cylinders and Tank 1 to remove any water from the gas. This was necessary in the dry gas experiments to remove water

impurities and was retained in the steam experiments to ensure that the steam in the gas in Tank 1 came only from the boiler.

3.1.2 Furnace and Combustion Chamber

The major component of the apparatus that was changed between the dry gas and the steam experiments was the combustion chamber. The chamber used for the nitrogen and oxygen-nitrogen experiments is shown in Figure 2-7. It was constructed of 316 stainless steel with an inner diameter of 2.22 cm, a depth of 3.1 cm and a wall thickness of 0.32 cm. The thermocouple well had a diameter of 0.476 cm ($\frac{3}{16}$ in.) and housed a type K thermocouple (rated to 1375°C). Originally the thermocouple was mounted on top of the chamber, but after it was damaged a number of times by the lithium flame it was moved to the bottom. The top and bottom pieces of the chamber were bolted together with the seal provided by an inconel O-ring. Gas flowed into and out of the chamber via the two lead pipes shown in the figure. The entire chamber was suspended in a furnace consisting of a hollow box (30.5 cm x 30.5 cm x 30.5 cm) of insulation (50% Al_2O_3, 50% SiO_2) with a stainless steel floor, heated by four 700 W ceramic space heaters.[4]

It was decided to change the chamber design to minimize the impact of the gas flowing directly down upon the pool and churning it up during a run. The churning would tend to increase the surface area of the pool and would lead to overestimation of the reaction rate, as the pool surface area was assumed to be equal to the cross-sectional area of the chamber. It was also desired to eliminate the direct attachment of the thermocouple to the chamber as it was damaged a number of times when, after an experiment, the chamber was soaked in water to remove built up reaction products[1]. The solution of lithium and its compounds in water is very corrosive.

The second combustion chamber design, shown in Figure 3-2, was used for the steam experiments. The first chamber fabricated using the second design was constructed of 304 stainless steel. After it was severely corroded by the lithium during

a trial run at 650°C, the following chambers were constructed of 316 stainless steel. Gas flowed in and out through the top piece of the chamber across the pool rather than down upon it. The two pieces were bolted together and sealed with a 321 stainless steel O-ring. 321 stainless was chosen over inconel to reduce the chance of corrosion by the lithium. The chamber was welded on both ends to 10.16 cm (4 in.) stainless steel lead pipes (0.95 cm ($\frac{3}{8}$ in.) dia.) which in turn were welded to bonnet valves. The entire assembly rested inside an insulated 1100 W clamshell furnace (30.48 cm (12 in.) long x 4.13 cm ($1\frac{5}{8}$ in.) dia.) rated to 1200°C. On the bottom of the inside of the furnace there was a type K thermocouple which was connected to a computer controlled power supply unit. The thermocouple was in direct contact with the bottom of the chamber and, in conjunction with the power supply unit, allowed the exact temperature of the lithium pool to be pre-selected before each experiment and observed during the experiment. That improved test accuracy in that previously the temperature had to be monitored manually and the experiment run as soon as the furnace reached the desired temperature[4]. The chamber assembly also allowed for loading the lithium under an argon atmosphere inside a glove box, which greatly reduced the chance of contamination.

3.1.3 Other Components

The flow meter was used to maintain a constant gas flow rate to the combustion chamber during the experiment. It employed either a black glass or stainless steel float and was rated at 7.7 and 14 liters/min respectively. A typical experiment had a gas flow rate of about 6 liters/min. This was higher than the flow rate of 2–3 liters/min used in the dry gas experiments[1]. The higher flow rate was used in an attempt to eliminate the flow rate dependence of the reaction rates observed previously.

The filter was used to trap the solid aerosol reaction products that left the combustion chamber and keep them out of Tank 2. It was made of a teflon membrane (rated to 0.2 microns) and was changed out every few runs. A few runs were aborted

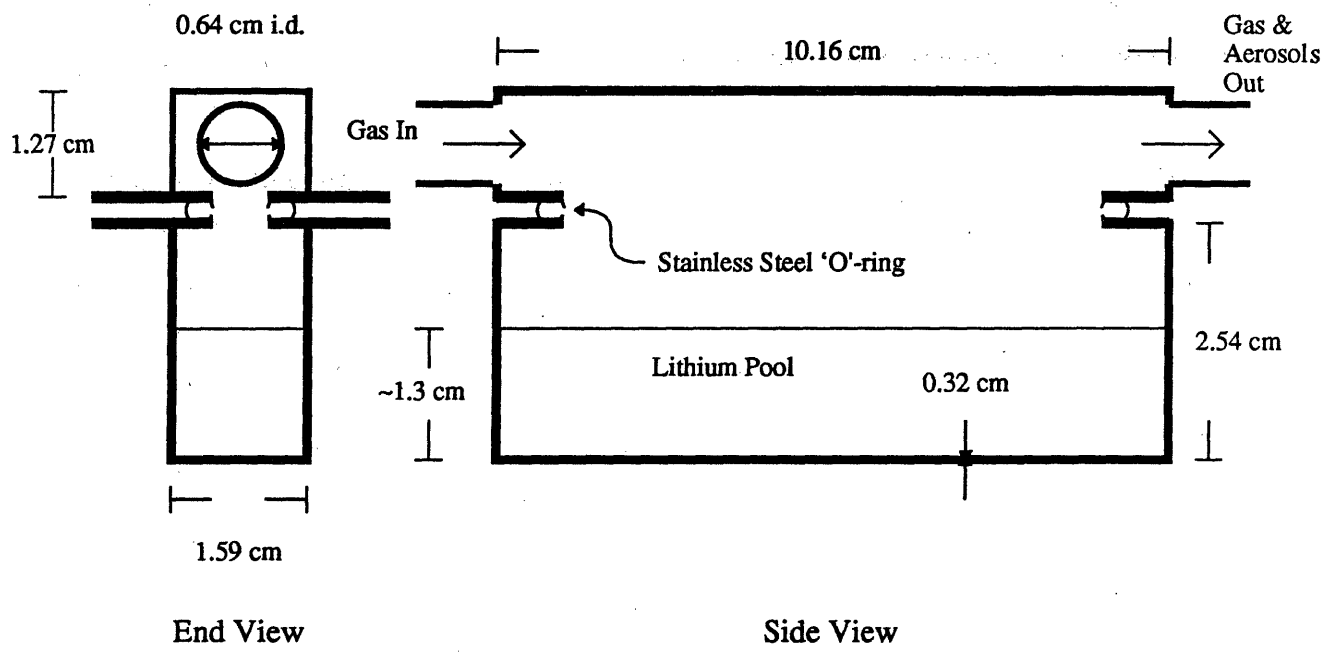

Figure 3-2: Second combustion chamber design

when it was realized that the filter was clogged. This occurred after about five runs with nitrogen-oxygen-steam mixtures, as both the lithium-oxygen and lithium-steam reactions produced aerosol reaction products (Li_2O and LiOH)[7].

A residual gas analyzer was used to determine the final gas composition in Tank 2. It was connected to each tank by a silicon capillary line (50 micron dia.) and used mass spectroscopy to determine the isotopes present in the tank. A turbomolecular pump was used to provide a vacuum (down to 10^{-8} torr) for the analyzer head; it was backed by a mechanical roughing pump.

The data acquisition system was connected to an IBM PC-AT which stored the recorded data. The system itself translated the incoming data signals from the thermocouples and pressure transducers into readable forms. It employed a 16 bit analog to digital converter and was rated as reading 500 channels per second[1]. The recorded data was stored in files on the PC with a different file for each run. Spreadsheet software (LOTUS-123) was used to convert the raw data into reaction rates.

3.2 Procedures

The actual reaction time in the experiments was approximately one minute, but they required extensive preparation which made each one take about three hours or so to complete. The post-test procedures took anywhere from two hours to overnight to finish.

3.2.1 Test Preparation

The first step in preparing an experiment was the preheating of the tanks and the boiler, and the pumping down of the vacuum system. The preheating took approximately one hour, while the pumping down (to $\sim 10^{-8}$ torr) took about half an hour. For a typical run the tank temperatures were set at 130°C, although this caused the pressure transducer on Tank 2 to overheat a number of times. Therefore Tank 2 was

preheated to only 100°C in the later runs. The boiler was usually allowed to pressurize to approximately 103.5 kPa, gauge (15 psig). This was determined by experimentation, as there was no pressure gauge on the boiler itself. It was determined after a number of trials that 40 minutes was usually sufficient to produce the necessary pressure to provide steam for Tank 1.

The next step, performed while the preheating and pumping was going on, was the loading of the lithium into the combustion chamber. This was particularly important, as a leak in the chamber could lead to lithium contamination, or worse, a lithium leak during the experiment. The actual loading took place inside a glove box with an argon atmosphere. This practically eliminated the problem of lithium contamination encountered in previous experiments, although some impurities were present when the lithium was received from the vendor. Before the chamber was actually placed in the glove box the O-ring was coated with the silver goop high temperature sealant and set into the bottom piece of the chamber. After about three grams of lithium were placed into the chamber, the top of the chamber was securely bolted onto the bottom, and the bonnet valves were closed to isolate the lithium from the outside atmosphere.

After the lithium was loaded, Tanks 1 and 2 were purged with nitrogen and argon, respectively. Tank 1 was filled with nitrogen because it was the major gas constituent in the mixture. Tank 2 was filled with argon so that the only other gases present at the end of the experiment would be those that did not react with the lithium. Purging was accomplished by pressurizing the tanks to 207 kPa (30 psig) and 69 kPa (10 psig) with their respective gases and then allowing the gas to bleed out of each tank slowly. This was repeated four or five times, until the gas in each tank was more than 99% pure (confirmed by the RGA).

Once the tanks were purged, the combustion chamber was connected in place with brass compression fittings. A slight overpressure of argon was maintained inside the gas lines (via the argon inlet shown in Figure 3.1) to prevent a small leak from

allowing air into the chamber. Both bonnet valves were opened, and the lithium was heated to the temperature selected on the furnace control unit. This usually took about half an hour.

While the lithium was being heated, the gas in Tank 1 was prepared. The law of partial pressures was used to determine the composition of the gas—the partial pressure of each constituent was monitored (using the pressure transducer) as it was added until the desired amount was present. A gas regulator was used to control the oxygen or nitrogen pressure and the valve between the boiler and Tank 1 was used to control the steam pressure. A typical run saw an initial total gas pressure of 345 kPa (50 psia) in Tank 1. Controlling the steam pressure in Tank 1 by using the valve was difficult at times. To compensate for under or overshooting the target steam pressure, the steam was added to the tank first and then more or less of the other gases were added as necessary to produce the desired gas composition. During this process care was taken to ensure that no hot steam was allowed to pass back from the boiler toward the gas supply tanks, as it would have damaged the silicone seals around the tubing fittings.

After the desired gas composition was made up in Tank 1, and the lithium had reached the desired temperature, the computer program used to record the data was loaded into the computer. The program recorded the time, the temperatures of the tanks and the pressures of the tanks during the run. In the previous experiments it also recorded the temperature of the combustion chamber, but that function was no longer necessary as the furnace temperature was controlled by the furnace control unit and the temperature reading could be observed on the front of the unit.

3.2.2 Test Execution

Once the data acquisition program was loaded, the experiment was ready to begin. The argon inlet was shut off to maintain a steady pressure in Tank 2, and the program was started. The valve between Tank 1 and the combustion chamber was then opened

to allow gas to flow. The flow rate was monitored on the flow meter and it was maintained at about 6 liters/min. Care was taken to maintain a steady flow, as sudden gas surges could give falsely high reaction rate readings by churning the pool. Once the pressure difference between the tanks had decreased to the point at which the flow rate could not be maintained, the valve was closed and the program was stopped. The entire reaction time was about one minute for the lower temperature runs and about 30 seconds for the higher temperatures. After the data had been taken, all heaters were shut off and the furnace was opened and allowed to cool. The gas composition of Tank 2 was then analyzed on the RGA and recorded.

3.2.3 Post-Test Procedures

Once the chamber was cool enough to handle, it was removed and opened. The bottom half usually contained a combination of reaction products and (at low temperatures) unreacted lithium. The chamber was placed into a large bowl of water and allowed to soak until it was clean. This took about two hours after low temperature runs, as the lithium quickly reacted with the water. After high temperature runs, most of the reaction product consisted of the solid lithium nitride, which took longer to dissolve (sometimes the chamber was left to soak overnight). The lithium nitride would usually have to be sanded off of the chamber with an emery cloth to avoid soaking it for longer times.

After the chamber had been soaked, the bolts and O-ring were checked for damage and replaced if necessary. This was usually the case after high temperature runs, and in fact the O-ring was replaced after every run after an O-ring failure caused the lithium to leak out of the chamber. After that the chamber was then cleaned off with paper towels until the metal surface upon which the O-ring would rest was clean. The upper part of the chamber was also cleaned if any aerosol reaction products had been deposited in the exit pipe.

During this time the water level in the boiler was also checked using a clear flexible

hose attached to the drain pipe at the bottom of the boiler. It was refilled if the water level fell below 25 cm, as exposing the immersion heater (at 15 cm) to vapor could have severely damaged it. Distilled water was used and it was added through the drain pipe until the boiler was approximately two-thirds full. The water level was checked after every five runs or so, and it was only necessary to refill it twice.

It was also occasionally necessary to test the apparatus for gas leaks and to determine the leakage rate if such leaks were detected. This was accomplished by performing a run as described in this chapter, but without using any lithium. The preparatory and execution steps were exactly the same, except for the ones involving the handling of the lithium. The run was executed and the "reaction rate" measured was due to gas leakage. Thus the experimental error caused by gas leakage was determined. The error measured in these experiments was approximately five percent. For further discussion of experimental error, see Chapter 4.

As stated earlier, the total time taken for one experiment was approximately three hours, with the lowest temperatures taking a little less and the highest temperatures taking a little more. Previous experiments (with the first combustion chamber) took one or two hours more because of the slower cooling time of the furnace and the greater difficulty of cleaning the chamber[1].

Chapter 4

Results and Data Analysis

4.1 Results and Observations

Forty-two experiments were conducted with nitrogen-steam mixtures and nitrogen-oxygen-steam mixtures to characterize the kinetics of the lithium-nitrogen-steam and lithium-nitrogen-oxygen-steam gas reactions. Three gas compositions were used: steam-nitrogen, steam-air (80% N_2, 20% O_2) and steam-90% nitrogen-10% oxygen. In order to determine the temperature dependence of the reactions, the experiments were conducted with lithium pool temperatures ranging from 400–1100°C, inclusive. The exact gas composition and lithium pool temperature for each run, and the total number of runs performed with each gas composition are shown in Table 4.1.

4.1.1 Reaction Rates as a Function of Lithium Temperature and Gas Composition

The various lithium-gas reactions were characterized by observing the lithium reaction rates with each gas constituent in the mixture. The reaction rates in each run were determined by applying the ideal gas law as follows:

$$RR_N = \frac{(6.93)\cdot(3)}{A\Delta t}\left(\frac{F_{N1}\Delta P_1 V_1}{RT_1} - \frac{F_{N2}\Delta P_2 V_2}{RT_2}\right) \tag{4.1}$$

Table 4.1: Lithium test matrix

Gas Molar Percentages and Lithium Temperature				
Oxygen	Nitrogen	Steam	Temperature (°C)	Number
Steam-Air				
19	76	5	400–800	5
17	68	15	400–800	5
14	56	30	400–800	5
Steam-Oxygen-Nitrogen				
9	76	15	400–800	5
Steam-Nitrogen				
0	95	5	400–1000	8
0	85	15	400–900, 1100	8
0	70	30	400–800	6

$$RR_O = \frac{(6.93)\cdot(2)}{A\Delta t}\left(\frac{F_{O1}\Delta P_1 V_1}{RT_1} - \frac{F_{O2}\Delta P_2 V_2}{RT_2}\right) \tag{4.2}$$

$$RR_S = \frac{(6.93)\cdot(2)}{A\Delta t}\left(\frac{F_{S1}\Delta P_1 V_1}{RT_1} - \frac{F_{S2}\Delta P_2 V_2}{RT_2}\right) \tag{4.3}$$

$$RR = RR_N + RR_O + RR_S \tag{4.4}$$

where RR_N, RR_O, and RR_S are the lithium reaction rates in grams lithium per second per square centimeter with nitrogen, oxygen, and steam, respectively. A is the lithium pool surface area, Δt is the time step length, 6.93 is the average molecular weight of lithium, F_{Nn}, F_{On} and F_{Sn} are the molar fractions of nitrogen, oxygen and steam present in Tanks 1 and 2, ΔP_n is the pressure drop in Tank 1 and the pressure increase in Tank 2 over the time step, V_n is the volume of the tanks and T_n is the absolute temperature of the tanks. It should be noted that Equation 4.3 assumes that the lithium oxide producing reaction between lithium and steam was occurring rather than the lithium hydroxide producing reaction. This is discussed further in Section 4.1.3. The same method was used for all mixed-gas experiments, just the compositions were different.

4.1.1.1 Lithium-Nitrogen Experiments

Twenty-two experiments were performed with nitrogen-steam mixtures to characterize the effect of the presence of water vapor on the reaction kinetics of the lithium-nitrogen reaction. Eight each were performed with 5% and 15% steam, while six were performed with 30%. It was found that at lower temperatures the water vapor acted as a catalyst and actually served to increase the nitrogen reaction rate above that observed in the pure nitrogen tests. The lithium-nitrogen reaction rates are shown in Figure 4-1 and the lithium-steam reaction rates are shown in Figure 4-2. Solid symbols in the figures indicate low temperature tests in which the lithium was preheated for an extended period of time to ensure complete melting. This is further discussed in Sections 4.1.2 and 4.1.3.

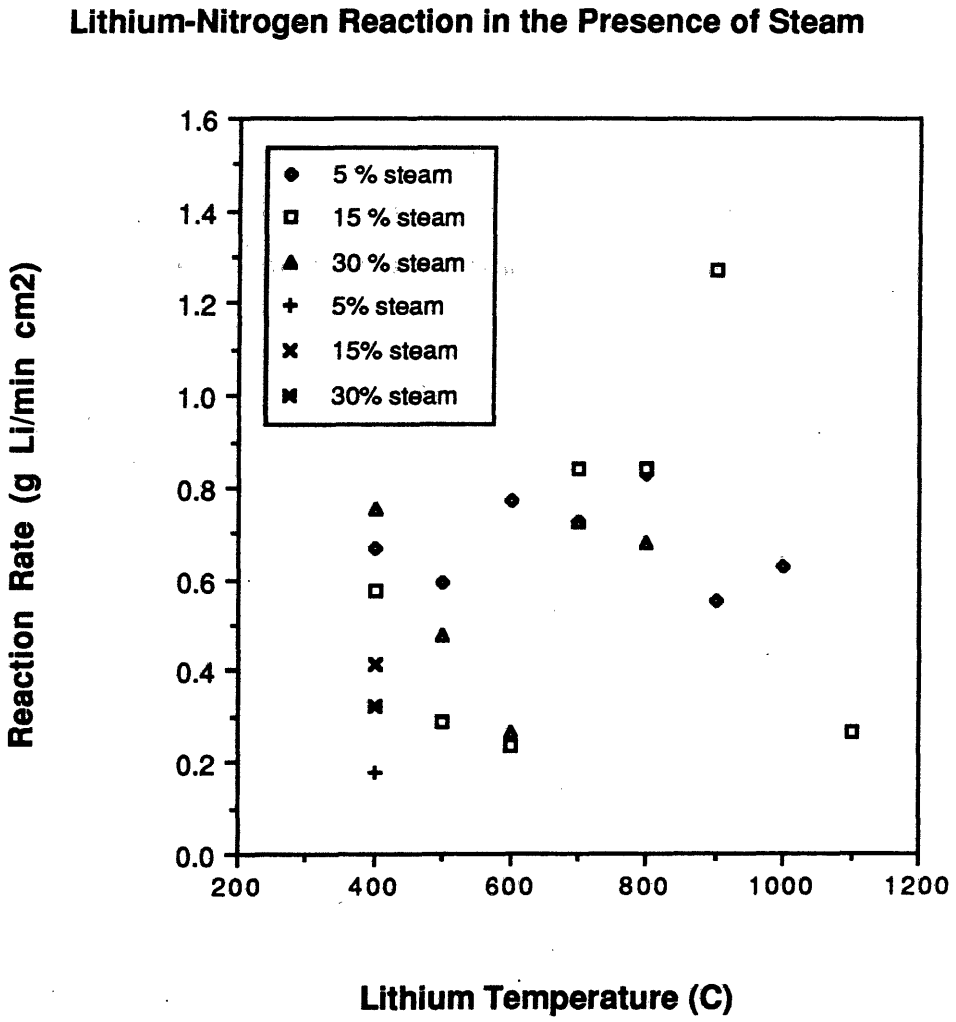

Figure 4-1: Lithium-nitrogen reaction rates in lithium-nitrogen-steam tests (lower symbols indicate preheated tests)

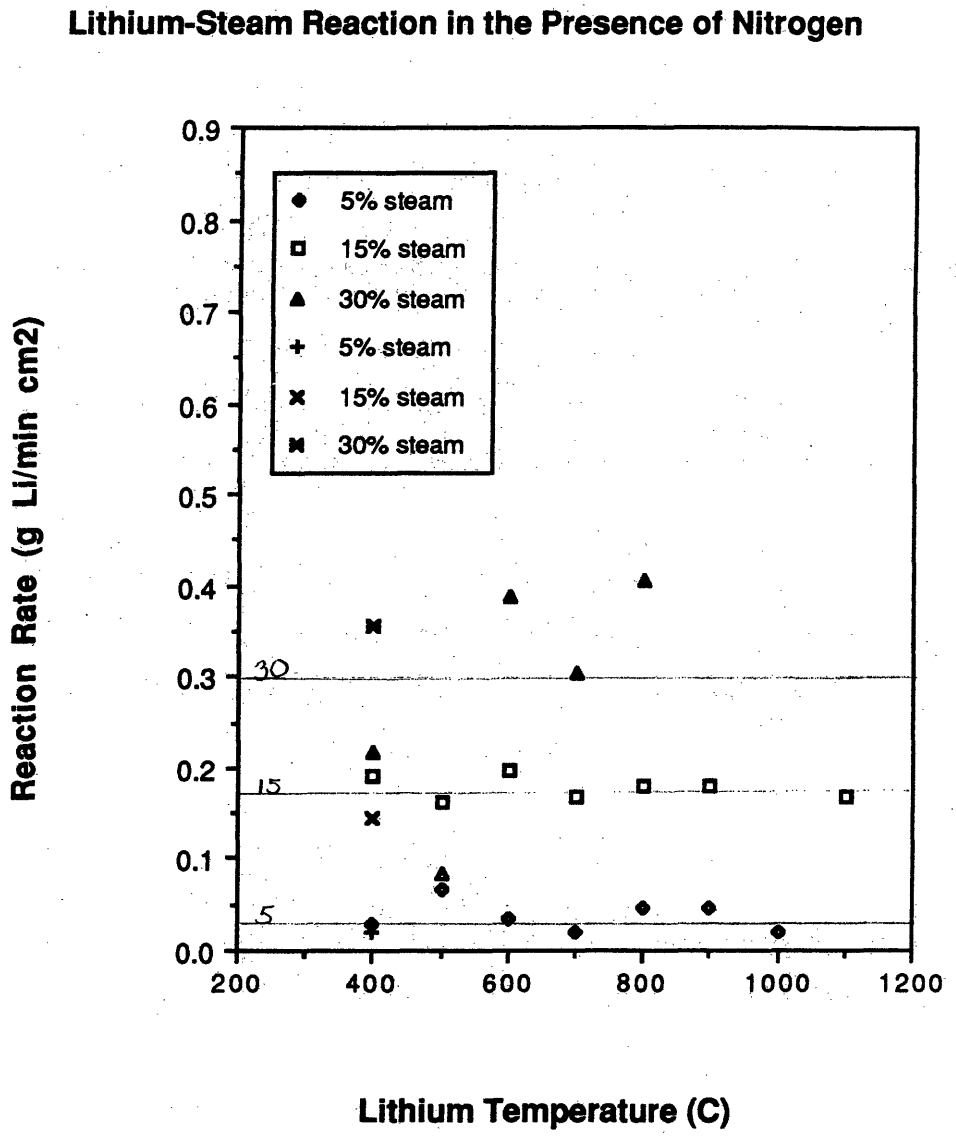

Figure 4-2: Lithium-steam reaction rates in lithium-nitrogen-steam tests (lower symbols indicate preheated tests)

4.1.1.2 Lithium-Air Experiments

Twenty experiments were performed with nitrogen-oxygen-steam mixtures to determine the effect of the presence of both oxygen and steam on the lithium-nitrogen reaction. Five runs were performed with 76% nitrogen, 19% oxygen and 5% steam (basically air with 5% steam), five were performed with 68% nitrogen, 17% oxygen and 15% steam (air with 15% steam), five more were performed with 14% oxygen and 30% steam (air with 30% steam), while the last five were performed with 9% oxygen, 76% nitrogen and 15% steam. All four sets were performed from 400 to 800°C, inclusive, at 100°C intervals. It was observed that the presence of water vapor tended to negate the inhibiting effect of the oxygen—the nitrogen reaction rates at low temperatures were slightly higher than the pure nitrogen rates, yet they were lower than the reaction rates measured in the steam-nitrogen tests. The lithium-nitrogen reaction rates in the steam-air tests are shown in Figure 4-3. The lithium-steam reaction rates and the lithium-oxygen reaction rates in the steam-air tests are shown in Figures 4-4 and 4-5, respectively. The reaction rates of lithium with nitrogen, oxygen and steam in the 10% oxygen-90% nitrogen-steam tests are shown in Figure 4-6

4.1.2 Reaction Products and Observations

As in the lithium-nitrogen-oxygen experiments, the chief reaction product was lithium nitride, but the secondary reaction product observed was a white aerosol deposited on both the bottom of the chamber and in the filter. This aerosol was believed to be either lithium hydroxide or lithium oxide. Both are formed by the lithium-steam reaction, while lithium hydroxide is also formed by the lithium oxide-steam reaction[7].

At low temperatures the lithium was not melted completely (it was present in lumps on the bottom of the chamber after the experiments). This effectively increased the surface area available and thus caused an overestimation of the reaction rates for the 400°C and 500°C cases. Thus it was decided to repeat the experiments at 400°C.

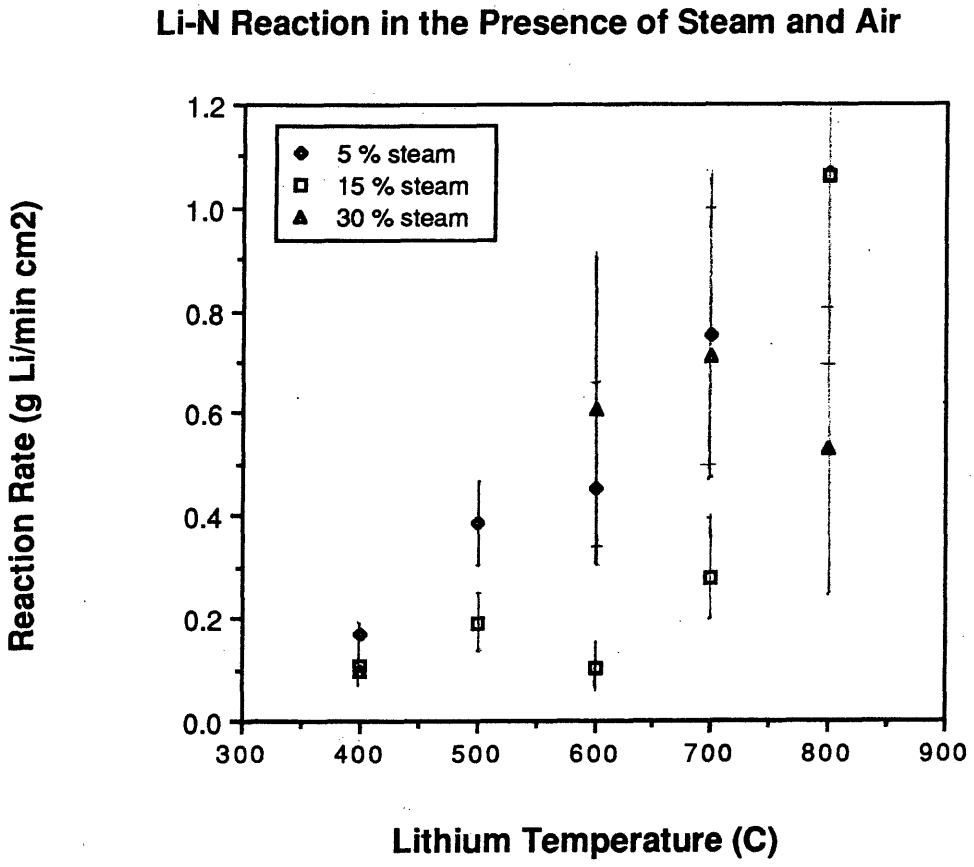

Figure 4-3: Lithium-nitrogen reaction rates in lithium-air-steam tests

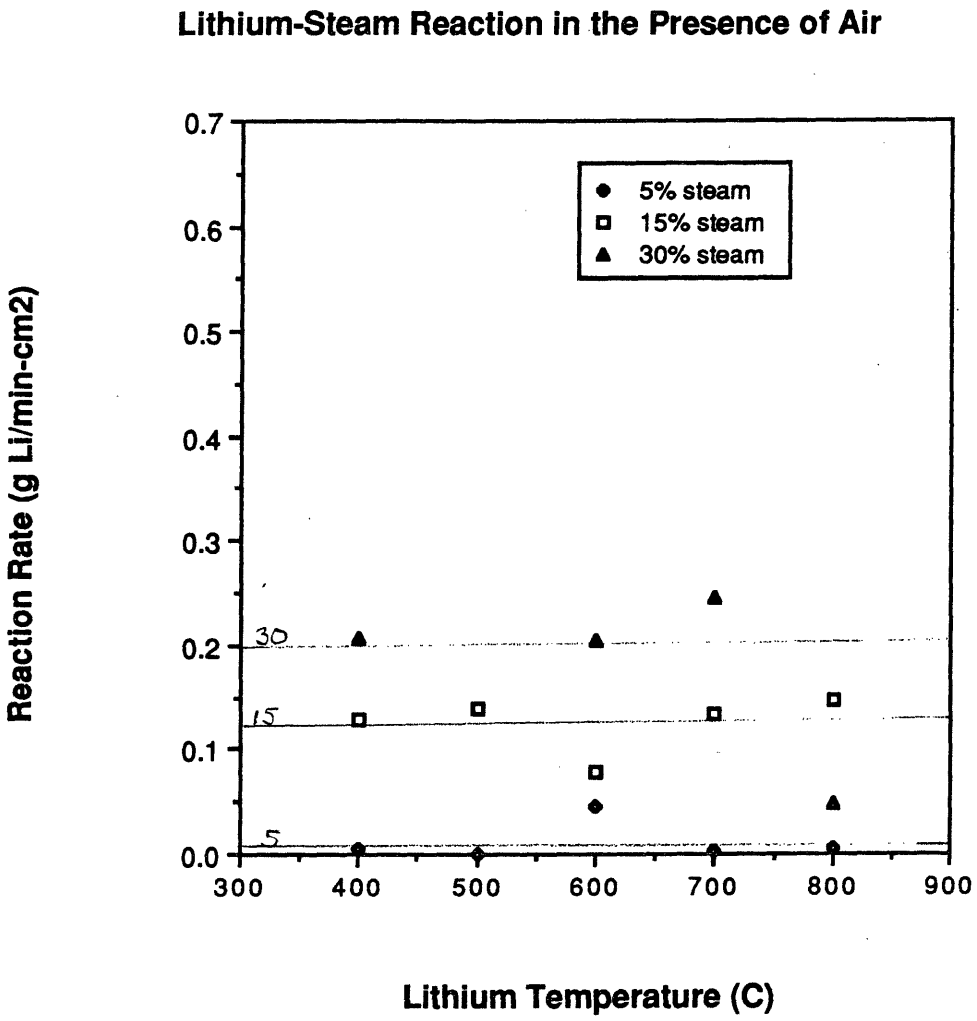

Figure 4-4: Lithium-steam reaction rates in lithium-air-steam tests

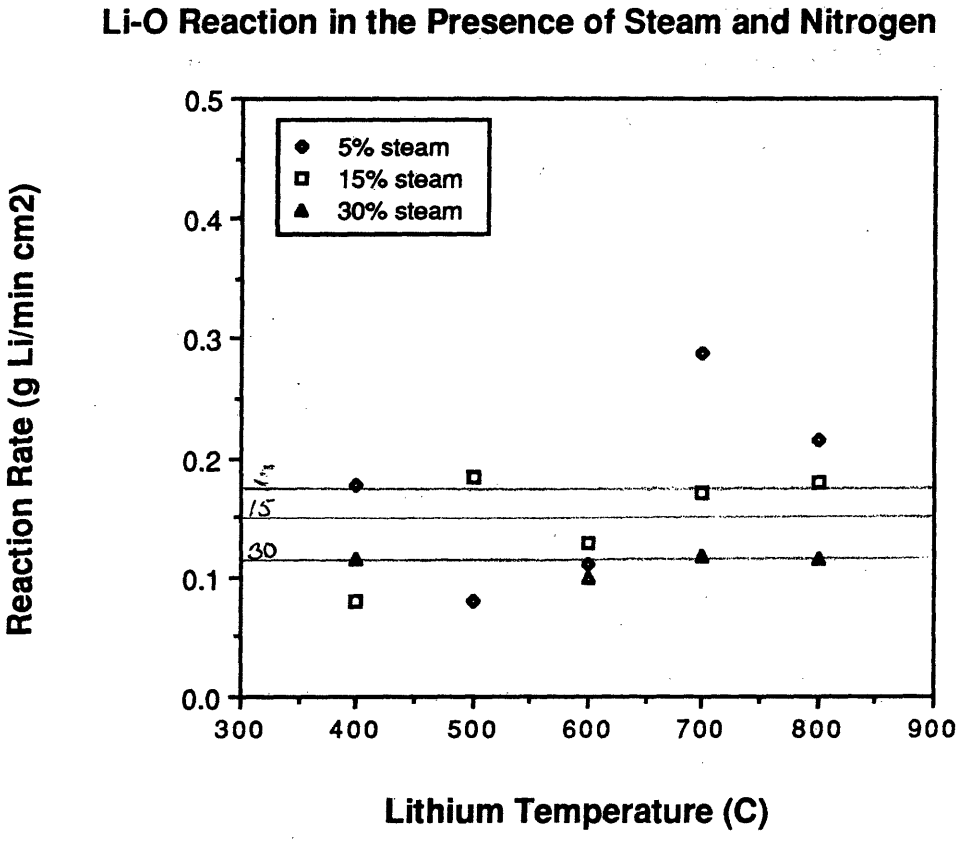

Figure 4-5: Lithium-oxygen reaction rates in lithium-air-steam tests

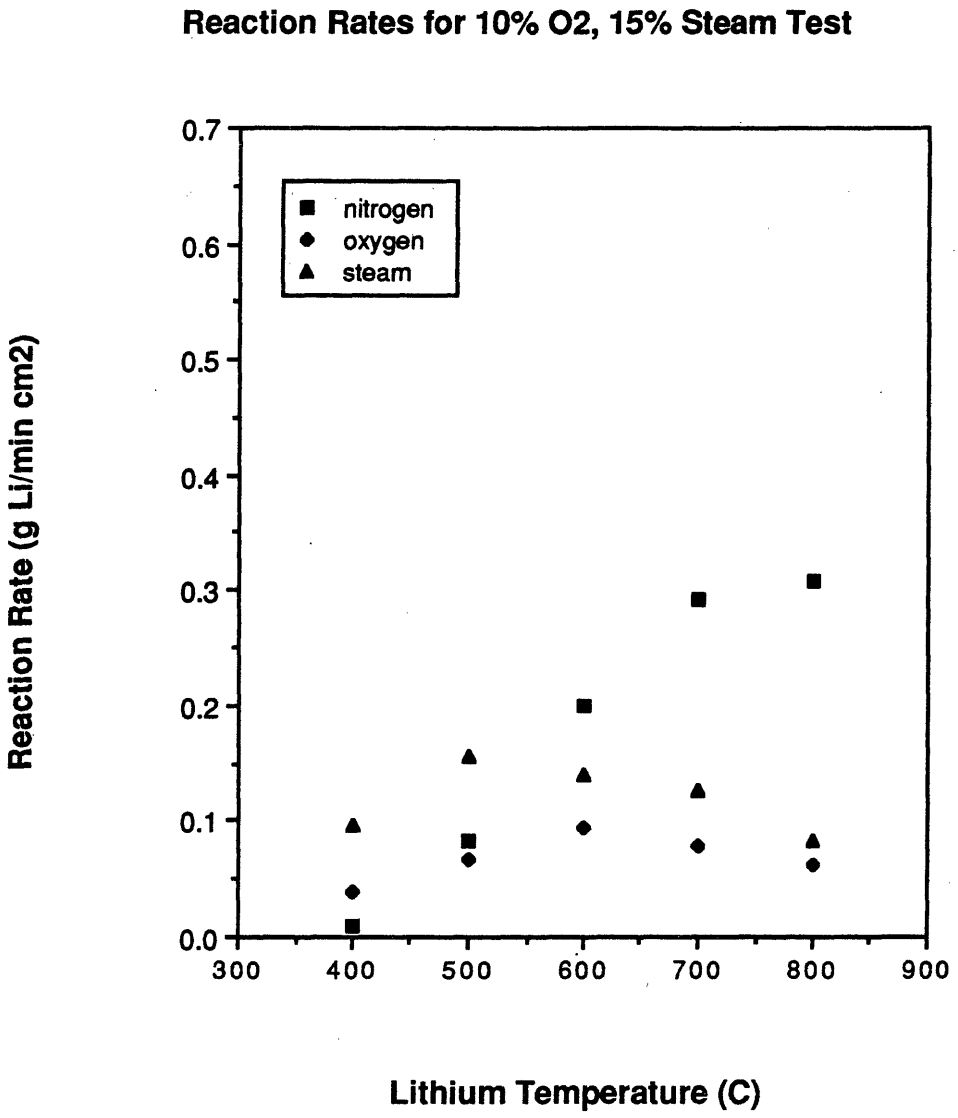

Figure 4-6: Lithium-gas reaction rates in lithium-10% oxygen-90% nitrogen-steam tests

In the second set of experiments, the lithium was heated up to 500°C and allowed to cool down to 400°C. The new test results are depicted by lower symbols in Figures 4-1 and 4-2. As it can be seen, this smoothed out the lithium surface, decreasing the available area and the measured reaction rate. Above 500°C the lithium was almost always completely melted and thus presented a more uniform (and smaller) surface area.

In the lithium-steam-air experiments the reaction products consisted of the black solid lithium nitride and the white aerosols lithium oxide and lithium hydroxide, although considerably more aerosols were generated; the filter had to be changed often to avoid clogging. It was also observed that considerably more lithium melting had occurred at the lowest temperature (400°C). After most tests the reaction products were present as coral-like formations on the bottom of the chamber.

4.1.3 Difficulties and Experimental Error

A number of problems arose during the performing of these experiments which caused runs to be aborted and/or equipment to be damaged. During successful runs, difficulties in taking measurements caused by a lack of instrument performance or natural phenomena caused a certain amount of error to be introduced into the experimental results. First, the difficulties that hampered the performing of experiments will be described to provide a total picture of the work; second, the sources and magnitudes of the experimental errors will be detailed and quantified to produce a final estimate of the accuracy of the data.

4.1.3.1 Experimental Difficulties

The difficulties that impeded the progress of the experimentation were few in number, and were mostly inconveniences that caused the abortion of runs or modification of procedures; however, one of them actually caused the final stoppage of work. The chief experimental difficulties are itemized below:

- Stainless steel corrosion
- Aerosol filter clogging
- Transducer overheating
- Combustion chamber lithium leakage

The problem with stainless steel corrosion occurred early on in the work. As mentioned in Section 3.1, it was decided to redesign the combustion chamber to eliminate some of the difficulties encountered by earlier experimenters. The first of the new chambers was designed like all of the later ones (see Figure 3-2) but was fabricated out of type 304 stainless steel. A test run was performed at 650°C in order to test the new apparatus design and the new equipment. After the test the furnace was opened to allow the chamber to cool, upon which it was discovered that the hot lithium had corroded through the bottom of the chamber (0.159 cm) and had attacked the heating unit in the furnace below. Fortunately the heater was not damaged, but the chamber was rendered useless. Subsequently all chambers were constructed out of type 316 stainless steel, which is more resistant to lithium corrosion. Corrosion of the chamber by the hot lithium was no longer a problem.

The clogging of the aerosol filter was the most recurrent event which caused runs to be aborted or discarded. The purpose of the filter was to remove combustion product aerosols from the gases that exited the combustion chamber to prevent them from building up in Tank 2 (see Figure 3-1). The problem with clogging occurred because almost all of the lithium-steam reaction product (LiOH or Li_2O) and lithium-oxygen reaction product (Li_2O) was in an aerosol form. In fact the aerosol generation was heavy enough to clog the chamber exit pipe between the chamber and the bonnet valve (see Figure 3-1) once during the course of the experiments. That was not the case in the lithium-nitrogen tests; however Gil mentioned a filter clogging problem in the lithium-nitrogen-oxygen tests[4,1]. Thus it became necessary to change out the filter every five runs when the lithium-steam-air tests were being done.

The overheating of the pressure transducers was a temporary problem caused by the heating of Tank 2 to prevent steam condensation (see Section 3.2). During a number of early runs it was discovered that the pressure transducer on Tank 2 was reading a negative number. After consulting the literature it was found that the maximum storage temperature of the transducers was 250°F (121°C), so it was decided to reduce the temperature of Tank 2 to 100°C. After that the problem did not recur.

The leakage of lithium from the seal between the two halves of the combustion chamber was the most serious difficulty encountered during these experiments. This problem was never really solved and ultimately led to the termination of the work after the loss of the third chamber. The first event occurred during a 1000°C nitrogen run with 5% steam. During the run, it was noticed that the gas flow rate was much lower than it should have been. After the run, the furnace was opened to allow the chamber to cool, when it was found that the lithium had seeped out around the O-ring seal near the middle of the length of the chamber. The lithium severly corroded the outside of the chamber and had oozed onto the side of the furnace near the chamber flange, where it corroded some of the heating element material. Reaction products were built up where the lithium had been, and it was not possible to open the chamber even after it had cooled, as the bolts holding the two halves together were sealed tight. That chamber had to be discarded.

After the leak it was thought that the severity of the high temperature reactions had caused the lithium to froth up, attack the O-ring seal, and seep out of the chamber. It was decided to limit future experiments to a maximum temperature of 800°C until all of them were finished, then attempt the high temperature runs again.

The next loss occurred after a second attempt at the lithium-nitrogen-steam run at 1000°C. This chamber had been used for most of the experiments and two small lithium leaks had been observed in previous lithium-steam-air runs at 800°C, but no permanent damage had been done. In this case the white light from the external

lithium fire was noticed inside the furnace. The furnace was opened and a small lithium fire was observed at the seal between the two chamber halves. It had the appearance of a small, bright white flare. As the chamber cooled down, the reaction products were scraped away from the location of the fire in an attempt to prevent them from sealing the chamber shut. After the chamber had cooled, it was opened. It was found that all of the lithium was gone and the reaction product formed only a thin layer on the bottom and sides of the chamber. From the location of the layer it appeared that the lithium had crept up the sides of the chamber and was burning right at the O-ring seal. An examination of the O-ring revealed that it had been severely corroded at the point of the external fire, and was somewhat corroded elsewhere. Previous to the run it had been brand new.

Though the chamber was determined not to have been damaged beyond repair, it was retired in light of its extended service. It was thought that the wear caused by the repeated use and cleaning (by sanding) had caused a slight unevenness in the surface at the seal that had allowed the lithium to seep past the O-ring.

The third chamber was then fabricated in order to collect as much high temperature data as possible before failure. No design changes were made, but in an attempt to prolong its life, the chamber was never filled more than half full and brand new O-rings were used to ensure a clean seal. The efforts were successful for one steam-nitrogen run with 5% steam run at 1000°C, but failed on a steam-nitrogen run with 15% steam at 1100°C. Fortunately, however, the data from the run was usable. The lithium-steam experiments were terminated at that point.

Another possible cause of the leaks may have been the selection of the O-ring material. It was decided to use type 321 stainless steel to increase the corrosion resistance over the Inconel O-rings used by Gil and Ijams[4,1]. However, stainless steel begins to lose some of its elastic strength at a lower temperature than Inconel[4]. Therefore, while the stainless steel O-ring may have been more corrosion resistant, by weakening it may have allowed the lithium to escape. That would explain the

exclusive occurrence at high temperatures.

The lithium leaks may also give some insight into a source of experimental error as well as providing general experience with lithium handling. As mentioned, the appearance of the distribution of the reaction products after the second 1000°C run would suggest that the lithium had crept up the sides of the chamber and burned. The creep phenomenon was known[4], but it was thought that the thin film would burn off shortly after the gas was allowed into the chamber and not seriously affect the reaction rate measurements[4,1]. This was perhaps not the case. If not, then lithium creep could have been a significant source of error, as the long, thin shape of the combustion chamber would have provided a large perimeter per unit surface area for the lithium to climb. The creep could have as much as doubled the surface area of the lithium, with a corresponding overestimation of the lithium reaction rates, although the effect would probably have been most pronounced only at the high temperatures near which the leaks occurred.

4.1.3.2 Experimental Error

A number of factors contributed to producing error in the measurements of the lithium reaction rates. They can generally be split into two categories based on their origin: natural phenomena and instrumental or experimental design deficiencies. The sources of error that have been identified are listed in Table 4.2 according to their category, in the order of decreasing significance. They will be described in detail and their effect on the accuracy of the data will be quantified in this section.

Lithium melting and creep (or spreading) were probably the most significant sources of error in these experiments. During low temperature (400 and 500°C) nitrogen runs partial melting of the lithium served to increase the surface area available to the incoming gas, which increased the measured reaction rate. Since the calculation of the reaction rate was based on the fixed cross sectional area of the combustion chamber, any increase above that would have given a falsely high result. On several

Table 4.2: Sources of experimental error

Natural Phenomena	Instrumental or Design Deficiencies
Lithium Melting and Creep	Residual Gas Analyzer
Lithium-Steam Reaction Products	Gas Leakage
Lithium Purity	Change in Lithium Pool Temperature
Steam Condensation	Gas Composition with Low Steam Content
	Gas Flow Dependence of Reaction Rates

occasions the lithium was found in small lumps at the bottom of the combustion chamber after a test. Based on the fact that the lithium ribbon was typically rolled into three small cylinders, and the chamber bottom was approximately 1 cm wide x 6 cm long, the surface area of the unmelted lithium rolls would be about 17 cm^2, slightly more that twice the area of a fully liquid pool. However, the lithium was never observed to be completely unmelted, and it was resting on the bottom of the chamber, so a maximum factor of 1.6 would probably be more correct. As this phenomenon was most prevalent in the 400°C nitrogen runs, they were repeated with a different procedure: the lithium was heated up to 500°C, held for 15 minutes or so, and then allowed to cool to 400°C. The results of the repeated tests are depicted by the lower symbols in Figures 4-1 and 4-2 and they show that the measured lithium-nitrogen reaction rates were indeed lower when the lithium was heated for a longer time period.

Lithium creep up the walls of the chamber was another source of error. As mentioned in the previous section, examination of the combustion chamber after high temperature runs showed that the reaction products were deposited on the sides of the chamber as high as the O-ring seal. In some cases this actually led to the penetration of the seal and the damaging of the chamber. The creep of the lithium could have effectively doubled the surface area if it had burned over the area indicated by the reaction product deposits for the duration of the run. It is believed from the observations, however, that the worst creep occurred only at or above 800°C—the temperature range in which the lithium leaks occurred, and that the lithium never covered the *entire* surface of the floor and walls of the chamber. Also, the reaction rates at high temperatures were higher and may have burned off the creeping lithium in a short time. Examination of the reaction rate data showed that reaction rates decreased with time in some of the high temperature tests. That may have been the lithium creep burning off. If the effect was obvious, it was not included in the calculation of the average reaction rate, but if not, the reaction rate was determined

normally. All things considered, a maximum factor of 1.4 for the highest temperature runs would probably be a best estimate.

Determination of the distribution of the lithium-steam reaction products was a problem in calculating the lithium-steam reaction rates. The lithium steam reaction may proceed in two branches:

$$2Li + H_2O \longrightarrow Li_2O + H_2 \tag{4.5}$$

or

$$2Li + 2H_2O \longrightarrow 2LiOH + H_2 \tag{4.6}$$

In these experiments the lithium-steam reaction rate was calculated from the difference between the amount of steam that entered the combustion chamber and the amount of unreacted steam that passed into Tank 2 (see Section 3.2). That provided an accurate calculation of the steam consumption rate, but, as can be seen from Equations 4.5 and 4.6, not necessarily the lithium reaction rate. Equations 4.5 and 4.6 show that either one or two lithium atoms can be consumed for each water molecule. Thus some estimate must be made of the distribution of the reaction products. From Table 2.3, if the dry air reaction product percentages (in percent of the total lithium reacted) are subtracted from the moist air reaction product percentages, one obtains a ratio of three or four to one in favor of the oxide producing reaction (Equation 4.5). Results of the steam test LPS-1 done at HEDL indicated that the ratio was closer to ten to one[8]. For these experiments it was assumed that the oxide reaction was the only one that occurred and that two lithium atoms were consumed for each water molecule. That would produce a slight overestimation of the lithium reaction rate: if the actual split was taken to be 85 to 15, oxide to hydroxide (over 5 to 1), the actual lithium consumption rate would be:

$$0.85 \cdot (2) + 0.15 \cdot (1) = 1.85 \text{ Li atoms per } H_2O \text{ molecule} \tag{4.7}$$

thus the reaction rate would have been overestimated by about eight percent.

The lithium purity may have affected the reaction rate measurements indirectly. If impurities were present in the lithium, they would cause the melting temperature to increase, and thus could aggravate the melting problem covered earlier in this section. The lithium used in these experiments was supposedly 99.9% pure when it was received from the vendor. However, small spots of corrosion were noticed on the ribbon and had to be removed when it was loaded into the chamber. The lithium reaction products are denser than the lithium itself, so they would sink to the bottom of the chamber once the lithium had melted. Any effect on the reaction rate measurements would be covered under the melting effect.

Another event that may have caused an error in the lithium-steam reaction rate measurements was the condensation of steam in the tubing between the tanks and the chamber. Condensation was never observed, except inside the flow meter after a run. The tanks were heated and the tubing was insulated, so it is unlikely that a significant amount of steam was lost in transit. Condensation in the capillary line may have affected the measurements of the gas composition in Tank 2 in the 30 percent steam runs. This will be covered in the discussion of error associated with the RGA.

The most significant source of error arising from a lack of instrument performance or design deficiency was due to the inability of the residual gas analyzer to measure hydrogen gas and the limited accuracy of the system in measuring water vapor. The RGA could not measure hydrogen gas. Throughout the series of experiments very little hydrogen gas was observed to have been generated. Even though runs were performed with 30% steam, the amount of hydrogen registering on the RGA was generally one or two orders of magnitude less than the amount of unreacted water vapor. When this problem was discovered, the vendor of the RGA, the Dycor Co., was contacted. They stated that hydrogen gas was difficult to measure on the RGA and suggested that another method should be used if possible. Researchers at JRC-Ispra encountered similar problems when they attempted to measure hydrogen gas in their steam kinetics experiments[5]. They turned to bubbling their steam-hydrogen

mixture through water to condense the steam and leave the hydrogen to be measured volumetrically. That option did not exist here, so it was decided to assume that the hydrogen content of the gas was zero, rather than assign an arbitrary value. This will maximize the error estimate due to this factor.

The assumption that the hydrogen content of Tank 2 was zero caused the unreacted gas pressure in the tank to be overestimated by an amount equal to the hydrogen pressure, but the gas ratios between the nitrogen, oxygen and steam were unaffected. That in turn caused the gas consumption rates to be underestimated by a factor of P_H/P, where P_H is the hydrogen pressure and P is the total gas pressure in Tank 2. The actual hydrogen pressure can be estimated from the amount of steam pressure in Tank 2 and the fraction of steam reacting. During a typical run about half of the steam would react with the lithium and the typical fraction of steam pressure in Tank 2 was about five percent. Since one hydrogen molecule is produced per water molecule consumed, the final hydrogen fraction would also be about five percent. That would lead to a total underestimation of the lithium reaction rates by about five percent.

The second problem with the RGA and the vacuum system as a whole was its inaccuracy in measuring the concentration of water vapor in Tank 2. The difficulty arose because water vapor is condensible. As such, it could condense in the capillary tube between the tank and the RGA, in the RGA head, or on the surfaces inside the turbo pump. When Dycor was consulted regarding this problem, they suggested heating the capillary tube and the pump. Heating the capillary tube was not practical, as it was very fragile. The pump, however, was equipped with its own heater, and in fact the pump vendor suggested in their literature to preheat the pump when water vapor was in the gas being pumped. The heating would cause the water molecules to desorb from the pump and RGA surfaces, and in principle they could be pumped away before the measurement. In practice the heating helped to increase the accuracy of the measurements, as they were checked using the law of partial pressures on a

steam-nitrogen mixture, but did not eliminate the problem.

Condensation in the capillary line from Tank 2 to the RGA was suspected only in the 30 percent steam runs, as the lithium-steam reaction rates were inconsistent compared to the 15 and five percent steam runs. Condensation in the line could have blocked the gas flow to the RGA head and thus obstructed a true measurement of the gas composition in the tank.

Dycor cautioned that the RGA measurements would probably be accurate only to within an order of magnitude, but the performance obtained was better than that. Test runs indicated and experimental results suggested that the error was at most plus or minus 40 percent. That would affect the steam reaction rates directly, but the others would be off by a maximum of 40 percent of the steam content of Tank 2, or about two percent.

A source of error less significant than the RGA was the gas leakage from the system during a run. Although the tubing connections were sealed with silicone rubber, and sealant was reapplied to the combustion chamber fittings before each run, small leaks still occurred as seals wore out. Some seals were relatively old and were somewhat degraded by the heating and cooling of the tubing during each run. Some valves also leaked slightly. The total leakage in the system was determined by doing a run without any lithium and measuring the "reaction rate" due to the leakage. It was found that the leakage corresponded to a reaction rate of 0.02 g Li/min cm^2, assuming that the gas leaked was all nitrogen (a worst case, as each nitrogen atom consumes three lithium atoms). That value in turn represented an error (overestimation) of approximately five percent.

Two other sources of error that were not observed here, but were observed by Gil and may have contributed slightly to the experimental error were the rise in the lithium pool temperature during a run, and variations in the gas composition for runs with five percent steam. The lithium pool temperature was observed to rise about 20-30°C during a typical high temperature run. That would cause some error in the

reaction rate if it accelerated as the lithium got hotter, but it was judged to be a relatively small effect. The variation in gas composition could have occurred if the pressure rise in Tank 1 was due not to the addition of the mass of the steam, but the heating of the gas by a small amount of hot steam. The temperature of Tank 1 was monitored during the gas make up, and no significant changes were observed. Therefore this, too, was probably not important.

An overall estimate of the experimental error can be made using the factors determined for each source. The use of these factors results in a maximum factor of overestimation and underestimation of the reaction rates for each test. The experimental error factors determined for each may be combined arithmetically to determine the total estimated error; that is the experimental error is the product of the factors of overestimation divided by the factors of underestimation. It should be remembered that the largest error factors discussed in this section, the change in the lithium surface area and the performance of the RGA (for the steam reaction rates only), apply to their fullest extent only in a few instances—they are estimates of the maximum probable error. Furthermore, since most of the sources of error would have caused the overestimation of the reaction rates, the data points are closer to the top of the band in which the true reaction rates could be expected to fall. The error for non-condensibles was approximately 25 percent at low temperatures and 40 percent at high temperatures. For steam the error was about 50 percent as the error associated with the RGA had a more direct effect on the measurements.

Lastly, it was stated in Section 3.2 that the gas flow rate in the experiments was kept high in order to characterize the kinetics of the lithium reactions and ensure that the reaction rates were not limited by the gas flow. An average gas flow rate of about 6 liters/min, approximately twice as much as was used by Gil, was used in order to do this[1]. In the air tests with 30% steam it was found that about 60 percent of the gas was consumed. It was also found in all of the steam tests that the steam reaction rate was roughly proportional to the steam content of the gas and that the oxygen

reaction rate was roughly proportional to the oxygen content of the gas, suggesting that the gas flow rate and the reaction kinetics were influencing the reaction rates. Furthermore, in the case of steam-gas mixtures, the reaction rates measured here were less than those measured for a pure steam atmosphere at JRC-Ispra[5]. In the dry air tests Gil observed no ultimate kinetics limit for oxygen[1]; the point at which the lithium-oxygen reaction rate was influenced only by the reaction kinetics may be significantly higher than the reaction rates measured in the kinetics experiments. That would mean that the lithium reaction with 44 percent of the gas in the tests was influenced by both the gas flow rate and the reaction kinetics. The proportionality of the reaction rates to the steam and oxygen content of the gas will be discussed further in the next section.

4.2 Data Analysis

Given the measurements of the lithium reaction rates with the various gases it is desirable to use that data to better understand large scale lithium fires. That can best be done by observing new parameters and examining the response of old parameters to the changes in gas composition and lithium temperature. Those observations can then be quantified, extrapolated and applied to the modeling of large fires. In this case the new parameter is the lithium-steam reaction rate, which had not been measured before; the old parameters are the lithium-nitrogen reaction rate kinetics limit and the lithium-oxygen reaction rate.

4.2.1 Steam Effects on Lithium-Nitrogen Reaction Kinetics

Contrary to the results of the oxygen-nitrogen experiments, the results of the nitrogen-steam experiments showed that the presence of water vapor served to increase the nitrogen reaction rates above those indicated in the pure nitrogen experiments. This result was not entirely unexpected, as it has been observed that lithium-gas reactions

are catalyzed by even trace amounts of water vapor and lithium hydroxide[2]. The effect was greatest at low temperatures, as the reaction proceeded rather vigorously at high temperatures to begin with. It can also be seen that the effect was relatively independent of the concentration of the water vapor, perhaps indicating that only a very small amount of steam is needed to cause it to occur. The catalytic effect can be defined in a manner similar to that used to define the inhibition factor for oxygen. That is, the catalytic factor is the ratio of the lithium-nitrogen reaction rate with steam present to the reaction rate of pure nitrogen.

$$C_{H_2O} = \frac{RR''_N}{RR_N} \tag{4.8}$$

where RR''_N is the nitrogen reaction rate in the presence of steam. A plot of C_{H_2O} versus T_{Li} is shown in Figure 4-7. It can be seen that C_{H_2O} decreases exponentially with temperature, but is relatively independent of the steam concentration. A curve was fit using the average catalytic factor for each temperature:

$$C_{H_2O} = 680e^{-.006T}, \tag{4.9}$$

where T is in K. The above equation is good to within 15% of the actual values measured.

The catalytic effect can be explained if the steam is assumed to counteract the previously observed reaction kinetics limit. Ijams observed that the lithium-nitrogen reaction rates at high temperatures may be dependent upon both the flow rate and the reaction kinetics[4]—as the temperature increased, the kinetics limiting effect was observed to weaken greatly. Therefore, as the temperature increased and the kinetics limiting effect weakened, the catalytic effect would also weaken. In Figure 4-7 the catalytic factor decreases until it approaches unity (no effect) at temperatures over 700°C. As stated earlier, the relative independence from the steam concentration could be explained if the effect was caused by a very small amount of steam, as the lowest concentration used here was five percent.

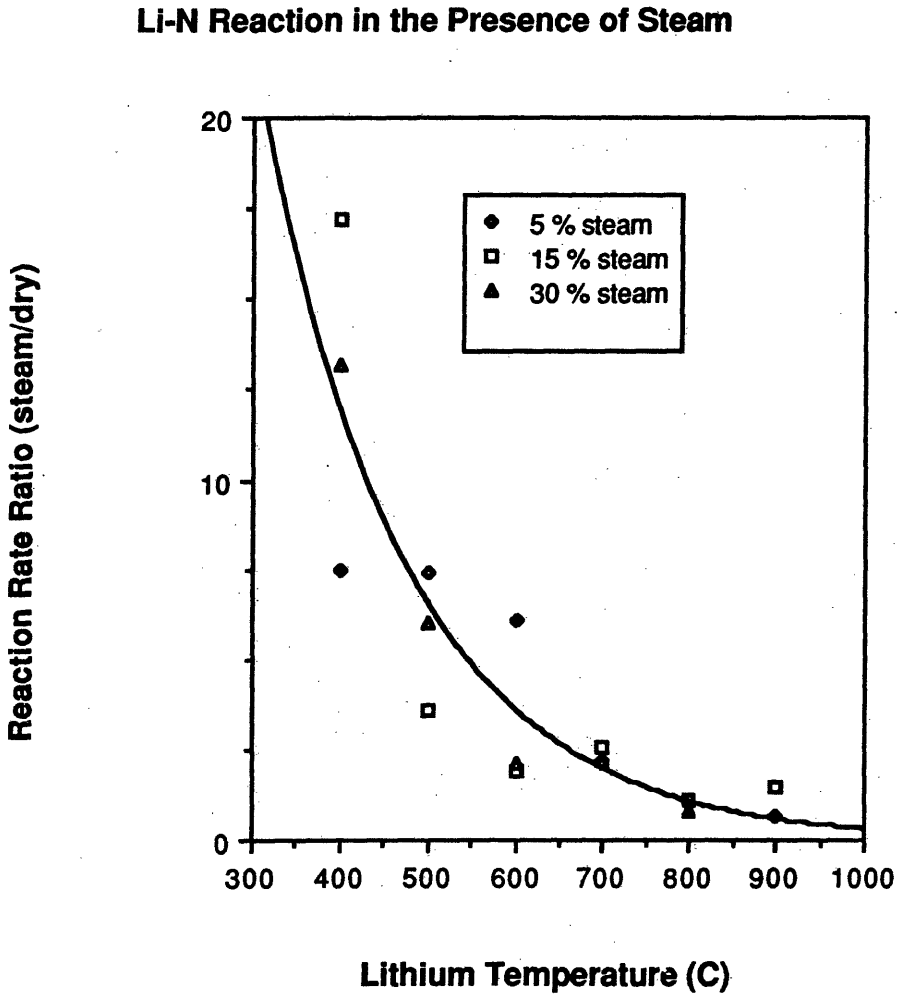

Figure 4-7: Lithium-nitrogen reaction rate catalytic factor in steam

It is interesting to note that the catalytic factors calculated from each group of runs followed an exponential decay with increasing temperature rather well and the decay coefficients for all of them were close. This would further suggest that the catalytic effect was caused by the presence of only a small amount of steam and that it was somehow affecting the lithium-nitrogen reaction at the reaction site. Addison and Davies performed experiments to measure the reaction rate of lithium and nitrogen over a number of hours and measured an activation energy for the lithium-nitrogen reaction[4]. They could not determine what the rate controlling mechanism was, but they speculated that it could have been the chemisorption of the lithium, followed by electron transfer, or it could have been the dissolving of the nitrogen in the lithium. The steam may have speeded up the process at the molecular level and thus increased the reaction rate.

4.2.2 Steam Effects on Lithium-Air Reaction Kinetics

The results of the steam-air experiments showed that the presence of steam served to counteract the inhibiting effect of oxygen on the lithium-nitrogen reaction. In all but one of the experiments, the nitrogen reaction rate was higher than in the pure nitrogen experiments, but lower than in the nitrogen-steam experiments. That would indicate that the inhibiting effect due to oxygen and the catalytic effect of steam offset each other to some degree. Figure 4-8 shows a plot of the ratio of the reaction rate of nitrogen in the steam-air experiments to that of nitrogen in air (C_{H_2O} in air), illustrating the effect of the presence of steam on the reaction rate of nitrogen in air. A curve was also fit to the average catalytic factor for each temperature for the air runs:

$$C_{H_2O} = 179e^{-.0033T} \tag{4.10}$$

where T is in K. The above equation is good to within twenty percent of the values measured.

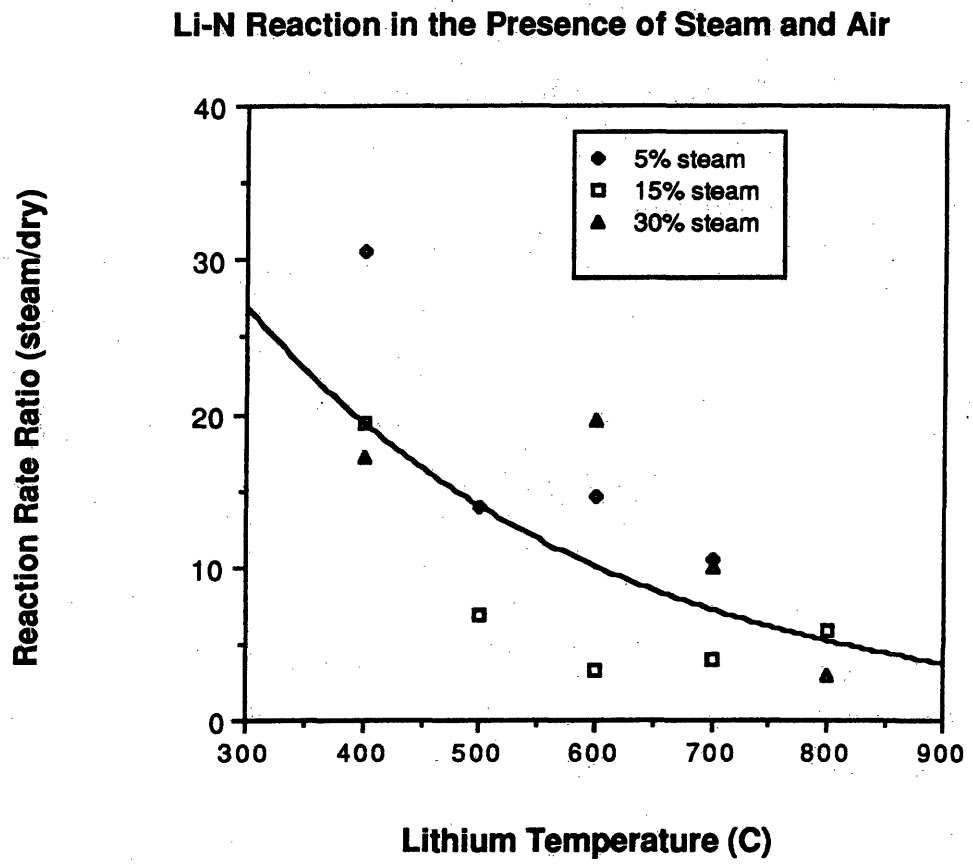

Figure 4-8: Lithium-nitrogen reaction rate catalytic factor of steam in air (ratio of nitrogen reaction rate with steam-air to that in dry air

The lithium-nitrogen-oxygen-steam experiments showed results similar to those of the lithium-nitrogen-steam experiments in that the catalytic factor decreased exponentially with increasing temperature. It is not entirely clear from the data, but the lithium-nitrogen reaction rates were generally lower with 15% steam than with five percent. That may indicate that as the steam content increased, the lithium-nitrogen reaction rate decreased, suggesting that in addition to catalyzing the nitrogen reaction, the steam was also competing with the nitrogen for the available lithium. This is not as evident from the 30% runs or the nitrogen experiments, but some concentration dependence can be seen. The same effect could be present but obscured by the experimental error mentioned earlier.

Comparing the catalytic factor in the air tests to that in the nitrogen tests, it is interesting to note the difference in the two values. The catalytic effect was stronger in the air experiments than in the nitrogen experiments, especially at high temperatures. That was probably due to the oxygen inhibiting the nitrogen reaction in the dry air experiments. In the nitrogen experiments, the lithium-nitrogen reaction rate was limited only by the kinetics effect. In the air experiments it was limited by both the kinetics effect and the oxygen inhibition effect. When steam was added to the nitrogen, it weakened the kinetics effect and allowed the nitrogen to react faster. When steam was added to the air, it did the same thing. However, since the nitrogen could react faster, it was then more able to compete with the oxygen for the available lithium, and thus reacted even faster in the steam-air experiments, relatively, than in the steam-nitrogen experiments. With regard to the temperature dependence, the kinetics effect was much weaker at high temperatures (over 700°C.) that at low temperatures, but the oxygen inhibition effect was not so strongly temperature dependent[1]. Therefore, the weakening of the kinetics effect would not be felt as much at higher temperatures as would the weakening of the oxygen inhibition effect.

4.2.3 Steam and Oxygen Reaction Kinetics

Before concluding the analysis of the experimental results, the lithium-steam and lithium-oxygen reactions must also be covered. While those data did not prove to be as interesting as the lithium-nitrogen data, some more insight into the nature of lithium fires can still be gained from them.

The lithium-steam reaction rates from the lithium-steam-nitrogen tests are shown in Figure 4-2. It can be seen from the figure that they did not exhibit any temperature dependence, unlike the lithium-nitrogen reaction rates. Additionally, it can be seen that the reaction rates were roughly proportional to the steam content of the gas. Figure 4-4 shows the lithium-steam reaction rates from the lithium-steam-air tests and the same things can be seen: the reaction rates appear to be independent of temperature, and roughly proportional to the steam content. Table 4.3 better illustrates the relationship between the average reaction rates and the steam content.

It can be seen that the lithium steam reaction rates were roughly, but not exactly, proportional to the steam concentration. As the steam concentration increased to 30 percent, the reaction rate began to fall off slightly, indicating perhaps that the reaction kinetics were becoming more limiting and that some ultimate kinetics limit might be reached if the steam supply was increased. It can also be seen that the reaction rates were lower in the air runs, as the steam had to compete with the oxygen for the available lithium. Figure 4-9 illustrates the effect of the presence of other gases on the steam reaction rate. It compares the lithium-steam reaction rates of all of the 15 percent steam runs, and additionally shows the reaction rates taken at JRC-Ispra from their pure steam experiments[5]. The effect of increasing oxygen content can be seen as the steam reaction rates decrease from pure nitrogen, to 10% oxygen to air. The data from the pure steam experiments would give a reason for the steam reaction rates to be slightly less than proportional to the steam content: the kinetics limit on the pure steam reaction rate appears to be not significantly higher than the average reaction rate calculated from the 30 percent steam runs with

Table 4.3: Lithium-steam reaction rates as a function of steam concentration

Steam Concentrations and Reaction Rates		
Concentration	Reaction Rate (g Li/min cm^2)	
(mole %)	in Nitrogen	in Air
5%	0.035	0.012
15%	0.174	0.125
30%	0.293	0.20

nitrogen.

Lithium-oxygen reaction rates in the presence of steam are shown in Figure 4-5. They, too, appeared to be proportional to the oxygen concentration, even more so than the steam reaction rates. This is better seen from Table 4.4 (the oxygen concentrations of 19, 15 and 14 percent correspond to steam concentrations of 5, 15 and 30 percent (see Table 4.1)). This would indicate that the lithium-oxygen reaction takes precedence over both the nitrogen and the steam reactions, as it does not appear to be hindered by the presence of steam, and is only very slightly affected by the presence of nitrogen[1].

Finally, the combined effect of the presence of the various gases can be seen in Figure 4-6, a plot of the lithium reaction rates with oxygen, nitrogen and steam from the 10% oxygen-90% nitrogen tests. It can be seen that at low temperatures the nitrogen reaction rate is very low but increases significantly with temperature. Meanwhile, the steam and oxygen reaction rates decrease slightly as the nitrogen begins to compete with them for the available lithium at high temperatures. The steam reaction rate is higher than the oxygen reaction rate due to the higher steam concentration.

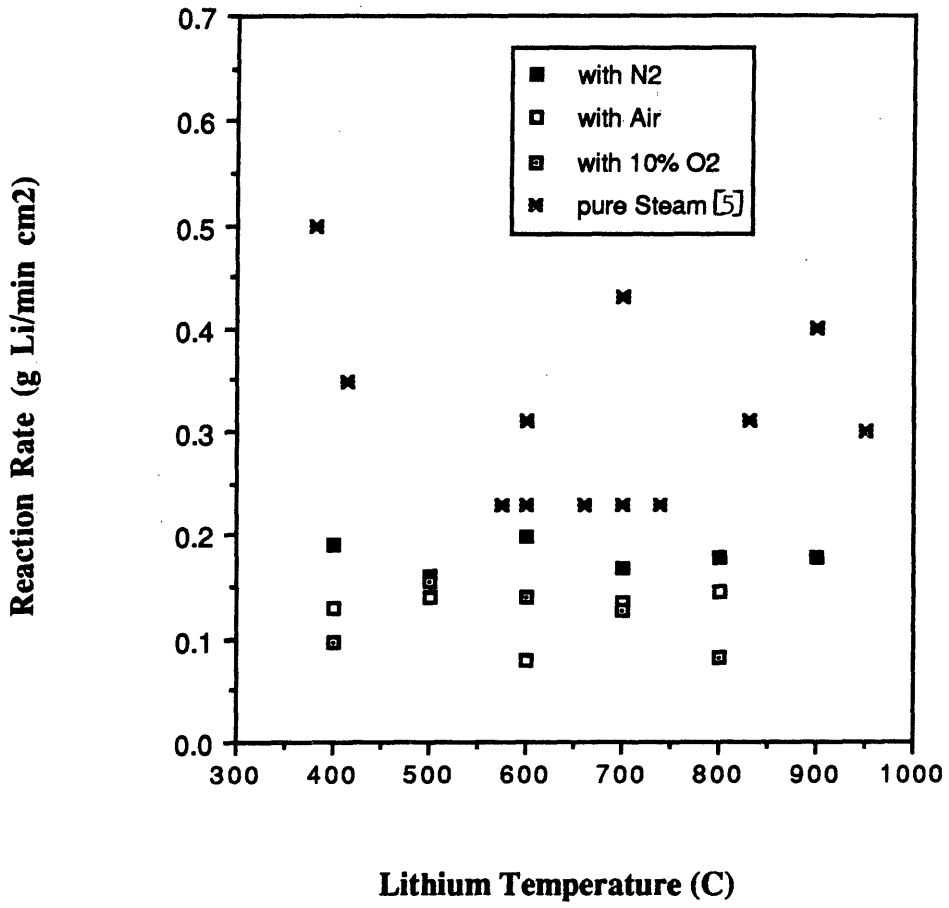

Figure 4-9: Li-steam reaction rates in the presence of nitrogen and oxygen, at 15% steam concentration

Table 4.4: Lithium-oxygen reaction rates in the presence of steam as a function of oxygen concentration

Oxygen Concentrations and Reaction Rates	
Concentration (mole %)	Reaction Rate (g Li/min cm^2)
19%	0.174
15%	0.148
14%	0.112

Chapter 5

The LITFIRE Code

5.1 Introduction

LITFIRE is a computer code which simulates lithium fires in fusion reactors by generating the time histories of the temperature and pressure profiles occurring in a reactor containment in response to a lithium or lithium-lead eutectic spill and fire. The fire may take place in a single cell optionally connected to a second cell, or within an insulated pan in a single cell. The lithium or lithium-lead may react with any mixture of oxygen, nitrogen or water vapor; any inert gas may also be included in the cell atmospheres. Lithium only may be burned in a carbon dioxide atmosphere without oxygen. The gases are assumed to travel via natural convection to a combustion zone just above the liquid metal pool. There they are consumed and energy is released. The thermal admittances between nodes are used in conjunction with nodal temperatures to determine the time rates of change of the temperatures. These rates of change are then integrated using Simpson's Rule or a fourth-order Runge-Kutta Method to give a time history for each node. Mass rates of change are determined from the lithium reaction rates and gas flow rates; they are integrated and combined with temperatures to determine gas pressure histories. A simple option for liquid metal-concrete interaction is available as well as the following options for mitigating

the effects of a fire: gas flooding, emergency space cooling, emergency floor cooling, aerosol removal and gas injection[10].

The LITFIRE code was first developed at MIT in 1978 from SOFIRE, a sodium fire simulation code[2]. It has been modified in the years since to increase its flexibility in modeling lithium fires. This chapter summarizes the work that has been done on LITFIRE up to the present time and includes a description of the physics of lithium fires, and the workings and capabilities of the code. Table 5.1 provides a brief chronology of the development.

The first section will cover the basic case of a lithium spill and fire inside a single cell containment building, while the second section will cover all of the optional capabilities of LITFIRE. The actual structure of the code and detailed descriptions of the numerical procedures used in the model are presented in the Appendix.

5.2 Basic LITFIRE

The basic case modeled by LITFIRE is a lithium spill and fire inside a single cell containment building. Within that case, the containment geometry, structural materials and containment atmosphere are specified by the user. A schematic of the one cell case with the heat transfer pathways is shown in Figure 5-1.

Heat generated by the fire is transferred to the structures and gas in the building and from there to the ambient. Containment gases are consumed by the fire, and the fire stops when either the lithium or the gas supply is exhausted. Lithium-gas reaction rates are limited either by the gas flow rate to the reaction site or by reaction kinetics limits. Temperature and pressure profiles of the containment are followed until either a predesignated time limit is reached or the containment temperatures and pressures have returned to normal. A diagram of the mass flow in LITFIRE is shown in Figure 5-2. The following subsections detail the modeling associated with each of the steps followed by the code during its execution.

Table 5.1: Chronology of the development of LITFIRE

Mod #	Principal Features	Year	Reference
1	Basic model: Single cell reactor containment building Lithium pool fire on the building floor Lithium-air reaction model Spray fire calculation Convective and radiative heat transfer from the pool Inert gas injection Emergency gas cooling Emergency floor cooling	1978	[2]
2	Additions: Pan fire option Two cell containment building option Lithium-concrete interaction option Lithium-nitrogen reaction kinetics Aerosol suspension effects	1980	[9]
	Modifications: Radiative properties of the combustion zone and cell gas		
3	Additions: Lithium-lead-air fire option	1983	[11]
	Modifications: Two cell containment building option Radiative properties of the combustion zone and cell gas Code structure		
4	Additions: Lithium-carbon dioxide reaction model	1986	[1]
	Modifications: Lithium-nitrogen reaction kinetics Lithium-air reaction model		

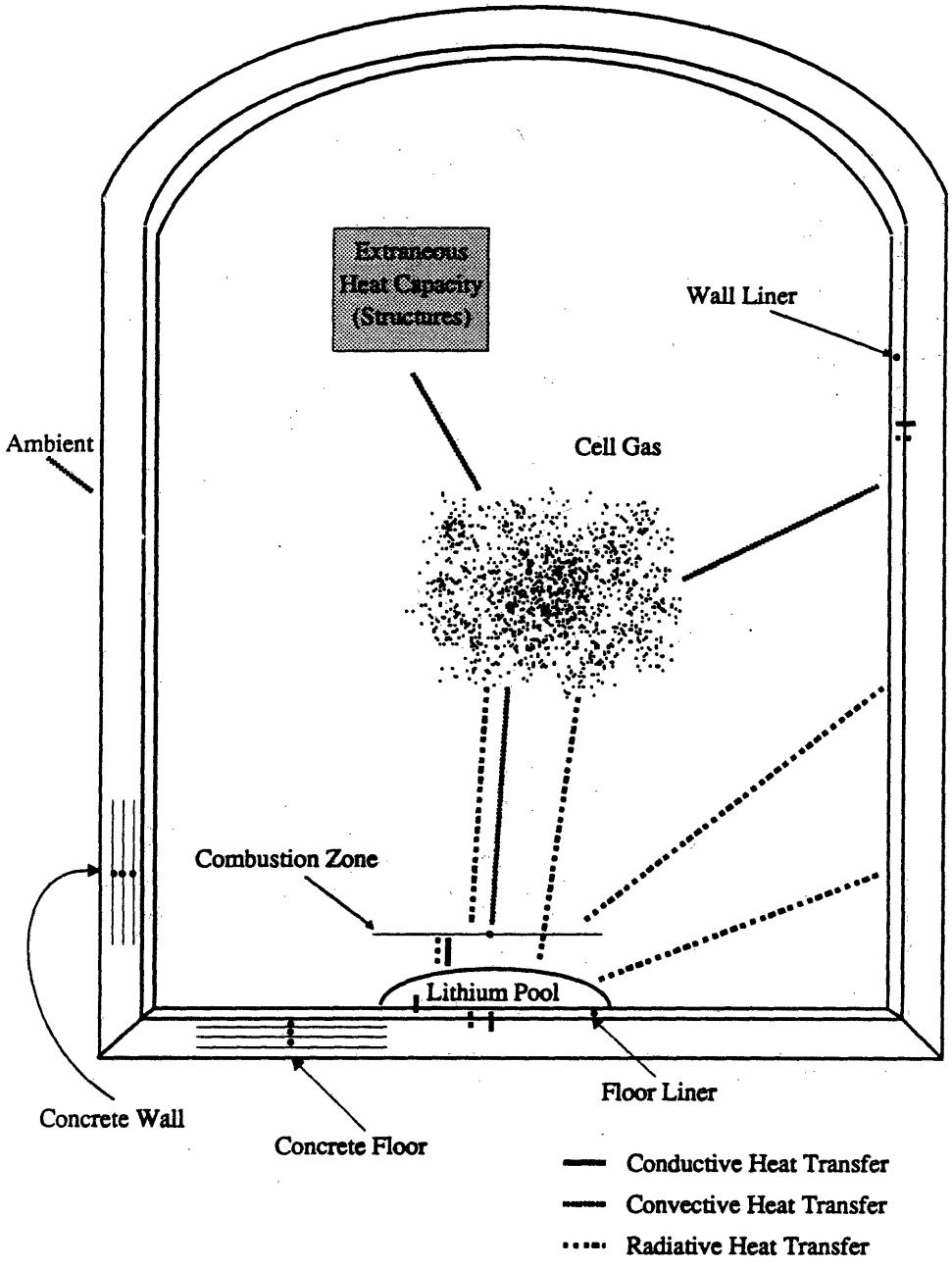

Figure 5-1: LITFIRE one cell case

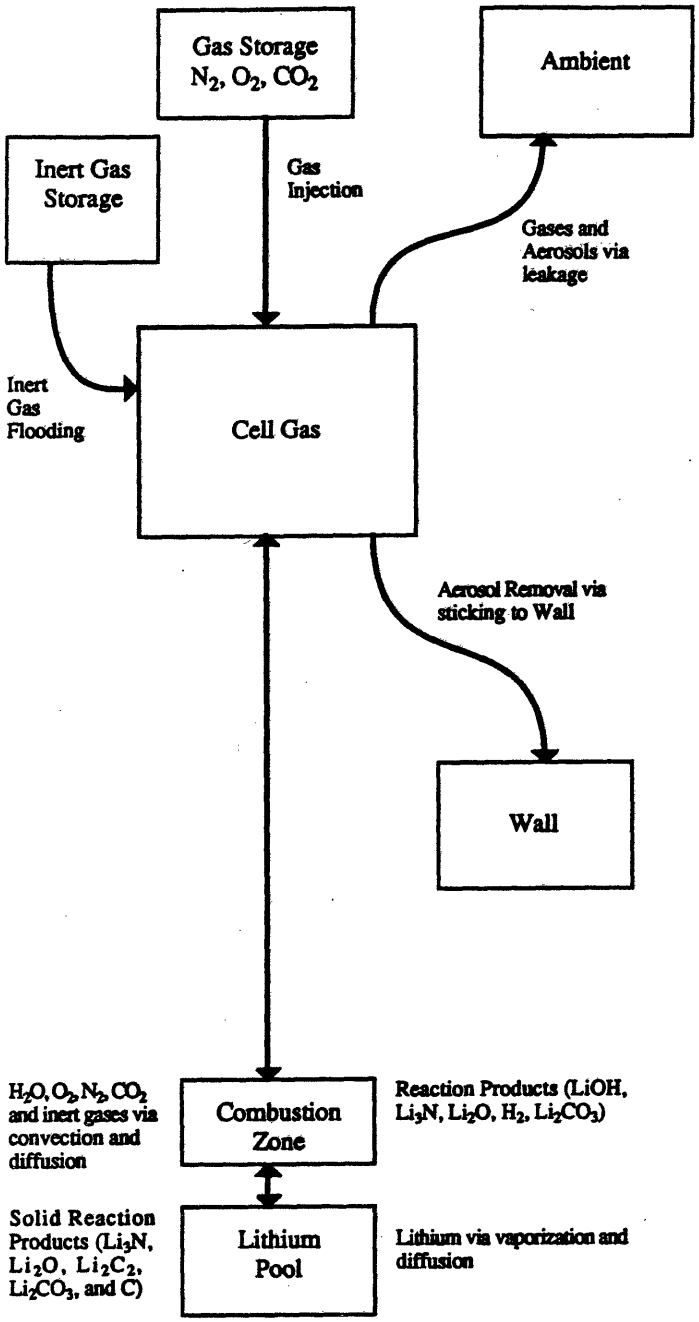

Figure 5-2: Mass flow in one cell LITFIRE

5.2.1 Preliminary Calculations

Before any calculations are performed by the code, the material properties of all of the nodes must be calculated. Most properties are assumed to be constant with respect to temperature, but the specific heats of some gases and combustion products, and most lithium properties, are calculated as functions of temperature. These are calculated at the beginning of each time step. The mass fraction and total mass of each of the individual gases is also calculated so that the total heat capacity of the gas may be calculated.

If lithium were spilled inside the containment building, a small fraction of the total spill mass would react with the atmosphere before reaching the floor. LITFIRE calculates the effect of the "spray" fire before beginning the calculations associated with the pool fire. The spray fire is accounted for by assuming that a fixed amount of lithium reacts instantaneously, adiabatically and stoichiometrically with the oxygen in the containment building atmosphere. The equilibrium temperature of the atmosphere is given by[2]:

$$\int_{T_o}^{T_p} M_L c_{p_L} dT_L + M_L Q_C = \sum_{i=1}^{n} \int_{T_{o_i}}^{T_f} M_i c_{v_i} dT_i \qquad (5.1)$$

where: T_o = initial atmospheric temperature

T_p = initial lithium temperature

M = mass

C_{v_i} = specific heat = $F(T_i)$

Q_C = heat of combustion per unit lithium mass

T_i = temperature of each gas constituent

T_f = final mixture (atmospheric) temperature

L = designation for sprayed lithium

Since the specific heats are functions of temperature, performing the integrations results in a fourth-order polynomial which is solved numerically.

The percentage of lithium that reacts during the spray stage is specified by the user. Studies performed with liquid sodium under a number of different conditions showed that no more that five percent of the metal reacted before striking a hard surface[2].

5.2.2 Heat Transfer Calculations

5.2.2.1 Radiative Heat Transfer

Thermal radiation within the containment building is a significant mechanism of heat transfer, as the temperatures reached by the lithium pool and the combustion zone are quite high, and the thermal conductivity of the cell gas is rather low. Radiative heat transfer rates in LITFIRE are calculated using the following basic equation:

$$Q_{1\to 2} = f A_1 \sigma (T_1^4 - T_2^4) \tag{5.2}$$

where $Q_{1\to 2}$ = heat transfer rate (W) from node 1 to node 2

A_1 = exposed area of node 1

f = radiative interchange factor based on A_1

σ = Stefan-Boltzmann constant

T_n = temperature of node n

The radiative interchange factor f is determined by the emissivities of the surfaces of the two nodes and the view factor between them. Thus the radiative emissivity of each node is required to account for radiative heat transfer within the containment building.

The emissivities of the solid elements in the containment building are specified by the input data and are assumed to be constant. The emissivity of the lithium pool is assumed by the code to be governed by the buildup of reaction products (Li_2O, Li_3N and Li_2CO_3) on the pool surface. Thus the radiative heat transfer from the pool will become more effective as the fire burns and reaction products are released.

The emissivity of the cell gas (in the absence of steam) is determined by the aerosol concentration in the gas:

$$\epsilon_g = 1 - \exp(-CA_aL) \tag{5.3}$$

where: C = aerosol concentration (particles/m^3)

A_a = aerosol particle surface area

L = optical path length (usually taken to be one-fourth the containment height)

The aerosol particle area is defined by the user in the input data and the concentration is calculated from the amount of aerosol reaction product generated by the fire. L is the average optical path length in the primary cell for the given case.

LITFIRE performs radiative heat transfer between multiple nodes by using the gray body electrical circuit analogy. The black body emissive power $E_b = \sigma T^4$ is regarded as the potential for a given node, while the radiative interchange factor is regarded as the resistance between the nodes. The resistance consists of a surface resistance for each surface given by $(1 - \epsilon)/\epsilon A$ and a spatial resistance given by $1/A_1F_{1\to2}$[12]. The net radiant heat transfer between two surfaces would be expressed as[12]:

$$Q_{1\to2} = \frac{E_{b_1} - E_{b_2}}{\sum R} = \frac{E_{b_1} - E_{b_2}}{\frac{1-\epsilon_1}{\epsilon_1 A_1} + \frac{1}{A_1 F_{1\to2}} + \frac{1-\epsilon_2}{\epsilon_2 A_2}} \tag{5.4}$$

where $F_{1\to2}$ is the view factor between the nodes. Thus the radiative interchange factor ($f = \sum R$ above) for each radiative heat transfer pathway between the nodes is determined from the emissivity of the surfaces, the emissivity of the cell gas between them and the view factor between them.

5.2.2.2 Natural Convection Heat Transfer

The heat transfer coefficients for convective heat transfer between surfaces and gases h are calculated from the temperature of the surface T_s, the temperature of the gas T_g, and the density of the gas ρ_g:

$$h = CF(T_s, T_g, \rho_g) \tag{5.5}$$

The function F is given in Appendix A. The constant C is used to adjust the value of h to fit each specific geometry for which Equation 5.5 is used. A recalibration of the code was performed after the experimental data regarding the oxygen inhibition factor were incorporated into the lithium reaction model (see Section 5.2.3 and Appendix A). Data from the HEDL tests LN-2 (a small nitrogen fire) and LA-5 (a large air fire) (see Chapter 2) were used in the recalibration to determine values of C that would best fit the experimental results. The results of the recalibration are given in Appendix C. Some recommended values for C are given in Table 5.2.

5.2.2.3 Conductive Heat Transfer

Once the heat capacities, the radiative interchange factors and the convective heat transfer coefficients for all of the nodes have been calculated, the thermal resistances between the nodes are calculated. Knowledge of the thermal resistance allows the temperature rate of change due to heat conduction and heat convection to be calculated. In LITFIRE the thermal resistance between adjacent nodes i and j is calculated as follows:

$$R_{ij} = \frac{l_i}{2k_iA} + \frac{l_j}{2k_jA} \tag{5.6}$$

or

$$R_{ij} = \frac{l_i}{2k_iA} + \frac{1}{h_{ij}A} \tag{5.7}$$

where l_n = characteristic length (thickness) of node n

k_n = thermal conductivity of node n

A = area of contact between nodes i and j

h_{ij} = convective heat transfer coefficient between nodes i and j,

depending on whether or not node j is a solid (Equation 5.6) or a gas (Equation 5.7).

The thermal resistance between the lithium pool and the combustion zone is determined somewhat differently, as the lithium is considered to vaporize and then react with the gases in the combustion zone. The pathway between the pool and the

Table 5.2: Typical values for the heat transfer correlation coefficient C

Condition:	Value
large (containment fire) pool surface	0.12 ± 0.01
small (HEDL) pool surface	0.16 ± 0.02
vertical surface inside enclosure	0.11 ± 0.01
vertical surface outside enclosure	0.07 ± 0.01
irregularly shaped objects inside enclosure	0.09 ± 0.01

zone is considered to consist of a mixture of atmospheric gas and lithium vapor. The thermal resistance is expressed as:

$$R_{pz} = \frac{d}{k_f A_p} \tag{5.8}$$

where d = thickness of the mixed vapor region

k_f = thermal conductivity of the vapor region

A_p = area of the lithium pool

The thickness of the vapor region is determined from:

$$d = D_L \frac{\rho_{Li_v}}{RR_{Li}} \tag{5.9}$$

where D_L = diffusion coefficient of lithium in air

ρ_{Li_v} = density of lithium vapor

RR_{Li} = lithium reaction rate (considered to be the lithium mass flow rate)

RR_{Li} is calculated as described in the next section, while D_L and ρ_{Li_v} are calculated from empirical expressions and the film conductivity k_f is calculated from a pressure weighted average of the thermal conductivities of lithium vapor and air as a function of the average temperature between the pool and the combustion zone (see Appendix A).

5.2.2.4 Temperature Rates of Change

The rates of heat transfer between all thermally adjacent nodes are calculated from the temperatures of the nodes, and the thermal resistances and radiative interchange factors between them. Once the rates of heat transfer to and from all of the nodes have been calculated, they are summed for each node, and the temperature rate of change of each node is calculated using its own heat capacity. The heat flow to or from a given node is determined by summing the heat flow by conduction, convection and radiation to and from thermally adjacent nodes:

$$Q_1 = \frac{(T_1 - T_i)}{\sum_i R_{1i}} + \sum_j A_1 f_{1j} \sigma (T_1^4 - T_j^4) \tag{5.10}$$

where: Q_1 = heat flow rate to or from node 1

T_n = temperature of node n

i = designation for physically adjacent node

R_{1i} = thermal resistance between nodes 1 and i (see Eqns. 5.6 and 5.7)

j = designation for optically adjacent node

A_1 = surface area of node 1

f_{1j} = radiative interchange factor between nodes 1 and j (see Eqn. 5.4)

Temperature rates of change for each node are calculated by dividing the energy gain or loss rate by the heat capacity of the node:

$$\frac{dT_1}{dt} = \frac{Q_1}{m_1 c_{p_1}} \tag{5.11}$$

where t is time, m_1 is the mass of node 1 and c_{p_1} is the specific heat of node 1. The combustion zone node adds the heat of combustion and the heat of vaporization of the lithium combusted to the above terms, while the lithium pool subtracts the heat of vaporization of the lithium combusted. That is due to the assumption that the lithium reaction takes place in the vapor phase.

5.2.3 Lithium Combustion

The temperature rates of change in the containment can differ greatly depending whether or not the lithium pool is actually combusting (reacting with the containment atmosphere). The criteria used to determine whether or not the lithium is combusting are:

- Liquid lithium must be available (between 180 and 1347°C)
- Oxygen, nitrogen, carbon dioxide or water vapor must be available

- If only nitrogen is present, the combustion zone temperature must be less than 1127°C

If none of the above conditions are met, then the combustion zone is considered to be nonexistent, and heat transfer from the lithium to the rest of the containment building is performed normally. If combustion is occurring, then the combustion rate and the heat liberated by the lithium reactions is calculated.

In LITFIRE the lithium combustion rate is governed by the flow rate of gas or (if lithium-lead is being burned) the diffusion of lithium to the combustion zone. The gas flow rate is determined by natural convection using Reynold's analogy between heat and mass transfer. Thus LITFIRE assumes:

$$h_m = \frac{h}{\rho_g c_{p_g}} \tag{5.12}$$

where h_m = mass transfer coefficient (m/s)

h = convective heat transfer coefficient

ρ_g = gas density

c_{p_g} = gas specific heat

That analogy is valid when the Schmidt number ($Sc \equiv \nu/D$) and the Prandtl number ($Pr \equiv \nu/\alpha$) are both approximately equal to one, where D and α are the mass and thermal diffusivities (m^2/s), respectively. In that case, the Lewis relation is necessarily correct, with:

$$D \simeq \alpha \tag{5.13}$$

An examination of the two diffusivities for nitrogen and oxygen in air indicates that this is the case, and the Reynolds analogy is valid[2]. The correlations used to calculate the heat and mass transfer coefficients are presented in Appendix A.

Once the gas flow rate to the combustion zone has been calculated, the lithium reaction rate may be calculated. The lithium is assumed to react with the gas quickly as it flows to the combustion zone, unless the chemical kinetics serves to further limit

the reaction rate. The unhindered lithium reaction rate is given by:

$$RR_{Li} = A_{\text{pool}} \sum_i RR_i \tag{5.14}$$

where

$$RR_i = h_m \rho_i R_{s_i} \tag{5.15}$$

where A_{pool} = surface area of the lithium pool

ρ_i = total density of the gas i (mass/containment volume)

R_{s_i} = stoichiometric combustion ratio between lithium and the gas i (mass of lithium/mass of gas)

As described in Chapter 2, the kinetics of the lithium-nitrogen reaction and the presence of oxygen serve to reduce the lithium-nitrogen reaction rate below the gas supply rate. The presence of nitrogen also serves to slightly reduce the lithium-oxygen reaction rate. In LITFIRE, the nitrogen reaction kinetics limit is expressed using a series of curves fit to Ijams' reaction rate measurements. The nitrogen reaction rate is limited to the lower of either the nitrogen flow rate or the kinetics limit:

$$RR_N = h_m \rho_N R_{s_N} \tag{5.16}$$

or

$$RR_N = K(T_{Li}) \tag{5.17}$$

where $K(T_{Li})$ is the experimentally determined kinetics limit.

After the kinetics limit is applied to the reaction rate, the inhibiting effect of the presence of oxygen is accounted for as a function of the oxygen concentration in the gas. The final lithium-nitrogen reaction rate RR'_N is found by multiplying the preliminary rate RR_N, determined from the gas flow rate or the kinetics limit, by an oxygen inhibition factor R_{N_2}. The oxygen inhibition effect was quantified by Gil using data taken from lithium-mixed gas kinetics experiments (see Chapter 2 and Figure 2-13)[1].

$$RR'_N = RR_N \cdot R_{N_2} \tag{5.18}$$

Gil also found that the oxygen reaction rate was slightly inhibited by the presence of nitrogen. The inhibiting effect was quantified and is shown below as a function of the fractions of oxygen F_O and nitrogen F_N present in the gas[1]:

$$R_{O_2} = \left[\frac{1 - F_N}{F_O + F_N}\right]^{0.02} \tag{5.19}$$

The preliminary oxygen reaction rate RR_O, determined by the oxygen flow rate, is multiplied by R_{O_2} to obtain the final reaction rate RR'_O:

$$RR'_O = RR_O \cdot R_{O_2} \tag{5.20}$$

Once the reaction rates have been calculated, the heat generated by combustion is calculated by summing the products of the reaction rates and the heats of combustion (see Table 1.1) of each of the reacting gases:

$$Q_c = RR_N \Delta H_{Li_3N} + RR_O \Delta H_{Li_2O} + RR_S \Delta H_{Li_2O \text{ or } LiOH} \tag{5.21}$$

The empirical expressions used to represent the kinetics limit and the oxygen inhibition factor are presented in Appendix A.

5.2.4 Containment Overpressure and Leakage

Gas leakage from the containment building is calculated as a function of the overpressurization of the containment building:

$$\dot{m} = Km(P_c - P_A)^a \tag{5.22}$$

where $\dot{m}$ is the mass flow rate, m is the mass of the containment gas, and $P_c - P_A$ is the difference between the containment pressure and the atmospheric (outside) pressure. Typical values of the constants are $a = 0.5$ and $K = 2.6 \cdot 10^{-9}$ sec^{-1} psi$^{-0.5}$[2].

5.3 Modeling Options

The basic one-cell version of LITFIRE is capable of simulating a wide variety of spill conditions. The containment volume, height, wall and floor areas, atmosphere, and

material composition may be specified as well as the mass and surface area of the lithium spilled. A number of options are available to cover other accident scenarios and to simulate the lithium pool fire experiments conducted at HEDL (see Chapter 2). Optional reaction geometries include a primary cell containing the lithium surrounded by a larger secondary cell, and a partially insulated pan holding the lithium inside the basic primary cell. A concrete floor and wall for the containment are optional as is a liquid metal-concrete reaction routine. Also, instead of elemental lithium, a lithium-lead eutectic may be selected for the spill with the composition chosen by the user.

Two new options were developed as part of this work: an option to simulate a lithium spill in the presence of a steam-air atmosphere, and an option to simulate a lithium spill and fire inside the plasma chamber of a fusion reactor (with decay heat generation). The development and application of the new options will be described in Chapters 6 and 7, respectively.

In addition to the above options, several options involving the mitigation of lithium fires are available. They are:

1. Containment inert gas flooding
2. Emergency containment space cooling
3. Emergency containment floor liner cooling
4. Aerosol removal
5. Cell gas injection

Each code option is discussed in the following subsections.

5.3.1 Two Cell Option

The two cell option was developed to model the effects of a fire inside a tokamak fusion reactor and to determine its effects on the structural integrity of the torus,

or to represent the encapsulation of the reactor in a subcontainment inside the main containment building[9]. In this option a separate secondary cell with its own material composition, atmosphere and geometry exists surrounding the primary cell. (See Figure 5-1) The provision for a crack between the primary and secondary cells, allowing the exchange of cell gases also exists. The code follows the composition, pressure and temperature of both cell gases during the run. The heat and mass flow paths in two cell LITFIRE are shown in Figures 5-3 and 5-4 respectively.

The gas flow rate between the two cells is calculated as a function of the pressure difference between them. The temperature change of the two cell gases is calculated from the enthalpy of the gas transferred. The composition of the mass of gas transferred is the same as the gas in the cell from which it came.

5.3.2 Pan Option

The pan option was created to model the lithium fire experiments performed at HEDL (see Chapter 2). It models a lithium fire inside a suspended, insulated pan in the primary cell. A diagram of the pan and cell is shown in Figure 5-5. The pan dimensions and composition are user defined and all of the normal mechanisms described in this chapter are used for heat transfer and lithium combustion.

5.3.3 Lithium-Concrete Reaction

The amount of energy released from a lithium-concrete interaction could be even greater than that released from a lithium-air fire (see Table 1.1). Since the lithium would probably fall onto the containment building floor, a lithium-concrete interaction would occur if the floor liner failed. Given the high temperature of the lithium pool, and the corrosiveness of liquid lithium, the failure of the liner is conceivable. Therefore an option was developed to model the reaction of lithium with the concrete floor under the liner. This includes lithium reactions with water driven from the concrete and certain components of the concrete itself. The model was not intended to treat

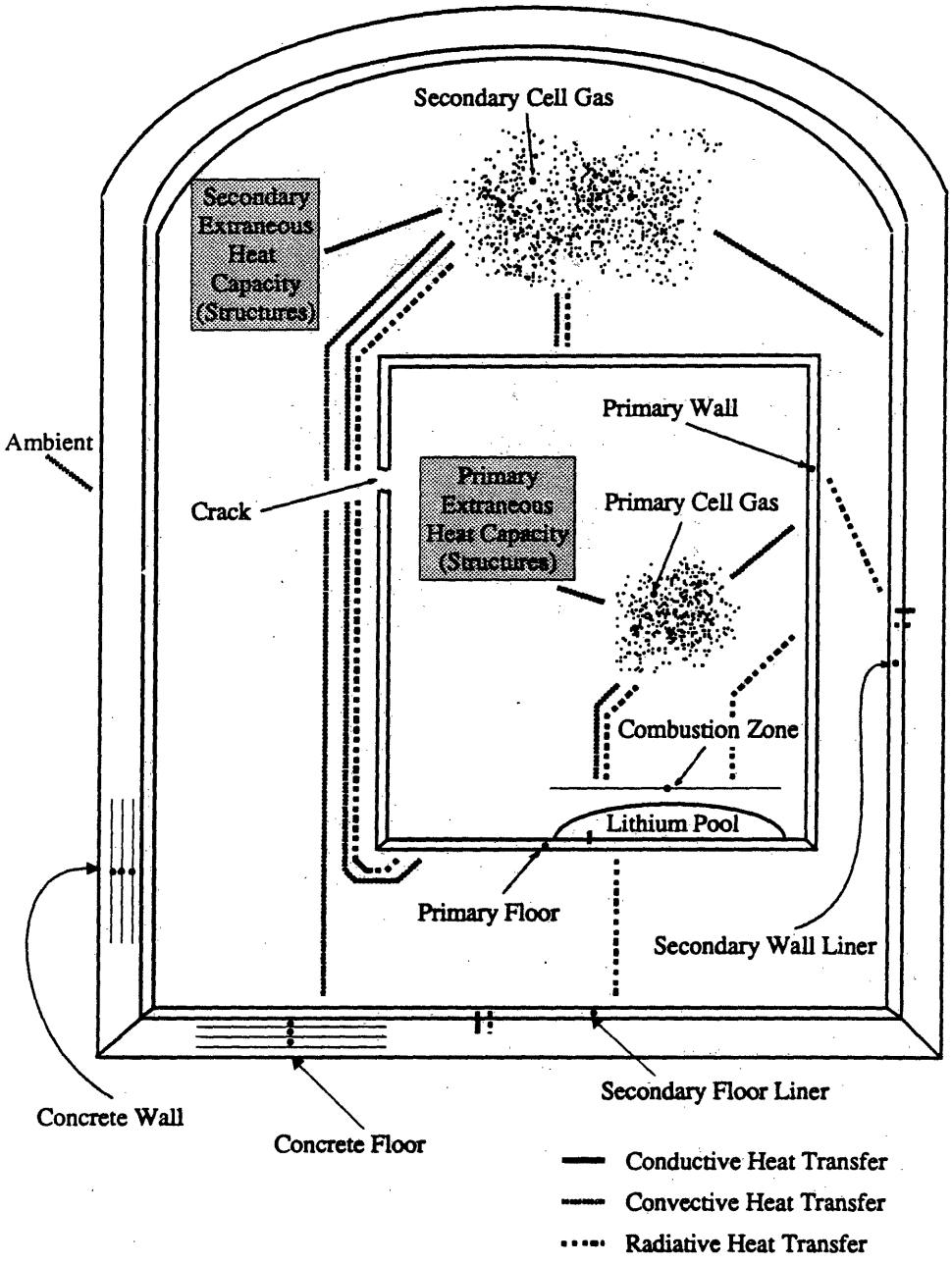

Figure 5-3: LITFIRE two cell option

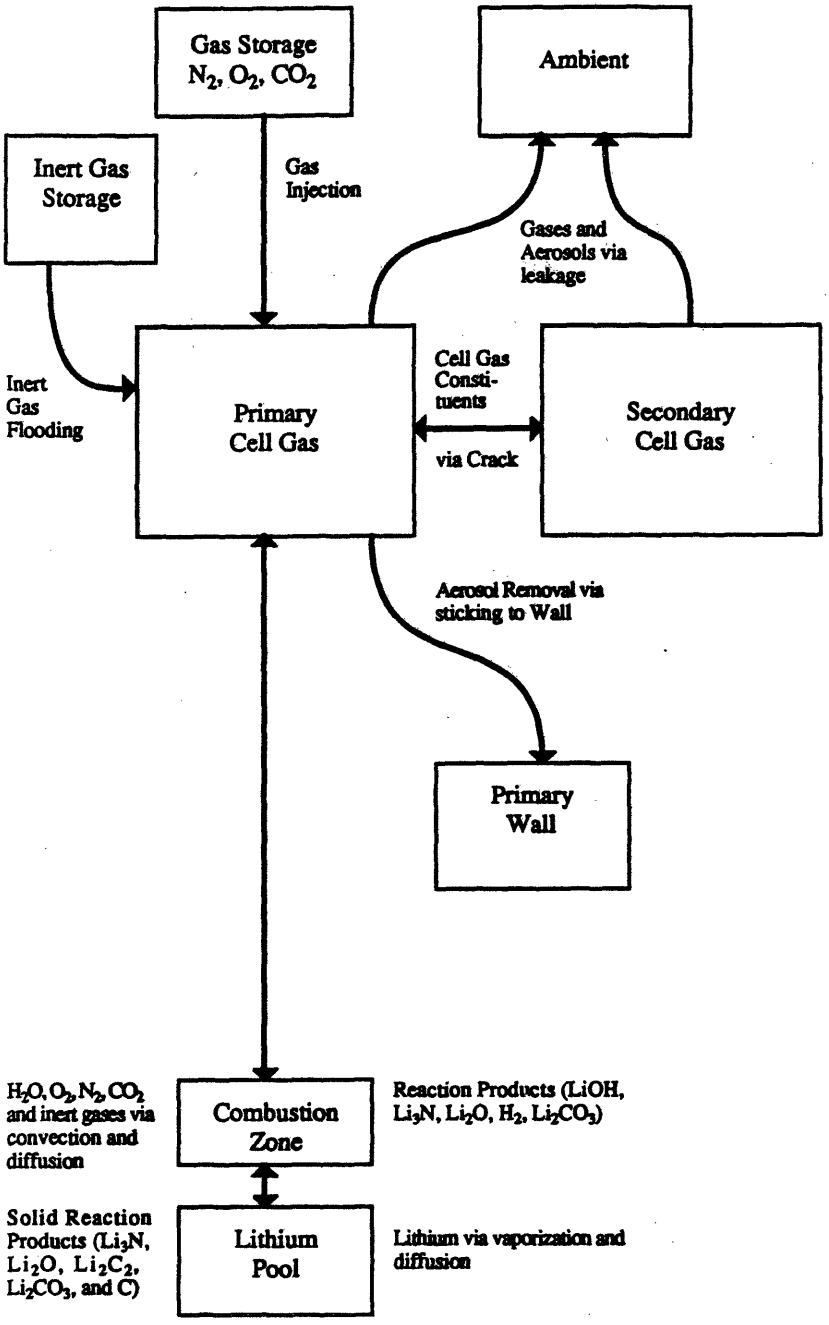

Figure 5-4: Mass flow in LITFIRE two cell option

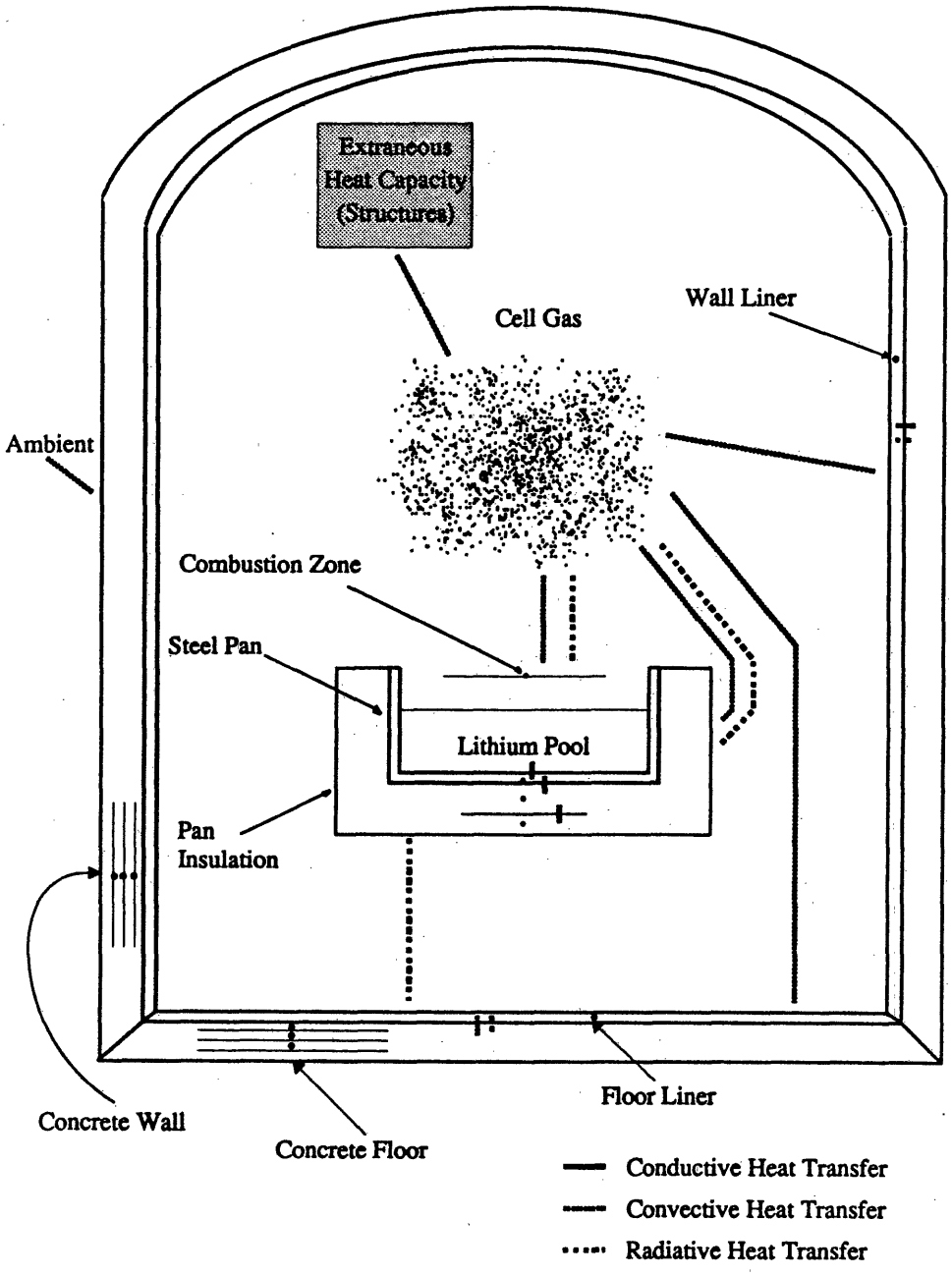

Figure 5-5: LITFIRE pan option

lithium-concrete interactions rigorously, but rather was intended to be a base upon which a more detailed model could be built[9].

In this model it is assumed that the containment floor liner has failed and that the lithium reacts with the solid compounds and the water in the concrete. The reaction is assumed to take place in a concrete combustion zone, a thin layer between the topmost floor concrete node and the bottom of the lithium pool. As the concrete reacts, the heat generated passes into the floor concrete and the lithium pool, and the concrete combustion zone grows by penetrating into the top floor concrete node. Once the reaction starts, the only events that could cause it to stop would be the exhaustion of the lithium supply or the cooling of the combustion zone below the concrete ignition temperature (250°C).

As the composition of concrete could vary fairly widely from one plant design to another, there are a large number of lithium-concrete reactions that are possible. Covering all of them would require a large number of code input variables and would tend to make the model rather complex. Since this is a simple model, it is assumed that only one homogenized lithium-concrete reaction occurs, with an average energy of 620 kJ/mol Li. That value was calculated from HEDL data taken from their lithium-magnetite test LMC-1[9].

However, the lithium reaction with the water driven from the concrete is handled separately. The water is assumed to react with the lithium as soon as it is driven from the concrete. Lacking data on water release rates from heated concrete, empirical data on the amount of water present in the concrete and an imposed exponential time constant are used to determine the release rate. The correlations used to determine the water release rate from the concrete are presented in Appendix A. Other simplifying assumptions are also made in the model[9]:

- The concrete combustion zone is assumed to be much smaller than the top floor concrete node to minimize the perturbation of the floor nodes' properties
- The heat generated by the interaction is transferred only by conduction to either

the top floor node or the lithium pool. All reaction products except hydrogen gas are confined to the concrete combustion zone. The amount of hydrogen released is assumed to be small, so it does not affect the cell gas temperature.

- Water vapor is driven from the top floor concrete node only, and is assumed to react immediately with the lithium pool. The lithium oxide producing lithium-water reaction is assumed.

- The concrete combustion zone is assumed to penetrate into the top concrete floor node at a constant rate during the interaction while the interaction surface area is held constant. The physical properties of the combustion zone are assumed to be the same as those of the concrete.

5.3.4 Lithium-Lead Combustion

This option allows for the substitution of a lithium-lead eutectic in the place of elemental lithium as the source of the fire. All LITFIRE options are compatible with the lithium-lead combustion option except the initial spray fire calculation. The difference between the standard lithium combustion option and lithium-lead combustion lies primarily in the extra limits imposed on the lithium reaction rate for the eutectic. The following discussion of the lithium-lead option is taken mostly from Gilberti[11]. The lithium-lead experiments performed at HEDL and JRC-Ispra are described in Chapter 2 and reference[6].

In general, the lithium-lead reaction rate is limited by the diffusion of lithium from the pool to the combustion zone as well as the gas supply. As seen in Chapter 2, the lithium-lead reaction rate can be much lower than the lithium reaction rate under comparable conditions. In this model the lithium is assumed to dissociate from the lead before reacting with the incoming gases. The lead is assumed to be completely inert. Thus the only influence of the lead upon the reaction rate is its influence on the lithium transport rate to the combustion zone. Since no lithium-lead pool fire

data were available when the model was developed, it was decided to "bound" the problem between a conservative view and an optimistic view[11].

The conservative view is that the eutectic pool is turbulent and well mixed. This model is the same as the basic lithium combustion model except that lithium-lead properties are used instead of lithium properties. The only limit on the reaction rate is the gas flow rate to the combustion zone. This is known as the "turbulent pool model".

The optimistic view is that the pool is not turbulent, and that as the lithium reacted, a thin depleted layer of pure lead would form on top of the pool. The remaining lithium would have to diffuse through this layer before it could react. In this model the depleted layer is assumed to be semi-stable, that is no mixing between the eutectic and the pure lead is assumed to occur. The layer is also assumed to grow in thickness as the lithium in the pool is consumed. This model uses an extra pool node to represent the depleted surface layer and is known as the "layered pool model". This model seems to match the HEDL data better.

5.3.4.1 Turbulent Pool Model

Changes were made to the basic lithium combustion model to account for the use of lithium-lead in only three areas: the lithium pool properties, the pool heat balance and the lithium-nitrogen film thickness.

The lithium pool properties were changed in that lithium-lead properties were used instead. Additionally, the lithium-lead properties are calculated as a function of lithium concentration, so the lithium-lead pool properties are time as well as temperature dependent.

The pool heat balance was modified in that the heat of dissociation of the lithium-lead is subtracted from the pool. Therefore some of the heat transferred from the combustion zone does not arrive at the pool. Since the dissociation process was assumed to be confined to the pool, the combustion zone heat balance is not affected.

The lithium-nitrogen film thickness was modified in that it is directly proportional to the lithium density at the pool surface (see Equation 5.9). Since the presence of lead serves to reduce the lithium atom density, the film thickness is reduced and therefore the heat conduction rate from the combustion zone to the pool is increased.

Another effect that served to reduce the film thickness was the reduction of the lithium vapor pressure. The lithium vapor pressure in lead at a given temperature is equal to the product of the pure lithium vapor pressure at that temperature and the activity of the particular alloy (< 1). The further reduction of the film thickness also increases the heat conduction rate between the combustion zone and the pool.

5.3.4.2 Layered Pool Model

The layered pool model assumes that a depleted surface layer of lead is formed when the lithium reacts and serves to hinder lithium transport to the combustion zone. Even though lead is denser than lithium and would tend to sink to the bottom of the pool, it is assumed that at steady state a thin layer of pure lead would remain at the surface as the lithium reacted.

The layered pool model incorporates the same changes to the pool properties as the turbulent pool model except that the lithium-lead concentration is held constant. As the lithium reacts, the excess lead is assumed to remain at the pool surface, so the depleted lead layer grows over time. The lead layer is modeled as a separate node at the surface of the pool. The eutectic underneath forms a second pool node. The growth rate of the layer is calculated from[11]:

$$m_{Pb}(t) = \int_0^t \frac{1-X}{X} A_p R R_{Li} dt' \tag{5.23}$$

where X is the weight fraction of lithium in the eutectic. The thickness of the layer can then be calculated[11]:

$$d_{Pb} = \frac{m_{Pb}}{\rho_{Pb} A_p} \tag{5.24}$$

The lithium transport rate to the combustion zone is determined by its diffusion rate through the depleted layer. This is calculated from[11]:

$$\dot{m}_{Li} = -D_{Li}\frac{-N_{LiPb}}{d_{Pb}} \tag{5.25}$$

where N_{LiPb} is the lithium atom density in the lithium-lead and D_{Li} is the diffusion coefficient of lithium in lead. In Equation 5.25 the lithium concentration at the surface of the pool is taken to be zero, as that gives the highest possible diffusion rate for a given eutectic composition[11]. The expression for D_{Li} is given in Appendix A[11].

5.3.5 Mitigation Options

The following is a list of options available to evaluate the effectiveness of certain techniques used to attempt to mitigate the consequences of a lithium fire:

- Containment inert gas flooding
- Emergency containment space cooling
- Emergency containment floor liner cooling
- Aerosol removal
- Cell gas injection

Each option allows the user to select additional heat removal mechanisms as desired. The individual options are described below.

Inert gas flooding could be used to mitigate the effects of a fire if it took place in a small space and the lithium combustion caused the depletion of the atmospheric gas. The gas depletion would cause a pressure decrease which would tend to suck in more gas from the ambient. Inert gas flooding could maintain the pressure and thus prevent the influx of air to refuel the fire[2]. In LITFIRE, the temperature of the gas, the mass flow rate and the starting and stopping times are specified.

Emergency space cooling could be used in a containment building to reduce the containment gas pressure in the event of an accident. This would both protect the containment building itself and help prevent the release of containment gases like tritium to the atmosphere. In LITFIRE, the total cooling rate of the gas (in BTU/sec), and the starting and stopping times are specified.

Similar to emergency space cooling, emergency floor cooling could be used in the event of an accident to protect the integrity of the floor liner and perhaps prevent a lithium-concrete interaction. In this option, the total cooling rate of the floor liner and the starting and stopping times of the cooling are specified.

LITFIRE also has the capability to model aerosol removal via sticking to the walls of the building. This is not a fire mitigation system, but as the gas emissivity increases with increasing aerosol concentration, it would serve to reduce the heat transfer rate from the combustion zone to the containment structures during a fire.

Aerosol removal is modeled by defining a "sticking time", the average time required for an aerosol particle near the containment wall to be removed. "Near the wall" is defined as within one inch, and the fraction of aerosol particles removed per second is equal to the fraction near the wall divided by the sticking time[9].

Gas injection is an option designed to simulate the gas injections to the test cell during the HEDL experiments. In those experiments it was occasionally necessary to inject more cell gas into the cell as the original gas was being consumed by the fire and the cell pressure was dropping close to atmospheric pressure. In order to prevent outside air from leaking into the cell, more gas had to be injected. In LITFIRE, the time of each injection, the composition of the injected gas (fraction of oxygen and nitrogen) and the cell gas pressure increase due to the injection may be specified. The injection and the resultant pressure increase is assumed to take place over one minute's time.

Chapter 6

Modeling Lithium Fires in the Presence of Steam

6.1 Introduction

The overall goal of this work was to determine the potential consequences of lithium-steam chemical and thermal interactions inside the reactor containment building of a fusion reactor and to assess the safety implications of the presence of water near the reactor. This included performing the lithium-steam-air reaction kinetics experiments described in Chapters 3 and 4. The other part of the effort was the modification of the LITFIRE code (described in Chapter 5) to enable it to model lithium-steam reactions. This involved the addition of the capability to model two-phase mixtures of steam and water, and the modification of the lithium-nitrogen reaction rates to account for the effect of the presence of steam determined from the results of the kinetics experiments. The modification of LITFIRE is described herein. The modified code was then used to predict the consequences of lithium spills and fires inside the reactor containment building and inside the reactor plasma chamber.

6.2 LITFIRE Modifications

The major changes made to LITFIRE involved the addition of water pool nodes in the primary and secondary cells to model the effect of water condensation and accumulation on the floors of the reactor and the building; the addition of an iterative energy balance routine to determine the temperatures of the cell gases; and the modification of the gas heat transfer coefficients to account for the condensation of steam in the presence of non-condensible gases. Most modifications described herein were developed along the lines of the CONTEMPT code that describes the response of a light water reactor (LWR) containment to loss-of-coolant accidents (LOCA)[13].

6.2.1 Water Pools

The new water pools are illustrated in Figure 6-1. The mass and energy of the liquid water present in each pool is tracked by the model. Mass and energy may be transferred to and from the pools via the pathways indicated in Figures 6-1 and 6-2. Mass transfer takes place via condensation/evaporation or boiling.

Condensation may occur on any of the exposed surfaces in containment or on the surface of the water pool itself. Condensation to or evaporation from the pool surface is a function of the concentration gradient of water vapor from the surface of the pool to the cell gas above it. In LITFIRE the following equation was used to determine the mass transfer rate to and from the pool[13]:

$$\dot{m} = A_{\text{pool}} 18 K_b (x_g - x_b)/x_{am} \tag{6.1}$$

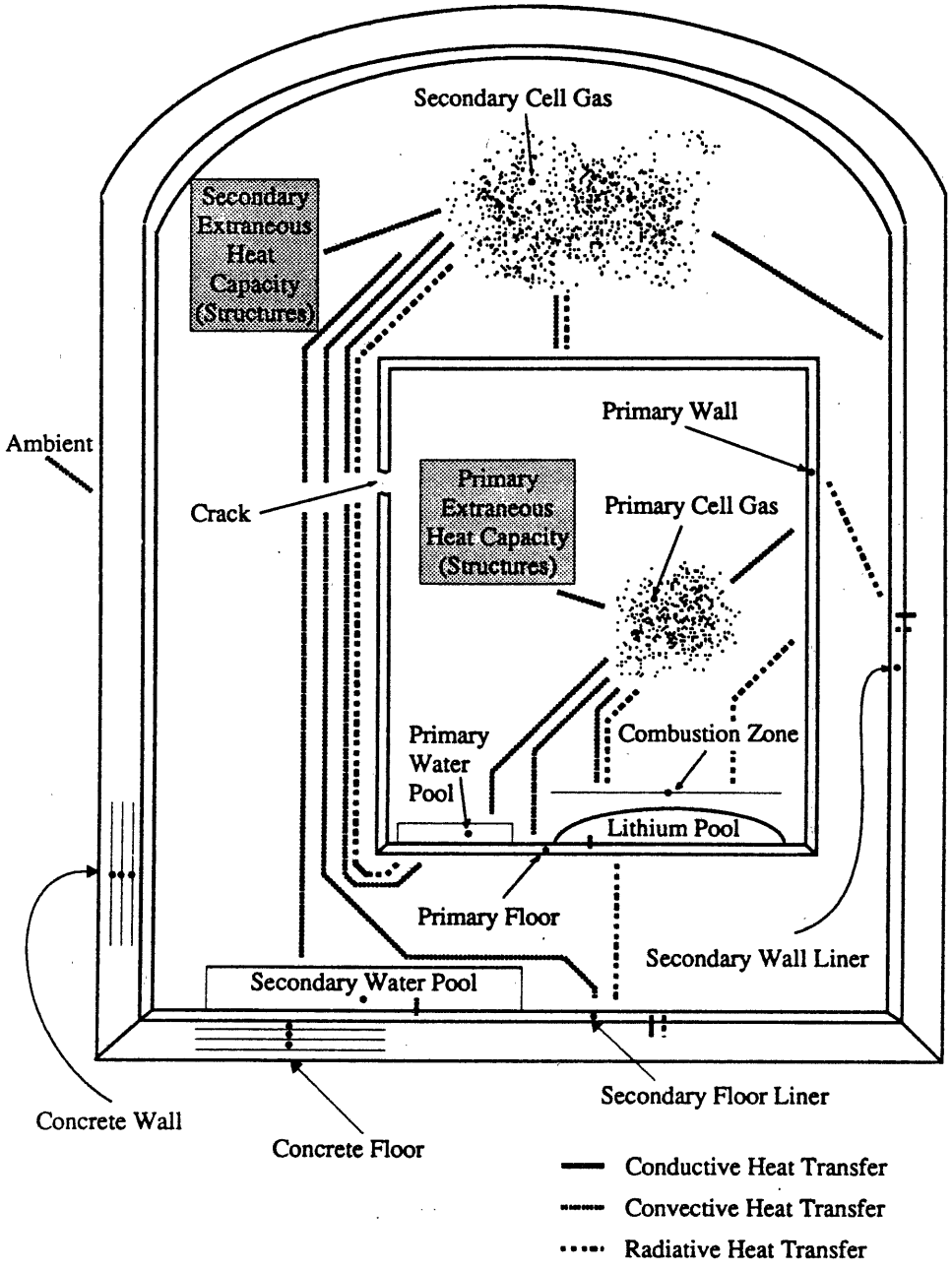

Figure 6-1: Energy flow in modified two-cell LITFIRE

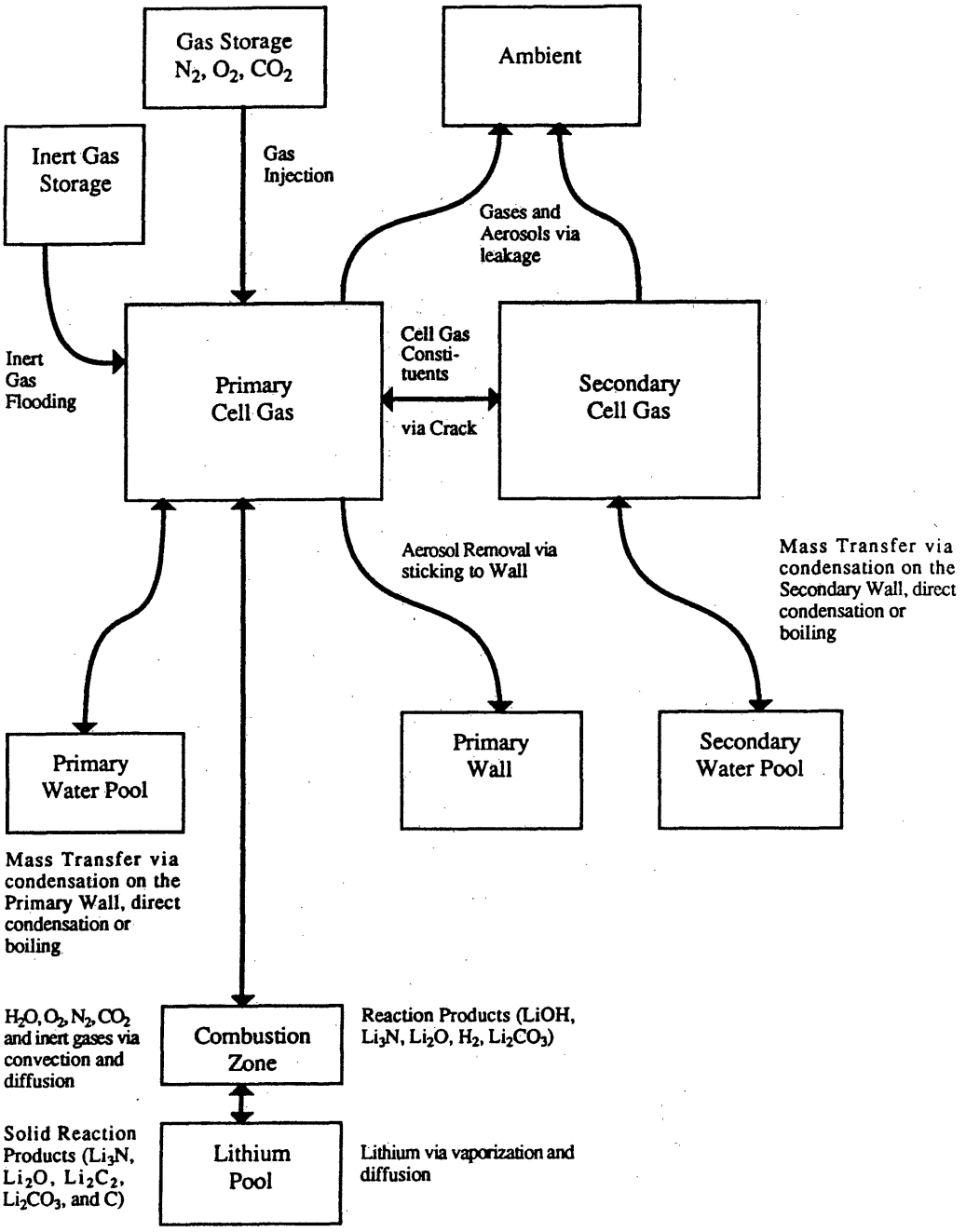

Figure 6-2: Mass flow in modified two-cell LITFIRE

where $\dot{m}$ = mass flow rate

A_{pool} = surface area of the water pool

K_b = mass transfer coefficient (see Appendix A)

x_g = molar fraction of water vapor in the cell gas

x_b = molar fraction of water vapor at the pool-cell gas boundary

x_{am} = logarithmic mean mole fraction of air
used to account for the resistance of the air to mass transfer

The heat transfer to and from the pool via condensation or evaporation is determined as follows:

$$\dot{q} = A_{pool} h_b' (T_g - T_b) + \dot{m} H_g \tag{6.2}$$

where h_b' = sensible heat transfer coefficient

T_g = cell gas temperature

T_b = boundary layer temperature
(assumed to be the water pool temperature)

H_g = specific enthalpy of saturated water vapor
at the cell gas temperature

Values for the heat transfer coefficient h_b' are determined from the Nusselt number relations shown in Appendix A.

Boiling occurs when the specific internal energy of the water pool U_l/M_l is greater than the specific energy of saturated liquid water at the cell pressure. If this is so, the excess mass of liquid water is immediately boiled off into the cell gas. The amount of water boiled off is given by:

$$\Delta m = \frac{U_l - M_l u_{f_p}}{u_{g_p} - u_{f_p}} \tag{6.3}$$

where u_{f_p} and u_{f_p} are the specific energies of saturated liquid water and saturated steam at the cell gas pressure, respectively. The water vapor and liquid mass rates of change due to boiling are:

$$\dot{m} = \pm \frac{\Delta m}{\Delta t} \tag{6.4}$$

The energy rates of change of the cell gas U_v and the water pool U_l due to boiling are calculated as follows:

$$\frac{dU_v}{dt} = \frac{u_{g_p}\Delta m}{\Delta t} \tag{6.5}$$

$$\frac{dU_l}{dt} = -\frac{u_{g_p}\Delta m}{\Delta t} \tag{6.6}$$

Condensation/evaporation does not take place if boiling occurs.

For a single cell analysis, heat transfer from the water pool to the cell floor is determined from the Nusselt number correlation in a manner similar to that used for sensible heat transfer from the water pool to the cell gas. In a two-cell analysis heat transfer takes place from the containment (secondary) water pool to the containment floor liner, but the torus (primary) floor communicates thermally only with the lithium pool directly above it (see Figure 6-1).

6.2.2 Iterative Energy Balance

In the original LITFIRE code, the cell gas temperature is followed like the other structural temperatures, by direct integration of the time rate of change of the temperature over each time step; and with the initial temperature specified by the user. In the case of a steam-air atmosphere, this would not be possible, as the effects of water changing phase must be taken into account. In this option, an iterative energy balance routine is used during each time step to determine the cell gas temperature, based on the total energy and specific volume of the steam-air mixture[13]. Values for the cell gas temperature are guessed and then substituted into the following equation to determine their accuracy:

$$F(T) = U_v - M_{w_v} u_w(T, v) - M_a c_{v_a} T \tag{6.7}$$

where M_{w_v} = mass of water in the cell gas

$u_w(T, v)$ = specific energy of the water
as a function of temperature and specific volume

M_a = mass of non-condensible gas in the cell

c_{v_a} = specific heat of the non-condensible gas

If the error in cell gas energy $F(T)$ is a sufficiently small fraction of the actual cell gas energy U_v, $(5/10,000)$, or the difference in temperature guesses is less than or equal to 0.005°R (0.0028°C), the guess is accepted as the correct gas temperature. The first guess is taken to be the temperature of the previous time step, and the second one is taken to be 0.5°R (0.28°C) higher or lower, depending on the sign of $F(T)$.

6.2.3 Heat Transfer between Structures and the Cell Gas

Modifications had to be made to the heat transfer coefficients between the cell gas and the containment structures to account for the presence of water vapor. The Uchida condensing steam heat transfer coefficient is used as a function of the mass ratio of non-condensible gas to steam[14]. If the structural temperature is less than the saturation temperature, the heat transfer rate for superheated steam conditions is given by:

$$\dot{q} = h_u A(T_s - T_w) \tag{6.8}$$

or (in British units):

$$\dot{q} = \frac{1}{1800} A(T_v - T_w) \tag{6.9}$$

whichever is greater, where h_u = Uchida heat transfer coefficient

A = surface area of the structure considered

T_s = saturation temperature
based on cell water vapor partial pressure

T_w = structural temperature

T_v = cell gas temperature

The $\frac{1}{1800}$ in Equation 6.9 is the lowest value of the Uchida heat transfer coefficient allowed (for a air-steam ratio of at least 50:1, in Btu/sec-ft^2-°F). For saturated conditions Equation 6.8 is used. The steam partial pressure is calculated as a function of the steam specific volume and the cell gas temperature T. Because of the large specific volume of the steam, the steam pressure can often be lower than the saturation pressure at the cell gas temperature and therefore the steam would be effectively superheated. Thus Equation 6.9 is the one often used to calculate the heat transfer rates. When $T_w > T_s$, heat is transferred between the wall and the gas as governed by the product of Grashof and Prandtl numbers (see equations in Appendix A).

Mass transfer to the liquid water pool via condensation is a function of the heat transfer rate as shown below:

$$\dot{m} = \frac{\dot{q}}{H_{fg}} \tag{6.10}$$

where H_{fg} is the specific enthalpy of vaporization for water at the cell gas temperature. Mass is transferred via condensation if the cell gas is superheated or saturated and the structural temperature is less than the saturation temperature. If the structural temperature is greater than the saturation temperature, heat is transferred without mass transfer.

6.2.4 Modification of Cell Gas Emissivity

In the original LITFIRE, the cell gas emissivity is determined as a function of the amount of combustion product aerosols generated by the fire (see Section 5.2.2.1). In

the case of a steam-air atmosphere, the emissivity must be modified to account for the presence of water vapor, which exists as polar, non-symmetrical molecules. These molecules absorb and emit radiation, as opposed to non-polar, symmetrical molecules such as N_2 or O_2, which do not contribute to the cell gas emissivity. To model the effect of the water vapor, the containment was assumed to be a hemisphere of gas radiating to an element at the base of the hemisphere and the solution of Hottel and Egbert was used to determine the emissivity of a hypothetical system at one atmosphere total pressure[12]. Their solution at 1200°R (667 K) was fitted to a curve using a least squares method:

$$\epsilon_{w1} = \begin{cases} 0.37(p_w L)^{0.67}, & \text{for } p_w L \leq 0.5 \\ 0.28 + .11 \ln(p_w L), & \text{for } p_w L > 0.5 \end{cases} \tag{6.11}$$

where p_w is the partial pressure of water in atmospheres, and L is the beam length (usually taken to be one-fourth the containment height) in feet. For open, relatively empty areas, the actual beam length was used for L to reflect the fact that heat could be radiated from one end of the cell to another. A temperature of 1200°R (667 K) was taken as a typical cell gas temperature based on previous calculations using LITFIRE. However, the variation of ϵ_{w1} with temperature is fairly small in that range, for typical values of $p_w L$ (~ 10). The actual emissivity of the steam-air mixture is then determined by considering the case in which the total pressure is not one atmosphere. Taking a linear approximation of Hottel and Egbert's solution[12]:

$$\epsilon_{wa} = 0.7(p_w + p)\epsilon_{w1} \tag{6.12}$$

where p is the total pressure in atmospheres. The actual cell gas emissivity is then taken to be the sum of the steam-air mixture emissivity and the combustion product aerosol emissivity (Equation 5.3).

$$\epsilon_g = \epsilon_{wa} + \epsilon_{g_c} \tag{6.13}$$

This equation is valid if the steam and the aerosols do not have overlapping absorbtion band structures. Since the aerosols are solids, they are considered to be gray bodies

and thus their emissivities are independent of radiation wavelength. The emissivity of the steam is a function of radiation wavelength, with high values at some wavelengths and values of almost zero at others[15]. That would indicate that Equation 6.13 is not valid. However, ϵ_{g_c} is limited by the code to a maximum value of 0.04 in order to match experimental results from fires in dry atmospheres[11]; the presence of steam causes the emissivity of the cell gas (without aerosols) to be on the order of 0.3. Thus the real effect of Equation 6.13 is to include the relatively small influence of the buildup of aerosol particles in the atmosphere over time; it would not significantly overestimate the total emissivity of the cell gas plus the aerosols.

6.2.5 Humidity and Steam Injection

Steam may be present in the reactor containment originally, through the humidity in the air, or may be injected into the containment during an accident. In the new version of LITFIRE (Mod 7), the initial humidity of each cell may be specified independently, which will determine the amount of water vapor initially present in the cell as:

$$M_{w_{vi}} = \eta \frac{V_c}{v_g} \tag{6.14}$$

where $M_{w_{vi}}$ = initial mass of water vapor present in the cell
η = fraction of 100% humidity
V_c = cell volume
v_g = specific volume of saturated water vapor at the cell gas temperature

Steam may be injected over any time period of the execution of the code. The mass flow rate and enthalpy of the steam are specified, and the rates of change of the mass of steam and cell gas energy due to steam injection are calculated as follows:

$$\frac{dM_{w_v}}{dt} = \dot{m}_s \tag{6.15}$$

$$\frac{dU_v}{dt} = \dot{m}_s H_s \tag{6.16}$$

where $\dot{m}_s$ is the mass flow rate of the injected steam and H_s is the specific enthalpy of the injected steam.

6.2.6 Reaction Kinetics and Experimental Verification

The reaction rates of oxygen and nitrogen are not limited only by the mass transfer rate to the reaction site, but also by the kinetics of the reaction. As described in Chapter 5, the maximum reaction rate of nitrogen and lithium as a function of temperature was determined experimentally and was incorporated into the old version of LITFIRE (Mod 4) as an additional limit[1]. The inhibition of the lithium-nitrogen reaction by the presence of oxygen, and the slight inhibition of the lithium-oxygen reaction by the presence of nitrogen were also determined experimentally and incorporated into the code as factors which reduce the reaction rates[1].

Since the oxygen and nitrogen reaction rates were found to be lower than would be expected from the mass transfer limit, it was postulated that the steam reaction rate could be limited by the lithium temperature and/or the presence of the other gases. Furthermore, the presence of steam could affect the reaction rates of oxygen and nitrogen. The results of the lithium-steam-air and lithium-steam-nitrogen kinetics experiments presented in Chapter 4 showed that indeed the presence of steam served to catalyze the lithium-nitrogen reaction at low temperatures and that the lithium-steam reaction was somewhat inhibited by the presence of oxygen.

The catalytic effect of the presence of steam on the lithium-nitrogen reaction rate was incorporated into the new version of LITFIRE. The kinetics limit on the lithium-dry nitrogen reaction rate as a function of the lithium temperature is now multiplied by the steam catalytic factor C_{H_2O}. Values of C_{H_2O} were determined for both nitrogen and air (20% oxygen) (see Equations 4.9 and 4.10). In the code, the catalytic factor as a function of the oxygen content of the atmosphere is determined by interpolation between the two values of C_{H_2O}

The inhibition of the steam reaction rate by the presence of oxygen was also determined from the experimental data and incorporated into the code. The inhibiting effect of the presence of oxygen is shown in Table 4.3, where it can be seen that the steam reaction rate in the presence of air was about 70% as fast as in the presence of nitrogen only. The inhibiting effect of oxygen is modeled in the code by assuming that the reduction of the steam reaction rate is proportional to the oxygen content in the atmosphere, that is:

$$RR'_S = RR_S \left(1 - 0.3\frac{F_{O_2}}{0.2}\right) \tag{6.17}$$

where RR'_S = final (inhibited) steam reaction rate

RR_S = initial (uninhibited) steam reaction rate

F_{O_2} = molar fraction of oxygen present

After the steam reaction model was installed into the code, it was tested against the results of two of the HEDL pool fire experiments involving steam: LPS-1 and LAM-2. LPS-1 was a test using a 75% steam-25% argon atmosphere, and LAM-2 was a test using a moist air (14% humidity) atmosphere (see Chapter 2). The results of the comparisons are shown in Figures 6-3–6-11.

6.2.6.1 The LPS-1 Test

Figures 6-3 and 6-4 show that LITFIRE predicted the combustion zone (flame) and lithium pool temperatures of LPS-1 fairly well, although both were somewhat underestimated at the end of the run. That was due to the fact that LITFIRE determined that all of the lithium had been consumed in about 4000 seconds. That can be seen in Figure 6-5 where the hydrogen concentration in the cell gas serves as an indicator of the cumulative amount of lithium that had reacted. It can be seen that LITFIRE overpredicted the reaction slightly and thus ran out of lithium before the experiment actually did.

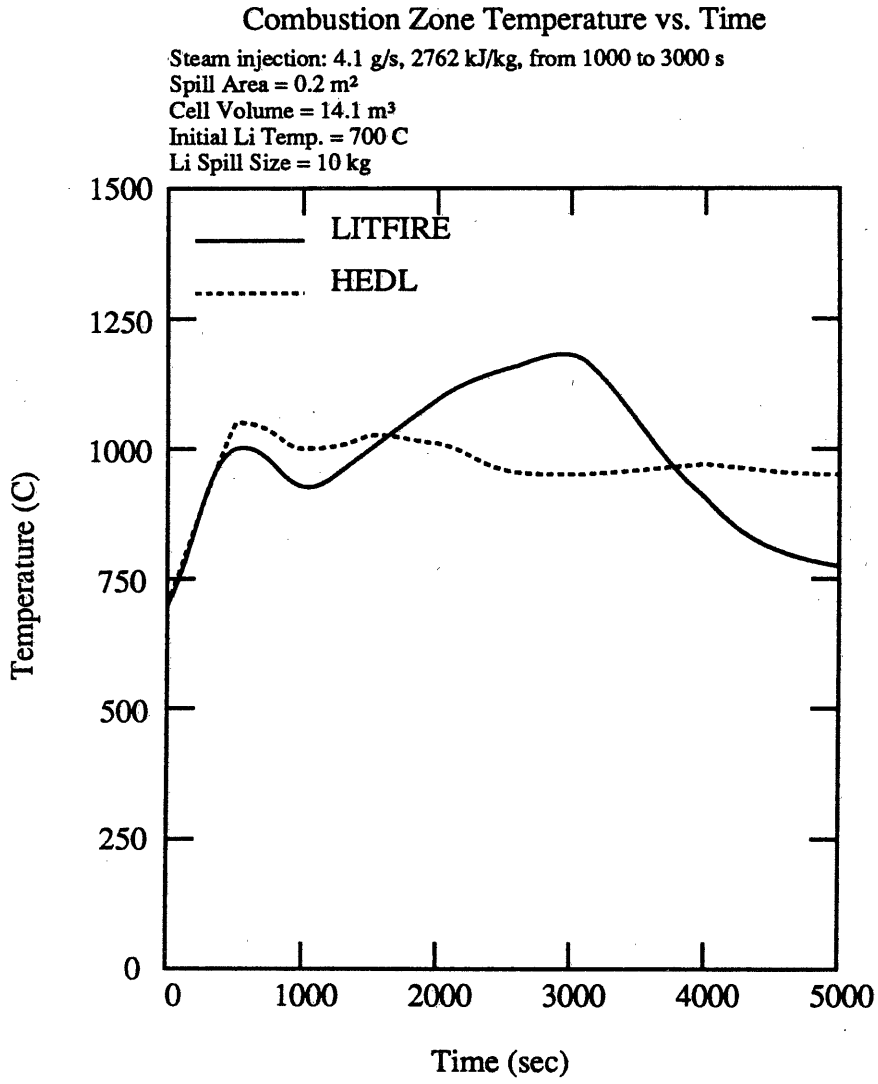

Figure 6-3: Test LPS-1 combustion zone temperature

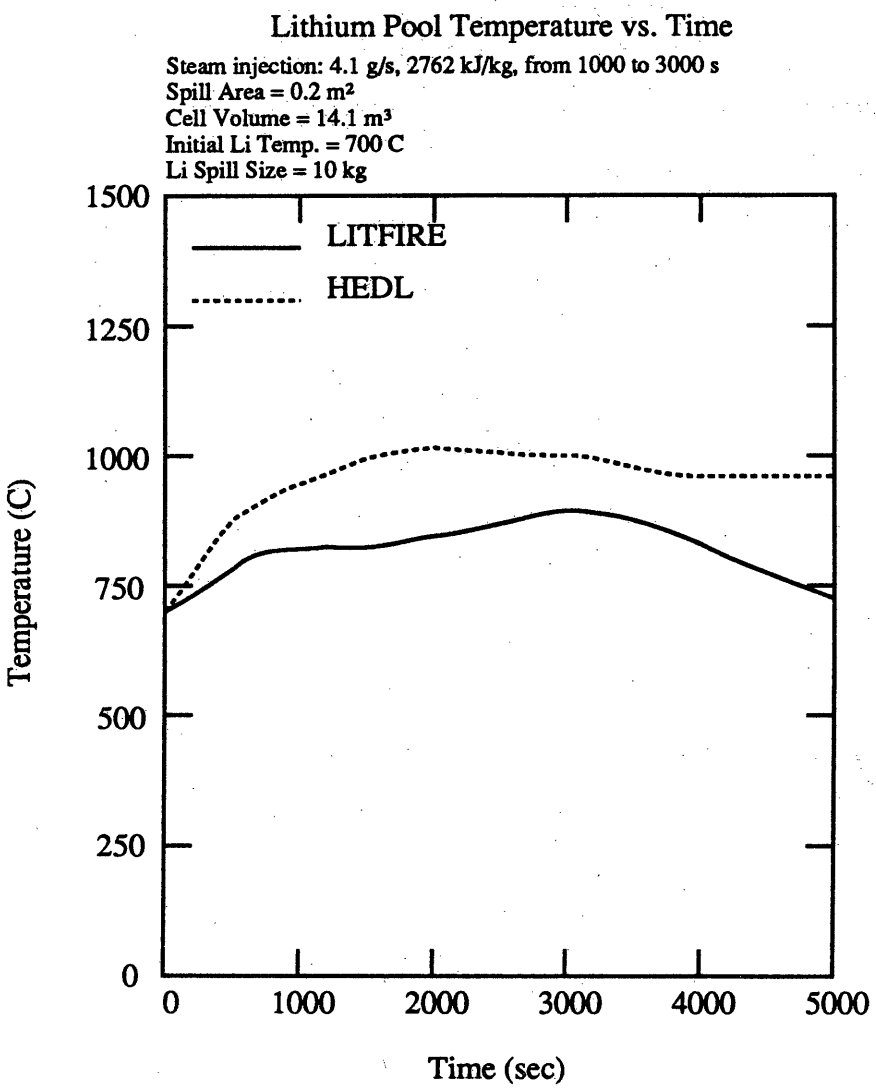

Figure 6-4: Test LPS-1 lithium pool temperature

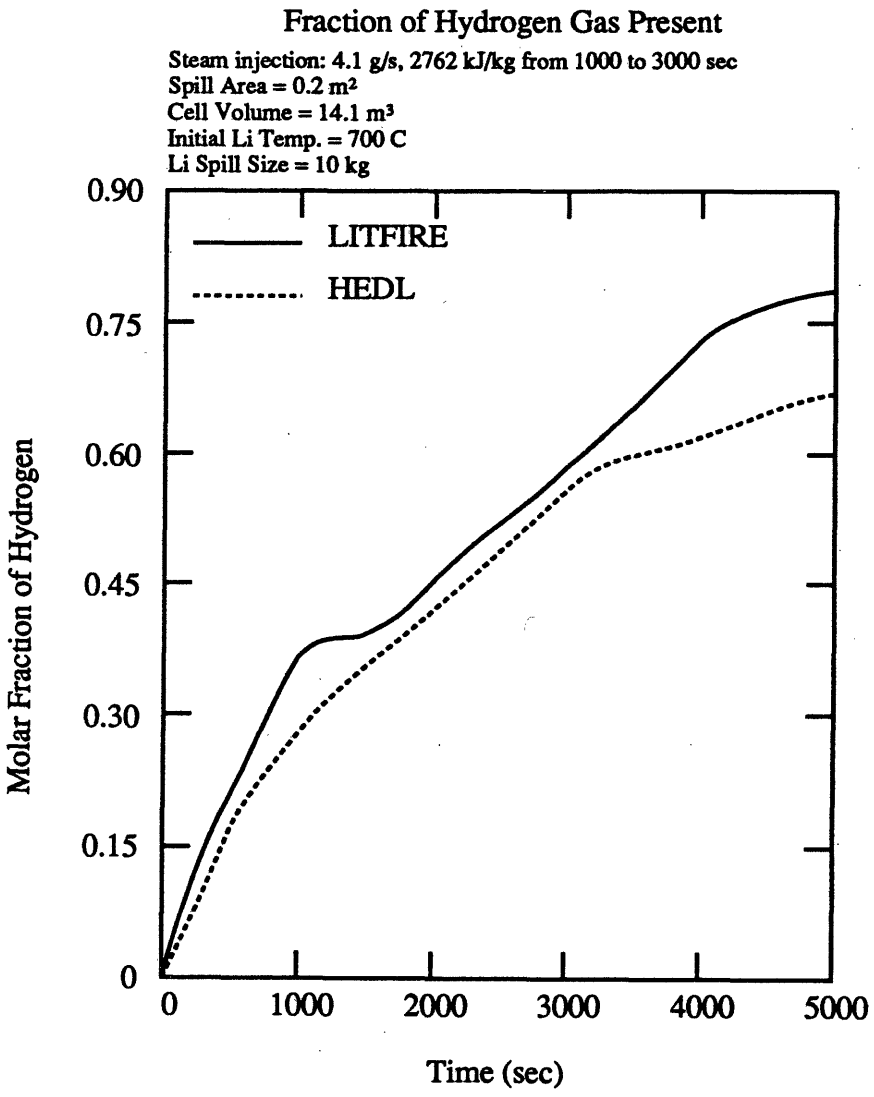

Figure 6-5: Test LPS-1 hydrogen gas molar concentration

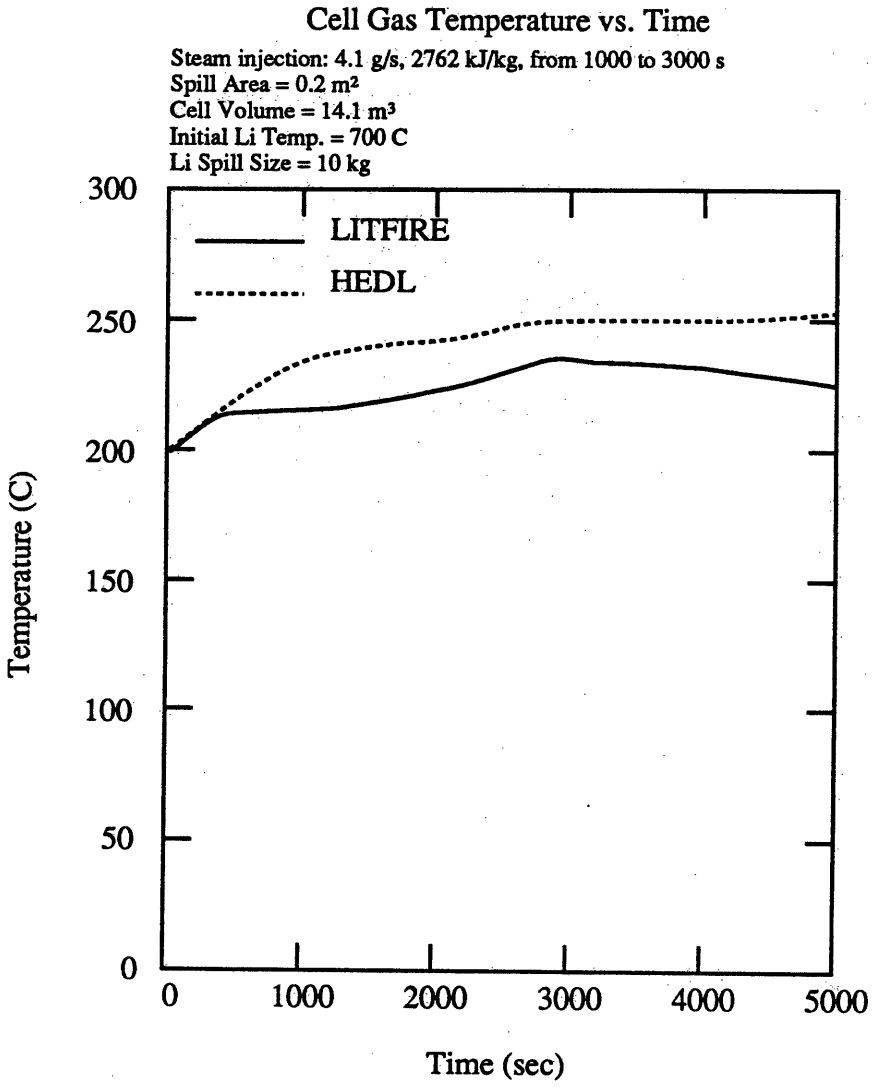

Figure 6-6: Test LPS-1 cell gas temperature

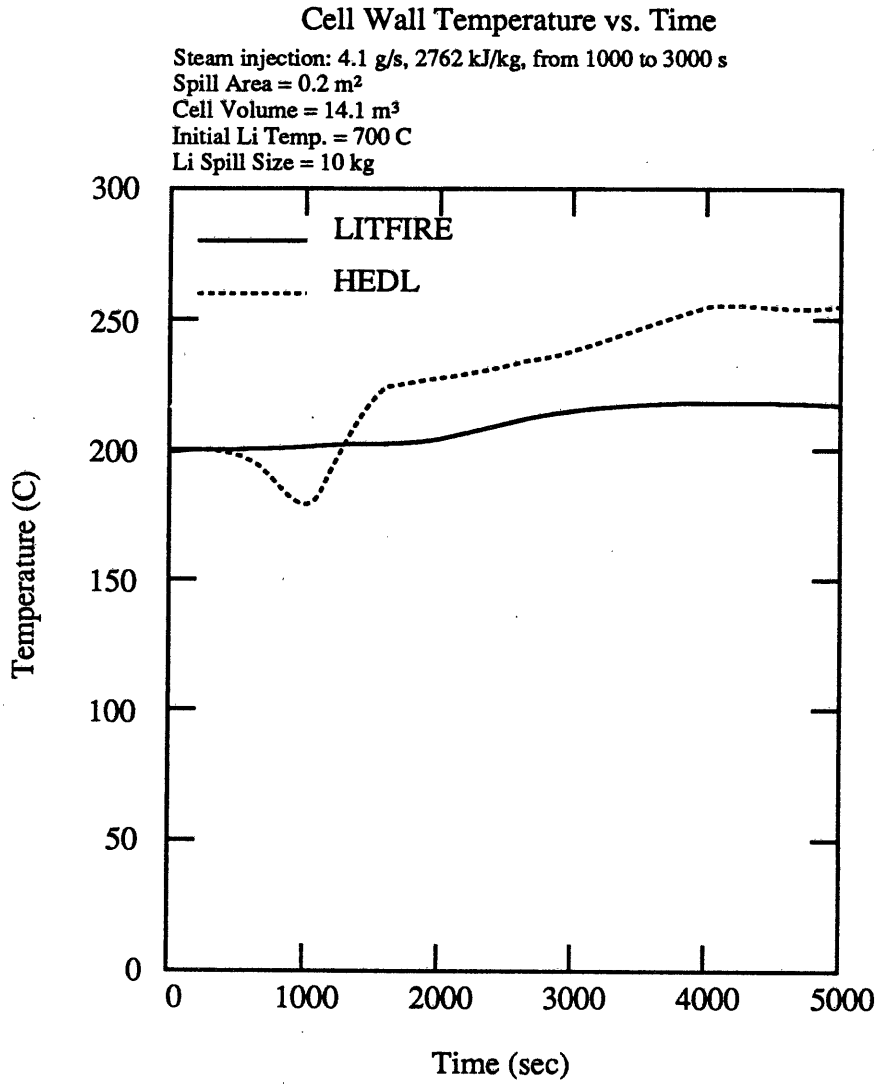

Figure 6-7: Test LPS-1 cell wall temperature

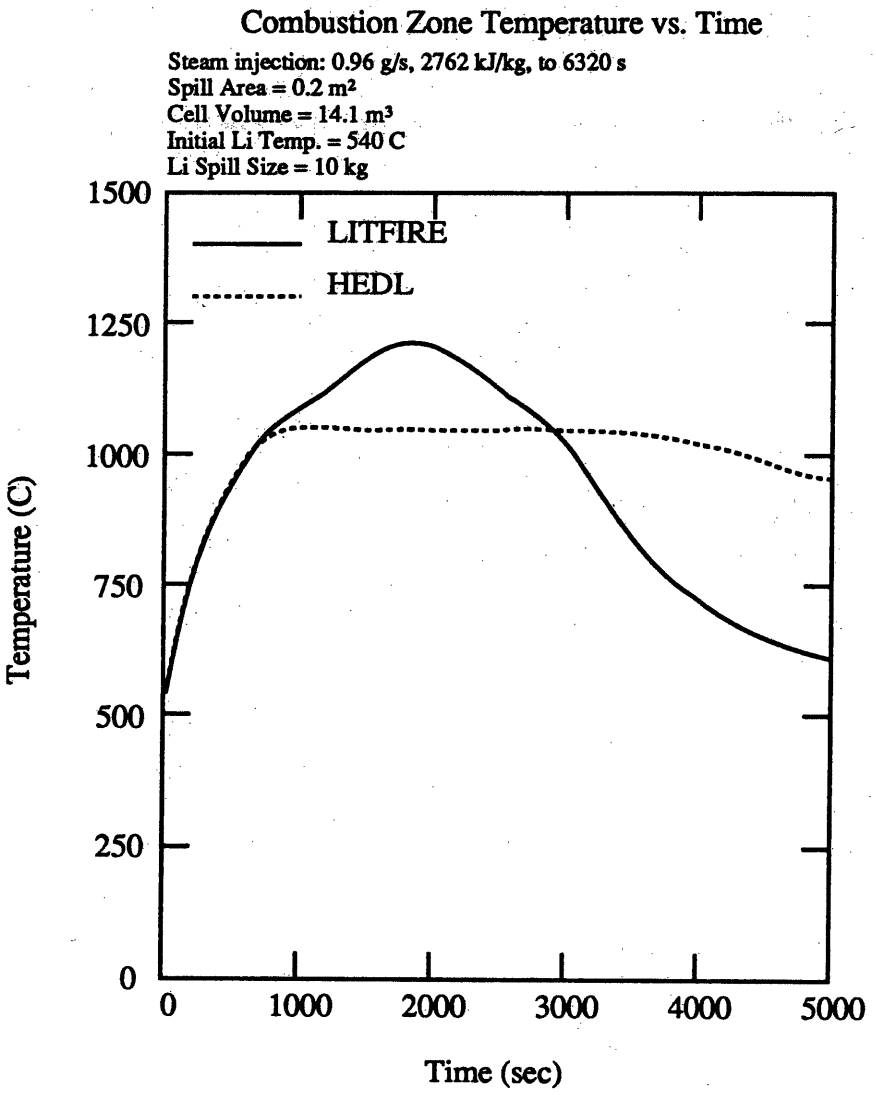

Figure 6-8: Test LAM-2 combustion zone temperature

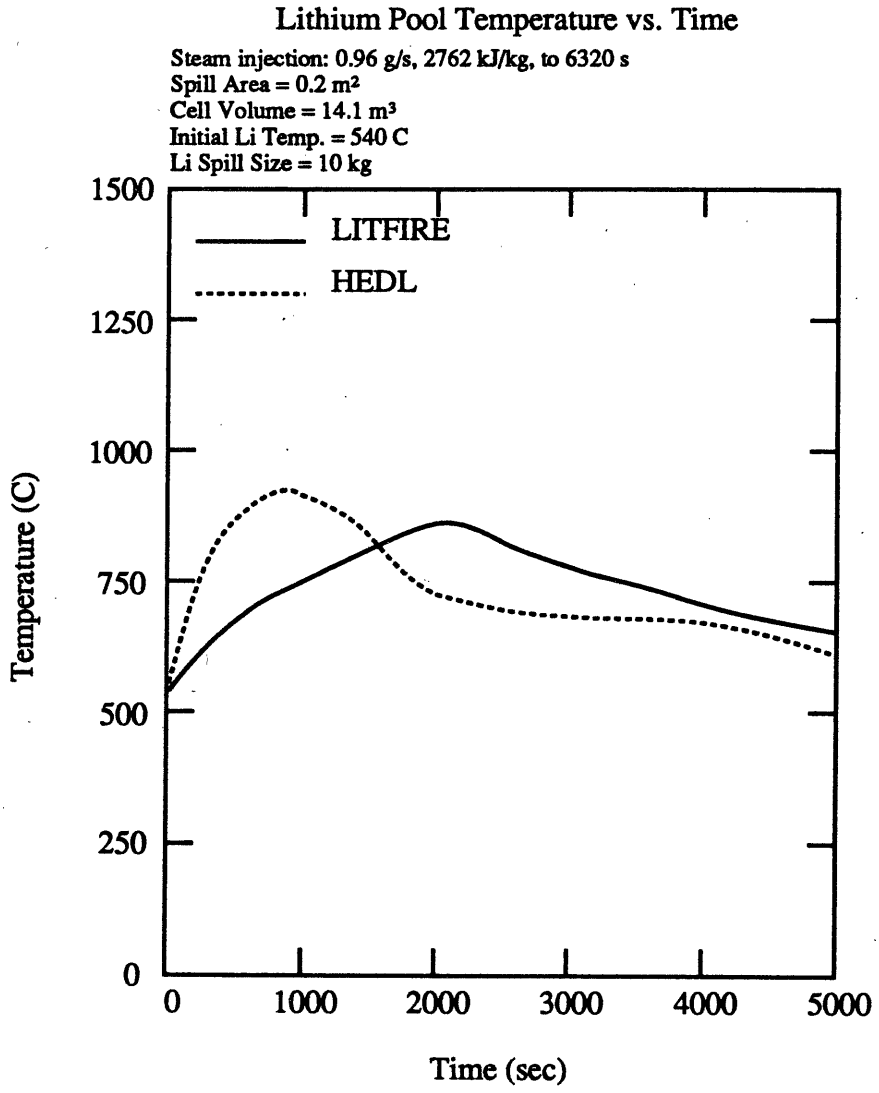

Figure 6-9: Test LAM-2 lithium pool temperature

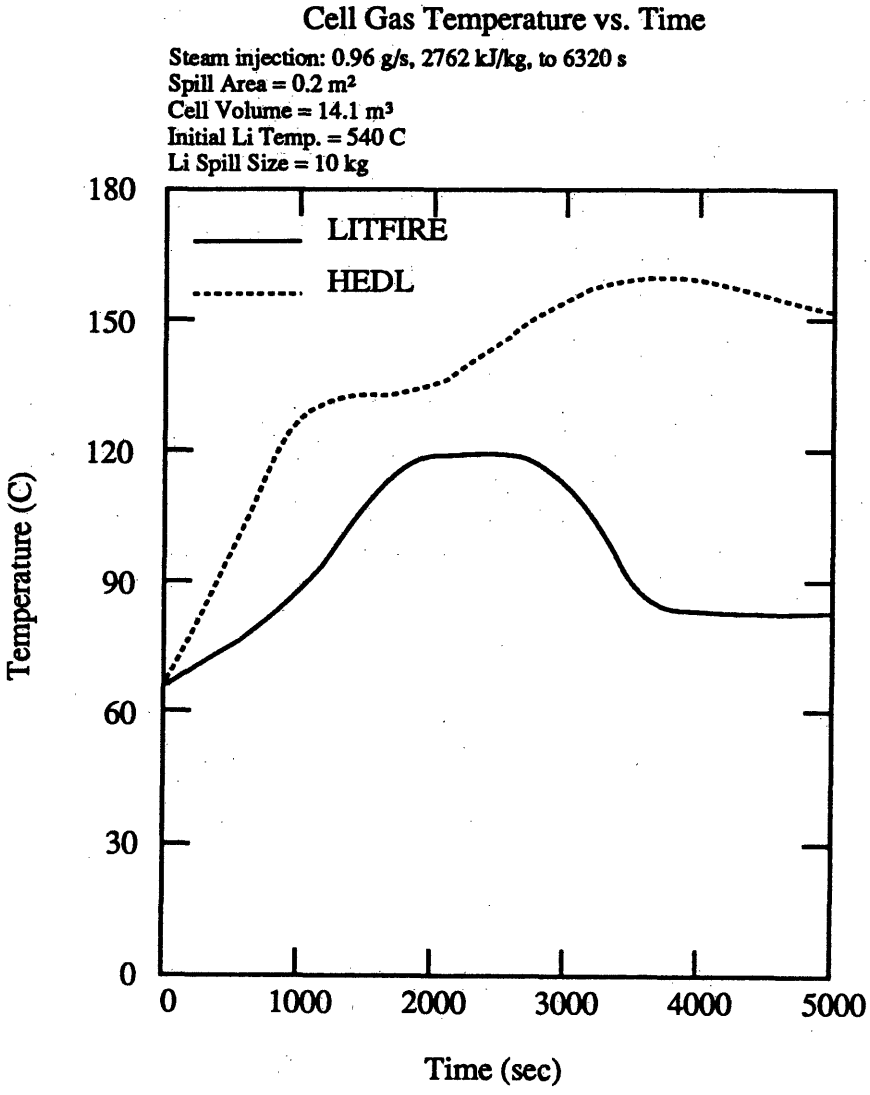

Figure 6-10: Test LAM-2 cell gas temperature

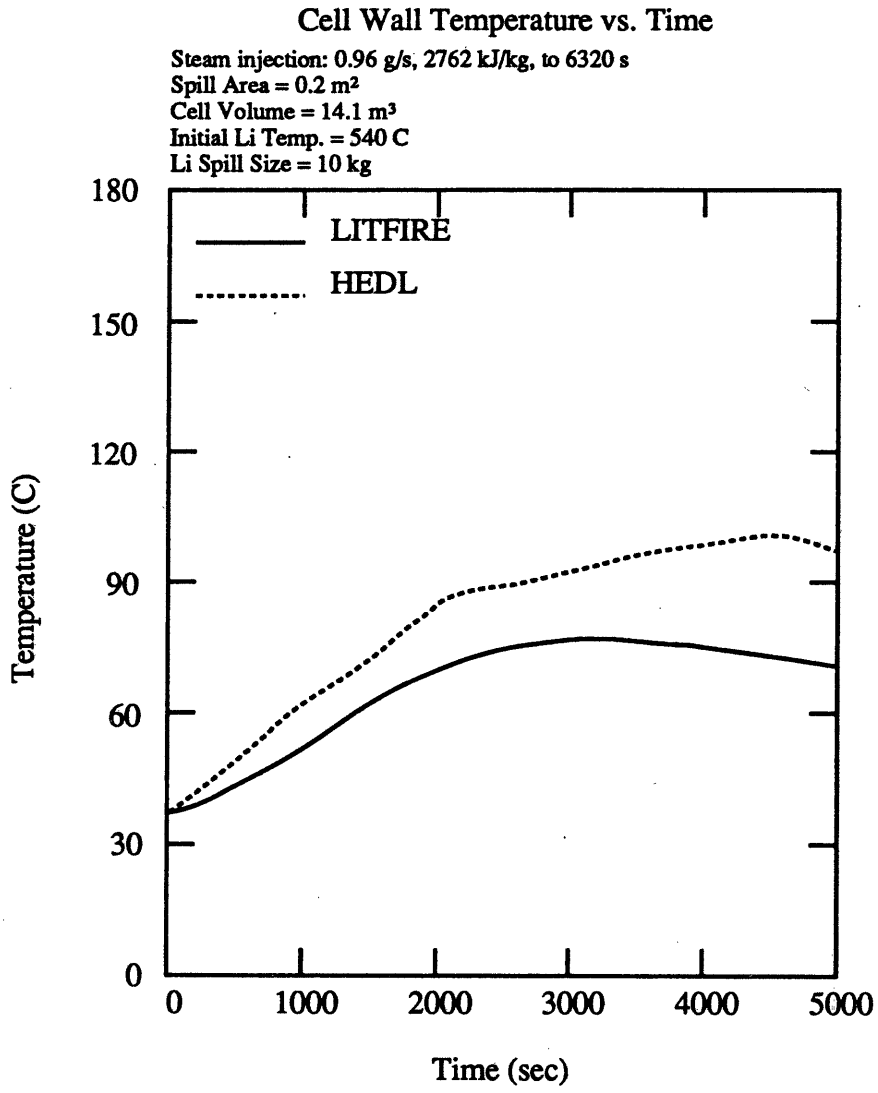

Figure 6-11: Test LAM-2 cell wall temperature

Figures 6-6 and 6-7 show the cell gas and cell wall temperatures, respectively. An examination of the HEDL data reveals that the temperature drop between the cell gas and the cell wall was rather small, about 15°C. Other mixed gas tests like LAM-2 had shown much greater differences. That would suggest that the steam was enhancing the heat transfer rate between the wall and the gas, even though the wall temperature remained above saturation throughout the experiment and condensation could not occur. Under those (superheated) conditions, LITFIRE uses the same heat transfer correlations as it does for an all non-condensible atmosphere. During the calibration of the code, it was found that they did not produce accurate results—the temperature difference between the gas and the wall was predicted to be about 60°C. Therefore it was necessary to increase the heat transfer correlation coefficient (see Table 5.2) between the wall and the gas from 0.13 to 0.8 (to reduce the temperature difference), and to reduce the coefficient between the wall and the ambient from 0.07 to 0.015 (to maintain the same total heat loss rate of the cell) to increase the accuracy of the prediction. Finally, the LITFIRE predictions were fairly good, albeit both temperatures were somewhat underpredicted. In the future it may be desirable to accurately determine the effect of superheated steam upon the heat transfer coefficient and incorporate it into the current model.

6.2.6.2 The LAM-2 Test

Figures 6-8 and 6-9 show plots of the combustion zone and lithium pool temperatures of the LAM-2 moist air test. It can be seen from the combustion zone temperature that LITFIRE again overpredicted the lithium reaction rate, as it determined that all of the lithium had been consumed in about 3000 seconds. Before the fire went out, however, the prediction of both the combustion zone and lithium pool temperatures were accurate. It should be noted that the comparison of the lithium pool temperatures used the center of the lithium pool from the HEDL data, as that is the temperature represented by LITFIRE. This was lower than the maximum pool

temperature measured near the surface.

The cell gas temperature is shown in Figure 6-10 and the wall temperature in Figure 6-11. The effect of the early termination of the fire by LITFIRE can be seen in the plot of the gas temperature. After the fire goes out, the combustion zone ceases to exist and no longer radiates heat to the cell gas; thus the gas temperature begins to drop off. The prediction of the wall temperature was more accurate, although it too dropped off somewhat after the lithium had been consumed. The heat transfer coefficients used to simulate test LAM-2 were the same as those used normally by LITFIRE, further suggesting that the presence of a high concentration of steam was the reason for the significant increase in the heat transfer between the cell gas and the cell wall in LPS-1.

6.3 Consequences of Lithium Fires in Steam-Air Atmospheres

Calculations were performed to determine the consequences of the presence of steam and air in the reactor containment in the event of a lithium spill and fire. Steam was assumed to be present in these cases as a result of initial humidity in the atmosphere and also as a result of a hypothetical steam line break. These results of these cases were then compared to calculations performed without humidity or steam injection to determine the effects of the steam on the pressure and temperature profiles of the containment.

6.3.1 Initial Conditions

Calculations were performed for three groups of accidents. In the first group the lithium was assumed to spill onto the floor of the containment of a hypothetical fusion reactor plant. A one-cell geometry (Figure 6-12) was used for these cases. Containment geometry and initial conditions are given in Table 6.1.

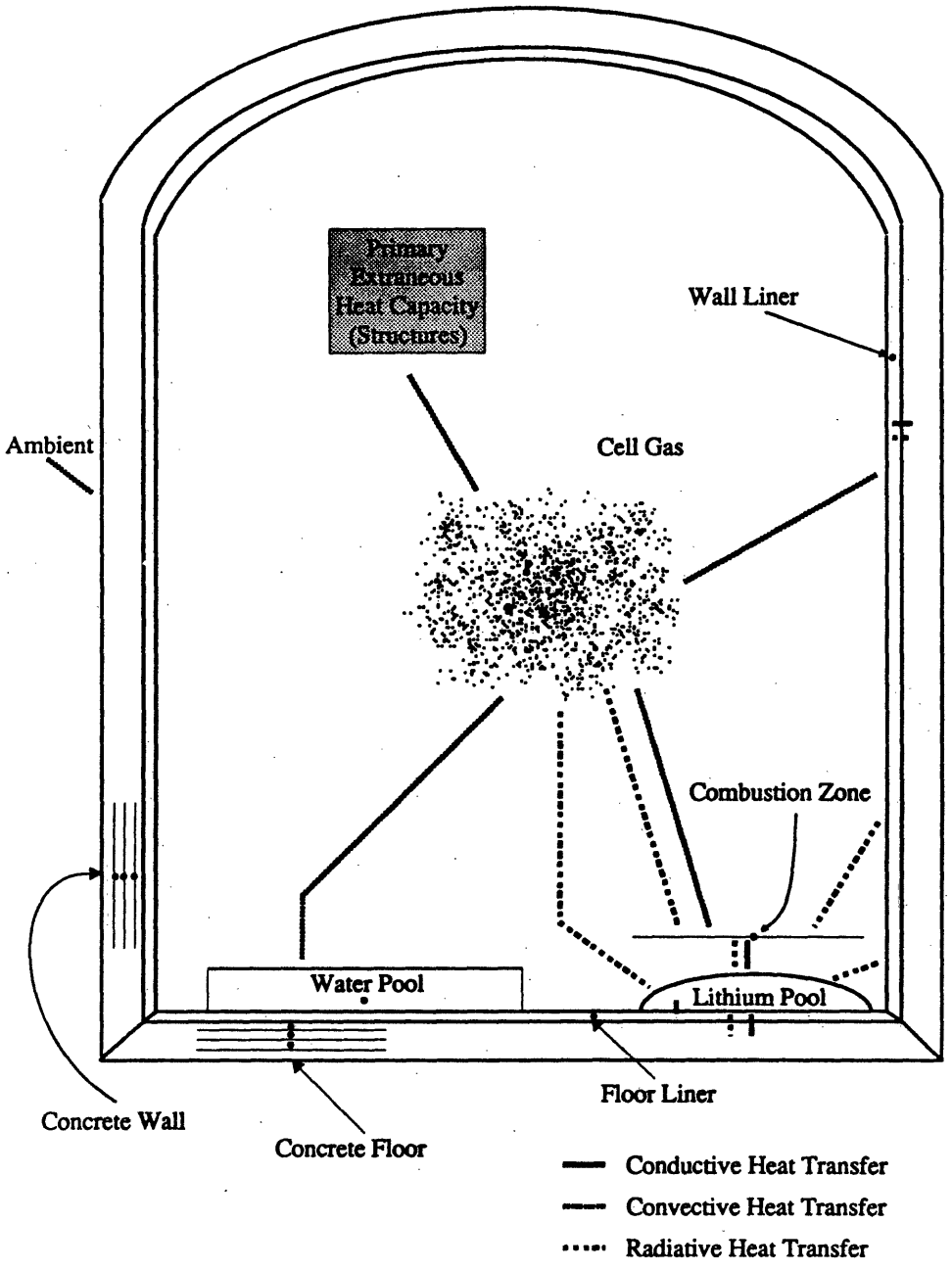

Figure 6-12: One-cell LITFIRE with steam option

Table 6.1: Containment geometry and initial conditions, first group of calculations

Lithium mass spilled:	22,000	kg
Lithium pool area:	1000	m^2
Spray fire fraction:	0	%
Containment volume:	250,800	m^3
Containment height:	45	m
Floor area:	5485	m^2
Wall area:	17,480	m^2
Ambient temperature:	25.5	°C
Gas pressure:	101.4	kPa
Gas composition:	Air	
Steel liner thickness:	0.63	cm

This group consisted of three cases, one performed with 70% humidity and no steam injection; one with humidity and steam injection from 600 to 4000 seconds into the accident at a rate of 4.53 kg/sec at 2727 kJ/kg (corresponding to a small leak in the secondary steam system); and one with no humidity or steam injection.

The second group of calculations was performed using the same containment building as the first but using the two-cell geometry to simulate the effects of a spill and fire inside the vacuum torus. A crack was assumed to exist in the wall of the inner cell, allowing the exchange of cell gases. The inner cell geometry and initial conditions are given in Table 6.2. The containment (outer cell) initial pressure and temperature were similar to those in Table 6.1.

Two calculations were performed in this group, one with 70% humidity in the outer cell (containment building); and one with dry air. In both cases the initial pressure in the inner cell (torus) was zero.

In the third group of calculations it was decided to determine the effects of steam injection into the containment building during a lithium fire inside the vacuum torus. The geometry and initial conditions were the same as in the second group of calculations (see Tables 6.1 and 6.2), but steam was injected into the outer cell for 4.5 seconds at the beginning of the calculation at a rate of 680 kg/s at 2875 kJ/kg (corresponding to a main steam line break with emergency shutoff)[16]. Two calculations were performed, one with humidity and steam injection and one without. The dry case was the same one that was performed in the second group.

6.3.2 Results of the First Group

The results of the first group of cases are shown in Figures 6-13–6-19. The effects of the steam on the lithium combustion can be seen in Figure 6-13, as the time to consume the lithium increased slightly and the maximum combustion zone temperature decreased from about 1250°C to about 1200°C. Similar observations can be made by inspecting Figure 6-14 for the pool temperature history. These effects were

Table 6.2: Inner cell geometry and initial conditions, second group of calculations

Cell volume:	872	m^3
Cell height:	4.9	m
Floor area:	105	m^2
Wall area:	572	m^2
Lithium mass spilled:	10,000	kg
Wall and Floor temperature:	550	°C
Gas pressure:	0	kPa
Wall and Floor thickness:	0.6	cm
Crack area:	100	cm^2

due to the increased cell gas emissivity, which increased the heat transfer rate from the combustion zone to the cell gas. The effect of the additional energetic reaction (6595 kJ/kg-Li consumed, compared to 8856 kJ/kg-Li for oxygen and 1952 kJ/kg-Li for nitrogen) was minimal due to the relatively small amount of water vapor present. The slight increase in combustion time was due to the lower lithium reaction rate as the reaction rate of lithium with nitrogen slows as the lithium pool temperature decreases.

The steam injection to the containment had no apparent effect on the combustion of the lithium since injection did not begin until 600 seconds into the accident and the total amount of steam injected during combustion was small compared to the amount of water vapor initially present in the containment as humidity (approximately 4000 kg of water vapor in a containment volume of 250,800 m^3 and 70% humidity).

The humidity and steam injection did have a significant effect on the heat transfer inside the containment building. As shown in Figure 6-15, the maximum gas temperature was much higher when steam was present than when the atmosphere was dry. This was caused by the higher emissivity of the cell gas which greatly enhanced the radiative heat transfer from the combustion zone. The cell gas emissivity was approximately 0.3 with humidity and 0.005 (initially) without. It can be seen in Figure 6-15 that the gas temperature increased rapidly during combustion and levelled off afterwards when humidity was present. In the case where steam was being injected into the containment, the containment gas temperature had increased to the point where the steam injected was at a significantly lower temperature (approximately 140°C) than the cell gas. This meant that the steam was actually cooling the gas slowly, as can be seen in the figure.

The effect on the containment gas pressure is shown in Figure 6-16. As was to be expected from Figure 6-15, the cell gas pressures were much higher when steam was present than when it was not. The maximum containment pressure reached was approximately 250 kPa, just as lithium combustion stopped. This compares with a

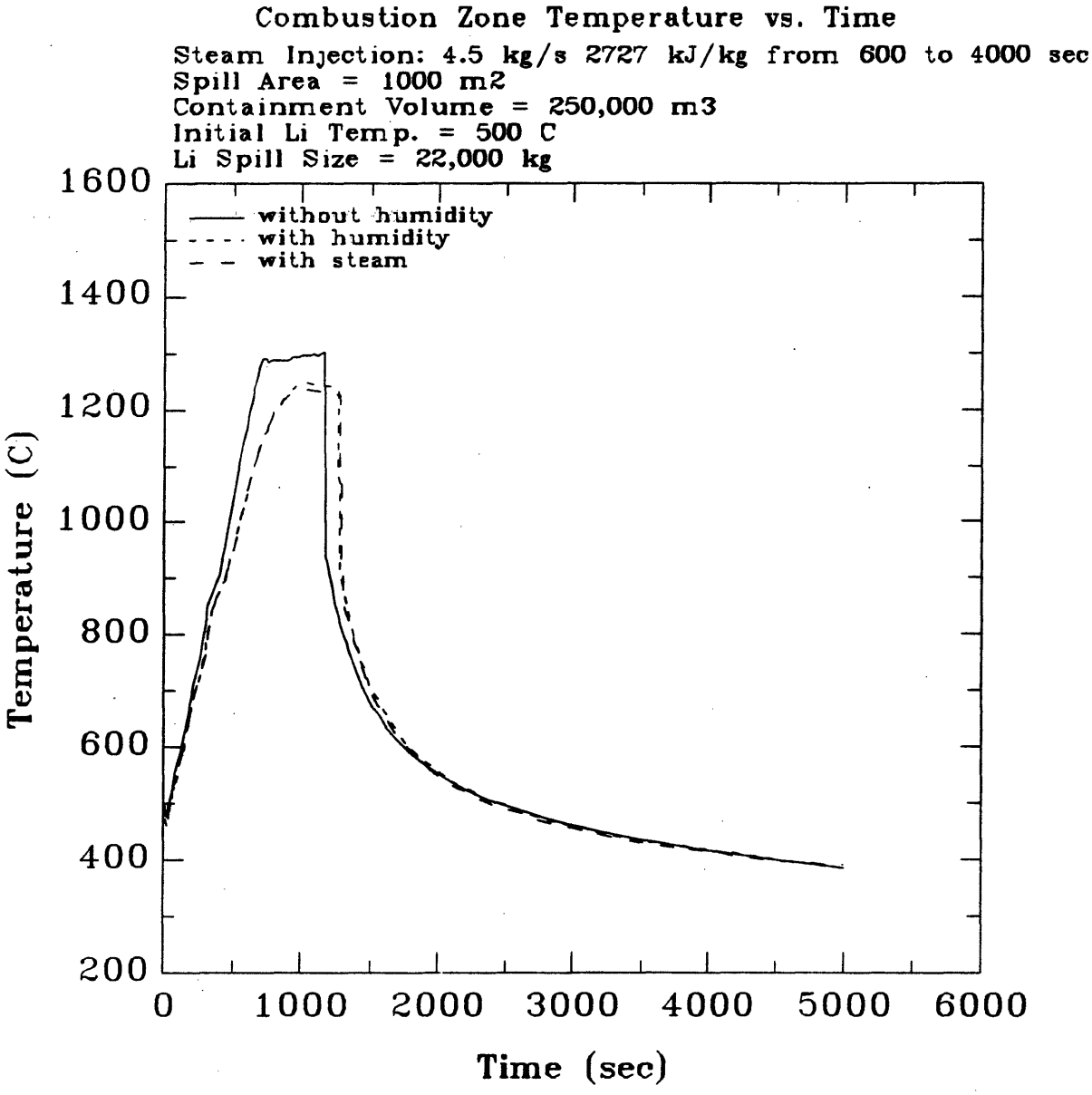

Figure 6-13: Combustion zone temperature versus time, one cell geometry

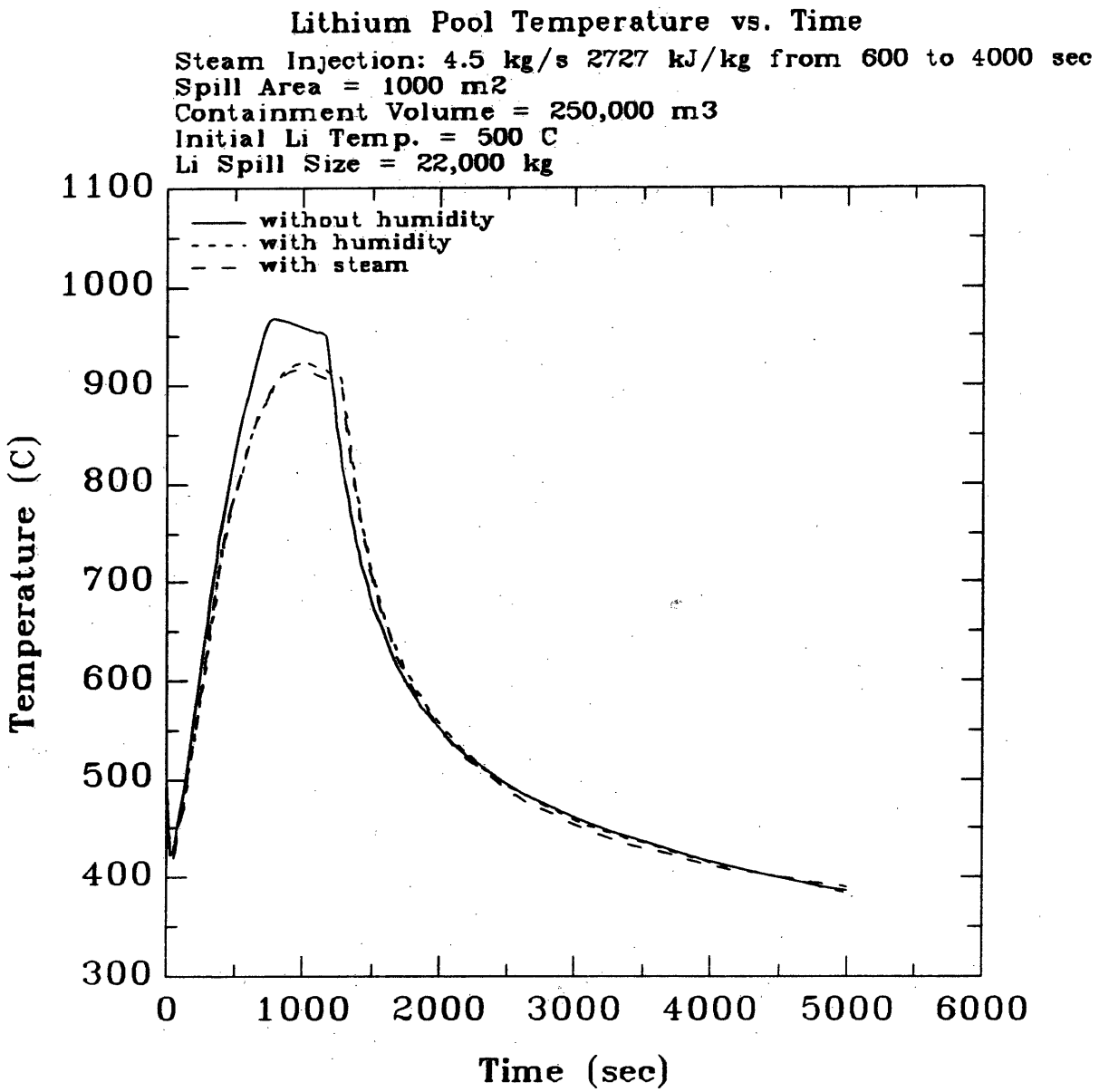

Figure 6-14: Lithium pool temperature versus time, one cell geometry

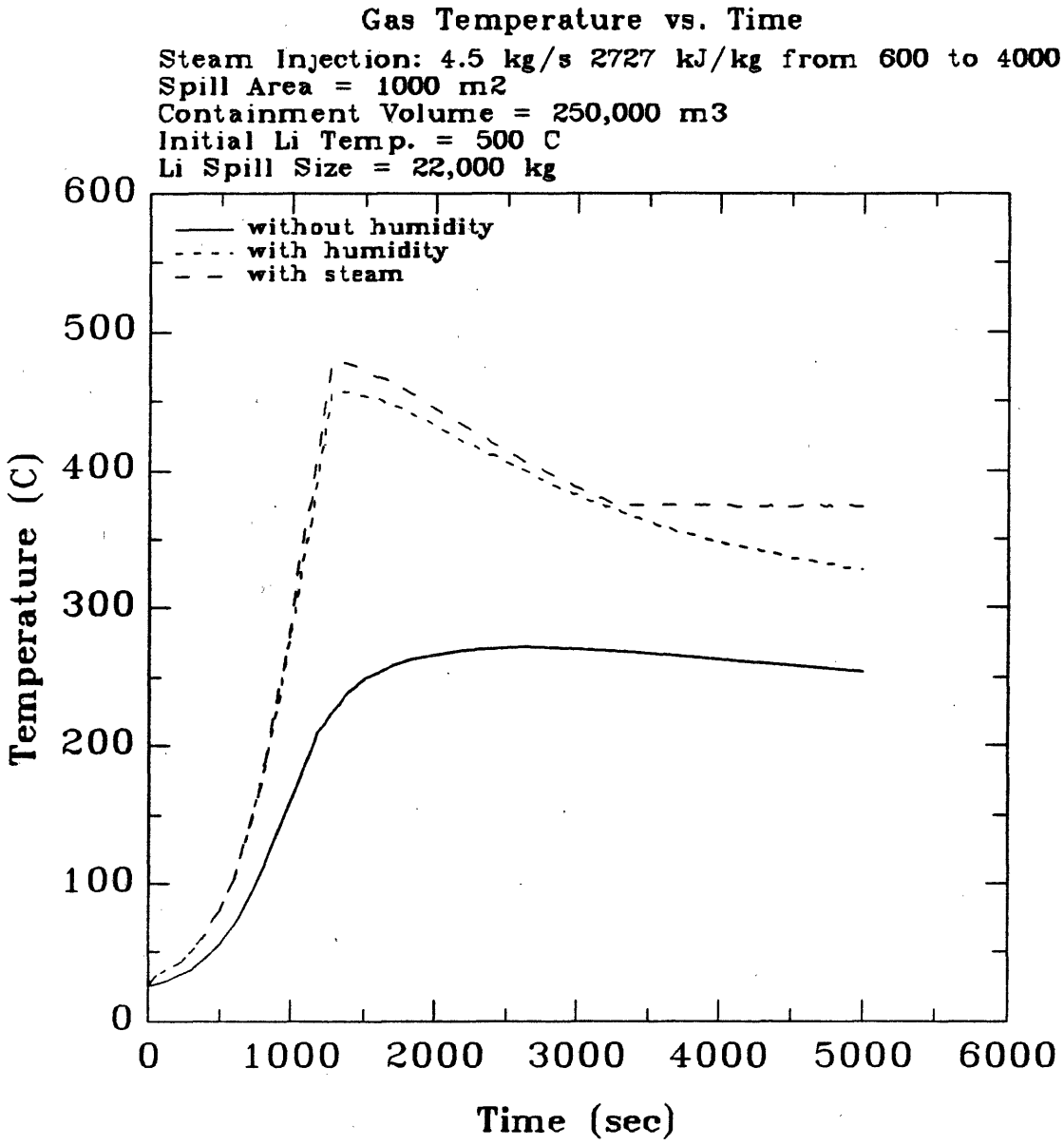

Figure 6-15: Cell gas temperature versus time, one cell geometry

maximum pressure of 170 kPa with a dry atmosphere, roughly a factor of two in containment overpressurization. The steam injection reduced the pressure by cooling the gas, but the addition of extra mass actually served to increase the gas pressure. The pressure was reduced to 230 kPa at the end of the steam injection period (4000 seconds).

The effect of the changes in the gas heat transfer properties can be seen in Figure 6-17. The maximum wall temperature was reached at the end of the combustion time in all three cases. This was due to the radiative heat transfer from the lithium pool and combustion zone. After the lithium was consumed the sources of heat were removed. The wall temperature then decreased as heat was lost to the surrounding concrete. The maximum wall temperature was slightly lower when water vapor was present, since the increased emissivity of the cell gas served to increase the amount of heat radiated to the gas instead of the wall.

The containment floor temperature closely followed the lithium pool temperature, as shown in Figure 6-18. In all the steam and humidity cases the maximum temperature was approximately 875°C, while in the dry case it was about 950°C. After the lithium had been consumed, the floor was cooled by the cell gas.

Figure 6-19 shows the molar fraction of hydrogen gas in the containment building. This is a matter of concern, as the hydrogen could explode if a sufficient amount of it accumulated in the containment during an accident. The maximum concentration reached, with a spill size of 22,000 kg was 0.2 mole percent. This is lower than the concentration needed for an explosion (a minimum of 4.0 mole percent in dry atmospheres and more when steam is present). In the presence of unlimited water vapor, the amount of hydrogen produced should be proportional to the amount of lithium consumed. Thus in the event of a much larger spill, or a smaller containment volume, the hydrogen might reach a higher concentration.

It should be noted that the results presented here represent those from a "typical" accident that may occur in a commercial reactor. Parametric studies of accident con-

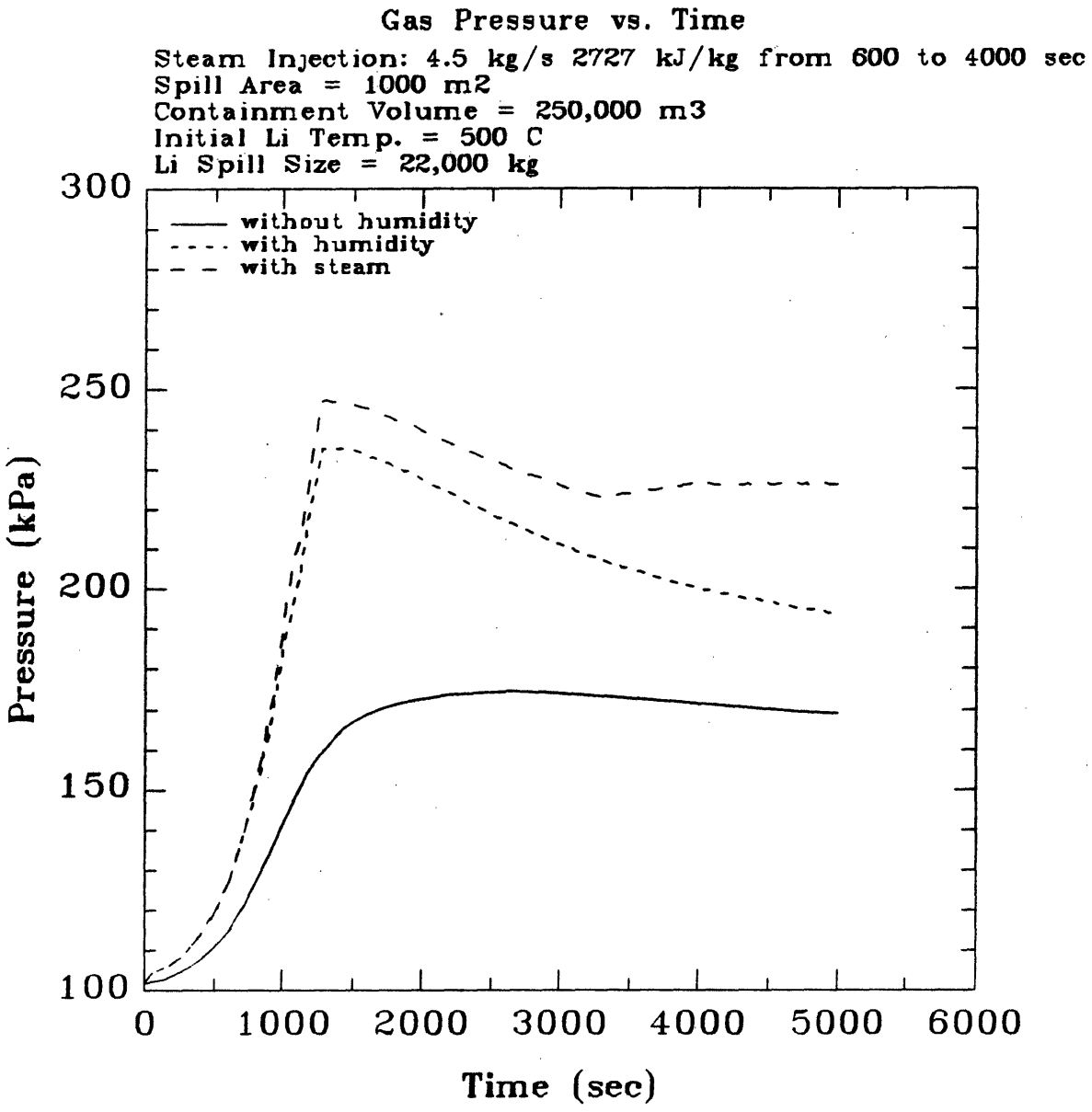

Figure 6-16: Cell gas pressure versus time, one cell geometry

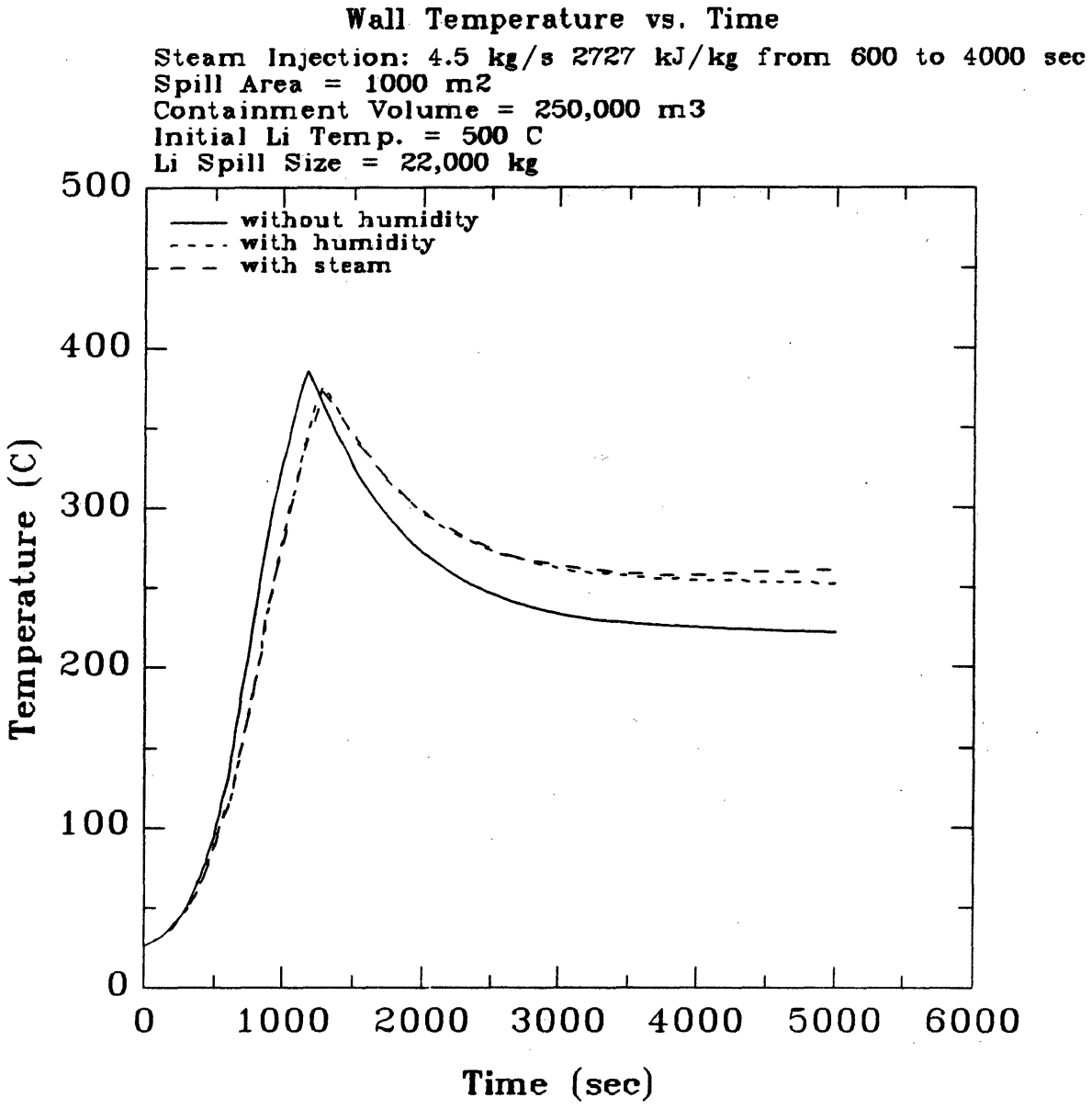

Figure 6-17: Containment wall temperature versus time, one cell geometry

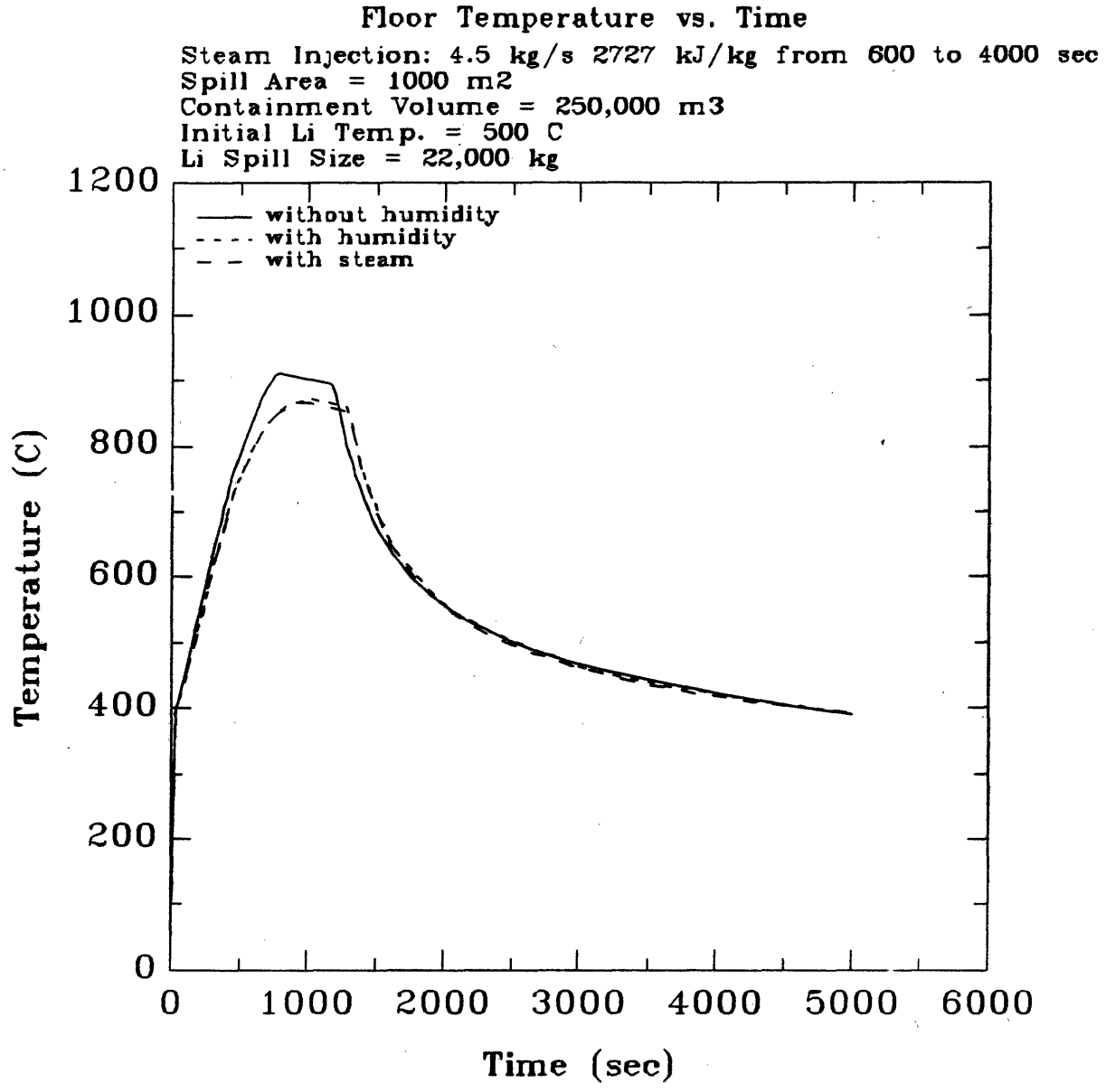

Figure 6-18: Containment floor temperature versus time, one cell geometry

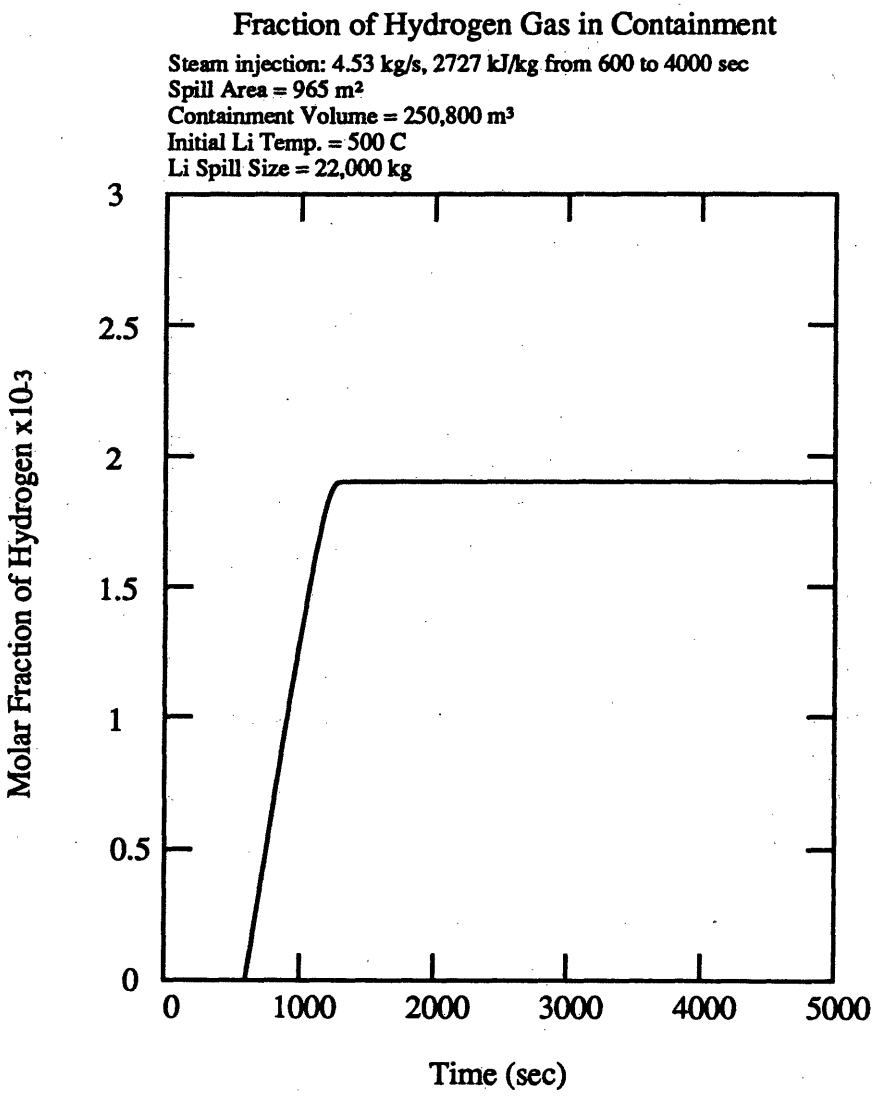

Figure 6-19: Containment molar fraction of hydrogen gas

sequences have been performed (without the presence of steam) in which the amount of lithium spilled was varied by up to a factor of two relative to this work. Those studies showed that the maximum lithium pool and combustion zone temperatures were relatively insensitive to the size of the spill; more sensitive were the containment cell gas temperatures and pressures[6]. Thus the maximum temperatures presented here would not be significantly affected by a moderate change in the amount of lithium spilled and could be considered characteristic of large scale lithium fires.

6.3.3 Results of the Second Group

The results of the second group are shown in Figures 6-20–6-24. The combustion zone temperature is shown in Figure 6-20 and the lithium pool temperature is shown in Figure 6-21. From these figures it can be seen that when humidity was present the combustion zone temperature increased to about 175°C above the pool temperature at 2000 seconds into the accident. It then remained nearly constant until the end of the calculation. In the case without humidity, the combustion zone temperature increased to about 200°C above the pool temperature and increased very slowly for the duration of the calculation, indicating that in both cases the lithium was burning the entire time.

The reason for the lower combustion zone and pool temperatures in the humid case was the lower lithium reaction rate caused firstly, and most significantly, by the lower gas flow rate from the primary cell gas to the combustion zone and secondly, and less significantly, by the hydrogen gas buildup in the primary cell. In Figure 6-21 one can see that while the humid lithium pool temperature remained flat throughout the calculation, the dry air lithium pool temperature increased slowly the entire time. This difference in pool temperature was caused by the lower lithium reaction rate, and thus heat generation rate in the humid air case.

The lower lithium reaction rate was primarily caused by the lower temperature difference between the combustion zone and the cell gas, as that provides the driving

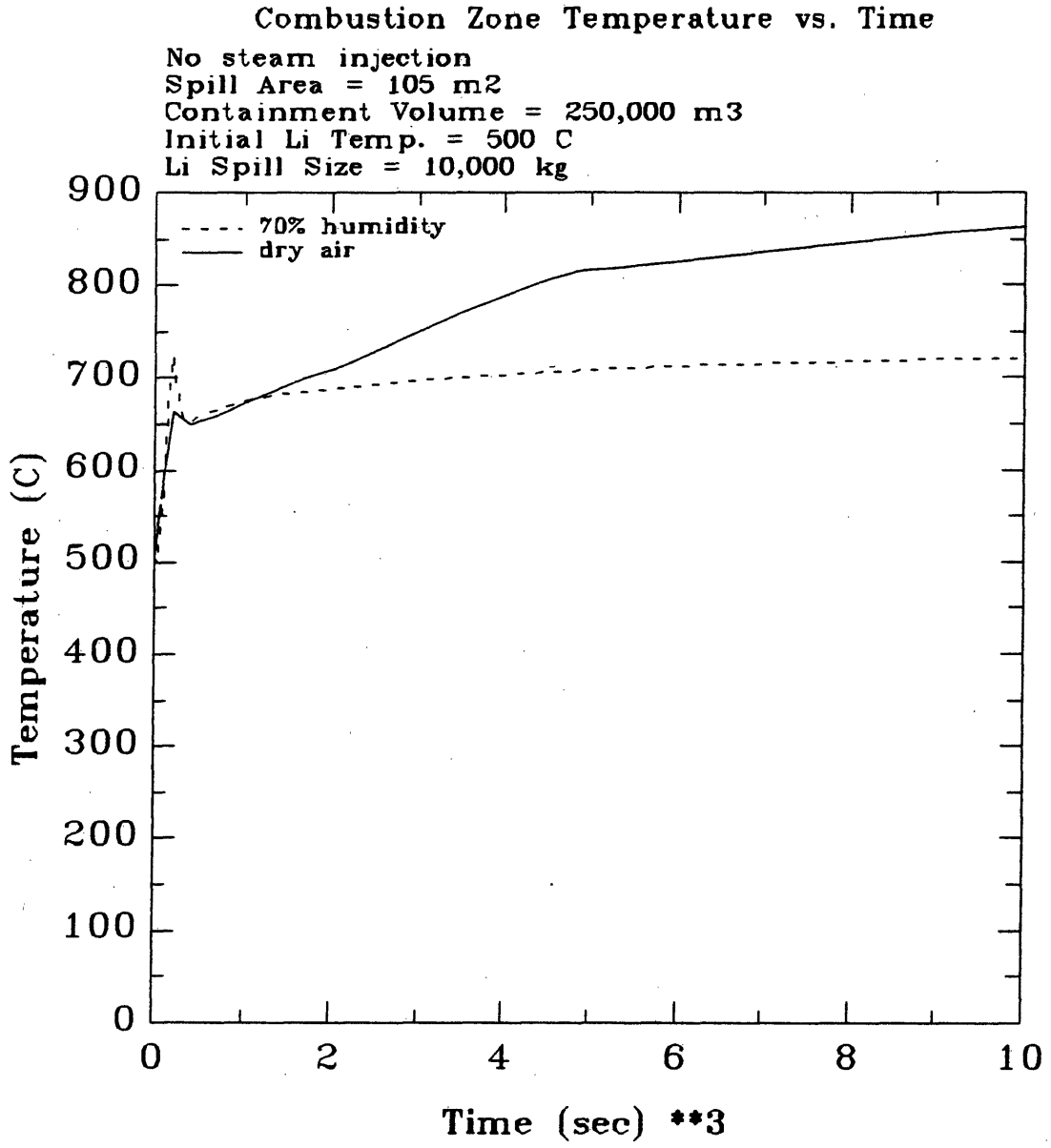

Figure 6-20: Combustion zone temperature versus time, two cell geometry

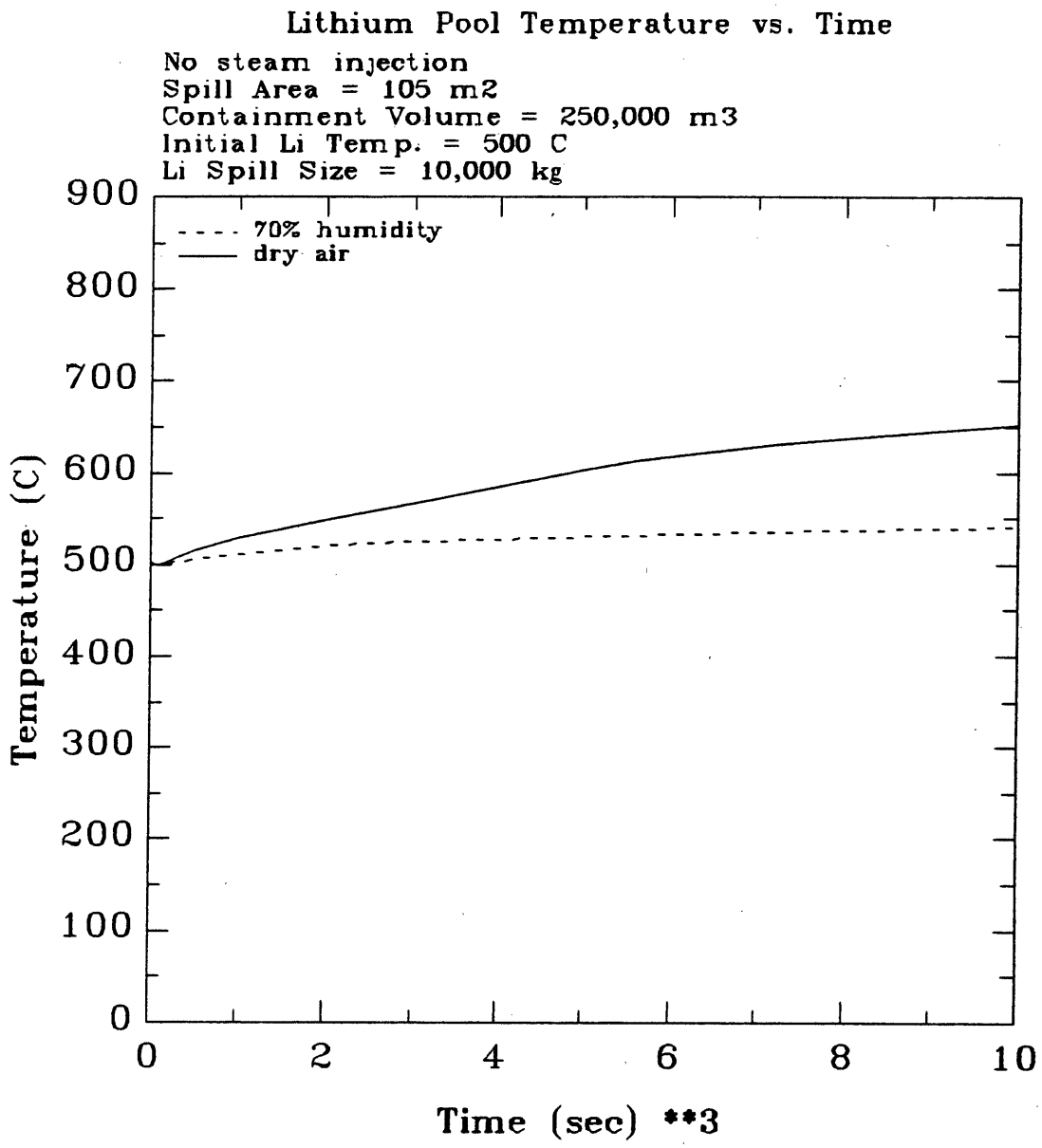

Figure 6-21: Lithium pool temperature versus time, two cell geometry

force behind the natural convection of the gas to the combustion zone. This can be seen in Figures 6-20 and 6-22, where the temperature difference between the combustion zone and the gas in the dry case went from about 225°C at the beginning of the calculation, to about 300°C at the end. In the humid case it went from about 175°C at the beginning to about 150°C at the end. Thus the gas flow rate from the cell gas to the combustion zone, the lithium reaction rate, and the heat generation rate were lower in the humid case.

The lower temperature difference between the gas and the combustion zone was caused by the increased radiative emissivity of the cell gas due to the presence of steam. That improved the thermal coupling between the combustion zone and the gas via radiative heat transfer and reduced the temperature difference between the two. That can also be seen in Figure 6-22, as the gas temperature was higher in the humid air case, even though the heat generation rate was lower. The lower heat generation rate in turn limited the rate of increase of the combustion zone temperature and the lithium reaction rate in a sort of positive feedback mechanism.

The hydrogen gas buildup helped to reduce the reaction rate somewhat by limiting the oxygen and nitrogen densities within the primary cell. As the fire was consuming the oxygen, nitrogen and steam in the cell, hydrogen was being generated in the humid air case. As the consumption of the gas reduced the cell gas pressure and drew in gas from the secondary cell, the hydrogen that had built up remained in the primary cell and did not allow as much oxygen and nitrogen to be drawn in to feed the fire. That caused the total oxygen and nitrogen densities in the primary cell to be lower, which in turn reduced the lithium reaction rate, since the non-combusting hydrogen was being convected to the combustion zone in the place of oxygen or nitrogen. This effect was not significant at the beginning of the fire, as the hydrogen concentration was zero, but it did become more influential by the end of the calculation as the concentration had increased to over 20%. The hydrogen buildup will be discussed further with the results of the third group.

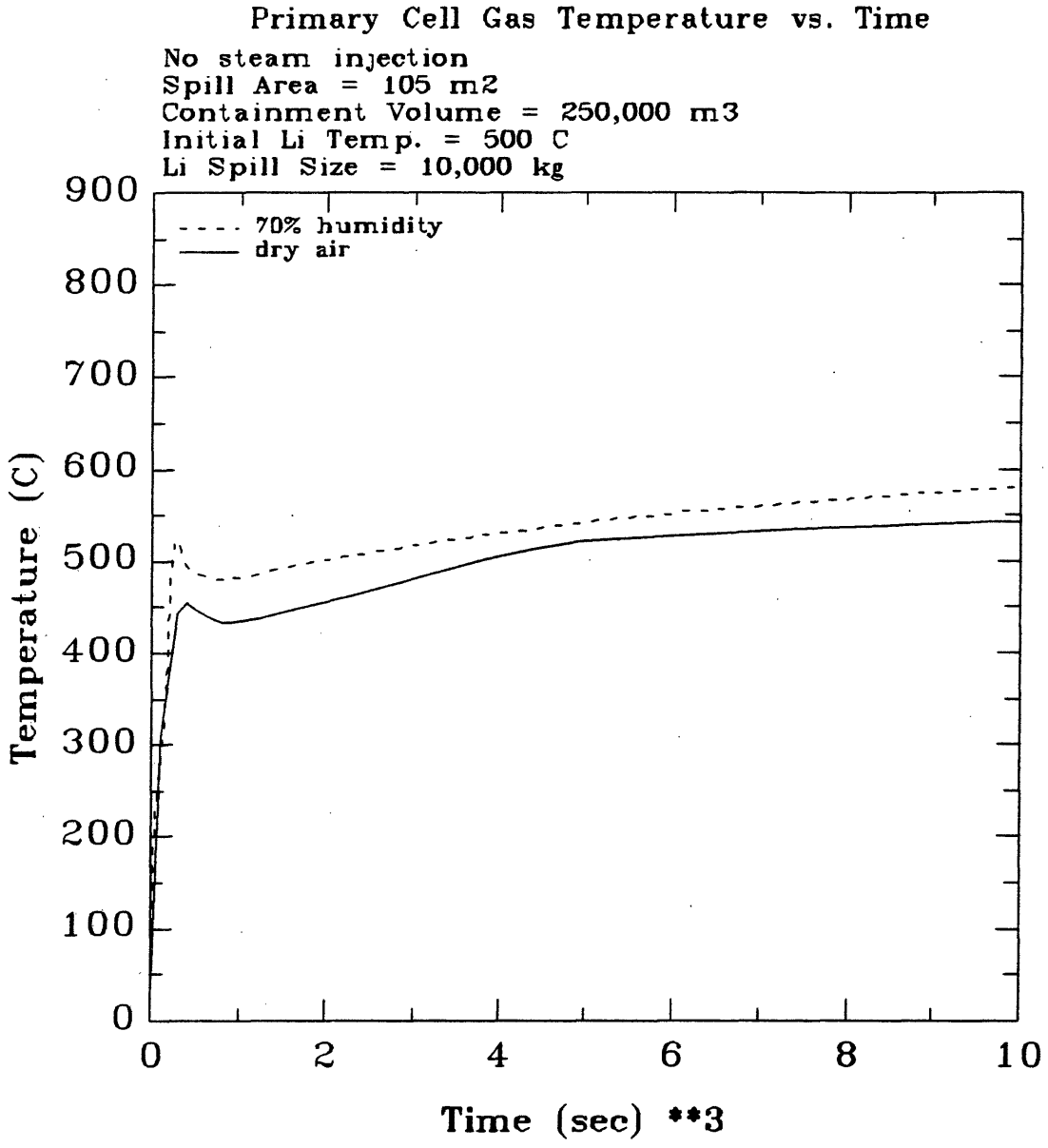

Figure 6-22: Primary cell gas temperature versus time, two cell geometry

The effect of the increased radiative heat transfer, in this case from the primary cell wall and floor to the secondary cell gas in the humid air case can also be seen in Figure 6-23—a plot of primary wall temperature versus time. In that figure the dry air wall temperature decreased from its initial value of 550°C to about 350°C at 1000 seconds, and then slowly increased to about 500°C. In the humid air case the wall temperature decreased to just under 300°C and then rose only slowly. Since the cell floor was in direct contact with the lithium pool and it, too, was radiating heat to the secondary cell gas more effectively, the lithium pool was cooled more effectively. This and the reduced lithium reaction rate served to reduce the pool temperature. Both of these effects illustrate the enhanced heat transfer caused by the higher cell gas emissivity.

The plot of primary cell gas temperature versus time further illustrates the effect of the higher emissivity of the cell gas. In both the dry air and humid cases, the maximum cell gas temperature was about 550°C, reached at the end of the calculation. Even though the lithium was reacting more slowly in the humid case, the cell gas temperature was nearly the same as in the dry case. This shows that the dominant effect of the presence of the water vapor was to raise the cell gas emissivity such that more heat was transferred from the combustion zone to the cell gas, so the temperature difference between the two, and thus the lithium reaction rate, was lower. The secondary cell gas was also significantly more effective in removing heat from the primary cell wall and floor. Both of these effects served to reduce the lithium pool temperature.

The primary cell gas pressure is shown in Figure 6-24. This is actually a plot of both cell gas pressures after about 2000 seconds, when they had equalized. The slightly higher pressure in the humid air case was due to the enhanced radiative heat transfer, even though the lithium reaction rate was lower. The crack in the primary cell was large enough that although the primary cell gas temperature was much higher than the secondary cell gas temperature the pressures were approximately equal. The

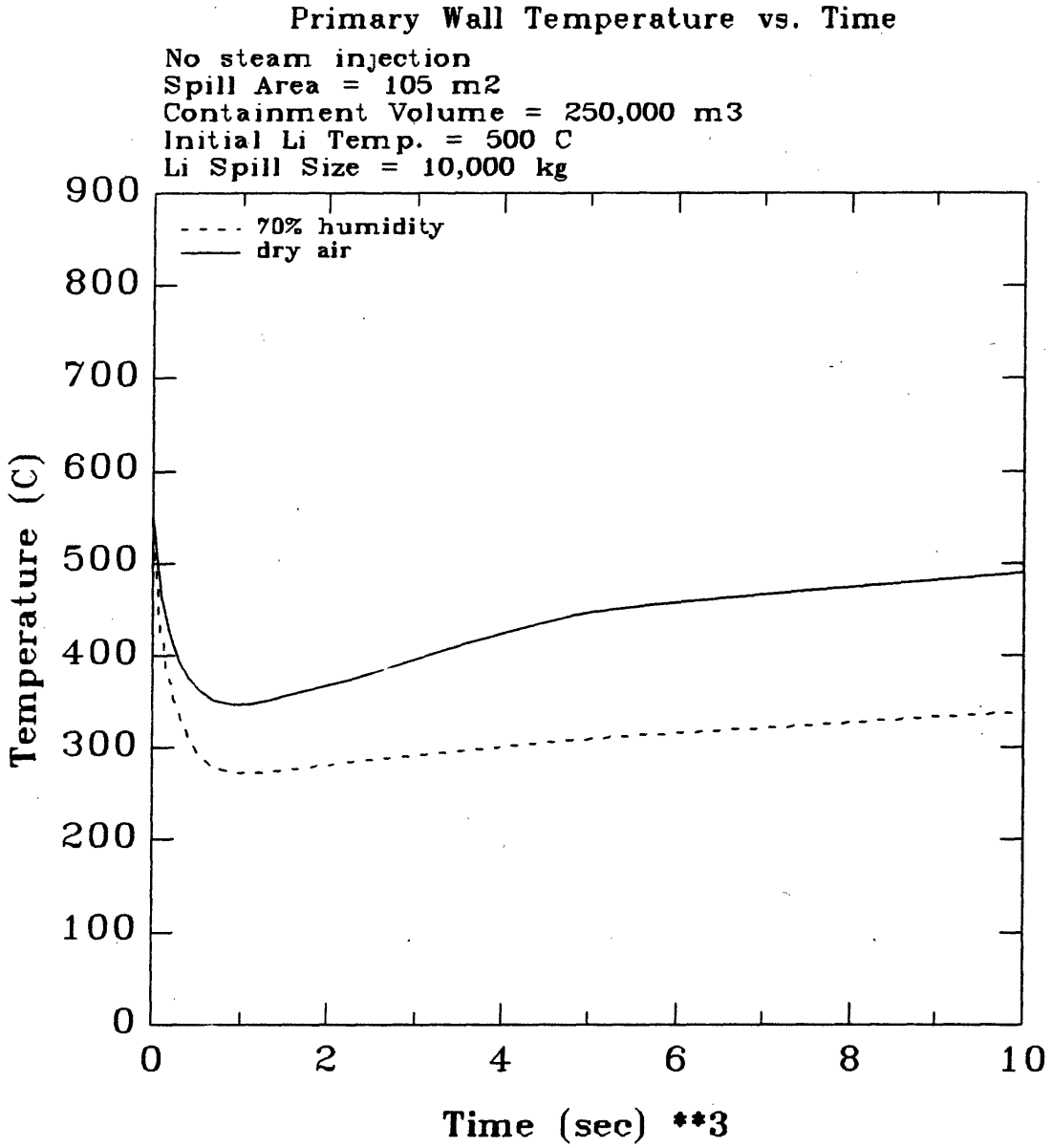

Figure 6-23: Primary cell wall temperature versus time, two cell geometry

maximum gas pressure in both cases was about 150 kPa.

The model used here for a fire inside the plasma chamber of a tokamak is a rough approximation in that while the heat capacities of the blanket and shield were included as the secondary cell extraneous heat capacity, their thermal resistances were not included between the primary cell and the secondary cell. However, in Chapter 7 a more detailed analysis which includes those thermal resistances and the decay heat produced in the reactor blanket and shield structures will be presented. It will be seen that the more detailed analysis produced similar trends with regard to the lithium pool and combustion zone temperatures (in the absence of steam); thus these results, while not exact, may be used to characterize the effects of the presence of steam on this type of lithium fire.

6.3.4 Results of the Third Group

The third group of calculations had similar initial conditions to those of the second group, but steam was injected into the humid air of the secondary cell at the beginning of the accident. This additional steam had the effect of increasing the water vapor content of the secondary cell, which further increased the cell gas emissivity and thus the heat transfer from the primary cell floor and wall by radiation to the gas surrounding them. However, the effect of this enhanced radiation was relatively small.

The lithium pool temperature (Figure 6-25) remained the same throughout most of the duration of the accident at just over 500°C. This can be compared to the dry air and humid air cases of the second group (Figure 6-21) and one can see that the cooling of the pool was more pronounced in this case than in the dry case, but essentially similar to the humid case. The lithium reaction rate was also reduced in a manner similar to the humid air case.

The cell wall temperature history also illustrates the increased heat transfer from the primary cell to the secondary gas. The wall temperature is shown in Figure 6-26 and one can see that it followed the same path as in the second group—it decreased

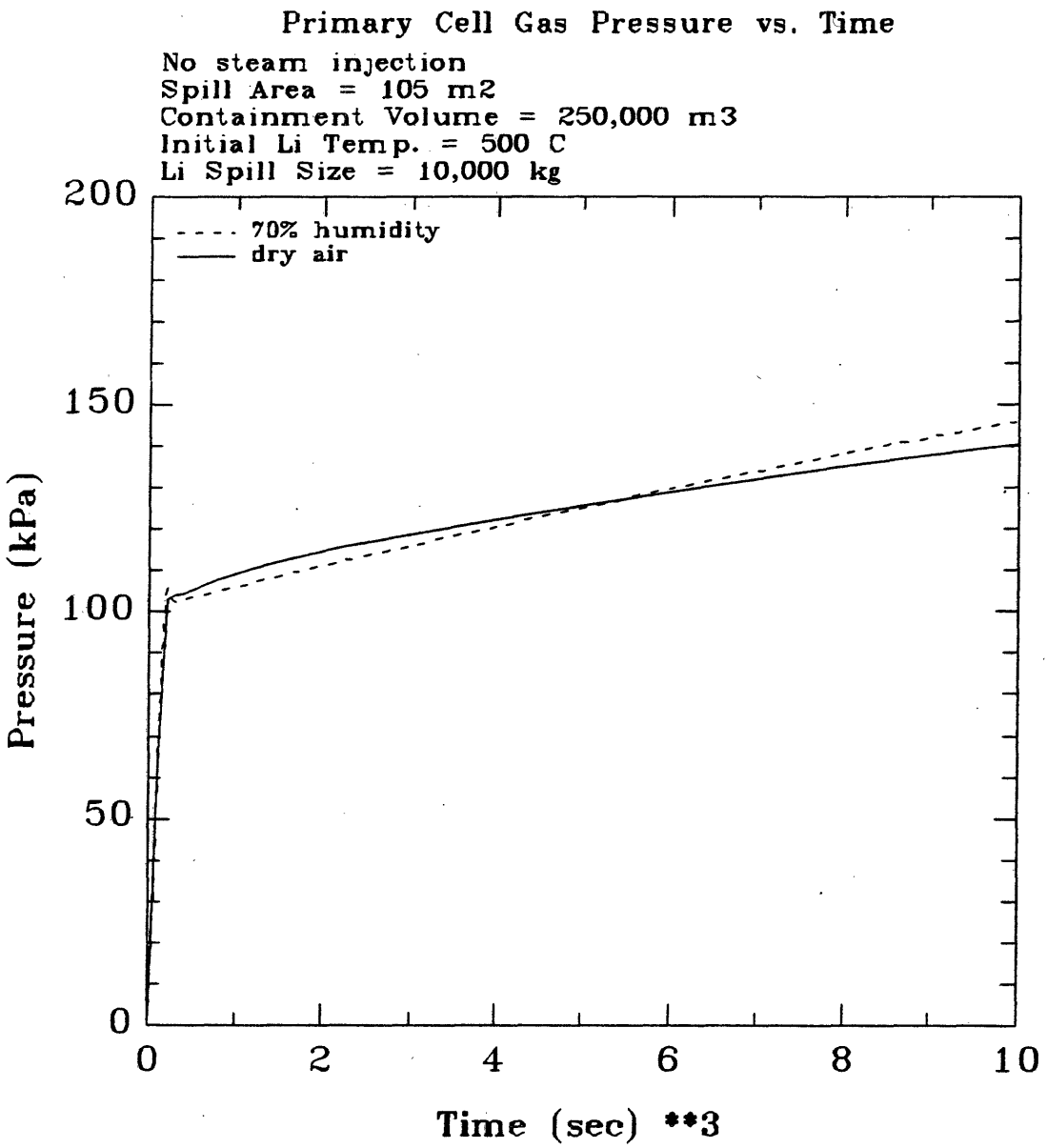

Figure 6-24: Primary cell gas pressure versus time, two cell geometry

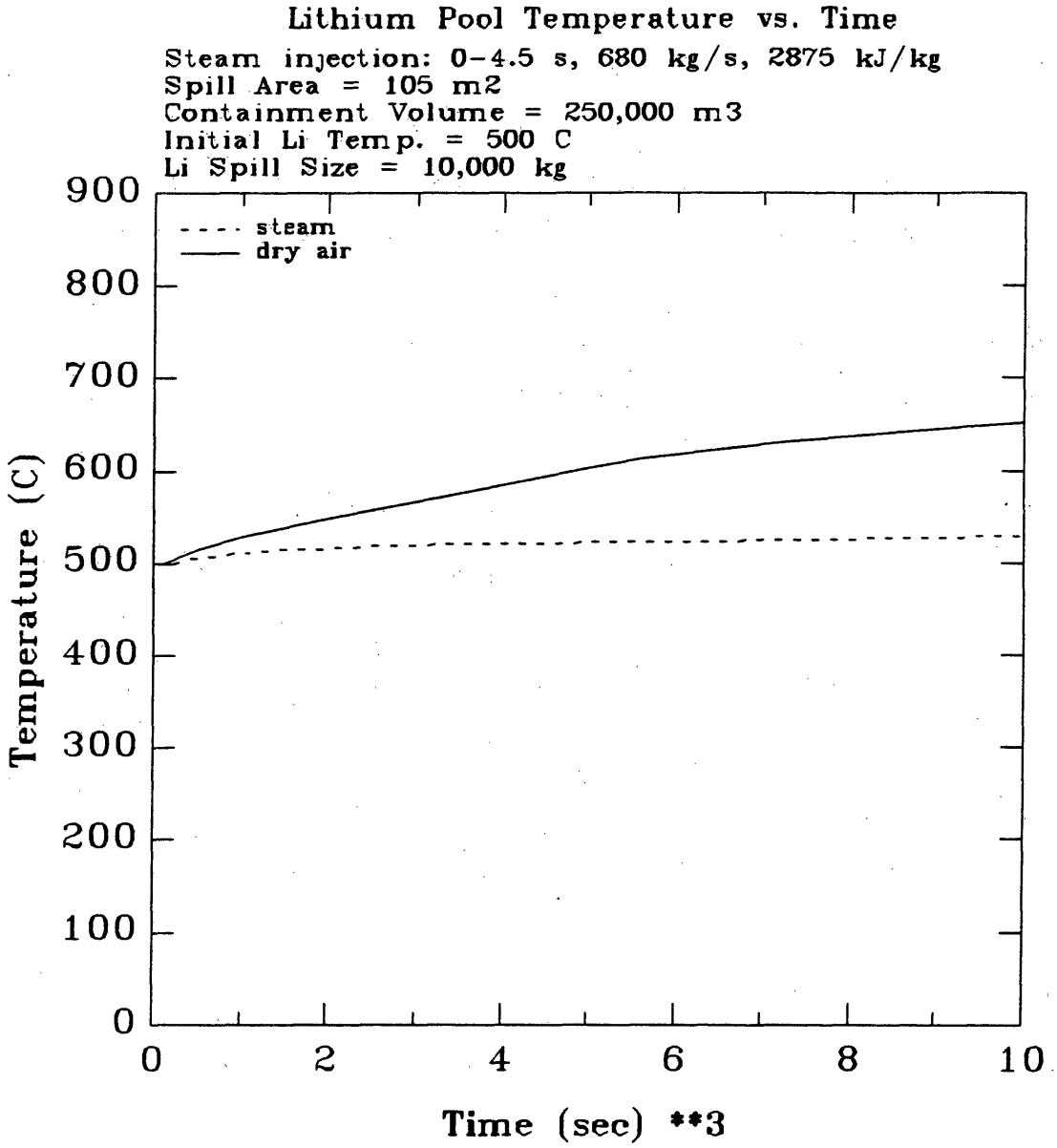

Figure 6-25: Lithium pool temperature versus time, two cell geometry with steam injection to the secondary cell

initially from an initial value of 550°C to level off at about 375°C. The slightly lower temperature was due to the increased cooling by the secondary cell gas. The temperature after the initial decrease was slightly lower than in the case with humidity only (Figure 6-23).

The primary cell gas pressure history is shown in Figure 6-27, and follows the same shape as the humid air in the second trial group (Figure 6-24). One can see that the secondary cell gas pressure was slightly higher in the steam case (155 kPa) than in the humid case as a result of the increased heat transfer to the cell gas and the injection of additional mass to the secondary cell.

Figure 6-28 shows the hydrogen molar concentration in the primary cell gas. The hydrogen concentration increased as the lithium reacted with the water vapor in the atmosphere to produce Li_2O, LiOH and H_2. Since the primary cell gas was being consumed as the fire was burning, and gas from the secondary cell was being drawn in to replace it, the hydrogen never had a chance to flow out of the primary cell. This caused the concentration in the primary cell to increase throughout the duration of the fire. As mentioned in the previous section, this served to reduce the oxygen and nitrogen densities in the primary cell somewhat, and thus the lithium reaction rate. The final molar concentration was just over 20% and increasing slowly as the lithium continued to react. That is a cause for some concern, as it is above the concentration needed for an explosion, although in the presence of a lithium fire in humid air one would expect the hydrogen to burn before exploding.

6.4 Conclusions

The major effect of the presence of water vapor in the one and two cell geometries appears to be the change in the heat transfer characteristics of the cell gases. The higher cell gas emissivities have the effect of increasing the primary cell gas temperatures above those of dry air. In the case of a fire on the containment floor, radiative

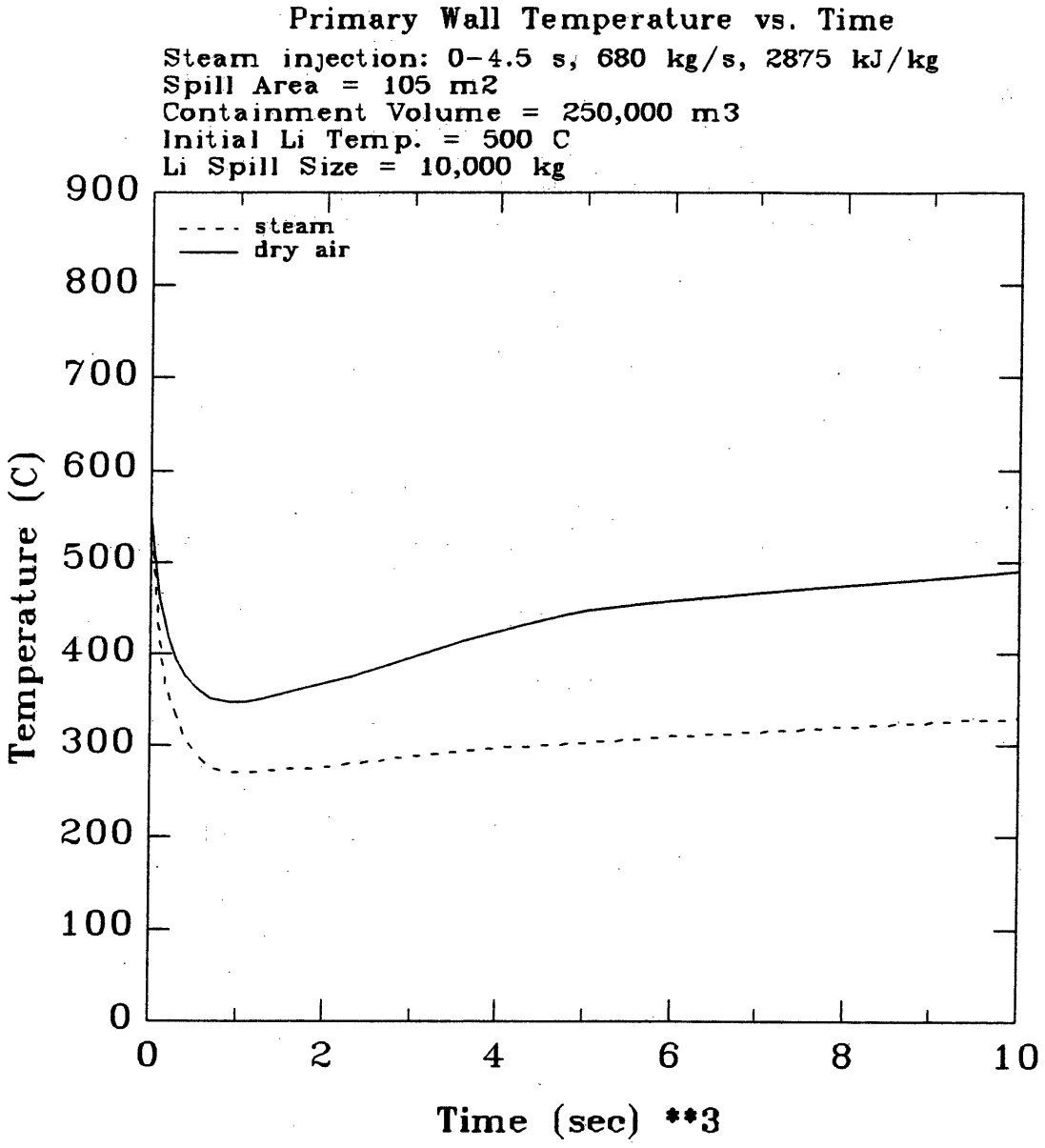

Figure 6-26: Primary cell wall temperature versus time, two cell geometry with steam injection to the secondary cell

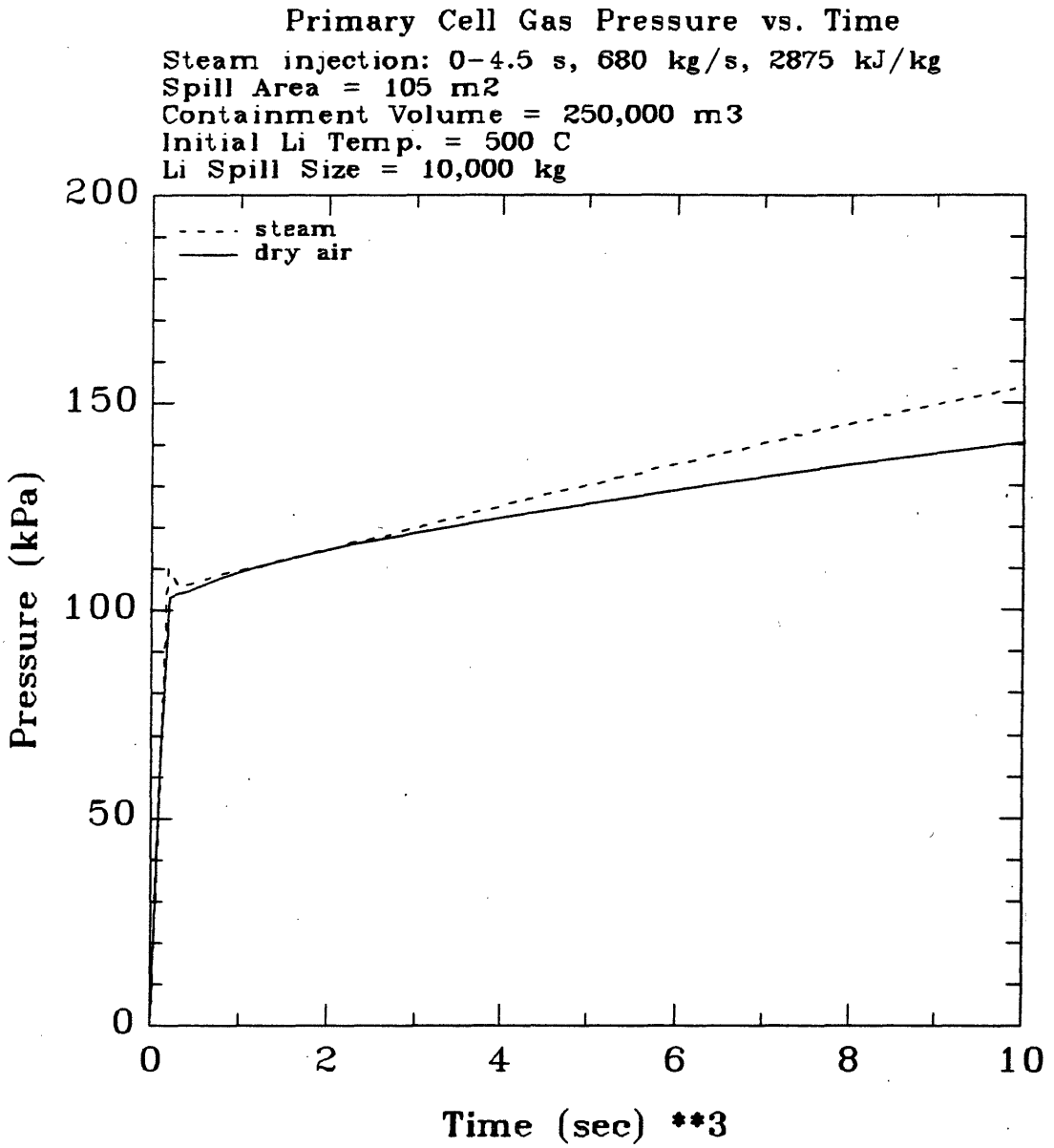

Figure 6-27: Primary cell gas pressure versus time, two cell geometry with steam injection to the secondary cell

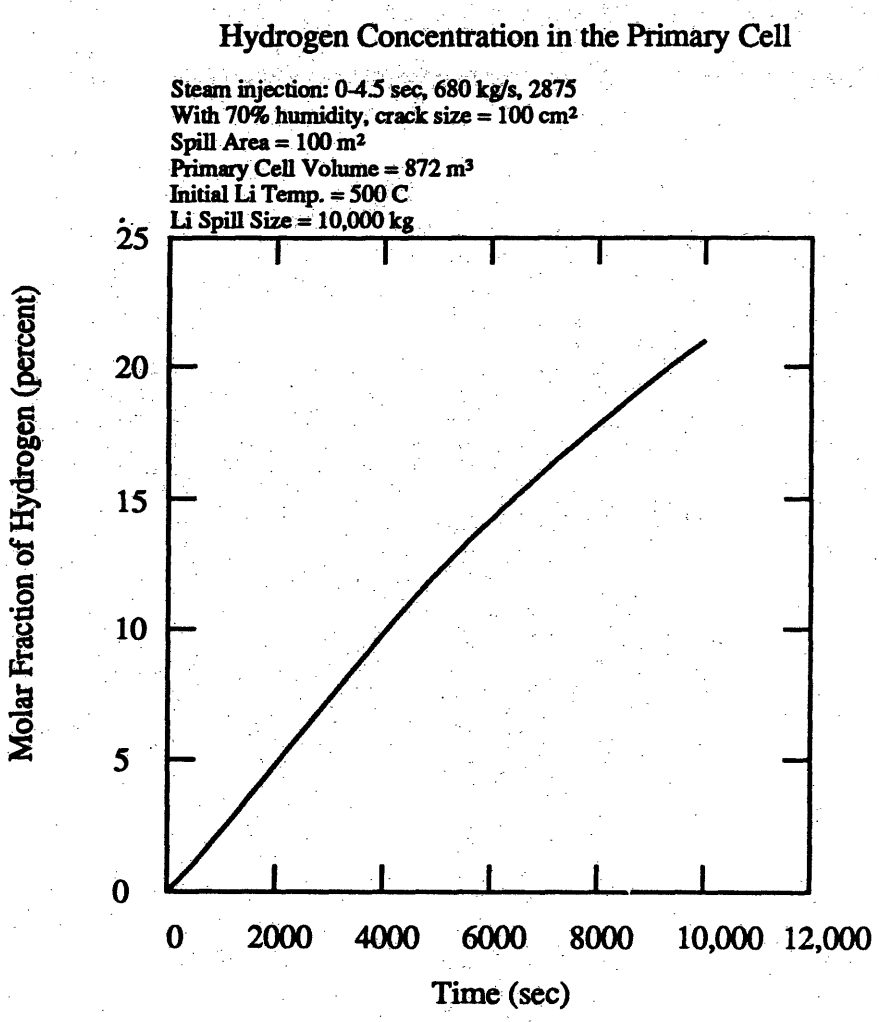

Figure 6-28: Hydrogen accumulation history for a torus fire

heat transfer between the combustion zone and the primary cell gas has the effect of cooling the combustion zone and the lithium pool somewhat and reducing the combustion rate, but substantially increasing the temperature and pressure of the containment atmosphere. The fire inside the torus appears to lead to much lower temperatures in the spilled lithium than possible in the containment fire case, due mainly to the cooling effect of the structures below the lithium pool and the small area of the pool. Again in the torus fire case steam has a net effect of lowering the temperature of the pool and structure below those calculated for dry air.

Chapter 7

Modeling Lithium Fires in the Plasma Chamber in the Presence of Decay Heat

In the event of a lithium spill and fire, a fusion reactor would be endangered by the heat produced by the burning lithium and by the decay heat produced by irradiated structural material. Such an accident would be a loss of flow accident (LOFA) if the lithium flow in the blanket was shut off before most of it escaped, or a loss of coolant accident (LOCA) if it was not. Therefore it is important to predict the consequences of not only lithium fires and LOCA/LOFA separately, but also the consequences of simultaneous occurrences. Work has been done previously in both areas separately. LITFIRE has been used to predict the consequences of lithium fires both inside and outside the plasma chamber of a tokamak, considering a number of containment geometries, containment atmospheres, spill sizes and geometries[17,1,11,9,2], and the consequences of decay heat following LOCA/LOFA events in a number of different blankets were recently predicted by Massidda[18]. None of these analyses attempted to predict the consequences of a simultaneous occurrence of the two events.

7.1 Development of the Torus Fire Model

LITFIRE, as previously described, has the ability to predict the consequences of a lithium spill inside the plasma chamber of a tokamak without considering the effects of decay heat[17]. Extra nodes represent the blanket and shield structures and the heat transfer pathways to and from those nodes. The lithium was assumed to be spilled into the torus and to burn, while an opening in the vacuum vessel allows gas from the containment into the torus. The maximum temperature reached by the first wall during such analyses was about 620°C[17]. This existing torus fire capability was used as the basis for the new torus fire/decay heat model. It was expected that the worst case accident would be a fire inside the torus adding heat directly to the first wall, which is the location of the maximum temperature in the blanket during a LOCA/LOFA[18].

7.1.1 Heat Transfer

In order to represent the material compositions of the different areas of the blanket and shield structures, they were divided into seven regions of different material composition. They are shown in Figure 7-1[18]. The regions were then either modeled as individual nodes or lumped together in one node. Each node was considered to possess its own thermomechanical properties. From inboard to outboard, the nodes and regions are shown in Table 7.1.

In the earliest version of the decay heat model, the blanket node represented a lumped approximation of the blanket structure from the part of the first wall directly adjacent to the plasma to the vacuum gap between the blanket back wall and the shield (regions 2 through 6). Since the blanket was composed mostly of lithium, which has a high thermal conductivity, one node was deemed sufficient for it. One node was also used for the shield, although the thermal conductivity of the steel and water was not nearly as high as the lithium in the blanket. With the changes in the

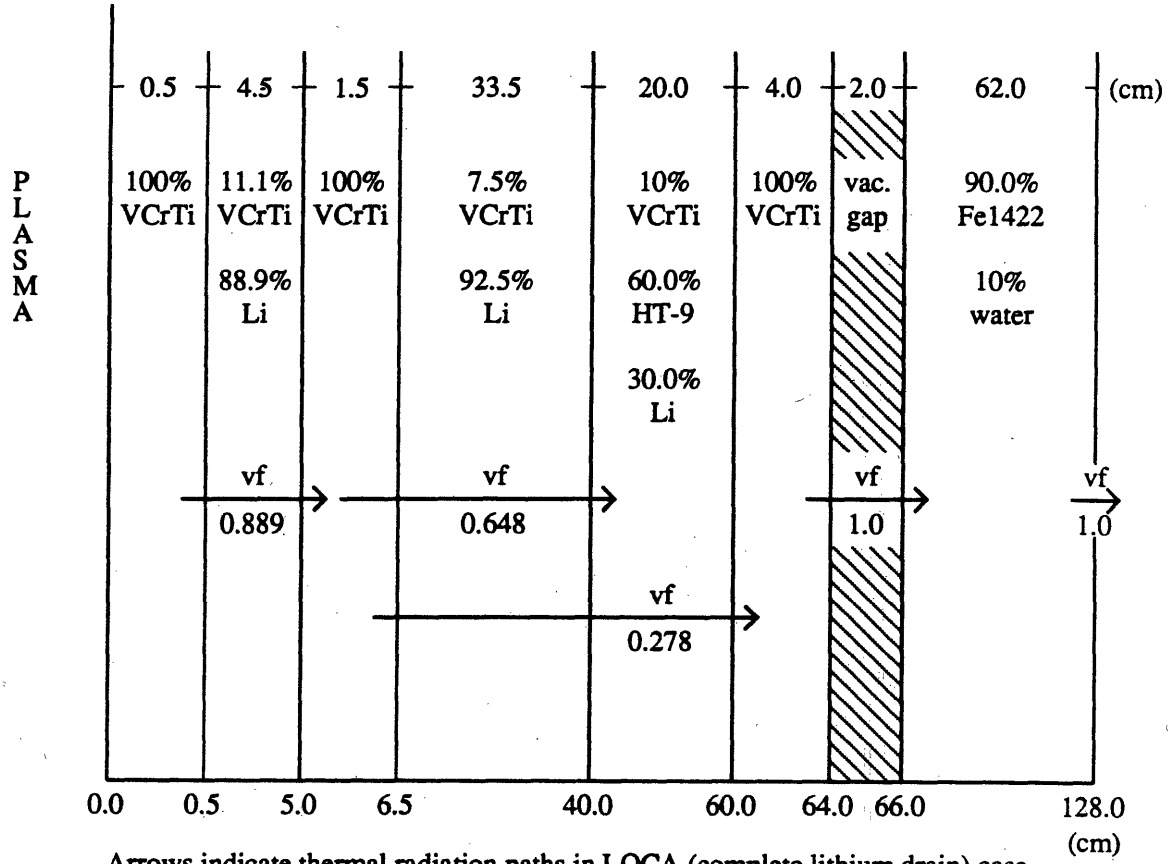

Arrows indicate thermal radiation paths in LOCA (complete lithium drain) case.
The vf parameters indicate the view factor for that particular path.
Thermal radiation from the back of the shield goes to either the containment building wall or floor.

Figure 7-1: Torus fire model blanket regions

Table 7.1: Torus fire model blanket nodes and regions

Region	Node
1. front of the first wall	first wall
2. inside of the first wall	breeder
3. back of the first wall	
4. breeder region	
5. manifold	manifold
6. blanket back wall	blanket back wall
7. shield	front of the shield
	bulk of the shield
	back of the shield

heat transfer pathways, heat flowed by conduction from the first wall to the blanket, then by radiation across a vacuum gap to the shield, and then by convection and radiation to the containment atmosphere and wall.

When the model was calibrated against the results of Massidda (for LOCA/LOFA without a fire), it was found that the LOFA results of this model agreed rather well, but the LOCA results tended to underpredict the temperature of the first wall. The calculated rate of radiative heat transfer between the blanket and the shield was seen as a possible source of error, as the lumped temperatures of the blanket and shield nodes were lower than the temperatures at the inboard surfaces of each node, and higher than the temperatures at the outboard surfaces. Thus the temperature difference across the vacuum gap between the blanket and shield (between the outboard surface of the blanket and the inboard surface of the shield) was higher than it should have been, and the radiative heat transfer rate between the two nodes was too high.

To correct the radiative heat transfer problem, surface nodes 4 cm thick (the thickness of the blanket back wall) were added to the blanket (adjacent to the vacuum gap) and to the shield (on both the inner and outer surfaces). These extra nodes better represented the temperature distribution in the blanket and allowed the full thermal resistance of the larger blanket and shield nodes to affect the radiative heat transfer rate. This version of the model tended to overpredict the temperature of the first wall, as the radiative heat transfer *inside* the blanket itself was not taken into account.

Since most of the breeder region of the blanket is assumed to be empty during a LOCA, radiative heat transfer from the front of the breeder region to the manifold and to the back wall could take place; this would enhance heat transfer away from the breeder region and lower the temperature. Modifications were made to allow radiative heat transfer from the first wall to the blanket (the first wall is actually composed of hollow tubes (6.5 cm across) carrying lithium—they would be empty during a LOCA), and from the blanket to the back wall (with an "average" view factor to account for

the different pathways). This produced an improvement, but still overpredicted the temperature by about 100°C. The final version of the model included an additional node for the manifold region of the blanket, as it had a different material composition and thus different thermal properties and internal heat generation rates from the rest of the structure. This final version was included in LITFIRE as a regular option that may be used in conjunction with all of the other options except the two-cell, pan fire and concrete reaction options (see Chapter 5). A schematic of the nodes and heat transfer pathways is shown in Figure 7-2.

Each node in the code has its own characteristics of geometry, mass, specific heat, thermal conductivity and thermal emissivity. The geometry specifies the area through which heat can be transferred and the thickness in the direction of heat flow. In the case of the breeder node, the area is either the inner surface (adjacent to the front of the first wall) or the outer surface (adjacent to the manifold), and the thickness is the perpendicular distance between the two surfaces. The areas of the front of the shield and the back of the shield nodes were taken to be the areas of contact between them and the shield bulk, respectively. The areas of the manifold, back wall and shield bulk nodes were taken to be the average surface area of each.

The mass of the blanket was taken to be the total mass of the structure, proportioned into the breeder, manifold and back wall nodes according to the volumetric ratios of each[18]. As shown in Table 7.1, the breeder node represents three regions of different material composition: the inside of the first wall (region 2), the back of the first wall (region 3) and the breeder region (region 4). The manifold node represents only the manifold region and the back wall node represents only the back wall region. The mass of lithium present in the blanket and manifold regions was added in LOFA cases.

The specific heat of each node c_p was determined by dividing the sum of the heat capacities of each material in that node by the sum of the masses of each material

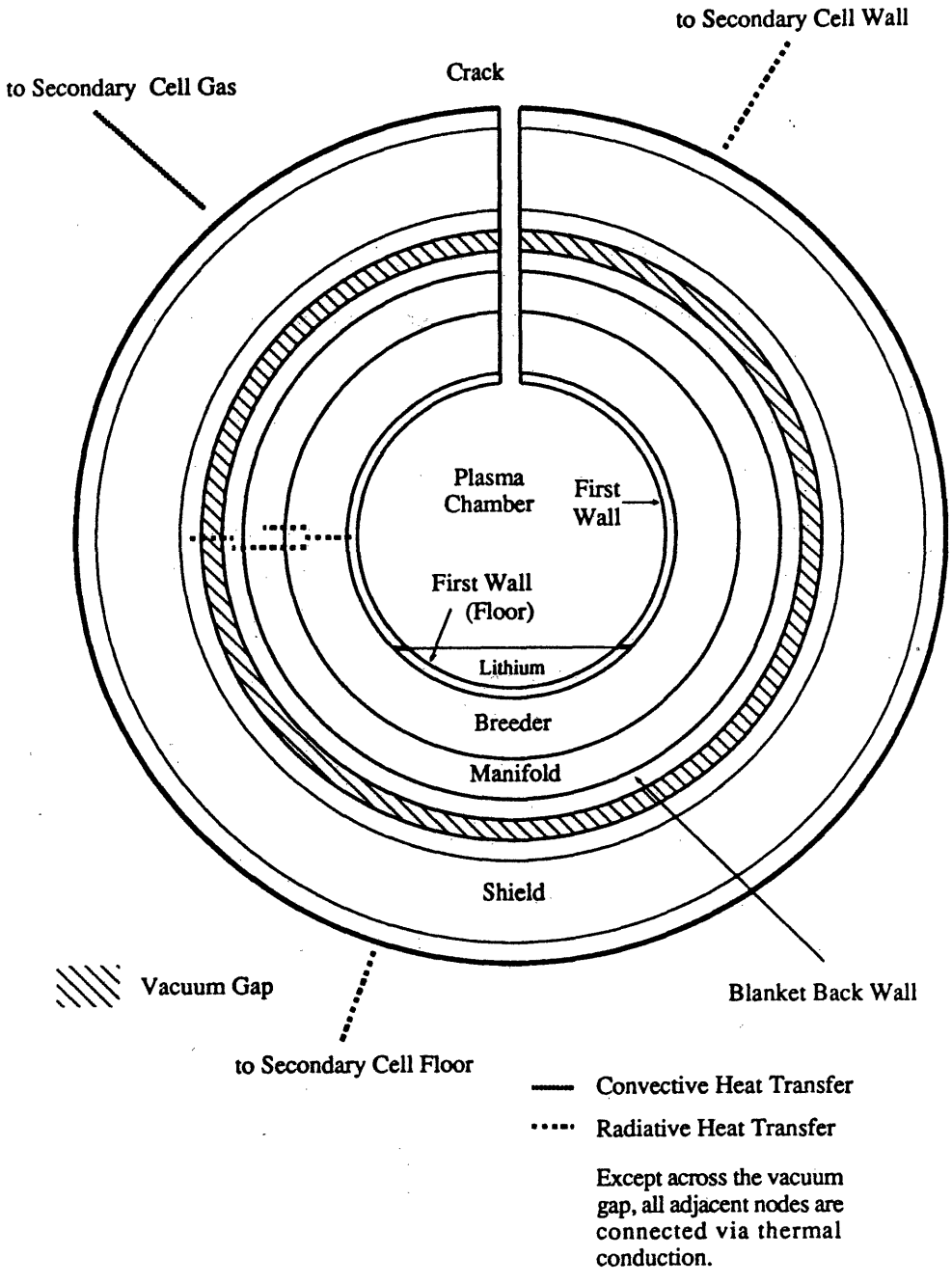

Figure 7-2: Energy flow in the LITFIRE torus fire option

(including the lithium for LOFA):

$$c_p = \frac{\sum_m M_m c_{p_m}}{\sum_m M_m}, \tag{7.1}$$

where M_m is the mass of each different material present in the node and c_{p_m} is the specific heat of each material in the node.

Thermal emissivities were specified for the blanket side of the first wall, the inside of the blanket, and the outside of the blanket (facing the shield); the emissivities of each surface may be different. The emissivity of the back of the shield is already user specified from the previous LITFIRE formulation[17].

The lumped thermal conductivity of the breeder node was found by calculating the total thermal resistance of each the three regions it encompasses, summing the resistances and from that sum determining the conductivity:

$$k = \frac{t}{A \sum_{i=1}^{3} R_i} \tag{7.2}$$

where t = node (breeder) thickness (m)

A = average cross sectional area of the node (m^2)

i = number of the blanket region

R_i = thermal resistance of the region (K/W)

(The 3 is for the regions 2 through 4 corresponding to the Li/Li/V blanket designated by Massidda (see Figure 7-1).

The thermal resistance of each region was determined in the following manner:

$$\frac{1}{R_i} = \sum_m \frac{k_m A_i f_m}{t_i} \tag{7.3}$$

where m = the number of the material type (each region was composed of one to three different types of material, including lithium for LOFA)

k_m = thermal conductivity of each individual material

A_i = cross sectional (average surface) area of each region

f_m = is the fraction of each material present in the region (vacuum is counted in the LOCA case)

t_i = thickness of each region

Thus each material is assumed to contribute a parallel heat transfer pathway, with its own thermal resistance dependent upon the thermal conductivity and fractional surface area of the material, and the thickness and total area of the region. The resistances of each material in the region are added in parallel, to determine the total resistance of the region (Equation 7.3). The regional resistances are then added in series to determine the total resistance of the breeder node, from which the thermal conductivity is calculated (Equation 7.2).

The manifold and the second wall are the other two blanket regions. Since they were considered to be separate nodes themselves, their thermal resistances were not lumped in with the others. The manifold consisted of three different material types (Li, V and HT-9) and its thermal conductivity was determined the same way as that of the blanket node with three different materials. The second wall was solid and its properties were determined as those of standard nodes in LITFIRE.

All three of the shield nodes had the same thermal conductivity and specific heat. Heat was transferred between them only via conduction and the thermal resistance between each node was calculated in the same manner as in standard LITFIRE.

7.1.2 Decay Heat Generation

In addition to the aforementioned characteristics, the first wall, breeder, manifold, second wall and shield nodes each have a decay heat source resulting from the irradiation of the reactor structure. The decay heat generation rates are entered into the

code in W/m^3 for each node, and then multiplied by the nodal volume to obtain the total decay heat generation rate.

The decay heat densities for the breeder and shield nodes were determined by taking an average over those nodes of the decay heat densities calculated by Massidda for each blanket and shield region they encompass. Massidda used the ONEDANT[19] and REAC[20] codes to calculate the neutron fluxes and resulting activities at a number of points between the first wall and the outer surface of the shield. The output from REAC in Ci/cm^3 for each radioisotope was converted to W/m^3 by multiplying the activity by the average decay energy for each isotope. This produced the heat generation rate from each isotope at each point selected for calculation, q'''_{r_o} and $q'''_{r_{t_i}}$, at the front and back of each region, respectively. The heat generation rate across the nodes was determined by assuming an exponential decrease from the front to the back of the node. Thus,

$$q'''_{r_{t_i}} = q'''_{r_o} e^{-\mu_r t_i} \tag{7.4}$$

where t_i is the thickness of the node and μ_r is the linear attenuation coefficient for each isotope. With the calculation of μ_r the decay heat generation rate can be determined at any point in the node by summing over the isotopes. Material fractions (including voids) were taken into account when the output from REAC was converted into W/m^3. The output from REAC showed that none of the top isotopes considered in the decay heat model arose from the irradiation of lithium, and thus the calculation is valid for both LOCA and LOFA[18].

The total decay heat generation rates for the nodes in the decay heat model were calculated by averaging the heat generation rate of the top total heat producing isotopes for each node. Massidda calculated the total heat produced by each isotope in each region over the first two days after the accident. The decay heat model uses the top three of those isotopes in each node. The breeder node uses the isotopes in the breeder region of the blanket. In all instances the top heat producing isotopes considered in the decay heat model account for at least 87% of the total heat

produced—this total was then adjusted to produce 100% of the heat generated over the first two days. The volumetric heat generation rate for each node as a function of time $q_i'''(\tau)$ is calculated from the local volumetric heat generation rate as follows:

$$q_i'''(\tau) = \sum_{r=1}^{3} \frac{1}{t_i} \int_0^{t_i} q_{r_o}''' e^{-\mu_r t_i} e^{-\lambda_r \tau} dt \tag{7.5}$$

where τ is the elapsed time, and λ_r is the decay coefficient for each radioisotope. This volumetric heat generation rate is then multiplied by the volume of the node to obtain the total internal heat generation rate for the node. During the execution of the code the decay heat generation rates are added to the normally calculated heat transfer rates to determine the total energy gain or loss rate and the temperature rate of change for each node.

7.2 Consequences of a Lithium Fire inside the Plasma Chamber

7.2.1 Initial Conditions

Once the model was developed, it was used to predict the consequences of a lithium fire inside the plasma chamber of a tokamak. Specifically, it was desired to ascertain the temperature rise in the blanket structures caused by the presence of a lithium fire following a loss of coolant or loss of flow accident. The blanket chosen for the analysis was the self-cooled lithium-vanadium alloy blanket from the Blanket Comparison and Selection Study (BCSS)[21], as it was rated as the best performing tokamak blanket of those studied. The geometry of the blanket is given in Table 7.2.

The same reactor geometry was used for both the LOFA and LOCA cases, but the thermal properties were changed to reflect the presence or absence of the lithium coolant. Selected reactor thermal properties from both cases are given in Table 7.3.

Table 7.2: Reactor geometry, torus fire analysis

Plasma chamber volume:	872	m^3
First wall area (exposed):	572	m^2
First wall area (covered):	105	m^2
First wall thickness:	5	mm
Breeder node thickness:	40	cm
Breeder node area:	724	m^2
Manifold thickness:	20	cm
Manifold area:	826	m^2
Back wall thickness:	4	cm
Back wall area:	880	m^2
Shield thickness:	62	cm
Shield outer area:	1125	m^2
Crack size:	100	cm^2

Table 7.3: Selected reactor thermal properties, torus fire analysis

Property	LOFA		LOCA	
First wall thermal conductivity:	31.0	W/mK	31	W/mK
First wall (exposed) heat capacity:	$8.69 \cdot 10^6$	J/K	$8.69 \cdot 10^6$	J/K
First wall (covered) heat capacity:	$1.59 \cdot 10^6$	J/K	$1.59 \cdot 10^6$	J/K
Breeder thermal conductivity:	58.3	W/mK	2.59	W/mK
Breeder heat capacity:	$6.09 \cdot 10^8$	J/K	$2.61 \cdot 10^7$	J/K
Manifold thermal conductivity:	34.7	W/mK	19.7	W/mK
Manifold heat capacity:	$2.35 \cdot 10^8$	J/K	$1.87 \cdot 10^8$	J/K
Back wall thermal conductivity:	31.0	W/mK	31.0	W/mK
Back wall heat capacity:	$3.38 \cdot 10^7$	J/K	$3.38 \cdot 10^7$	J/K
Shield thermal conductivity:	24.6	W/mK	24.6	W/mK
Shield heat capacity:	$1.26 \cdot 10^9$	J/K	$1.26 \cdot 10^9$	J/K

The initial conditions of the reactor were the same for both calculations—they were derived from estimated operating conditions of the reactor and structural temperatures given in the BCSS[17,21]. The accident was assumed to occur as the blanket was punctured and lithium flowed (instantaneously) into the plasma chamber. A crack was assumed to exist between the plasma chamber and the containment building to allow air to enter the chamber and sustain the fire. Since the plasma chamber of a reactor would contain a hydrogen plasma at a very low pressure (unless the plasma is assumed to be shut off, i.e. at low temperature), the initial pressure of the chamber was taken to be zero, and the air had to flow into the chamber via the crack. Ten thousand kilograms of lithium was assumed to have spilled into the chamber. This is less than was spilled in the containment building fire analysis, as it was assumed that the geometry of the reactor would prevent all of the lithium in the ruptured blanket module from being drained into the chamber. The initial conditions for both cases are given in Table 7.4.

7.2.2 Results

The results of the LOFA and LOCA calculations are presented in Figures 7-3 and 7-4, respectively. The figures show plots of the temperature profiles of the exposed first wall, the covered first wall (floor), the lithium combustion zone and the first wall in the absence of a fire (with decay heat only). The first wall temperature is presented, as in all cases the first wall was the hottest region of the blanket, and thus it is there that the greatest damage caused by high temperatures would occur. The first wall temperature in the absence of a fire is presented for comparison, to determine the additional temperature rise caused by the fire.

7.2.2.1 Loss of Flow Accident

In the loss of flow case, it can be seen in Figure 7-3 that the lithium burned for about 30,000 seconds ($\sim$ 8 hours) until it was entirely consumed. During that time the first

Table 7.4: Initial conditions for the torus fire analyses

Lithium spill mass	10,000	kg
Lithium spill temperature	500	°C
First wall temperature	550	°C
Breeder temperature	550	°C
Manifold temperature	500	°C
Second wall temperature	450	°C
Shield temperature	100	°C
Plasma chamber pressure	0	kPa

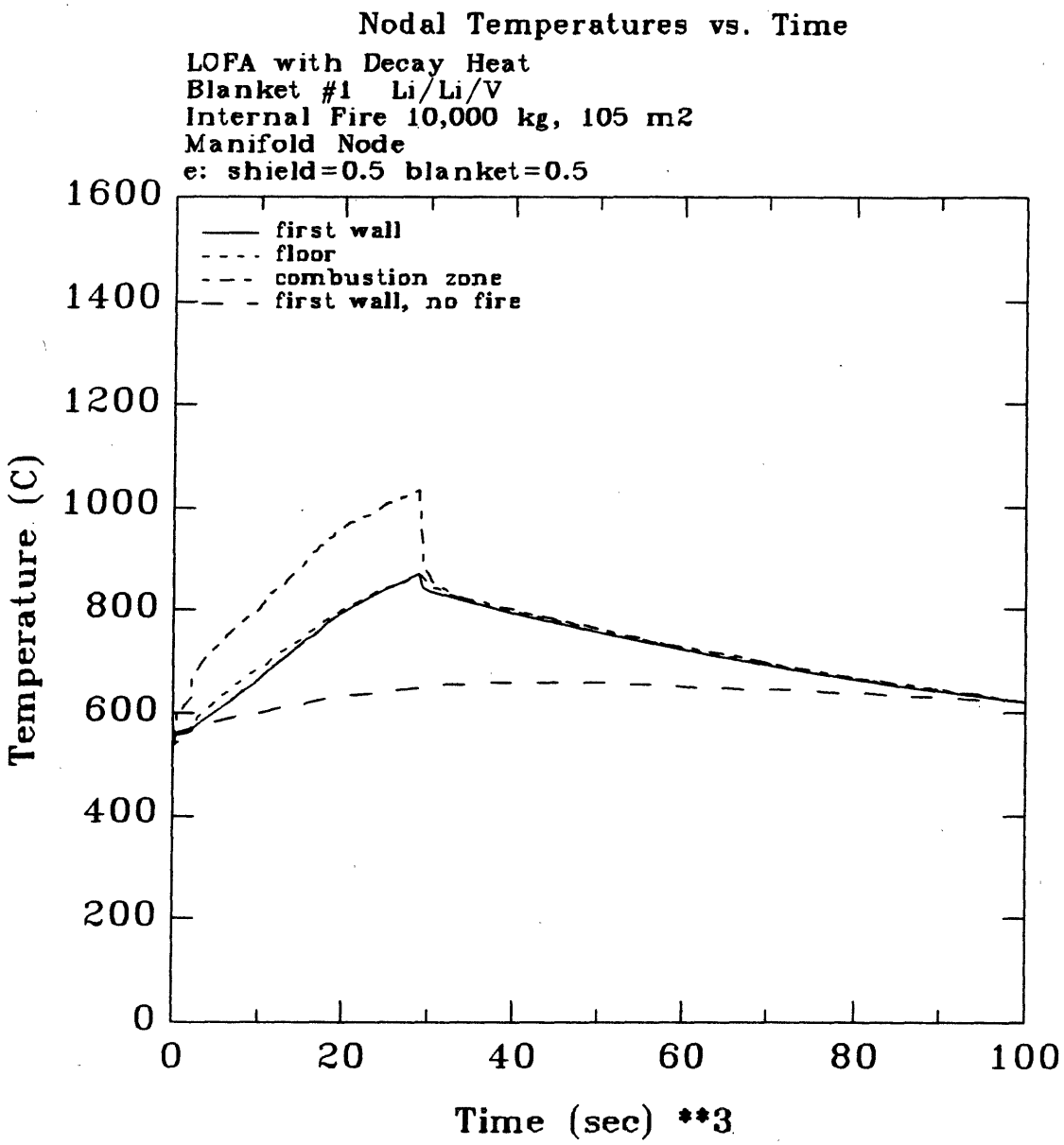

Figure 7-3: Results of the LOFA/torus fire calculations

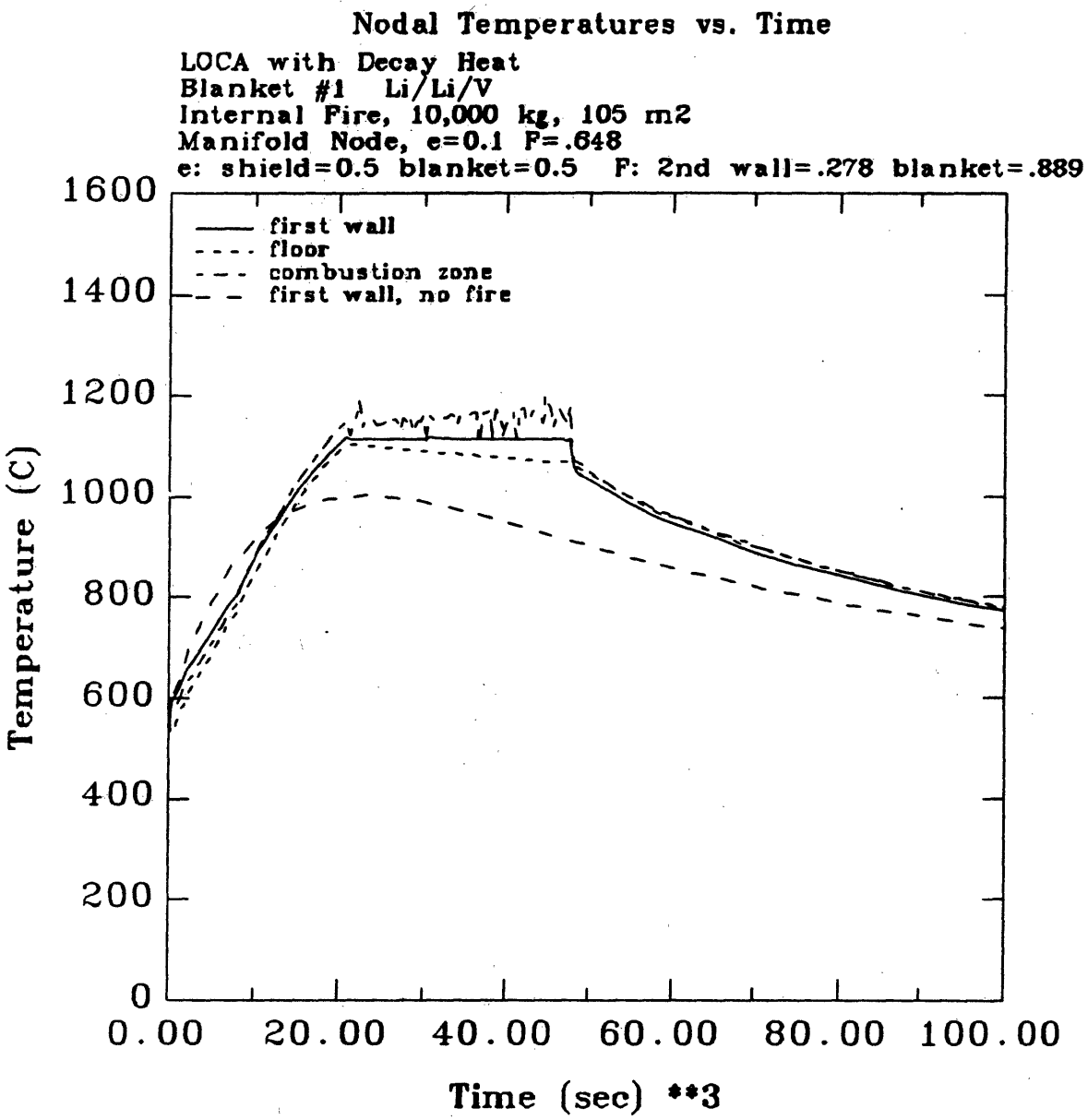

Figure 7-4: Results of the LOCA/torus fire calculations

wall temperature (both covered and exposed areas) rose to about 875°C by the time the fire had burned out. The temperature then decreased slowly until the effects of the fire were no longer visible, about 100,000 seconds ($\sim$ 27 hours) after the start of the accident. In the absence of the fire, the first wall temperature rose slowly until it reached a maximum of approximately 650°C at 40,000 seconds ($\sim$ 11 hours) into the accident. It then decreased slowly for the duration of the calculation.

Comparing the two cases, the effect of the fire was to raise the maximum first wall temperature about 225°C above that expected during a LOFA without a lithium fire. The maximum wall temperature of 875°C could pose somewhat of a threat to a vanadium structure under a load, as that is slightly over half the absolute melting temperature of the alloy (2173 K), and thermal creep effects could begin to set in if the temperature was maintained for a significant length of time[22]. In this calculation the first wall temperature was over 800°C for about five or six hours and the maximum temperature was not much over half the melting temperature, so the temperature rise would probably not lead to a catastrophic creep rate at the first wall[18].

However, in the case of a fire inside the plasma chamber, it was assumed that a crack in the blanket existed through which air could flow to feed the fire. Vanadium oxidizes readily at temperatures over 650°C, and the oxide has a melting temperature of about 670°C. Oxidation experiments performed in air with vanadium have shown that at temperatures ranging from 650–680°C, the time required to form a molten oxide is approximately 15 minutes[18]. This molten oxide could then slide off of the wall, exposing unreacted metal, which would then oxidize and slide off of the wall, exposing more metal. In the case analyzed, the first wall temperature remained over 700°C for nearly 20 hours, so this process could repeat itself until the wall was destroyed. Thus the prime threat to the integrity of the first wall is the elevated temperature caused by the fire (in addition to that caused by the decay heat) in combination with the ingress of air to the plasma chamber through the crack in the blanket. This finding has serious reactor design implications. It is essential that

no oxygen be allowed to come into contact with a vanadium structure at elevated temperatures. Therefore, in the event that a vanadium alloy was used for the structure of the first wall and one could not be certain that oxygen could be kept out of the plasma chamber, it would be necessary to use a cover gas (without any oxygen) over the reactor.

The results of this analysis can be applied to reactor designs employing a structural material other than vanadium by considering only the effects of the temperature increase caused by the fire. As stated earlier, the vanadium blanket was chosen for the analysis because of the favorable rating it received from the BCSS. Massidda also found that it was the safest blanket in terms of the thermal response to undercooling transients[18]. Other blankets would be expected to experience higher temperatures without a fire. With the simultaneous occurrence of a fire the maximum first wall temperature could be expected to be an additional 200° higher. This would further aggravate the problem of thermal creep and could cause the wall to fail. Massidda estimated the failure temperature of HT-9 to be 900°C, based upon an estimated ultimate tensile strength of near zero and the recrystallization of the material (which greatly reduces its ductility) between 900 and 1000°C[18]. In this analysis, the fire raised the maximum temperature of a vanadium wall from 650 to 875°C. If an HT-9 wall reached a higher temperature under a LOFA alone, it could quite conceivably reach 900°C in the event of a LOFA with a fire. Thus the additional temperature increase of 200°C or so could be significant, depending upon the material composition of the structure.

7.2.2.2 Loss of Coolant Accident

In the loss of coolant case, the first wall temperature rose from its initial temperature of 550°C to approximately 1100°C in about 20,000 seconds ($\sim$ 5 1/2 hours) and remained there until about 50,000 seconds ($\sim$ 14 hours) into the accident, when the lithium had been consumed. The temperature then decreased slowly until the end of

the calculation (100,000 seconds) when it was just under 800°C. In the case without the fire, the first wall temperature rose to reach a maximum of just over 1000°C in approximately 20,000 seconds, when it began to cool off very slowly until the end of the calculation.

In the LOCA with the fire, the temperature of the area of the first wall covered by the lithium (the floor) was slightly lower than that of the exposed first wall during the fire. That can be attributed to the fact that the combustion zone was radiating heat to the exposed first wall, but could not radiate through the lithium pool to the floor. The longer burn time for the fire (14 hours, compared to eight hours in the LOFA case) can be attributed to the extremely high lithium pool temperature. As shown in Chapter 2, the lithium-nitrogen reaction rate drops off very sharply above 1100°C, and the reaction does not take place at all above 1127°C. In this case, the extremely high temperature of the surrounding structures drove the lithium pool temperature high enough that the lithium-nitrogen reaction kinetics limit was taking effect and reducing the total lithium reaction rate. Thus the lithium took longer to burn.

Comparing the two cases, the effect of the fire was to raise the maximum first wall temperature by an additional 100°C and maintain that maximum temperature for about eight and a half hours, until all of the lithium had been consumed. Similar to the LOFA case, maintaining an elevated first wall temperature over an extended period of time could lead to structural damage. In the LOCA case the threat is even greater due to the higher temperature and a peculiar property of vanadium: it undergoes a phase change at 1000°C which could cause the first wall to be non-reusable[18]. The oxidation problem mentioned earlier would also be exacerbated by the increase in temperature.

It is interesting to examine the effect of the decay heat on the maximum combustion zone temperature reached during a fire. The maximum combustion zone (flame) temperature is of interest as the surface temperature of the first wall near the point which the lithium pool surface and the wall meet could be higher than the average

wall temperature. That means that radioactive material present on the wall at that point could be volatilized and released while material on the rest of the surface would not be. A plot of the nodal temperatures in the absence of decay heat, presented in Figure 7-5, helps to illustrate the effect of the decay heat upon the combustion zone temperature in the event of a LOCA. Comparing the case with decay heat (Figure 7-4) to the case without, it can be seen that, indeed, the presence of decay heat served to increased the maximum combustion zone temperature markedly, from approximately 980°C to approximately 1200°C. Thus the decay heat would make a significant difference in the maximum temperature seen by the first wall, and would also increase the potential for volatilization and release of radioactive material.

The case without decay heat is also interesting to examine from the point of view of determining the relative impact of the decay heat and the fire upon the temperature increase of the first wall. It can be seen from Figures 7-4 and 7-5 that the decay heat serves to increase the maximum first wall temperature by about 250°C above and beyond the increase caused by the fire. That compares with an extra 100°C increase caused by the fire in Figure 7-4. Thus the presence of decay heat is the dominant reason for the temperature increase of the first wall.

The higher temperature of the first wall caused by the fire may not drastically increase the overall threat to the integrity of a vanadium wall. Certainly, the presence of oxygen in the plasma chamber, postulated to enable the fire to burn, would be a grave threat at those temperatures; but the 100°C temperature increase caused by the fire does not seem be a terrible threat beyond that posed by a loss of coolant accident in which the blanket is penetrated and the lithium (or other coolant) spills *out* of the blanket onto the floor of the containment building. Such an accident would result in a lithium fire outside the reactor (if lithium was the coolant) and would raise the structural temperatures somewhat, but the principal threat to the safety of the reactor would come from the oxygen that flowed into the plasma chamber and oxidized the vanadium.

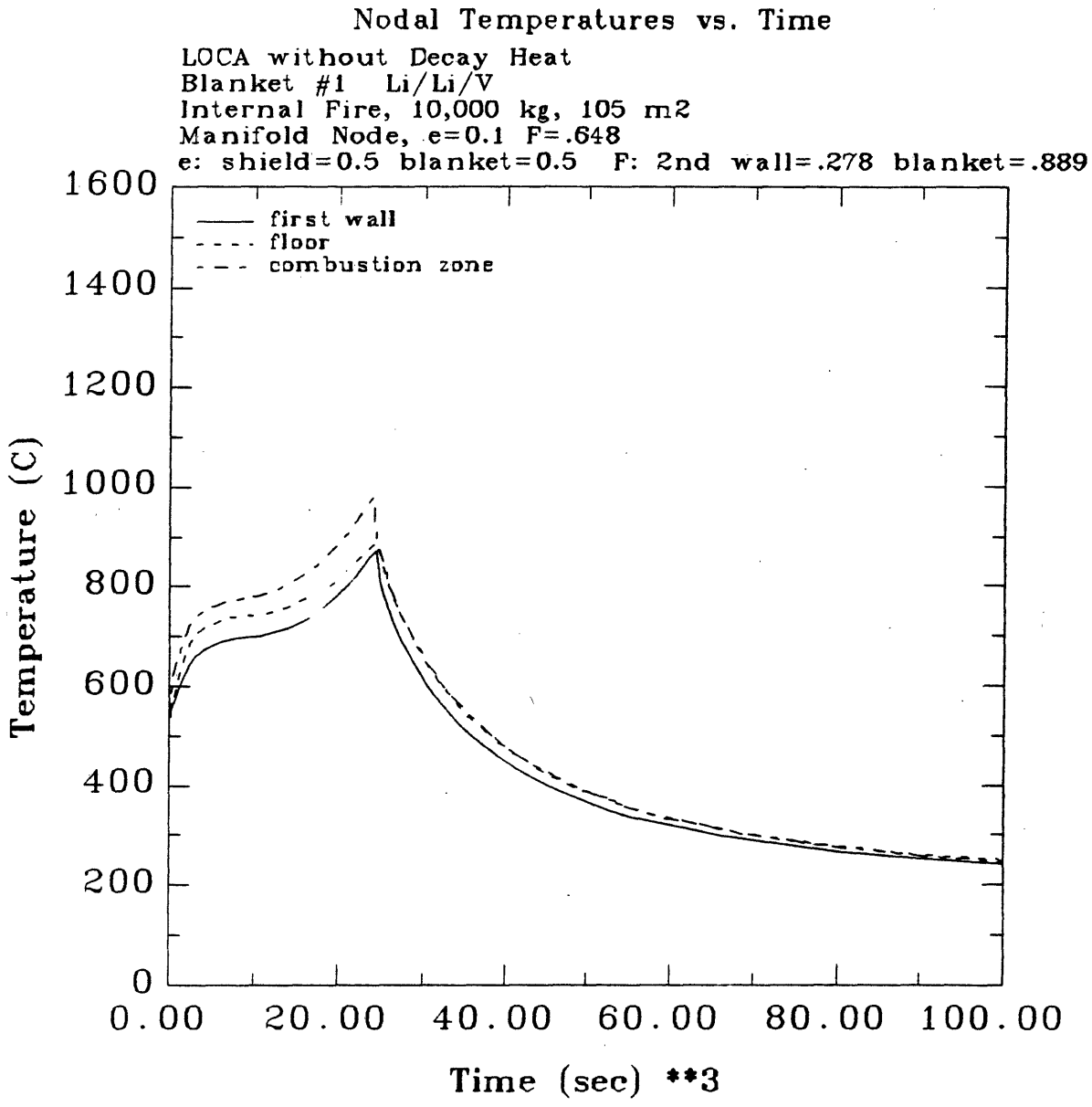

Figure 7-5: Results of the LOCA/torus fire calculation without decay heat

In the event that a different material was chosen for the reactor structure, the temperature increase due to just the loss of coolant accident would probably be greater than that experienced by the vanadium blanket[18]. Since the maximum first wall temperature of the vanadium blanket was 1000°C, in the event of a fire, any first wall temperature increase due to the thermal or nuclear properties of the structure would serve to drive the lithium temperature closer to the lithium-nitrogen reaction cut-off point of 1127°C. That would greatly reduce the lithium reaction rate (the non-reacting nitrogen in the air would then serve as an inert gas) and the extra temperature rise due to the fire would thusly be reduced. The higher first wall temperature caused by the LOCA would probably also exceed the temperature limit of the structural material[18]. Therefore, since the fate of the first wall would probably already have been sealed by the occurrence of the LOCA, the additional occurrence of a lithium fire inside the plasma chamber would probably not increase the threat to the integrity of the structure greatly.

Chapter 8

Conclusions and Recommendations for Future Work

8.1 Conclusions

This work consists of three parts: lithium reaction kinetics experiments performed with steam-nitrogen and steam-air mixtures; development and application of a model to simulate large lithium fires associated with hypothetical fusion reactors in the presence of a steam-air atmosphere; and development and application of a model to simulate lithium fires in the plasma chamber of a tokamak in the presence of radioactive decay heat. Each part was described in detail in earlier chapters. The impact of the results of each part on the future design or operation of fusion reactors may now be assessed.

8.1.1 Impact of Steam on Lithium Fires

8.1.1.1 Experiments

Forty-two kinetic experiments were performed, in each of which approximately three grams of lithium were burned in steam-nitrogen and steam-nitrogen-oxygen mixtures. The lithium reaction rates with each of the individual gases was measured and characterized as a function of the gas composition and the lithium pool temperature. The results of the reaction kinetics experiments show that the lithium-nitrogen reaction rate is significantly affected by the presence of steam. Steam, in addition to reacting with the lithium itself, serves to catalyze the lithium-nitrogen reaction . In this work the catalytic effect of steam is defined as the ratio of the lithium-nitrogen reaction rate in the presence of steam to the the reaction rate in the absence of steam. The catalytic effect is most pronounced at low temperatures but decreases exponentially with increasing temperature until it disappears above 700°C. Thus the presence of steam allows the nitrogen to react more quickly at low temperatures; it serves to reduce the kinetics limiting effect on the lithium-nitrogen reaction rate.

When lithium is burned in the presence of nitrogen, oxygen and steam, the inhibiting effect of the oxygen and the catalytic effect of the steam counteract each other to some degree, as the nitrogen reaction rate is higher than in the presence of dry air, but lower than in the presence of only steam. The catalytic effect of the steam falls off exponentially with increasing temperature but at higher temperatures it is stronger in the presence of air than in the presence of nitrogen alone, that is the ratio of the kinetics limited lithium-nitrogen reaction rates (steam:dry) is higher in air than in pure nitrogen. As the kinetics limited reaction rate increases with temperature, the nitrogen is better able to compete with the oxygen for the available supply of lithium and in turn the oxygen inhibition effect on the lithium-nitrogen reaction rate is reduced. Therefore, as a result of the reduction of the kinetics limiting effect *and* the oxygen inhibition effect, the total catalytic effect of the presence of steam on the lithium-nitrogen reaction rate is greater in air than in nitrogen.

The steam reaction rate itself is affected by the presence of oxygen. It was found that the oxygen in air (20% concentration) served to reduce the lithium-steam reaction rate by approximately 30% below that measured in the steam-nitrogen runs.

The results of the kinetics experiments may be a cause for some concern regarding the use of nitrogen as a cover gas for fusion reactors employing liquid lithium. The catalytic effect of the steam necessitates that the atmosphere be kept very dry, as a small amount of water vapor (from, say, a small steam line leak) could cause a lithium-nitrogen fire to burn more fiercely than was previously thought.

8.1.1.2 Analysis

Three groups of calculations were performed with LITFIRE to assess the effect of the presence of steam due to humidity in the air and/or a small steam line break in the event of a lithium spill onto the floor of a reactor containment building, and in the event of a lithium spill into the plasma chamber of a fusion reactor. The results of the containment building fire calculations showed that the principal effect of the steam was to enhance the heat transfer from the lithium pool and the combustion zone to the containment building atmosphere via thermal radiation. The presence of non-polar water vapor molecules served to increase the cell gas emissivity and thus the amount of heat radiated to the gas during a fire. The effect of the enhanced heat transfer was to raise the peak cell gas temperature in the containment building fire calculation by approximately 200°C. This in turn doubled the overpressurization of the containment building atmosphere compared to that calculated for a lithium fire in a dry air atmosphere. It was also found that the injection of additional steam from a steam line leak (4.53 kg/s) into the containment building had little effect above and beyond that seen with humidity (70%) in the air.

When lithium was assumed to have spilled into the plasma chamber instead of onto the containment building floor, the steam actually served to reduce the lithium pool and combustion zone temperatures by enhancing the radiant heat transfer from

the walls of the reactor to the surrounding containment building. The steam also increased the gas temperature inside the chamber, which served to reduce the gas flow rate from the gas to the combustion zone and thus the lithium reaction rate. This was due to the fact that the gas flow rate to the combustion zone is governed by natural convection, which is driven by the temperature difference between the combustion zone and the cell gas above. The combination of the enhanced cooling of the reactor and the reduction in the lithium reaction rate both served to reduce the temperatures of the lithium pool and the first wall below those calculated for a dry air atmosphere. Similar to the containment building fire case, it was seen that the injection of steam into the containment building during the fire (680 kg/s for 4.5 s) had little effect above and beyond that caused by the humidity in the air.

The results of the LITFIRE calculations have serious design implications for the containment buildings of fusion reactors, as the increased overpressurization caused by the presence of steam would directly increase the stress on the containment building walls. Therefore it will be necessary to increase the strength of the containment building or to ensure that steam could not possibly be present in the atmosphere in the event of a lithium spill. This could be accomplished by isolating the reactor in a subcontainment, separate from the steam generators or intermediate cooling loop.

The results of the plasma chamber fire calculations are somewhat encouraging in that the steam was seen to have a slightly favorable effect upon the temperature response of the first wall. That would indicate that the presence of steam inside the plasma chamber during a fire in the chamber would not be devastating, but one could not be sure that the lithium would spill only into the chamber and not out onto the containment building floor. If that was to occur the results of the containment building fire calculation would apply and the integrity of the containment building could be endangered. Therefore, it is recommended that steam be kept out of the containment building atmosphere as long as liquid lithium is used as the reactor breeder or coolant, or that the building design requirements include the effects of

steam on lithium fires.

8.1.2 Impact of Decay Heat on Lithium Fires

A model was created to simulate a lithium fire inside a tokamak plasma chamber and account for the presence of radioactive decay heat generation in the blanket structures of the reactor. The model accounts for the heat transfer pathways from the plasma chamber to the containment building through the blanket structures as well as the decay heat generated in them. Two calculations were performed, one simulating the simultaneous occurrence of a loss of flow accident (LOFA) and a lithium fire, and one simulating a simultaneous occurrence of a loss of coolant accident (LOCA) and a lithium fire. The self-cooled lithium/vanadium structure blanket from the BCSS was used for the calculations, as it was rated as the best performing tokamak blanket[21]. It was also calculated to respond relatively well to hypothetical undercooling transients[18].

The results of the calculations showed that the effect of the fire in the LOFA case was to raise the maximum temperature of the first wall by about 200°C (to 875°C), and in the LOCA case to raise it by about 100°C (to 1100°C). The reason for the lower temperature rise in the LOCA case was that the lithium pool temperature approached the cut-off point for the lithium-nitrogen reaction (1127°C). Therefore the lithium-nitrogen reaction rate was reduced by the kinetics limit and less energy was liberated by the lithium combustion.

In the event of a LOCA without a fire, the first wall temperature was calculated to reach a maximum temperature of 1000°C. Vanadium undergoes a phase change at 1000°C that greatly reduces its ductility and would make it non-reusable. Therefore the incremental effect of a temperature increase of 100°C caused by a fire would not greatly increase the already large threat caused by the LOCA. In the event of a LOFA without a fire, the first wall temperature was calculated to reach a temperature of 650°C; with the fire it was calculated to reach 875°C. Raising the temperature to

650°C would not be sufficient to cause the material to creep. Since 875°C is slightly above half the absolute melting temperature of vanadium, thermal creep would begin to occur which could damage the first wall. The threat to the integrity of the first wall would be increased, albeit not drastically so.

The thermal response of a blanket composed of a different material such as HT-9 could be expected to be similar to the Li/Li/V blanket, as blankets composed of HT-9 have also been analyzed and found to perform similarly to vanadium in the event of LOFA/LOCA in the absence of a fire[18]. Therefore it would be expected that an HT-9 blanket would respond to a lithium fire in a similar manner. HT-9 has a failure temperature of about 900°C[18]. Thus a peak first wall temperature of 875°C with a fire, compared to 650°C without one would be much more threatening to the structural integrity of the wall. A temperature of 1000°C reached during a LOCA without a fire would cause the wall to fail, so the simultaneous occurrence of a fire would be a moot point with regard to the first wall—the fate of the first wall would already have been sealed. Therefore the greatest *increase* in the threat to the safety of the reactor caused by a fire in the plasma chamber would come about in the event of a LOFA, rather than a LOCA.

This finding also has design and operational implications for future reactors: a lithium spill into the plasma chamber could turn an accident (LOFA) previously believed to be less than catastrophic into a significant threat to the safety of the reactor. The consequences of such an accident could be mitigated by designing the reactor so that natural circulation could remove more of the decay heat after the accident. If one can assume that any reactor employing a liquid lithium coolant or breeder would have a modular blanket, then natural circulation in the intact loops could remove heat even though one loop had been punctured and a fire was burning inside the plasma chamber. If natural circulation was insufficient to remove enough decay heat, the time scale of the accident could give operators a chance to restart the reactor coolant pumps on the other modules and use forced convection to remove the

heat. Barring either of those options, a passive system could be designed to flood the vacuum gap between the blanket back wall and the shield, thus improving the heat transfer away from the blanket and into the shield. Any solid, liquid or gas would enhance the heat transfer via conduction or convection.

The effects of the fire itself could be mitigated through a fire suppression system. Such a system could be designed to inject an inert gas like helium or argon into the plasma chamber to suppress the fire. The inert gas would serve to reduce the amount of air that was supplied to the fire which would in turn reduce the lithium reaction rate. The reduction of the lithium reaction rate would reduce the maximum temperature reached during the accident. In order to maximize the effectiveness of such a system, the inert gas would have to be injected directly into the plasma chamber. Injection into the surrounding containment building would cause a mixture of inert gas and air to seep slowly through the crack into the plasma chamber; the suppressive effect would be greatly reduced. The fire suppression system could be designed to operate in conjunction with the plasma quenching system used to shut off the plasma in the event of an undercooling transient. As soon as the transient was initiated an inert gas accumulator could inject the gas into the plasma chamber, simultaneously quenching the plasma and suppressing any fire that might start. If the injection rate was faster than the rate of influx of air into the chamber the fire might be prevented altogether.

8.2 Recommendations for Future Work

8.2.1 Lithium Reaction Kinetics

Lithium reaction kinetics experiments have been performed with mixtures of nitrogen, oxygen and steam, nitrogen and steam, nitrogen and oxygen, and nitrogen and steam alone[4,1,5]. All of the experiments measured the lithium reaction rate with the individual gases as a function of the lithium temperature and the composition of

the gas mixture. The range of gases expected to be found in the containment building of a future fusion reactor, with the possible exception of some inert gas like argon or helium, has been covered. Although most of the steam-air and steam-nitrogen experiments were performed at low to moderate temperatures, the trends in the results of those experiments and previous dry gas experiments indicate that further experimentation with steam at high temperatures would be unlikely to yield significant useful information with regard to assessing the safety of employing liquid lithium as a coolant or breeder in a reactor. At those temperatures the kinetics limit on the lithium-nitrogen reaction would be high enough that the steam catalytic effect would not be evident and, in the case of a large lithium fire, the lithium reaction rate would be limited by the gas flow rate to the reaction site.

Further experimentation with hydrogen gas in the presence of air or nitrogen could yield useful information about the reactions of lithium and oxygen in air with the hydrogen released by the lithium reaction with steam. Currently LITFIRE assumes that the hydrogen reacts neither with the lithium nor the oxygen, but merely builds up in the primary cell gas. Such an assumption may not be correct, as the hydrogen may react with lithium to form lithium hydride or oxygen to form water. If it reacted to form water, the water could then react with the lithium to release hydrogen and an equilibrium concentration of hydrogen could be established inside the primary cell. Kinetics experiments could provide information as to whether or not that was the case. Regarding the hydrogen issue, the branching ratio between the lithium-steam reactions that produce lithium oxide and lithium hydroxide was taken from the results of one HEDL pool fire test (LPS-1). Lithium-steam reaction tests that included a precise measurement of the reaction product distribution would enable the hydrogen generation rate from the lithium-steam reaction to be more accurately determined.

Kinetics experiments may be useful in determining the reactivity of lithium-lead with steam-air mixtures. Previous experiments have measured the reaction rate between lithium-lead and pure steam[5], and large pool tests have been done with

lithium-lead and air[6], but no experiments have been done with lithium-lead and steam-air mixtures. The results of the air tests showed that in all cases the temperature of the metal did not increase, and the steam tests measured a very low reaction rate between $Li_{17}Pb_{83}$ and steam[6,5]. Steam-air kinetics tests are likely to show the same low reaction rates, but a catalytic effect, similar to the one observed in the lithium-steam-nitrogen and lithium-steam-air experiments, may be discovered. Such an effect could raise the reaction rates above those expected based upon the results of the previous air and steam experiments.

Besides the chemical reaction kinetics tests, experimentation could be done in the area of radiative heat transfer in steam-air mixtures to determine the accuracy of the correlation currently used to calculate the emissivity of the atmosphere in LITFIRE. The increase in the emissivity caused by the presence of steam has a significant effect on the gas temperature and the gas pressure. Confirmation of the accuracy of the emissivity correlation would lend greater confidence to the results of the calculations, while revelation of the inaccuracy of the correlation would necessitate that changes be made to the code and the calculations performed again.

8.2.2 Lithium Fire Modeling and the LITFIRE Code

The LITFIRE code currently has the capability to model lithium and lithium-lead reactions with all gases expected to be present in the containment building atmosphere of a fusion reactor. The code has been calibrated by using the results of lithium pool-gas tests conducted at HEDL and lithium reaction kinetics experiments conducted at MIT. Further improvements can be made by using the results of future lithium-lead kinetics tests to calibrate the lithium-lead reaction model.

Further improvements could perhaps also be made by reexamining the interpretation of the results of the lithium-nitrogen-oxygen kinetics experiments. Those results are currently modeled by the code as a pure nitrogen reaction kinetics limit (determined from the lithium-nitrogen kinetics experiments) and an oxygen inhibition

factor. The inhibition factor currently reduces the lithium-nitrogen reaction rate as a function of the lithium temperature and the oxygen concentration. It is applied regardless of whether or not the lithium-nitrogen reaction rate is being governed by the flow rate of nitrogen to the combustion zone or the nitrogen reaction kinetics limit. Chemical kinetics would suggest that if the reaction rate is truly flow rate dependent, that is the gas flow rate to the combustion zone is so low that even if all of the gas reacted immediately the reaction rate would still be below the measured kinetics limit, then other kinetics effects, like the oxygen inhibition effect, should not take effect, and all of the gas should, in fact, react immediately. LITFIRE assumes that the oxygen inhibition factor affects not only the nitrogen kinetics limit, but also the lithium-nitrogen reaction rate in the flow dependent regime. This assumption may not be correct. The code should be recalibrated with the oxygen inhibition factor affecting only the lithium-nitrogen kinetics limit. The results of the recalibration could then be compared to the old results to determine which assumption was more correct. Care should be taken during the recalibration and comparison to consider not only the temperature response of the test cell (most likely a HEDL test) but also, and importantly, the lithium reaction rates with each of the component gases. It should be noted that the results of the steam-air experiments, expressed in terms of the steam catalytic factor, have been applied in LITFIRE only to the lithium-nitrogen kinetics limit.

It is clear from the results of previous calculations performed with LITFIRE that the consequences of a lithium fire in an air atmosphere (moist or dry) would be quite severe and would pose a definite threat to the safety of the reactor and containment building. Therefore air should be considered to be undesirable as a containment atmosphere from a safety point of view. Because of this, it is desirable to study other options available to use as containment building atmospheres. One possibility that in fact allowed a lithium cooled blanket to receive the highest safety rating from the BCSS is the use of nitrogen as a reactor cover gas. Nitrogen reacts more

slowly with lithium and releases less energy per unit mass of lithium consumed. It is also cheap and compatible with any reactor structural material. Calculations should be performed with LITFIRE to predict the temperature and pressure response of a reactor containment building with a nitrogen atmosphere over a wide range of conditions. These conditions should include the presence of steam due to a steam line break. Such calculations would be valuable in quantifying the enhancement of the safety of the reactor and could perhaps disclose some heretofore unknown problems.

Calculations performed with LITFIRE to assess the consequences of lithium fires in nitrogen atmospheres would, when combined with the results of previous calculations performed with air atmospheres, provide a significant data base for assessing the safety of using liquid lithium as a breeder or coolant in a fusion reactor. Such a data base does not exist, however, for lithium-lead. It is believed that the low reactivity of lithium-lead would greatly reduce the chemical reaction safety hazard compared to that of lithium[6], but that has not yet been confirmed by modeling large fires. LITFIRE calculations have been performed with lithium-lead but not nearly over the range of conditions that has been covered for lithium[23]. After the results of the lithium-lead kinetics experiments were used to improve the lithium-lead reaction model, such calculations could be performed and the safe use of lithium-lead could be assessed.

Appendix A

Calculations Used by LITFIRE in Modeling Lithium Fires

A.1 Emissivity of the Lithium Pool

The emissivity of the lithium pool is assumed to increase as reaction products are generated and they accumulate on the surface of the pool. The pool is assumed to start with an emissivity of 0.2 which increases linearly with the thickness of the reaction product buildup until the buildup is two millimeters thick, at which time the the pool emissivity ϵ_p is taken to be 0.9.

$$\epsilon_p = 0.2 + 0.7 \cdot t_p/(2\text{ mm}) \tag{A.1}$$

where

$$t_p = \frac{1}{A_{\text{pool}}} \sum_p \frac{m_p}{\rho_p}. \tag{A.2}$$

A_{pool} is the area of the lithium pool, m_p is the mass of an individual reaction product and ρ_p is the density of an individual reaction product.

A.2 Heat and Mass Transfer Coefficients

This section details the correlations used in LITFIRE to calculate heat and mass transfer coefficients.

A.2.1 Gas Natural Convection

In LITFIRE, natural convection heat transfer coefficients, used to calculate the heat transfer rates between the containment structures or combustion zone and the atmosphere, are calculated as functions of the structural or combustion zone temperature T_s or T_{cz}, the gas temperature T_g, and the gas density ρ_g:

$$h = 1.73C\,(0.014 + 1.92 \cdot 10^{-5}(\overline{T} - 460))\left[\frac{32.17\overline{\beta}|T_s - T_g|}{\overline{D}}\right]^{0.3333} \text{ W/mK} \qquad \text{(A.3)}$$

where

$$\overline{D} = \left[\frac{4.94 \cdot 10^{-5}\overline{T} + 0.0188}{3600\,\rho_g}\right]^2 \text{ ft}^4/\text{s}^2, \qquad \text{(A.4)}$$

$$\overline{\beta} = \frac{1}{\overline{T}} \qquad \text{(A.5)}$$

and

$$\overline{T} = \frac{T_s + T_g}{2}. \qquad \text{(A.6)}$$

The mass transfer coefficient, used to calculate the natural convection gas flow rate from the bulk gas to the combustion zone, is calculated in a similar manner:

$$h_m = 8.47 \cdot 10^{-5} C\,241.7\frac{(\overline{T}/493.2)^{2.5}}{132.0 + \overline{T}/1.8}\left[\frac{32.17\overline{\beta}|T_{cz} - T_g|}{\overline{D}}\right]^{0.3333} \frac{\text{m}}{\text{s}} \qquad \text{(A.7)}$$

If no combustion is occurring, the lithium pool temperature T_{Li} is substituted for the combustion zone temperature T_{cz}. As these calculations take place within the code, all temperatures and densities are in British units (°R and lbm/ft^3).

A.2.2 Water Vapor and Liquid Water Natural Convection

Heat transfer via natural convection involving a water pool is determined somewhat differently. Nusselt number Nu correlations are used to calculate the heat transfer coefficients between the pool and the cell gas h_b:

$$h_b = \frac{k}{L} Nu \tag{A.8}$$

$$Nu = C(GrPr)^n \tag{A.9}$$

where Gr and Pr are the Grashof and Prandtl numbers, respectively:

$$Gr = \frac{\beta g \Delta T L^3}{\nu^2} \tag{A.10}$$

$$Pr = \frac{\mu c_p}{k} \tag{A.11}$$

where ΔT = temperature difference between the cell gas and the pool

L = characteristic length of the pool (taken as $A_{pool}^{\frac{1}{2}}$)

k = thermal conductivity of the steam-air mixture at the boundary layer temperature

All other properties are evaluated at the boundary layer temperature and the water is assumed to be saturated liquid. Values for C and n are dependent upon the value of the product $GrPr$ as shown in Table A.1[12].

h_b is not the final sensible heat transfer coefficient, as rapid mass transfer by evaporation or condensation may increase its value. If the mass transfer rate is high, the sensible heat transfer rate will be increased due to sensible heat transfer by vapor molecules. Thus h_b is modified to include this effect:

$$h_b' = \left[\frac{a}{e^a - 1}\right] h_b \frac{\text{Btu}}{\text{s ft}^2\ ^\circ\text{R}} \tag{A.12}$$

where

$$a = \frac{18 K_b c_{p_g} (x_g - x_b)}{h_b x_{am}}. \tag{A.13}$$

Table A.1: Water pool heat transfer correlation coefficients

$GrPr$	C	n
Heated Surface		
$> 3 \cdot 10^{10}$	0.021	0.4
$2 \cdot 10^{7} - 3 \cdot 10^{10}$	0.14	0.333
$10^{5} - 2 \cdot 10^{7}$	0.54	0.25
Cooled Surface		
$3 \cdot 10^{5} - 3 \cdot 10^{10}$	0.27	0.25

The mass transfer coefficient K_b was determined by:

$$K_b = \frac{h_b}{18 c_{p_g}} \left(\frac{Pr}{Sc}\right)^{2/3} \frac{\text{lbm}}{\text{s ft}^2} \tag{A.14}$$

where c_{p_g} is the specific heat of the cell gas, and Sc is the Schmidt number, given by:

$$Sc = \frac{\nu}{D_{AB}} \tag{A.15}$$

where D_{AB} is the diffusivity of the steam-air mixture. An expression for D_{AB} has been determined experimentally:

$$D_{AB} = \frac{1.742 \cdot 10^{-9} T^{2.334}}{p} \frac{\text{ft}^2}{\text{s}} \tag{A.16}$$

If ΔT and thus the Grashof number and h_b are zero, a different expression is used for K_b:

$$K_b = \frac{p D_{AB}}{LRT} \left[\frac{L^3 g(\rho_o - \rho_b)}{\mu D_{AB}}\right]^{0.373} \tag{A.17}$$

where R = universal gas constant

ρ_o = bulk water vapor density (lbm/ft^3)

ρ_b = boundary layer water vapor density (lbm/ft^3)

Liquid water convective heat transfer coefficients, used to calculate heat transfer rates from the water pool to the floor liner underneath, are calculated from $GrPr$ in a manner identical to that used to determine h_b, except that liquid water properties are used in place of boundary layer properties.

A.2.3 Lithium Pool-Combustion Zone Conduction

Heat transfer between the lithium pool and the combustion zone takes place via thermal radiation and heat conduction through a mixture of atmospheric gas and lithium vapor. The thermal resistance between the zone and pool is calculated from the thickness of the vapor region, the thermal conductivity of the region, and the

lithium pool area (see Equation 5.8). The thermal conductivity of the vapor region k_f is calculated using a pressure weighted average of the lithium vapor conductivity and the gas conductivity:

$$k_f = \frac{p_{Li_v}(k_{Li_v} - k_{N_2}) + p_g k_{N_2}}{14.7} \frac{\text{Btu}}{\text{s ft °R}} \tag{A.18}$$

where the lithium vapor pressure p_{Li_v} is given by:

$$p_{Li_v} = 14 \cdot 10^{4.8831 - 14180.2/T_{Li}} \text{ psia} \tag{A.19}$$

The lithium vapor conductivity k_{Li_v} and the gas conductivity k_{N_2} are given by:

$$k_{Li_v} = 0.55 + \hat{T}(-4.99 \cdot 10^{-4} + 1.206 \cdot 10^{-7}\hat{T}) \frac{\text{Btu}}{\text{s ft °R}} \tag{A.20}$$

$$k_{N_2} = 0.0432 + \hat{T}(0.0078 - \hat{T}(8.2 \cdot 10^{-4} + 2.08 \cdot 10^{-4}\hat{T})) \frac{\text{BTU}}{\text{s ft °R}} \tag{A.21}$$

where

$$\hat{T} = 0.002\frac{T_{cz} + T_{Li}}{2} - 3.92 \tag{A.22}$$

where p_g = atmospheric pressure (psia)

T_{Li} = lithium temperature (°R)

T_{cz} = combustion zone temperature (°R)

The thickness of the vapor region is calculated from the density of the lithium vapor, the lithium mass flow rate (taken to be the combustion rate) and the diffusion coefficient of lithium in air (see Equation 5.9). The density of the lithium vapor ρ_{Li_v} is calculated as:

$$\rho_{Li_v} = \frac{144\, p_{Li_v}}{RT_{Li}} \text{ lbm/ft}^3 \tag{A.23}$$

and the diffusion coefficient of the lithium in air D_L is calculated as:

$$D_L = 3.56 \cdot 10^{-3}\frac{(T_{Li}/460)^{1.81}}{p_g} \text{ ft}^2/\text{s} \tag{A.24}$$

Thus the thermal resistance between the lithium pool and the combustion zone is determined.

A.3 Lithium Reaction Kinetics Calculations

In LITFIRE the lithium-nitrogen reaction rate is limited by either the nitrogen flow rate to the reaction site or the reaction kinetics limit observed in the lithium nitrogen-kinetics experiments (see Chapter 2), whichever is lower. The kinetics limit curves, with their ranges of applicability in terms of the lithium pool temperature (°C), are shown below (reaction rates RR are given in (g Li/min cm^2)):

$$
\begin{aligned}
&\text{for } T < 400 && \text{RR} = 0.008\,\tfrac{T-200}{200} \\
&\text{for } 400 \le T > 450 && \text{RR} = 0.008 + 0.001\left(\tfrac{T-400}{50}\right) \\
&\text{for } 450 \le T < 500 && \text{RR} = 0.009 + 0.008\left(\tfrac{T-450}{50}\right) \\
&\text{for } 500 \le T < 550 && \text{RR} = 0.017 + 0.011\left(\tfrac{T-500}{50}\right) \\
&\text{for } 550 \le T < 600 && \text{RR} = 0.028 + 0.022\left(\tfrac{T-550}{50}\right) \\
&\text{for } 600 \le T < 650 && \text{RR} = 0.050 + 0.043\left(\tfrac{T-600}{50}\right) \\
&\text{for } 650 \le T < 700 && \text{RR} = 0.093 + 0.307\left(\tfrac{T-650}{50}\right) \\
&\text{for } 700 \le T < 725 && \text{RR} = 0.400 + 0.225\left(\tfrac{T-700}{25}\right) \\
&\text{for } 725 \le T < 750 && \text{RR} = 0.625 + 0.125\left(\tfrac{T-725}{25}\right) \\
&\text{for } 750 \le T < 800 && \text{RR} = 0.750 + 0.066\left(\tfrac{T-750}{50}\right) \\
&\text{for } 800 \le T < 950 && \text{RR} = 0.89\sin\left(\tfrac{T}{600} - 0.175\right) \\
&\text{for } 950 \le T < 1050 && \text{RR} = 0.875 - 0.015\left(\tfrac{T-950}{100}\right) \\
&\text{for } 1050 \le T < 1100 && \text{RR} = 0.860 - 0.235\left(\tfrac{T-1050}{50}\right) \\
&\text{for } 1100 \le T < 1127 && \text{RR} = 0.625\left(\tfrac{1127-T}{27}\right)
\end{aligned}
\qquad \text{(A.25)}
$$

The presence of oxygen was also observed to reduce the lithium-nitrogen reaction rate. That effect is modeled by multiplying the preliminary lithium-nitrogen reaction rate (determined from the gas flow rate or the kinetics limit) by an oxygen inhibition factor R_{N_2}. The expressions used to calculate R_{N_2} as a function of the lithium temperature (°C) and the oxygen concentration are shown below:

5% oxygen:

$$500 \leq T \leq 750$$

$$R_{N_2} = 11.751 - 41.255U + 53.022U^2 - 22.962U^3 \quad \text{(A.26)}$$

$$750 \leq T \leq 1100$$

$$R_{N_2} = 13.173 - 55.058U + 77.625U^2 - 35.276U^3 \quad \text{(A.27)}$$

10% oxygen:

$$350 \leq T < 750$$

$$R_{N_2} = -0.176 + 5.925U - 6.998U^2 + 2.218U^3 \quad \text{(A.28)}$$

$$750 \leq T \leq 1100$$

$$R_{N_2} = 16.936 - 73.32U + 104.629U^2 - 48.067U^3 \quad \text{(A.29)}$$

20% oxygen

$$200 \leq T < 750$$

$$R_{N_2} = 0.391 + 4.128U - 8.161U^2 + 3.8U^3 \quad \text{(A.30)}$$

$$750 \leq T \leq 1100$$

$$R_{N_2} = 26.456 - 109.284U + 148.31U^2 - 65.412U^3 \quad \text{(A.31)}$$

where $U = T/750$. For values of oxygen concentration other than 5%, 10% or 20%, R_{N_2} is determined by interpolation.

A.4 Gas Transfer Between the Primary and Secondary Cells

In the two-cell option of LITFIRE, gas may flow between the primary and secondary cells through a crack in the primary wall. The gas mass flow rate from one cell to another is calculated from the pressure difference between the two cells using the following relation:

$$\dot{m} = 12 C_d A \sqrt{2 g_c \rho \Delta P} \text{ lbm/s} \quad \text{(A.32)}$$

where $\dot{m}$ = mass flow rate from one cell to another

C_d = coefficient of discharge (unity in LITFIRE)

A = area of crack (ft^2)

g_c = constant (32.2 lbm ft/s^2 lbf)

ρ = gas density (lbm/ft^3)

ΔP = pressure drop between the cells (psia)

The applicability of Equation A.32 is limited to the subsonic flow velocity regime, or:

$$\frac{P_{\text{high}}}{P_{\text{low}}} \leq \left(\frac{\gamma+1}{2}\right)^{\frac{\gamma}{\gamma-1}} \leq 1.89 \text{ for air} \tag{A.33}$$

where γ is the ratio of specific heats (c_p/c_v). For greater pressure ratios, the flow velocity is sonic, and the mass flow rate is determined from:

$$\dot{m} = 12 C_d A \sqrt{0.94 g_c \rho P} \tag{A.34}$$

where P is the higher of the two pressures.

The temperature change of the two cell gases caused by the mass flow is calculated from:

$$\frac{dU_n}{dt} = \pm \dot{m} h \text{ Btu/s} \tag{A.35}$$

where U_n is the internal energy of the gas in cell n and h is the specific enthalpy of the gas being transferred. Applying the following relations:

$$U_n = m_n c_{v_n} T_n \text{ Btu}, \tag{A.36}$$

$$h_n = c_{p_n} T_n \text{ Btu/lbm}, \tag{A.37}$$

using the definition of γ and performing some algebra, one obtains the following expressions for the temperature rates of change of the two cell gases due to the mass flow between them[9]:

$$\frac{dT_1}{dt} = \frac{\dot{m}(1-\gamma)T_1}{m_1 - \dot{m}\Delta t} \ ^\circ\text{R/s} \tag{A.38}$$

and

$$\frac{dT_2}{dt} = \frac{\dot{m}(\gamma T_1 - T_2)}{m_2 + \dot{m}\Delta t} \ ^\circ\text{R/s} \tag{A.39}$$

The mass flow rate $\dot{m}$ is taken to be positive from cell 1 to cell 2.

A.5 Lithium-Concrete Reaction

In the lithium-concrete reaction option, the lithium is assumed to penetrate the floor liner and react with the concrete underneath. The lithium reacts with the solid compounds in the concrete at a predetermined fixed rate, but it reacts with the water in the concrete as soon as the water is driven out. The following correlations are used to determine the water release rate from the concrete. The total amount of water ultimately remaining in the concrete at a given temperature (as $t \rightarrow \infty$) is given by:

$$W_f = W_i\{1 - \exp\left(26.207 + T_c\left[-0.0721 + T_c\{6.96 \cdot 10^{-5} - 2.26 \cdot 10^{-8} T_c\}\right]\right)/11.7\} \tag{A.40}$$

where W_i is the amount of water initially present in the concrete (lb/ft^3) and T_c is the temperature of the concrete (°R).

The water release *rate* is determined by assuming that the remaining water to be released eventually will be released in 30 seconds, that is:

$$\dot{W} = \frac{(W(t) - W_f)V_{con}}{30 \text{ sec}} \text{ lbm/s} \tag{A.41}$$

where

$$W(t) = W_i - \frac{1}{V_{con}} \int_0^t \dot{W} dt \text{ lbm/ft}^3 \tag{A.42}$$

and V_{con} is the volume of the topmost concrete node. If the concrete temperature is greater than 816°C, all of the water is assumed to be released in 30 seconds (i.e. $W_f \rightarrow 0$):

$$\dot{W} = \frac{W(t)V_{con}}{30 \text{ sec}} \tag{A.43}$$

In the HEDL experiment it was observed that the onset of the concrete reaction was delayed for five hours[9]. Thus it was decided to impose the condition that the concrete reaction not begin until $T_c \geq 250°C$.

A.6 Lithium Diffusion Through Lead

The diffusion coefficient for lithium diffusing through lead (used in the layered pool lithium-lead combustion model (see Equation 5.25)) is determined using the following expression:

$$D_{Li} = 6.0 \cdot 10^9 \exp\left(\frac{-680}{T_{Li}}\right) \text{ m}^2/\text{s} \tag{A.44}$$

where T_{Li} is in K.

A.7 Integrals

Every time dependent quantity in the code is expressed in terms of a first order ordinary differential equation. All time rates of change are integrated over each time step to calculate the values of the quantities during the execution of the code. The form of the integrals is:

$$S(t) = S_o + \int_0^t \frac{dS}{dt} dt \tag{A.45}$$

where $S(t)$ is the quantity being calculated, S_o is the initial value of S and dS/dt is the time rate of change of S. The code uses a fourth order Runge-Kutta Method or Simpson's Rule (user specified) to simultaneously solve all of the differential equations.

Appendix B

LITFIRE Program Description

The LITFIRE code is broken down into an initial routine and a dynamic cycle. The initial routine prepares the code for execution; then the dynamic cycle calculates and integrates the time rates of change of the code variables over each time step to calculate their values. The dynamic cycle is repeated until execution is terminated either by the code or as predetermined by the user.

B.1 Initial Routine

The initial routine prepares the code for execution. The four parts of the initial routine are:

1. Read input data
2. Write input data to a file
3. Initialize variables
4. Calculate spray fire effects

B.1.1 Reading and Writing of Input Data

The input data consist of titles and headings, control flags for the choice of options, containment building geometries, initial conditions and material properties. In this step the input data are read from separate files for use by the code. After the data are read by the code, they are immediately written into an output file to confirm that the data were read properly.

B.1.2 Variable Initialization

The initialization section sets all time rates of change to zero for the first step. Some constants are defined and initial conditions such as temperatures or gas masses and densities are determined using the input data. Since the code was originally written using British units, if input data were written in SI units they are converted over to the following units to be consistent with the rest of the code:

°R, BTU, pounds mass, feet, seconds

B.1.3 Spray Fire Calculation

The spray fire calculation is performed at the beginning of the execution of the code to determine the effect of the lithium reacting with the containment atmosphere as it sprays out of a pipe and onto the floor. This calculation is detailed in Chapter 5.

B.2 Dynamic Cycle

The dynamic cycle in LITFIRE calculates the temperature, pressure and mass profiles of the reactor containment over the time of the execution. Most of the dynamic cycle consists of calculating the thermal admittances between nodes, which are then used in conjunction with the nodal temperatures to determine the time rates of change of those temperatures. The time rates of change are then integrated over the time

step by use of the fourth order Runge-Kutta Method or Simpson's Rule. All of the calculations performed in the dynamic cycle are listed below in the order which they are performed:

1. Perform gas injection if necessary
2. Calculate temperature dependent heat capacities
3. Calculate individual gas fractions
4. Calculate gas emissivities and radiative interchange factors
5. Perform an energy balance to determine the gas temperature if the steam in containment option is used
6. Calculate natural convection gas heat transfer coefficients
7. Calculate thermal admittances
8. Perform steam injection if necessary
9. Perform lithium-lead diffusion calculation if necessary
10. Test for and calculate lithium or lithium-lead combustion
11. Calculate temperature rates of change from heat flow
12. Calculate lithium-concrete reaction if necessary
13. Calculate gas overpressure and leakage
14. Calculate aerosol removal rate via aerosol sticking
15. Perform integrations
16. Check for terminating execution
17. Perform time step control

18. Write the output to data files

19. Display error pointers if necessary

All but the last four of the steps performed in the dynamic cycle are described in Chapters 5 and 6. The last four are described below:

B.2.1 Termination Checks

The conditions that will terminate the code are:

- The lithium temperature reaches a value at which the lithium vaporizes (1347°C) or solidifies (180°C)
- The primary cell gas temperature returns to ambient temperature with no over-pressurization
- The code reaches the user specified stopping point (TIME≥TIMEF)

B.2.2 Time Step Control

Time step control is important for maintaining numerical stability. Three criteria are used to determine the size of the time step used during each dynamic cycle. They are:

- The time step must be smaller than a user defined fraction (RELERR) of the inverse rates of change:

$$\Delta t < \text{RELERR}\ T / \left(\frac{dT}{dt}\right)$$

- The conduction heat transfer limit must be satisfied:

$$\frac{\alpha \Delta t}{(\Delta x)^2} < 0.3$$

- The user imposed maximum and minimum time steps must be observed.

Although LITFIRE uses the most sensitive criteria to set the time step, instability may still occur if a node is too thin or is given too high of a thermal conductivity.

B.2.3 Writing the Data to Output Files

As the calculations of the temperature and pressure histories of the containment building are calculated, values of the nodal temperatures and the cell gas pressures are recorded in data files which may be printed at the end of the execution of the code.

B.2.4 Error Pointers

The execution of the code is terminated and error pointers are printed for the following reasons:

- Incompatible options are used together
- The spray fire calculation cannot be solved for $T < 10^6$°R
- The combustion zone temperature is negative
- The aerosol removal fraction is too large
- The depleted lead layer thickness $\geq 1/3$ the pool depth

Appendix C

Recalibration of the LITFIRE Code

After the experimental data on the oxygen inhibition factor were incorporated into the code (see Section 5.2.3 and Appendix A), it was deemed necessary to recalibrate the code in order to improve its performance, and to ensure that the results of calculations performed by LITFIRE still fit the results of the HEDL lithium pool fire experiments that were used to calibrate it previously. The older version of the code had used an oxygen inhibition factor that was determined empirically by fitting the results of LITFIRE calculations to the HEDL results, rather than the one determined from the lithium-mixed gas kinetics experiments[1]. It was decided to use the data from the HEDL tests LN-2 and LA-5 (see Chapter 2), as they were rather different from each other, and if LITFIRE predicted their results reasonably well, it would show that the code could more confidently be used to predict the temperature and pressure response of a containment building or some other test cell to a lithium fire.

The LA-5 test was chosen because it was the largest test performed by HEDL (100 kg Li, 850 m^3 test cell) and it comes the closest to representing a lithium spill and fire inside a containment building. The LN-2 test was chosen because it was a small (10 kg Li, 14.1 m^3 test cell), moderate temperature (532°C) nitrogen fire—it

was the farthest test from LA-5 that actually ignited.

C.1 The LA-5 Test

The final results of the simulation of the LA-5 test are shown in Figures C-1–C-4. It can be seen from the figures that LITFIRE agreed rather well with the HEDL data, although it was conservative in that it tended to overpredict the temperatures and the gas pressure. The difference between the HEDL values and the LITFIRE calculations at the end of the run was due to the fact that the HEDL experiment was terminated 3900 seconds after it was begun. The results obtained would tend to lend confidence to the belief that LITFIRE could reasonably predict the response of a reactor containment building to a lithium fire.

C.2 The LN-2 Test

The results of the simulation of the LN-2 test are shown in Figures C-5–C-7. It can be seen that LITFIRE predicted the lithium pool temperature fairly well, although it underpredicted the cell gas and cell wall temperatures somewhat. That suggests that the thermal coupling between the lithium pool and the cell wall and gas could be a little too low. It should be noted, however, that the same modeling input for the heat transfer coefficients and radiative emissivities were used for both cases. Increasing the thermal coupling between the pool and the gas could cause LITFIRE to be even more conservative in the large fire case. Since that case is closest to a fire inside a containment building, it would be better to err slightly on the side of it rather than on the side of the small nitrogen fire.

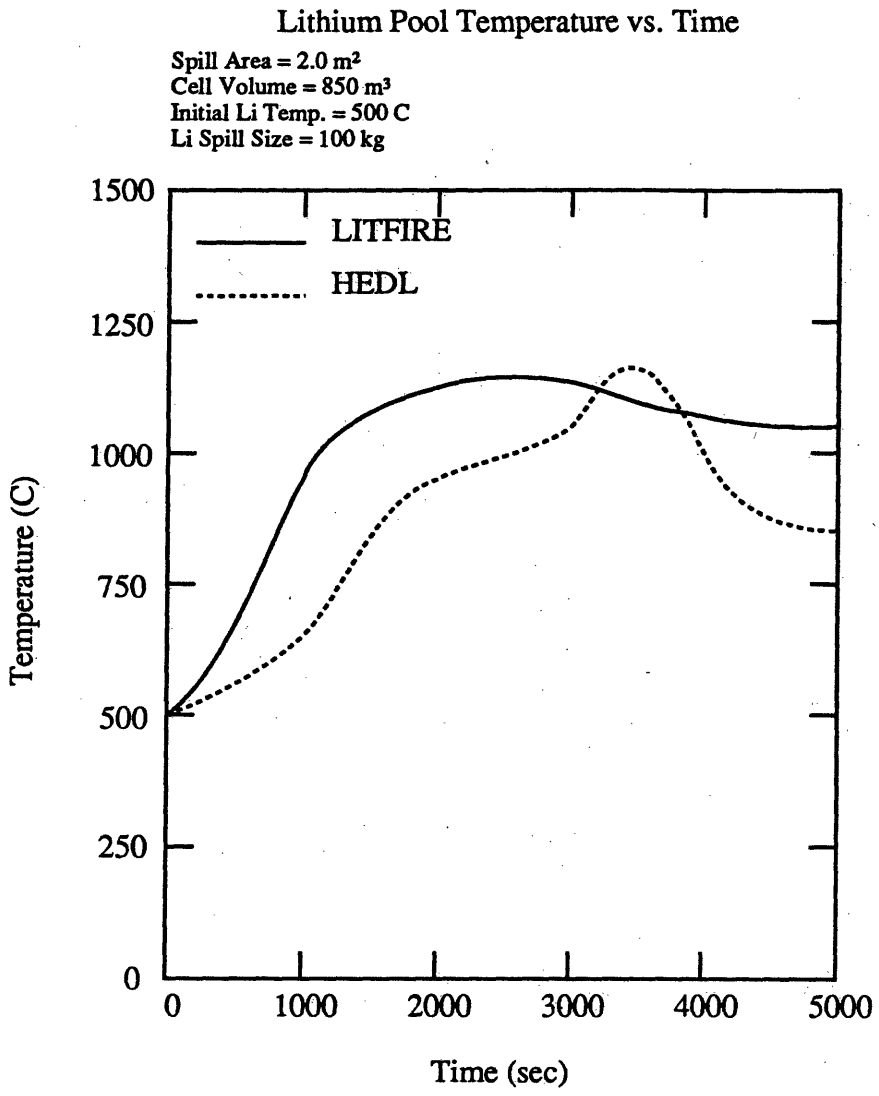

Figure C-1: LA-5 lithium pool temperature

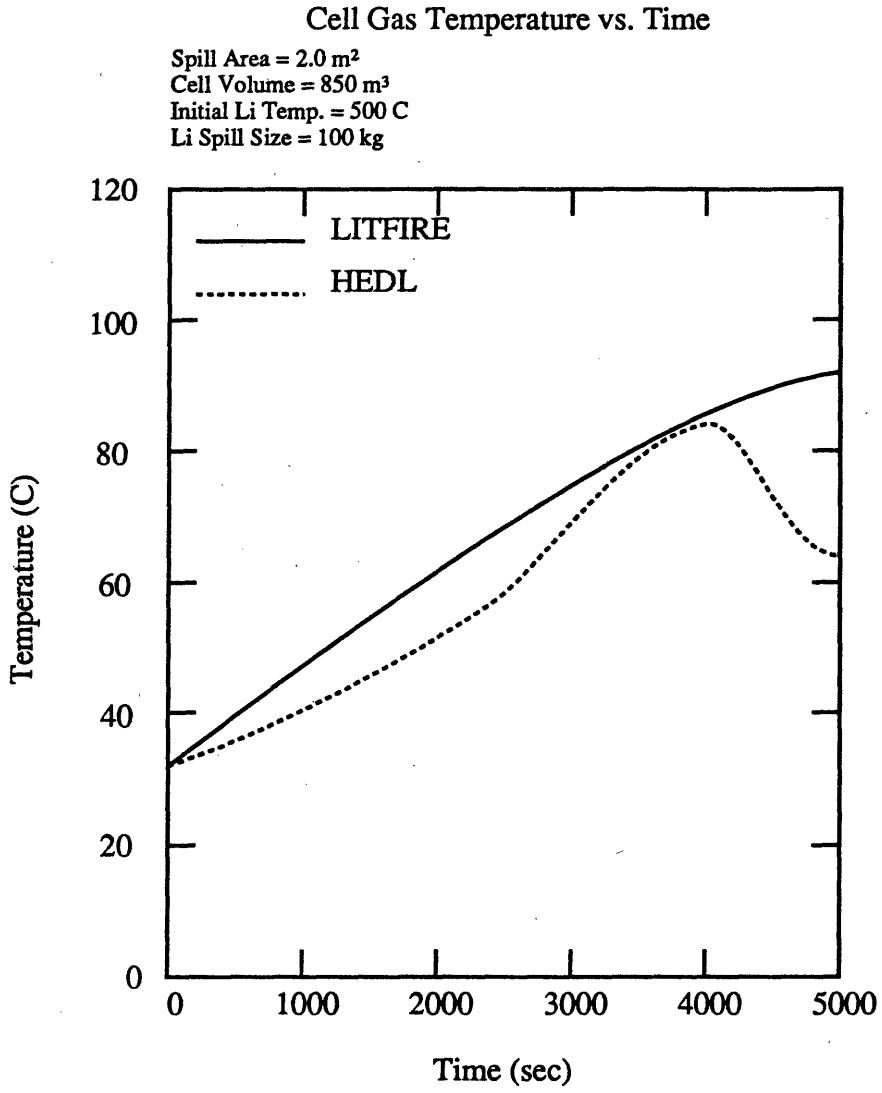

Figure C-2: LA-5 cell gas temperature

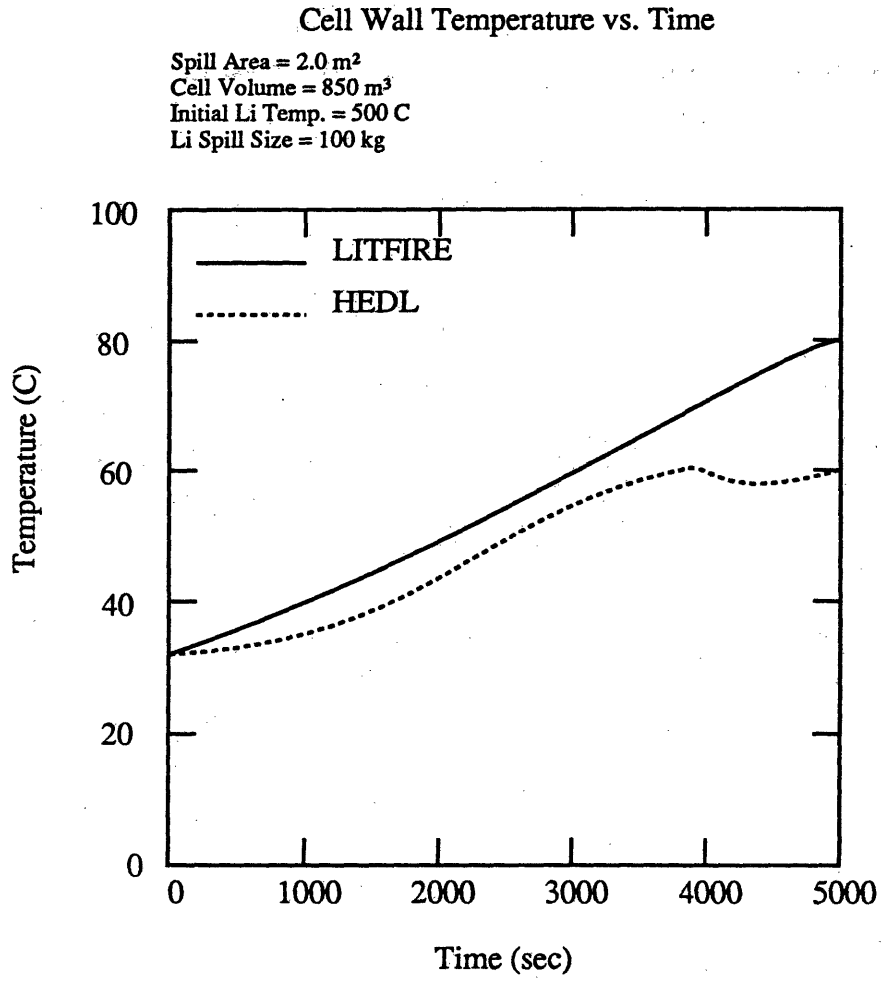

Figure C-3: LA-5 cell wall temperature

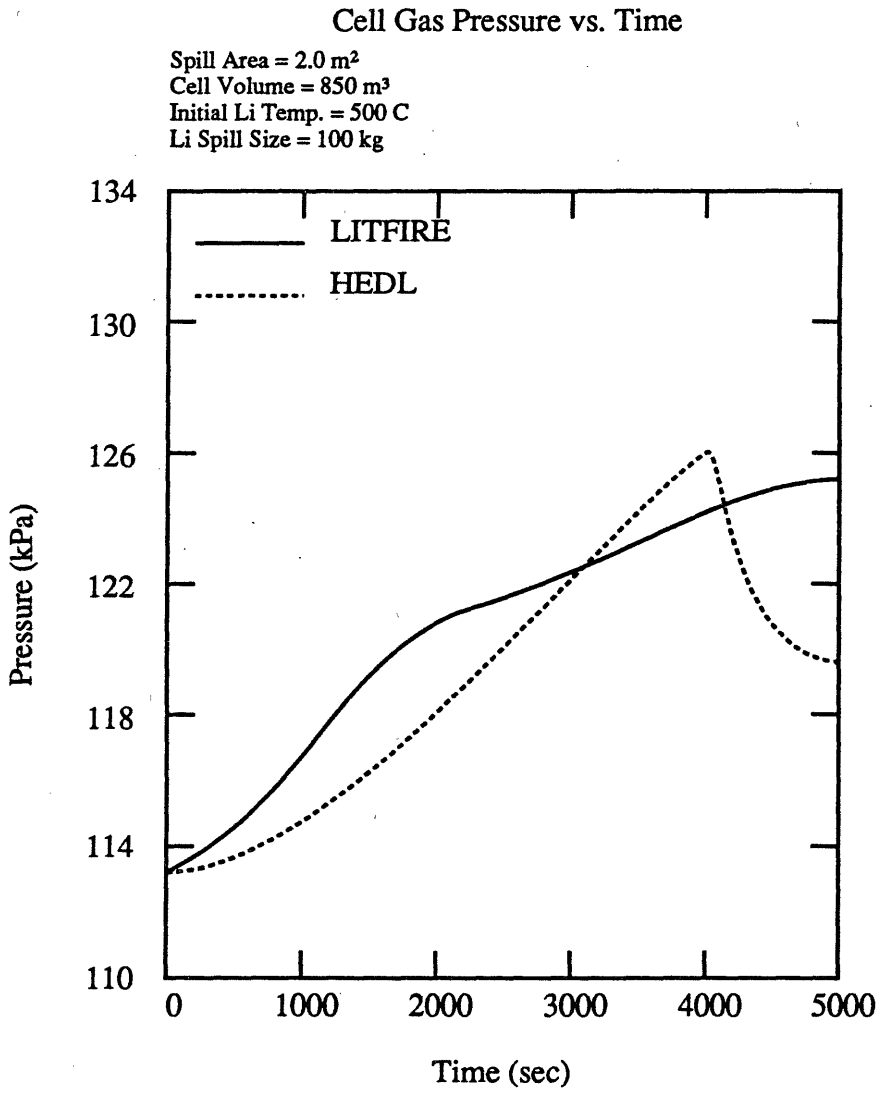

Figure C-4: LA-5 cell gas pressure temperature

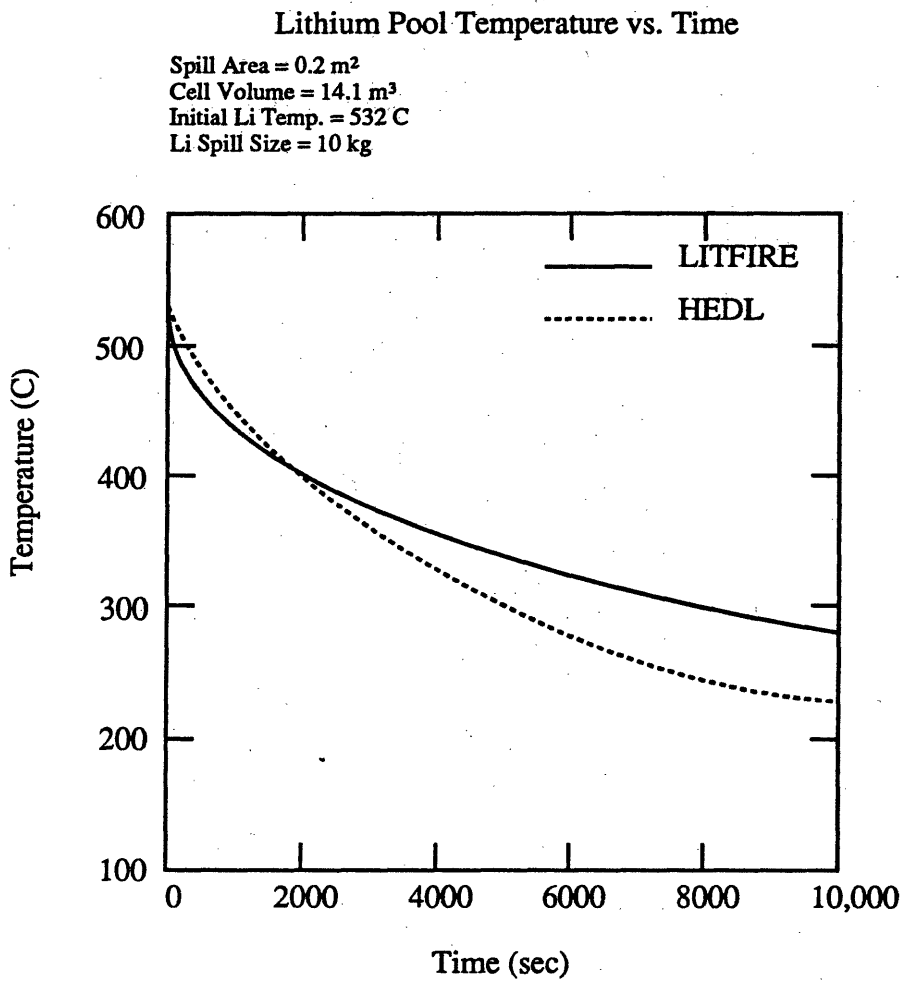

Figure C-5: LN-2 lithium pool temperature

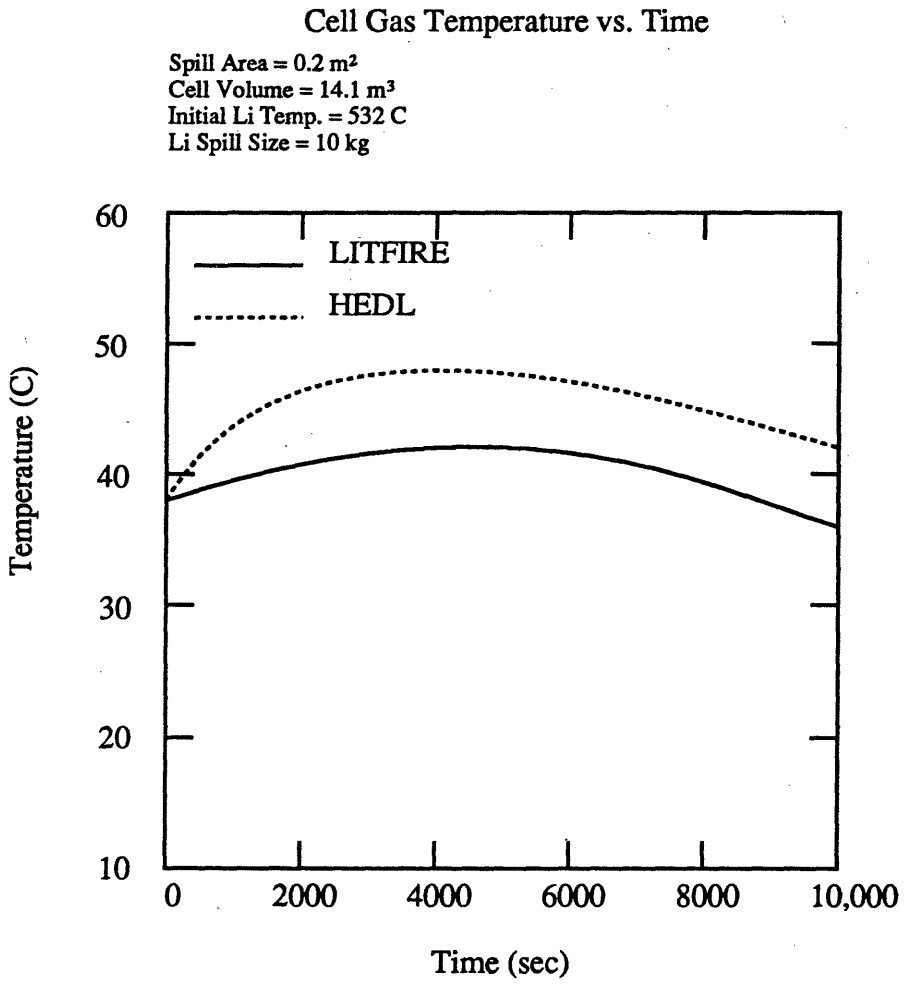

Figure C-6: LN-2 cell gas temperature

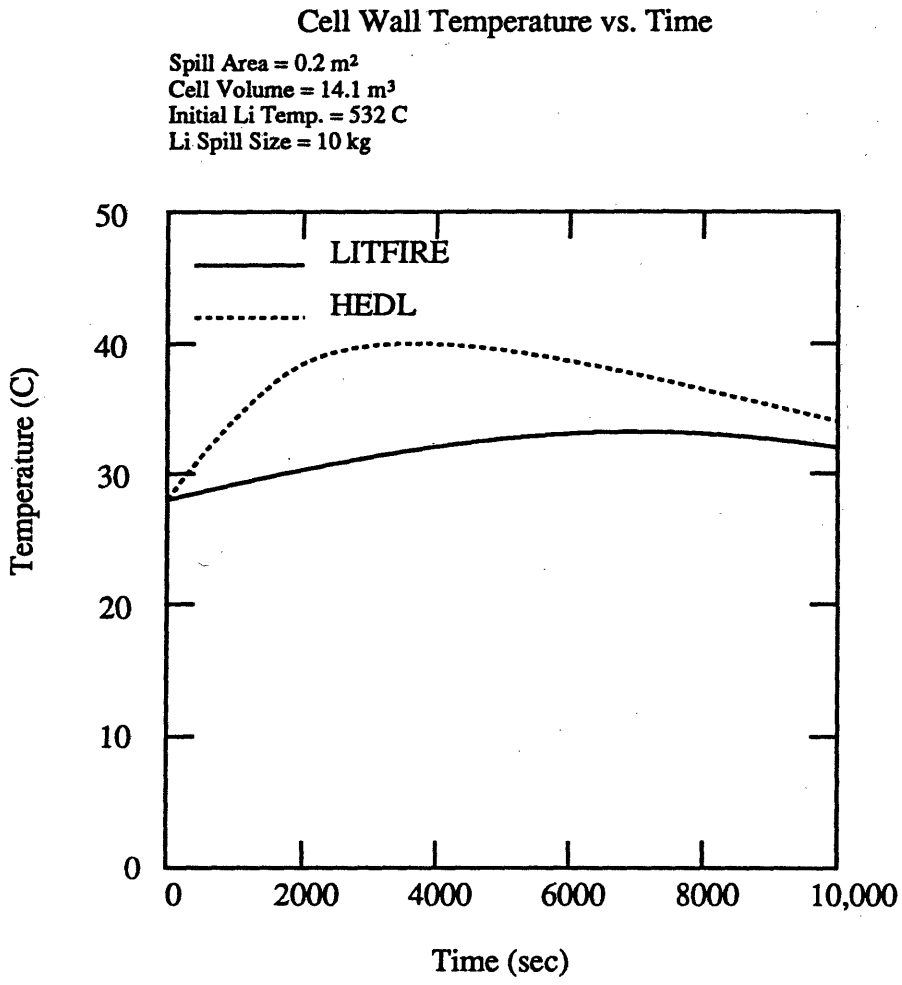

Figure C-7: LN-2 cell wall temperature

C.3 Input Data Used for the Recalibration

Table C.1 gives the values of the thermal properties and coefficients used to arrive at the results given in the previous sections.

All other input data were determined from actual physical properties such as mass, density, specific heat and thermal conductivity, or actual physical dimensions.

Table C.1: Input data used in recalibration of LITFIRE

Property	Value	
Combustion zone emissivity	0.9	
Combustion zone transmissivity	0.1	
Aerosol fraction	5	%
Aerosol radius	5	μ
Spray fire fraction	0	%
Wall emissivity	0.85	
Floor emissivity	0.85	
C†pool-gas	0.18	
C gas-wall	0.11	
C wall-ambient	0.07	
C floor-ambient	0.06	
C gas-floor	0.09	
Pan insulation emissivity	0.9	

†: C corresponds to the heat transfer correlation coefficients of Table 5.2

Appendix D

Experimental Data

Tables D.1, D.2 and D.3 give the lithium reaction rates measured in the kinetics experiments.

Table D.1: Lithium reaction rates of the steam-nitrogen experiments

Test No.	Lithium Temp. (°C)	Reaction Rates (g Li/min cm^2) N_2	O_2	H_2O	Total
5N400	400	0.669	-	0.028	0.697
5N3400	400†	0.179	-	0.021	0.200
5N500	500	0.593	-	0.067	0.660
5N600	600	0.774	-	0.035	0.809
5N700	700	0.724	-	0.019	0.743
5N800	800	0.830	-	0.047	0.877
5N900	900	0.553	-	0.046	0.599
5N000	1000	0.630	-	0.020	0.650
15N400	400	0.573	-	0.191	0.764
15N3400	400†	0.413	-	0.146	0.559
15N500	500	0.288	-	0.161	0.449
15N600	600	0.237	-	0.198	0.435
15N700	700	0.841	-	0.168	1.009
15N800	800	0.843	-	0.179	1.022
15N900	900	1.270	-	0.178	1.448
15N100	1100	0.263	-	0.169	0.432
30N400	400	0.752	-	0.216	0.968
30N3400	400†	0.323	-	0.357	0.680
30N500	500	0.480	-	0.084	0.564
30N600	600	0.265	-	0.389	0.654
30N700	700	0.724	-	0.305	1.029
30N800	800	0.677	-	0.404	1.081

†: preheated test

Table D.2: Lithium reaction rates of the steam-air experiments

Test No.	Lithium Temp. (°C)	Reaction Rates (g Li/min cm^2) N_2	O_2	H_2O	Total
5O400	400	0.171	0.178	0.004	0.353
5O500	500	0.387	0.080	0.000	0.467
5O600	600	0.454	0.111	0.046	0.611
5O700	700	0.754	0.288	0.003	1.045
5O800	800	1.066	0.214	0.006	1.286
15O400	400	0.109	0.079	0.129	0.317
15O500	500	0.190	0.184	0.139	0.513
15O600	600	0.101	0.129	0.079	0.309
15O700	700	0.279	0.170	0.134	0.583
15O800	800	1.059	0.180	0.146	1.385
30O400	400	0.096	0.115	0.208	0.419
30O500	500	‡			
30O600	600	0.606	0.100	0.205	0.911
30O700	700	0.709	0.118	0.246	1.073
30O800	800	0.530	0.114	0.048	0.692

‡: lost due to clogged filter

Table D.3: Lithium reaction rates of the steam-nitrogen-oxygen experiments

Test No.	Lithium Temp. (°C)	Reaction Rates (g Li/min cm^2) N_2	O_2	H_2O	Total
5O2400	400	0.000	0.038	0.096	0.134
5O2500	500	0.082	0.066	0.155	0.303
5O2600	600	0.199	0.095	0.140	0.434
5O2700	700	0.291	0.078	0.127	0.496
5O2800	800	0.308	0.062	0.082	0.452

Bibliography

[1] T.K. Gil and M.S. Kazimi. *The Kinetics of Liquid Lithium Reaction with Oxygen-Nitrogen Mixtures.* Technical Report PFC/RR-86-01, MIT Plasma Fusion Center, January 1986.

[2] D.A. Dube and M.S. Kazimi. *Analysis of Design Strategies for Mitigating the Consequences of Lithium Fire Within Containment of Controlled Thermonuclear Reactors.* Technical Report MITNE-219, Massachusetts Institute of Technology, July 1978.

[3] D.W. Jeppson. *Interactions of Liquid Lithium with Various Atmospheres, Concretes and Insulating Materials; and Filtration of Lithium Aerosols.* Technical Report HEDL-TME 79-7, Hanford Engineering Development Laboratory, June 1979.

[4] W.J. Ijams and M.S. Kazimi. *Temperature Effects on Lithium-Nitrogen Reaction Rates.* Technical Report PFC/RR-85-06, MIT Plasma Fusion Center, August 1985.

[5] H. Kottowski, Joint Research Center-Ispra, Liquid Metal Safety Workshop, Eighth Topical Meeting on the Technology of Fusion Energy, October 1988.

[6] S.J. Piet, et al. Liquid metal chemical reaction safety in fusion facilities. *Fusion Engineering and Design*, 5, 1987.

[7] D.W. Jeppson. *Scoping Studies—Behavior and Control of Lithium and Lithium Aerosols.* Technical Report HEDL-TME 80-79, Hanford Engineering Development Laboratory, January 1982.

[8] D.W. Jeppson, Hanford Engineering Development Laboratory, Liquid Metal Safety Workshop, Eighth Topical Meeting on the Technology of Fusion Energy, October 1988.

[9] M.S. Tillack and M.S. Kazimi. *Development and Verification of the LITFIRE Code for Predicting the Effects of Lithium Spills in Fusion Reactor Containments.* Technical Report PFC/RR-80-11, MIT Plasma Fusion Center, July 1980.

[10] D.S. Barnett, et al. *LITFIRE User's Guide.* Technical Report PFC/RR-87-11, MIT Plasma Fusion Center, August 1987.

[11] V.J. Gilberti and M.S. Kazimi. *Modeling of Lithium and Lithium-Lead Reactions in Air Using LITFIRE.* Technical Report PFC/RR-83-08, MIT Plasma Fusion Center, January 1983.

[12] D.R. Pitts and L.E. Sissom. *Heat Transfer.* Mc Graw-Hill Book Company, New York, 1977.

[13] L.L. Wheat, et al. *CONTEMPT-LT A Computer Program for Predicting Containment Pressure-Temperature Response to a Loss of Coolant Accident.* Technical Report ANCR-1219, Idaho National Engineering Laboratory, June 1975.

[14] H. Uchida, A. Oyama and Y. Tago. Evaluation of post-incident cooling systems of LWR's. In *Proceedings of the Third International Conference on the Peaceful Uses of Atomic Energy*, United Nations, New York, 1965. (A/CONF.28/P.436).

[15] J.H. Lienhard. *A Heat Transfer Textbook.* Prentice-Hall, Inc., Englewood Cliffs, NJ, 1981.

[16] The Babcock and Wilcox Company. *Steam/Its Generation and Use.* The Babcock and Wilcox Company, New York, 1978.

[17] D.S. Barnett and M.S. Kazimi. *Consequences of a Lithium Spill inside the Containment and Vacuum Torus of a Fusion Reactor.* Technical Report PFC/RR-87-9, MIT Plasma Fusion Center, June 1987.

[18] J.E. Massidda. *Thermal Design Considerations for Passive Safety of Fusion Reactors.* PhD thesis, Massachusetts Institute of Technology, October 1987.

[19] R.D. O'Dell, et al. *User's Manual for ONEDANT: A Code Package for ONE-Dimensional-Diffusion-Accelerated, Neutral-Particle-Transport.* Technical Report LA-9184-M, Los Alamos National Laboratory, February 1982.

[20] F.M. Mann. *Transmutation of Alloys in MFE Facilities as Calculated by REAC (A Computer Code System for Activation and Transmutation).* Technical Report HEDL-TME-81-37, Hanford Engineering Development Laboratory, August 1982.

[21] D.L. Smith, et al. *Blanket Comparison and Selection Study.* Technical Report ANL/FPP-84-1, Argonne National Laboratory, September 1984.

[22] W.M. Stacey, Jr. *Fusion.* John Wiley and Sons, New York, 1984.

[23] E. Yachimiak, Jr. and M.S. Kazimi. *Safety Analysis of Liquid Lithium-Lead Breeders in Fusion Reactor Geometries.* Technical Report PFC/RR-84-10, MIT Plasma Fusion Center, June 1984.